THE UNIVERSITY OF EDINBURGH

INSTITUTE OF ECOLOGY AND RESOURCE MANAGEMENT

THE EXCHANGE OF CARBON DIOXIDE IN TROPICAL FOREST

Patrick William Meir

A thesis submitted for the degree of Doctor of Philosophy

April 1996

Declaration

This thesis has been composed by myself from the results of my own work, except where stated otherwise, and has not been submitted in any other application for a degree.

Patrick Meir

April, 1996.

To all my family,

for their unconditional love and support.

Everthing that man esteems
Endures a moment or a day.
Love's pleasure drives his love away,
The painter's brush consumes his dreams;
The herald's cry, the soldier's tread
Exhaust his glory and his might:
Whatever flames upon the night
Man's own resinous heart has fed

*from '**The Resurrection**'*
William Butler Yeats, 1931

Abstract

This study investigated the structure of, and carbon dioxide fluxes at, a 'primary' rain forest in SW Amazonia, Brazil (PRF), and a disturbed secondary rain forest in SW Cameroon (SRF). The total above-ground biomass and leaf area index (LAI) at PRF were respectively 220 (±95% c.l. 48) Mg ha^{-1} and 4.0 (±95% c.l. 0.7) m^2 m^{-2}, and at SRF 90 (±95% c.l. 9.4) Mg ha^{-1} and 4.4 (±95% c.l. 0.9) m^2 m^{-2}. A novel method was devised to quantify the vertical profile in LAI: SRF was distinguished from PRF by a higher concentration of leaf area near the ground.

Three methods were used to determine the flux of CO_2 from soil and gave overall agreement (static and dynamic chambers, and eddy covariance). The mean soil efflux in PRF and SRF was respectively 5.5 µmol m^{-2} s^{-1} (±95% c.l. 0.2; n = 42) and 4.5 µmol m^{-2} s^{-1} (±95% c.l. 0.2; n = 178) at 20 - 24 °C. The temperature response was higher in PRF than SRF (Q_{10} = 2.3 *vs* 1.9). Soil efflux rates were also obtained from cerrado vegetation in central Brazil, where the efflux was 3.2 µmol m^{-2} s^{-1} (±95% c.l. 0.2; n = 10) and the Q_{10} 1.6, at 16 - 23 °C. Heterogeneity in emissions was higher in SRF than in PRF and could be described by a non-linear model incorporating the variables: soil temperature, organic carbon and total nitrogen (r^2 = 0.82). Carbon was the most important variable determining respiration in SRF; soil moisture was not limiting. There was no observable effect of season on efflux rates in either rain forest, but a decline occurred in cerrado during the dry season.

Effluxes of CO_2 were measured from stems and branches of diameter 0.002 m - 1.6 m in 24 species in PRF and 17 species in SRF; emission rates were 0.1 - 3.3 µmol m^{-2} s^{-1} with a Q_{10} of 1.8 in PRF, and 0.2 - 5.2 µmol m^{-2} s^{-1} with a Q_{10} of 1.6 in SRF. Bark temperatures ranged between 18 °C and 28 °C. Maintenance respiration was 80% and construction respiration 20% of total woody tissue respiration (R_t) in SRF. A functional model described the relationship between R_t and diameter in SRF better than a purely empirical one (r^2 = 0.66). A novel method was devised to estimate sap CO_2 concentrations which in SRF were 1.2 - 11.0 mmol dm^{-3} for *Distemonanthus benthamianus* and *Musanga cecropioides*. Sap CO_2 levels were sensitive to sap pH, and represented 1 - 30% of cuvette-measured leaf photosynthesis.

Maintenance leaf respiration (R_m) was measured through the vertical profile during the night in PRF and SRF. R_m increased with height at both sites: ~0.2 in PRF *vs* ~0.3 in SRF at 1.5 m, and ~0.5 in PRF *vs* ~0.9 in SRF at 26 m (values normalised to 22 °C, units: µmol m^{-2} s^{-1}). Leaf nitrogen and potassium concentrations (N_{leaf} and P_{leaf}) declined with height in the canopy. P_{leaf} concentrations were higher in SRF than PRF where P_{leaf} appeared to limit respiration. R_m was not significantly related to N_{leaf} or P_{leaf} on a mass basis, but was strongly correlated with these variables on an area basis, partly as a consequence of variation in specific leaf area. A molar ratio, R_m:N_{leaf} explained variation in R_m with height. A biochemical model was fitted to measurements of leaf photosynthesis (A_l) made throughout the vertical profile of the SRF canopy. Stomatal conductance (g_s) was highest in the morning at the canopy-top, and declined during the day; maximum g_s was 0.3 - 1.0 mol m^{-2} s^{-1}. A_l followed the same pattern, though a delayed peak was observed near the ground. A_{max} was 11 - 14 µmol m^{-2} s^{-1} at the canopy-top and 6 µmol m^{-2} s^{-1} near the ground; α, the quantum efficiency, varied from 0.04 - 0.06 mol mol^{-1}. Fitted photosynthetic parameters varied with height and were significantly related on an area basis to N_{leaf} and P_{leaf}.

Forest stand respiration models were made for both sites by component summation. For SRF, a multilayer model of photosynthesis was constructed using leaf level photosynthetic parameters, and compared with a 'big-leaf' one parameterised using eddy covariance measurements. Respiration estimates were combined with both to retrieve net forest assimilation at 0.7 - 0.9 µmol m^{-2} s^{-1}; a model estimated an annual carbon sink for PRF during 1992/3 of 0.3 µmol m^{-2} s^{-1} (0.9±0.2 Mg ha^{-1} yr^{-1}; Grace *et al.*, 1995, *Science*, 270, 778-780). Both forests were highly sensitive to CO_2 concentration and temperature. The temperature sensitivity of effluxes from soil was found to determine strongly the sink-source strength of both forests and should remain a focus for further work.

Acknowledgements

Above all I would like to thank my supervisor, John Grace, for his guidance since my arrival in Edinburgh. His amazing enthusiasm in the field for almost everything was matched only by his interest in editing this thesis. Thanks must go as well to my second supervisor, Adrian Newton, whose assistance at various intervals was timely and generous. I am also grateful to Paul Jarvis for allowing me the flexibility to complete this thesis at the end of the write-up.

Antonio and Heloisa Miranda provided a great base for us upon arrival in Brasilia; working with them and Rocha was fun as well as productive. The staff at INCRA in Ji-Parana provided invaluable advice and logistic support for all our boat journeys to the Reserva Jaru. Joao, Maria, 'Ready Eddy' and Jose Carlos stick out as particularly memorable characters, and Divons Lancheonete deserves a special mention too.

My thanks go to Dieudonne Nguele for his help with all things official in Cameroon, and his good company. Also to Paulinus Ngeh, Zak Tcheundjeu, Gerry Lawson and Andy Roby who provided support at FMRP in Mbalmayo. But special gratitude is reserved for John and Rose Jenks who coped with any number of problems, were immensely hospitable, and looked after me so expertly when I caught scarlet fever. And, of course, I could not leave out 'our' nuns who looked after us with such kindness at the convent in Mbalmayo.

The Edinburgh group also collaborated with IH (UK) and ANU (Australia). Many thanks are due to John Gash for his generous interest and help at conferences and in the field. Colin Lloyd, Anna McWilliam, Alaistair Culf and Ivan Wright were great entertainment on boats, towers and in forests and night-clubs, as well as being good colleagues. Thanks also go to Jon Lloyd for making his data available, and to Lins Vellen for analysing so many samples.

The number to mention from Edinburgh is legion, but my particular thanks go to John McIntyre for his technical brilliance and wacky personality, to John Massheder for expert (and patient) help with analysing the eddy covariance data, to Sophie Hale and Bart Kruijt for more discussion, to Craig Barton for his Stanley knife (and general advice), to Peter Levy for discussion over the minutiae of gas exchange and for exaggerating my knowledge of pop music. I owe an especially large debt of thanks to Shiela Wilson for her friendly and reliable help at times of stress. I am also grateful to Alex Harrower, Dave Mackenzie and Peter Davis in the workshop, who put up with my constant stream of questions and impractical ideas. Slightly further afield, thanks are also reserved for Linda Sharp for her patience, and to Stephen Gundry and Jim Wright for access to some late-breaking map technology. Jim was also responsible for making life in Edinburgh so enjoyable, as was 'Dennis' and my other flatmates, and of course, Lorraine.

Table of contents

1. INTRODUCTION

Background 1

Thesis aims and structure 4

2. THE RESEARCH SITES

PRF: Reserva Jarú, State of Rondônia SW Brazil 6

SRF: Mbalmayo Reserve, Central Province, Cameroon 10

3. FOREST STRUCTURE: BIOMASS AND LEAF AREA

3.1 Introduction 15

3.2 Methods

Woody biomass 16

Leaf area and biomass 17

3.3 Results 23

3.4 Discussion 30

3.5 Conclusions 34

4. THE FLUX OF CO_2 FROM THE FOREST FLOOR

4.1 Introduction 35

4.2 Methods

Closed chamber 39

Open chamber 41

Eddy covariance 42

Soil composition 44

4.3 Results 45

4.4 Discussion 63

4.5 Conclusions 69

5. THE FLUX OF CO_2 FROM WOODY TISSUE

5.1 Introduction 70

5.2 Methods

Measurement systems and chambers 74

The relationships among CO_2 efflux rate, T, D_w, R_m and R_c 77

Detection of CO_2 in the transpiration stream 78

5.3 Results 81

5.4 Discussion 93

5.5 Conclusions 98

6. LEAF RESPIRATION AT NIGHT

6.1 Introduction 99

6.2 Methods 100

6.3 Results 102

6.4 Discussion 111

6.5 Conclusions 115

7. PHOTOSYNTHETIC LEAF GAS EXCHANGE

7.1 Introduction 117

7.2 Methods 123

7.3 Results and Discussion 125

7.4 Conclusions 140

8. FOREST - ATMOSPHERE GAS EXCHANGE

8.1 Introduction 141

8.2 Methods

Measurement and estimation of the driving environmental variables 143

Measurement and processing of above-canopy eddy covariance data 145

Modelling respiration and assimilation 147

8.3 Results 150

8.4 Discussion 172

8.5 Conclusions 181

CONCLUDING REMARKS 183

BIBLIOGRAPHY 185

APPENDICES

A1. Design of soil temperature probe 199

B1. Woody tissue respiration in light and dark/ 200

C1. The measurement of photosynthesis using the LCA3 200

C2. Analytical solution for A_1 202

D1. Formulae to calculate λ, e_s, s, $\rho_{a,}$, γ, Ψ_M and Ψ_H 204

D2. Empirical relationships used to obtain in-canopy meteorological variables 205

E1. Species lists for SRF and PRF 207

List of symbols

Roman Alphabet

$[CO_2^*]$	Concentration of CO_2 dissolved in stem sap (mmol dm^{-3}).
$[CO_2]_i$	Initial CO_2 system CO_2 concentration (μmol mol^{-1}).
$[H^+]$	Concentration of H^+ ions in sap (mmol dm^{-3}).
A_{ch}	Surface area enclosed by chamber (m^2).
A_l	Rate of net photosynthesis by individual leaves (μmol m^{-2} s^{-1})
B_{bole}	Bole biomass (kg or Mg *per* tree or unit area)
B_{branch}	Branch biomass (kg or Mg per tree or unit area).
C	Open dry forest vegetation type, cerrado (*sensu stricto*).
c, c'	Ambient CO2 concentration, and instantaneous departure from the mean c (μmol mol^{-1}).
C_a,	Ambient concentration of CO_2 in air (μmol mol^{-1}).
C_{ac}	Above-canopy C_a (μmol mol^{-1}).
C_c	Concentration of CO_2 in the chloroplast (μmol mol^{-1}),
C_i	Internal concentration of CO_2 in the intercellular spaces at the surface of the cell walls in the leaf (μmol mol^{-1}),
c_p	Specific heat of dry air (J kg^{-1} K^{-1}).
C_{st}	Concentration of CO_2 at the site of evaporation within the sub-stomatal cavity (μmol mol^{-1}).
D, D_c	Water vapour pressure deficit of air (mol mol^{-1}). D_c refers to above-canopy D.
$d[CO_2]$	Difference between the initial and final CO_2 concentration (μmol μmol^{-1}).
d_{bh}	Tree diameter at breast height (1.3 m).
E	Flux of water vapour between forest canopy and the atmosphere (mmol m^{-2} s^{-1}).
$E_{c/o/v/j}$	Arrhenius activation energies for K_c, K_o, V_{max} and J_{max} respectively (kJ mol^{-1})
F_c	Flux of CO_2 about a plane at height, z (μmol m^{-2} s^{-1}).
F_n / $_c$ *etc*	CO_2 flux between the forest stand and the atmosphere, or ecosystem exchange (units in μmol m^{-2} s^{-1}). The subscripts n, c, cs, eco, ecom and ecob refer repectively to: net measured fluxes, canopy photosynthesis (corrected for respiration terms

	from soil and wood), selected dataset of canopy photosynthesis, storage corrected [biotic] fluxes, and modelled net fluxes using the multilayer and big-leaf models.
g	Coefficient determining the respiratory cost of constructing a unit of tissue.
g_a	[Canopy] aerodynamic conductance (mmol m^{-2} s^{-1})
g_c	Somatal conductance to CO_2 (mmol m^{-2} s^{-1}),
g_i	Internal conductance from the sub-stomatal cavity to the sites of carboxylation within the chloroplasts (mmol m^{-2} s^{-1}),
g_j	Fraction of leaf area in leaf angle inclination class *j*.
g_s	Stomatal conductance to H_20 (mmol m^{-2} s^{-1})
$g_{s\,/\,sc}$ *etc*	Stomatal conductance to water vapour (mmol m^{-2} s^{-1}). The subscripts s, sc, scm and scb refer respectively to leaf-level conductance, canopy conductance, and modelled canopy conductance using the multilayer and big-leaf models.
h	Tree height (m)
H_J/S_J	Parameters defining J_{max} at low and high temperatures (J mol^{-1} & kJ mol^{-1}),
h_{max}	Maximum predicted tree height (m).
i	Zenith angle or angle class of leaves in a canopy (°).
IRGA	Infra-red gas analyser.
j	Leaf inclination angle or angle class of leaves in a canopy (°).
k	Coefficent for the exponential response in CO_2 efflux to temperature ($°C^{-1}$).
k	von Karman's constant (~ 0.41).
$K_{1\text{ or }2}(T)$	Dissociation constants for carbonate ions.
K_c	Michaelis-Menten constant for carboxylation by Rubisco (μmol mol^{-1}),
$K_H(T)$	Henry's Constant for CO_2.
K_i	Fraction of true leaf area in angle class *i* that is projected onto the horizontal.
K_o	Michaelis-Menten constant for oxygenation by Rubisco (mol mol^{-1})
L, LAI	Leaf area index of a canopy (m^2 leaf area m^{-2} ground area).
LAD	Leaf angle distribution.
m	Coefficient determining the respiratory cost of maintaining a unit of tissue.
N	Number of leaf contacts with an infinitely thin rod inserted through a canopy.
N_{leaf}	Amount of nitrogen *per* unit leaf matter (in g m^{-2}, mol m^{-2} and g g^{-1}, mol mol^{-1}).
P	The probability of an infinitely thin [light] probe passing through a gap in a plane of a leaf canopy.
P	Pressure in (kPa).
P_{leaf}	Amount of phosphorus *per* unit leaf matter (in g m^{-2}, mol m^{-2} and g g^{-1}, mol mol^{-1}).

pO	Ambient concentration of oxygen (mol mol^{-1}),
PRF	Undisturbed, 'primary', rain forest site at Reserva Jarú, Rondônia, SW Brazil.
Q, Q_c	Photosynthetically active photon flux density (μmol quanta m^{-2} s^{-1}). Q_c refers to above-canopy Q.
Q_{10}	Relative increase in the rate of a [bio]chemical reaction in response to an increase in temperature of 10 °C (dimensionless).
R	Efflux rate of CO_2 (μmol m^{-2} s^{-1}).
$\boldsymbol{R}$	Universal gas constant (8.314 J mol^{-1} K^{-1}).
R_0	Fitted rate of CO_2 efflux at 0 °C (μmol m^{-2} s^{-1}).
r_a	[Canopy] aerodynamic resistance (s m^{-1}).
R_c	Respiration rate required to construct tissue (*e.g.*, μmol m^{-2} s^{-1}).
R_d	Daytime leaf respiration rate at $Q = 0$ (μmol m^{-2} s^{-1}),
RGR	Relative growth rate of trees (m^3 m^{-3} $time^{-1}$).
R_m	Night-time respiration rate in fully expanded, non-senscing leaves, *i.e.*, at zero growth rate (μmol m^{-2} s^{-1}).
R_m	Respiration rate in at a growth rate of zero, *i.e.*, maintenance (*e.g.*, μmol m^{-2} s^{-1}).
R_n	Net radiation (W m^{-2}).
R_r	(Raw) rate of efflux of CO_2 from woody tissue (μmol m^{-2} s^{-1}).
r_s	[Canopy] stomatal resistance to water vapour (s m^{-1}).
R_t	Efflux rate of CO_2 from woody tissue normalised to 25 °C (μmol m^{-2} s^{-1}).
R_t	Efflux rate of CO_2 of a whole forest, *i.e.*, modelled forest respiration (μmol m^{-2} s^{-1}).
R_{td}	Efflux rate of CO_2 from woody tissue normalised to 25 °C and to the mean D_w of all trees in SRF measured with RGR ≥ 0. Normalisation by diameter was achieved using the linear relationship between ln D_w and ln R_t (μmol m^{-2} s^{-1}).
s	Rate of change of the saturation vapour pressure with temperature (Pa K^{-1}).
SA	Surface area of woody tissue section (m^2).
SLA	Specific leaf area (cm^2 g^{-1}).
SRF	Secondary rain forest site at Mbalmayo Reserve, SW Cameroon.
t, t'	Air temperature, and instantaneous departure from the mean t (°C).
T_{ab}, TAGB	Total above-ground biomass (kg or Mg per tree or unit area).
T_b, TB	Total biomass; above- and below-ground components (kg or Mg *per* tree or unit area).
TBGB	Total below-ground biomass (kg or Mg per tree or unit area).
T_l	Leaf temperature (°C or, as T_{lK},in K).

T_t, T_s, T_{pred}, T_c	Temperature (°C). The subscripts t, s, pred and c refer respectively to tissue, soil, predicted and above-canopy temperatures.
u^*	Friction velocity (m s^{-1}).
u, u'	Streamwise wind speed, and instantaneous departure from the mean u (ms^{-1}).
V	Volume of woody tissue section (m^3).
v, v'	Lateral wind speed, and instantaneous departure from the mean u (ms^{-1}).
V_{ch}	Chamber volume (m^3).
V_g	IRGA system volume (m^3).
V_s	Gas sample volume (m^3).
w, w'	Vertical wind speed, and instantaneous departure from the mean w (ms^{-1}).
z	Distance to the top of the canopy or between target and observer (m).
z_{oM} , z_{oH}	Roughness length for momentum and heat respectively. z_{oH} also represents the roughness lengths for H_20 and CO_2 in this treatment (m).

Greek Alphabet

β	Maximum predicted increase in h with d_{bh} (m m^{-1}).
$\Delta[CO_2]_{ch}$	Change in chamber CO_2 concentration (μmol μmol^{-1}).
γ	Psychrometer 'constant' (Pa K^{-1}).
Γ^*	Leaf CO_2 compensation concentration in the absence of dark respiration (μmol mol^{-1}),
κ	The contact number for a light probe, calculated according to Lang (1987).
λ	Latent heat of vaporisation of water vapour (J g^{-1}).
ρ_a	Density of dry air (kg m^{-3}).
σ_w	Square root of the variance in w (ms^{-1}).
τ	The transmitted fraction of light incident on a canopy.
Ψ_M , Ψ_H	Adiabatic correction factors for momentum and heat respectively (Paulson, 1970).

1. Introduction

This thesis considers some processes governing the global carbon cycle on land, and especially the exchange of carbon dioxide between tropical forest and the atmosphere. Data are presented that quantify the rates of key physiological processes in the forest canopy and below-ground. The information is used in models that simulate the carbon dioxide exchange of soil and vegetation in order to improve the understanding of carbon cycling in one of the world's major biomes.

BACKGROUND

An appreciable amount of current political and scientific activity addresses the effects of human disturbance on the environment (Tickell, 1977; Quarrie, 1992). One of the primary scientific observations driving this activity is the rise in atmospheric carbon dioxide concentration (C_a) over the past 120 years from 280 to 360 μmol mol^{-1} (Friedli *et al.*, 1986; Keeling *et al.*, 1995). Anthropogenic land-use changes and the burning of fossil fuels have been causally linked with this increase (Keeling, 1994). There exists broad consensus that a doubling of C_a could result in a 'global warming' of 2 - 4 °C (Arrhenius, 1886; Plass, 1956; Houghton *et al.*, 1994). The physical, chemical and biological responses to such a climatic change are complex and far-reaching. They require investigation.

A global carbon budget can be computed by incorporating changes in C_a with the estimated carbon fluxes resulting from land-use change, fossil fuel combustion, and oceanic uptake (Houghton, 1995; Marland *et al.*, 1994; Francey *et al.*, 1995). But only 56% of the increase in C_a is explained by this (Keeling *et al.*, 1995) - an extra sink for CO_2 is needed to close the balance (Figure 1.1). The isotopic composition of C_a (the ^{13}C:^{12}C ratio) measured in a global 'flask network' has been used to quantify terrestrial and oceanic exchange rates, and thereby infer the location of possible sinks. However, the calculations are not without uncertainty, and indeed remain divergent in their conclusions, suggesting that there may be strong CO_2 absorption in the northern temperate zone or at tropical latitudes (Tans *et al.*, 1990; Ciais *et al.*, 1995; Enting *et al.*, 1995), or that the sink 'anomaly' can be explained by reference to small fractional increases in globally important carbon stores, such as in soil (Amthor, 1995).

Global carbon budgets necessarily depend on models of the carbon cycle. Current estimated values for net primary productivity are small relative to the overall fluxes of which they are composed. Gross primary production fixes 90 - 130 Pg C yr^{-1} (Bolin 1983; Bolin & Fung, 1992), whilst respiration in soil and terrestrial plants releases 64 - 72 Pg C yr^{-1} (Raich & Schlesinger, 1992) and 40 - 60 Pg C yr^{-1} (Bolin & Fung, 1992) respectively[1]. Clearly a small fractional change in one of these flows could have net consequences for C_a that would be larger than the contribution anthropogenic disturbance makes to the climate. Uncertainty in these gross processes needs to be reduced. Direct measurement of CO_2 transport in the major biomes is required to refine and constrain climate and carbon cycle models (Jarvis & Dewar, 1990; Henderson-Sellers, 1991).

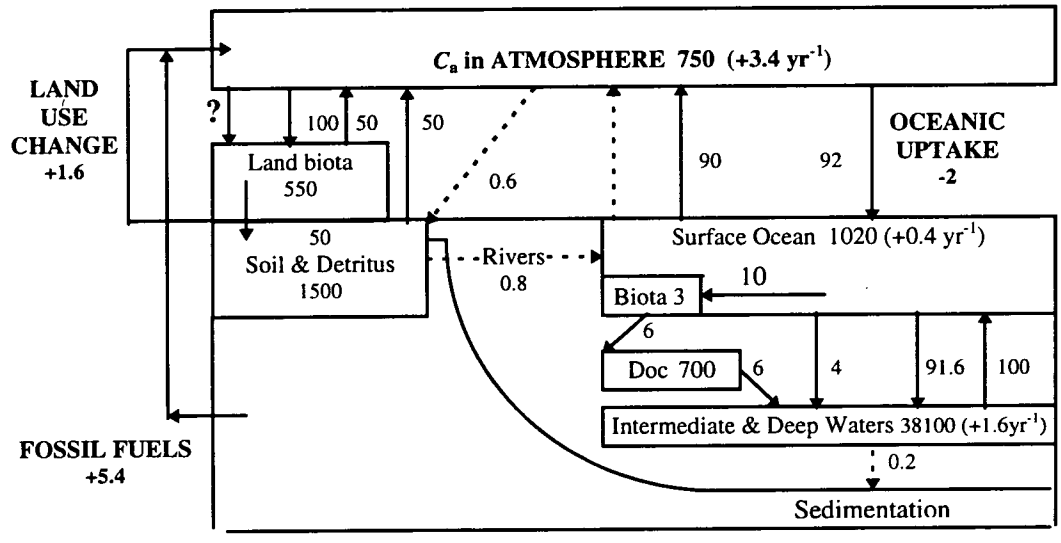

Figure 1.1. Reservoirs and fluxes in the global carbon cycle for 1980-89 (adapted from Siegenthaler & Sarmiento, 1993; units are Gt or Gt yr^{-1}). The figures in capitals can be used to constrain the net carbon balance; their sum leads to a 'missing' sink marked as a **?**. The latest estimates for each of these figures are now: increase in C_a = +2.1 (Amthor, 1995); emissions from land-use changes = +1.6 (±0.7) (Houghton, 1995); fossil fuel combustion = 5.7 (±0.3) (Gifford, 1994; Marland *et al.*, 1994); oceanic uptake = +3.5 to -0.8 (Francey *et al.*, 1995). Most estimates of the 'missing' sink are positive; Siegenthaler & Sarmiento (1993) estimated ? = 1.8 (±1.3).

THE TIGER AND ABRACOS RESEARCH PROGRAMMES

The carbon cycle does not exist in isolation from other natural processes. Acknowledging this, in 1990 the UK Natural Environment Research Council (NERC) set up a large multidiscplinary research programme, TIGER (Terrestrial Initiative in Global Environmental Research), to address the potential

[1]*One petagram, Pg (10^{15}g) = one gigatonne, Gt (10^9 tonne); one megagram, Mg (10^6g) = one tonne*

effects of climate change on land. The aim was to focus on the biosphere at its intersection with the hydrosphere, atmosphere and lithosphere, by means of measurement and modelling. It comprised four components, TIGERs 1-4: respectively, the carbon cycle on land; trace greenhouse gas emissions; the energy and water budgets; and ecosystem impacts (NERC, 1993).

The large extent of, and rapidly changing land-use patterns in tropical forests was addressed in TIGER1 as a study of the flux of carbon between tropical forest and the atmosphere. Direct measurements of forest gas exchange were planned using the newly-developed eddy covariance technique. This method has the capability of measuring the net fluxes over hours, days and weeks, but does not provide measurements of the the underlying physiology that comprises the component processes. This information is important in the interpretation of eddy covariance data, and facilitates modelling. The need for such measurements created an opportunity to link plant and soil ecophysiological studies with research into ecosystem processes.

The main field sites for this study were an undisturbed Amazonian rain forest in Brazil, and a secondary rain forest in Cameroon. For Brazil, the Edinburgh University group were invited to join the Anglo-Brazilian Amazonian Climate Observation Study (ABRACOS). ABRACOS was funded by the UK Overseas Development Administration (ODA) to improve the predictions of the climatic effects of deforestation in Amazonia using General Circulation Models (GCMs). Direct collaboration took place with Drs A. and H. Miranda at the University of Brasilia (UnB) and with the UK Institute of Hydrology. The UnB collaboration also made possible additional measurements in an open forest vegetation type, cerrado (*sensu stricto*). In Cameroon, the Edinburgh group collaborated directly with the Cameroonian Ministry for Forests, the Institute of Hydrology, Imperial College London University, and the Forest Management and Regeneration Project of the Office National de Développement de Fôrets / ODA, under the auspices of TIGER1 & 3. Field work for this thesis took place in 1993 - 94.

NON-LINEARITY AND HETEROGENEITY IN COMPOSITE AND COMPONENT ECOSYSTEM PROCESSES

The goals of both TIGER and ABRACOS were to confer greater credibility and accuracy upon climate and ecosystem models through field validation. In this context, the perceived goal of a model is to simulate a process under conditions or in places where it is either inexpedient or impossible to make measurements, such as the effects of climate or land-use change on the land - atmosphere interactions. The responses of a system to changes in the driving variables (*e.g.*, temperature, radiation, moisture,

C_a) are usually non-linear. For example, the predicted mean photosynthetic fixation of CO_2 by a leaf according to a linearly averaged radiation regime may be significantly different to that calculated using a 60 second time-step (*e.g.*, Hari *et al.*, 1984). If a flux is the result of several non-linear processes which may also depend on state variables, additional complexities ensue.

Clearly, to get a satisfactory answer the important processes must be represented with sufficient accuracy, and where they vary in space and time (*e.g.*, variability in soil quality and seasonality in growth), heterogeneity should be accounted for. In doing this, phenomena at one point of reference are mapped onto, or scaled up to another. The principle is as relevant to the representation of biochemistry in physiology as to the representation of local species diversity changes in whole forested regions (*for further discussion see:* Grace, 1991; Ehleringer & Field, 1993; Körner, 1995; Jarvis, 1995). A correct scaling approach may also lead to the identification of emergent system properties. For example, the feedback effects between canopy foliage and the atmosphere may significantly change leaf-to-air vapour pressure deficits, and hence stomatal conductance (Jarvis & McNaughton, 1986). At the still-larger mesoscale, atmospheric circulation resulting from interactions with heterogeneity at the land surface may create locally high CO_2 concentrations (Grace *et al.*, 1996). In the context of understanding the terrestrial carbon cycle, it was important to quantify the site-specific biological processes contributing to whole-forest carbon dioxide exchange in Brazil and Cameroon. The physiologically active compartments in a forest through which carbon flows are: soil, woody tissue and leaves. They form an armature around which this thesis is organised.

THESIS AIMS AND STRUCTURE

This study addressed key questions concerning the rôle of tropical forests in the global carbon cycle by quantifying the following attributes, using measurement and modelling techniques:

- forest structure: biomass and leaf area
- respiration in soil, leaves and woody tissue
- leaf-scale photosynthesis
- forest stand gas exchange

There are eight chapters. Chapter 2 describes the research sites; the remainder contain data and analysis. The underlying theme of comparison between the two forests is maintained throughout.

Chapter 3: The variation in canopy leaf area in the horizontal and vertical planes was measured using an established and a novel method. Estimates were made of above- and below-ground biomass in woody and foliar tissue. These data were used for scaling up the gas exchange measurements described below.

Chapter 4: The hypothesis that respiration in soil is related to soil temperature, moisture, and nutrient concentration was tested by the measurement of soil CO_2 effluxes and soil constituents. The linked hypothesis that spatial variability in efflux rates could be explained using a model incorporating these variables was also tested. The modelling of respiration in soil is critically discussed and two empirically determined models are presented.

Chapters 5 - 7: Measurements were made in order to test the hypotheses that woody and foliar tissue gas exchange is determined by organ temperature, size, position and nutrient concentration. The functional relationship between woody limb diameter and CO_2 efflux was investigated. The hypothesis that respiratory enrichment of the transpiration stream with dissolved CO_2 may be large enough to affect net photosynthesis was tested. Models were generated to predict woody tissue and leaf respiration rates. Leaf photosynthesis data were analysed using a biochemical model that correctly simulated stomatal conductance as well as photosynthesis.

Chapter 8: Whole-forest gas exchange was calculated using two independent methods. First, for Cameroon, a multilayer model was generated using the data in Chapter 3 to scale the relationships reported in Chapters 4 - 7 to a forest stand. Second, eddy covariance measurements for the same site in Cameroon were used to parameterise a 'big-leaf' model using the same photosynthesis equations presented in Chapter 7. Both *models* were constrained by component-summed respiration estimates and critically compared with the whole-canopy *measurements*. A component-summed respiration estimate was also calculated for the rain forest site in Brazil, and by incorporation with published results (Grace *et al.*, 1995b), an annual carbon budget was estimated. The potential effects of climatic changes on forest ecophysiological processes were modelled, and the results discussed.

2. The research sites

The two main sites visited for this study were separated not only in a biological and geographical sense by the Atlantic Ocean, but also by their respective histories. The forest in Brazil was apparently undisturbed, whilst that in Cameroon had experienced a limited degree of exploitation. For reference in this thesis, the former site is called 'primary rain forest' (PRF) and the latter 'secondary rain forest' (SRF). They are described separately in this chapter.

PRF: RESERVA JARÚ, STATE OF RONDÔNIA, SW BRAZIL

Location

Brazil is the largest country in South America. It spans from north of the fourth parallel in the northern hemisphere to south of the thirty-second parallel in the southern hemisphere. From east to west at its widest point the distance is almost as great, ranging from 35 °W - 74 °W. The catchment areas of the Amazon river cover about six million square kilometres in the north of the country, and form a conduit for the passage of approximately one sixth of all freshwater that is transported by rivers to the oceans (Junk & Furch, 1985). Much of this catchment area is found in Brazil, in the states of Amazonas, Pará, Mato Grosso, and Rondônia (Map 2.1).

The PRF study site was in the Reserva Jarú, Rondônia, and formed one of three sites used for the ABRACOS project referred to in Chapter 1. Rondônia has experienced considerable economic development since 1950, but retains regions of complete forest cover (Lisboa, 1990). There is no history of human disturbance at Jarú, and the physiognomy of the *terra firme* forest reflected this. The area is an ecological reserve administered by the Brazilian environmental protection agency, Instituto Brasileiro de Meio Ambiente e Recursos Renováveis (IBAMA). It is situated 80 km to the north of the nearest large settlement, Ji-Paraná, and is accessed by boat, and then by foot to the north-east of the Machado river. The micrometeorological tower was located at 10° 05' S and 61° 55' W. Land to the south-west of the river had suffered disturbance, characterised by the typical fishbone landscape pattern visible from space (Map 2.1).

Map 2.1. South America, with Brazil unshaded. Expanded below right is part of the State of Rondônia; the region of the field site is marked with a box. Expanded further is a satellite image of the field site (white arrow). The light stripes in the SW of the photograph denote anthropogenic disturbance; to the NE is undisturbed forest in the Reserva Jarú.

Scale: ~ 5km

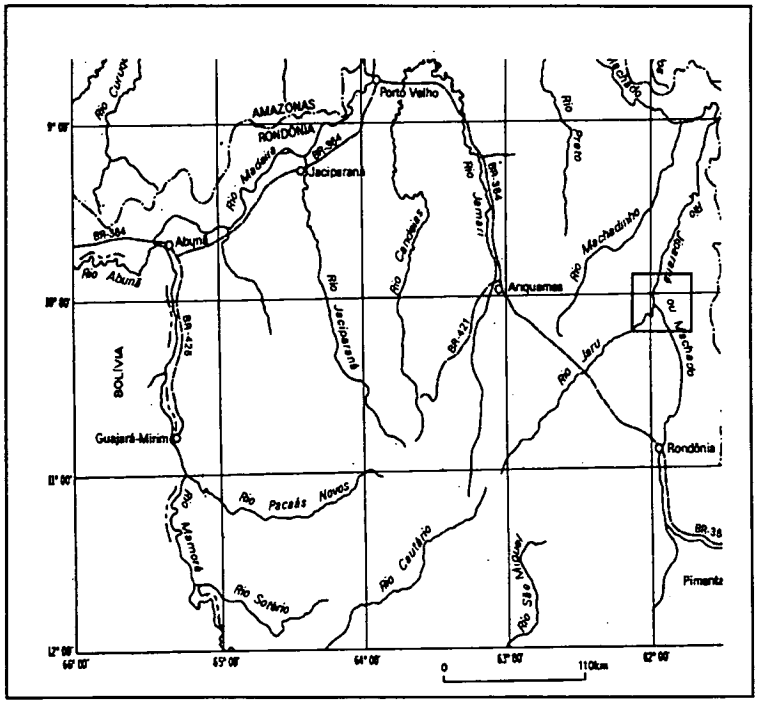

Climate

According to the Köppen nomenclature, the climate is classified as AM, where 'A' refers to 'tropical latitude and mean monthly temperature higher than 18 °C, and 'M' refers to precipitation greater than 1000 mm *per annum*, with one dry season (Amaral Filho *et al.*, 1978). Day length at 10 °S differs only a little from 12 hours, and long term data from the nearest city, Porto Velho, indicate that mean temperatures range between 25 °C and 27 °C, whilst total annual rainfall is less than 2400 mm, with a dry season from June to September and a wet season from December to May (Salati, 1985). The prevailing air flows of the Amazon region come from the east, as part of the trade winds. A feature of the climatic regime is the invasion of periodic cool fronts, or *'friagens'*, characterised by northerly penetration of cold polar air masses. These can cause the air temperature to drop temporarily (1 - 3 days) to as little 14 °C (Salati, 1985).

Site data were measured at Jarú for the year 1992-93 (Culf *et al.*, 1996), and are consistent with those for Porto Velho. Rainfall was 1900 mm with a similar timing for the wet and dry seasons, though 1992 / 3 was a drier than average year. The mean monthly temperature ranged from 23.2 °C to 25.7 °C, and the average water vapour pressure varied between 22 and 28 mbar. For the mid-range values, this corresponded to 81% relative humidity, and a water vapour pressure deficit of 0.006 mol mol^{-1} (Figure 2.1). The lower temperatures at Jarú presumably reflect higher urban maxima in Porto Velho, as average temperatures over pasture were similar to those over the forest (Culf *et al.*, 1996).

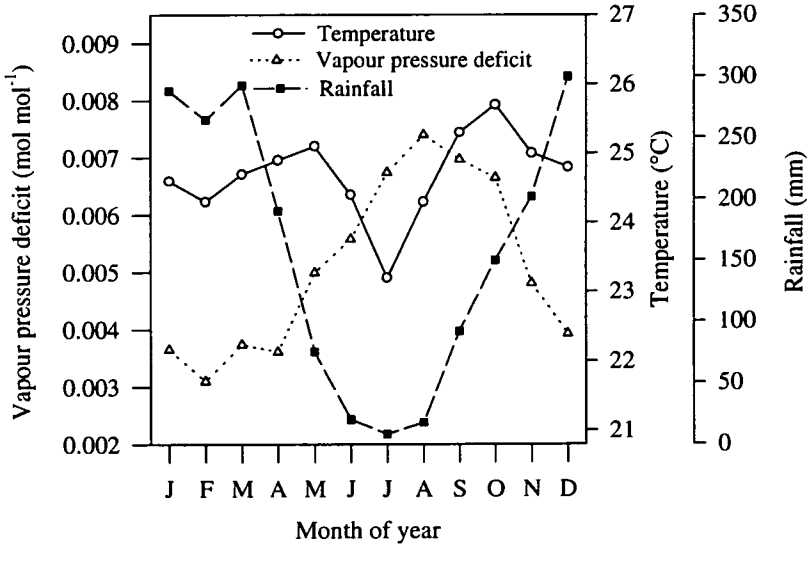

Figure 2.1. Climate data for PRF at Reserva Jarú, recorded in 1992/93 by the ABRACOS project.

Geology, Geomorphology and Pedology

Three geological provinces are identified in Rondônia (Leal *et al.*, 1978). Reserva Jarú is situated in the Xingu Complex and comprises Late Pre-Cambrian and Middle-to-Late Pre-Cambrian granite formations. Although on a fluvial terrace less than 200 m above sea level, the morphostructural unit to which the area belongs is described as the 'Southern Amazon Dissected Highland'. This is itself a part of a larger morphoclimatic unit comprising both depressions and regions of submontane character.

A soil description for Jarú is given by Hodnett *et al.* (1996). The soil type was a red-yellow orthic acrisol (U.S. Soil Taxonomy), with a high sand content near the surface. At 0.6 m the texture was a sandy loam and below this the clay content rose to between 17% and 34%. In most places the soil merged downwards into saprolite and then hard-weathered granite bedrock at a depth varying between 1.6 m and 4.0 m. The bulk density of the soil was 1.38 Mg m^{-3} near the surface (Table 2.1). Soil nitrogen and organic carbon concentrations for two nearby sites on similar soils and under similar vegetation types are reported as 1.0% and 1.03% - 1.33% respectively (Amaral Filho, 1978).

Vegetation

The most common natural vegetation type in Rondônia is described as 'open forest' or '*floresta aberta ombrofila*' (Lisboa, 1990; IBGE, 1993). This is characterised by a relatively low stature (tree height = 30 m - 35 m), wide spacing of trees, and sometimes with an abundance of palms of the genera *Iriartea*, *Euterpe*, *Astrocaryum* or *Maximilliana*. In the latter condition there may also be a local abundance of Brazil nut trees, *Bertholletia excelsa* (Pires & Prance, 1985). In contrast, 'dense forest' is characterised by a slightly greater stature (30 m - 40 m), more tightly knit tree crowns, and a relative absence of palms. The physiognomic differences between the two can be seen clearly from the air (Lisboa, 1990; page 195).

The forest at Jarú possessed features of both forest types. A full floristic survey was not carried out for the site, though a species list is given in Appendix E. The dominant families of both dense and open forest, Moraceae and Leguminoseae, were also common at Jarú. The local abundance of the palm *Maximilliana maripa* was indicative of open forest, but the above-canopy physiognomy as viewed from the 56 m tower and aircraft suggested the presence of denser forest (Plate 2.1). The mean canopy height was 33 m, though the tallest emergent tree reached up to 44 m. Intergradation of forest

types is a common feature throughout the Amazon basin (Pires & Prance, 1985), indeed similar forest formations can be found at other points on the periphery of the Amazon Basin (Pennington, 1994).

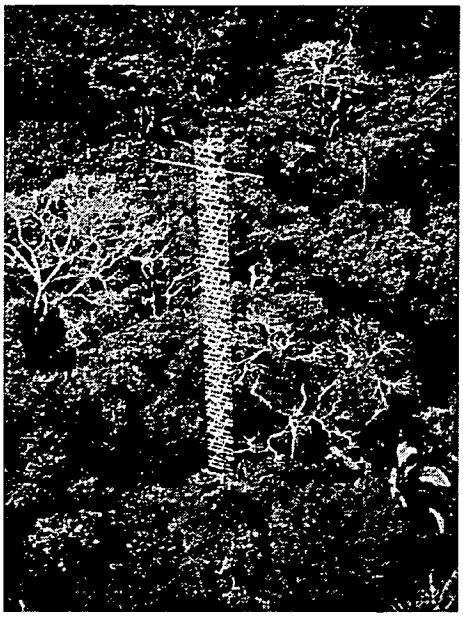

Plates 2.1a&b. Photographs of the PRF forest from the air, and from the tower.

SRF: MBALMAYO RESERVE, CENTRAL PROVINCE, CAMEROON

Location

Cameroon is centrally located on the western seaboard of Africa. Lying between 3° N and 13° N, it is bounded to the west by Nigeria and the Atlantic Ocean, to the north by Lake Chad, to the south by Equatorial Guinea, Gabon and Congo, and to the east by the Central African Republic (Map 2.2).

The SRF study site was in the Mbalmayo Reserve, approximately 10 km from the town of Mbalmayo and 60 km south of the capital Yaoundé, in the Central Province of Cameroon. The reserve has existed since 1947, and has experienced varying degrees of human-related disturbance. It comprises areas of relatively undisturbed forest, degraded secondary forest, plantations, abandoned fields and small cultivated gaps (Lawson, 1995). The variation in land use reflects the activities of the French Colonial Forest Service (Lanthony, 1958), the Centre Technique Forestier Tropical (Foahom, 1982),

the Office National de Régéneration de Forêts with the UK Overseas Development Administration (*e.g.*, Tchoundjeu & Roby 1995), and the proximity of the reserve to nearby settlement. In the northern part of the reserve, the International Institute for Tropical Agriculture have a Humid Forest Station where experimental plots and undisturbed secondary forest are found. The micrometeorological tower was accessed by road to the reserve, and then by a small track to a point 0.8 km south of all current forestry activities, at 3° 23' N and 11° 30' W (Figure 2.2). The surrounding forest was secondary and had been logged more than once, most recently in 1988-9 (Lawson, 1995), but the volume of extracted wood was not recorded.

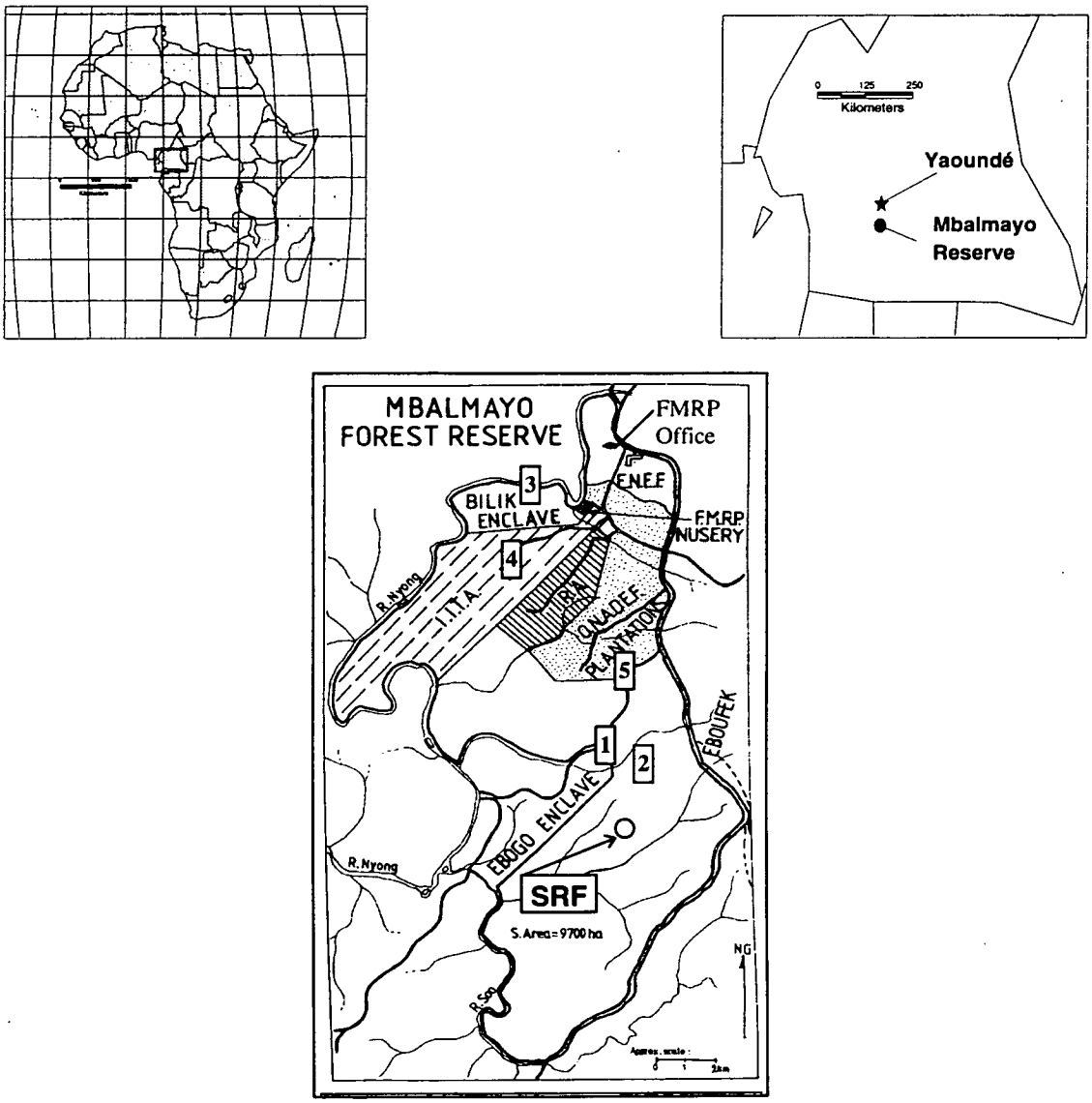

Map 2.2. Top left: Africa with Cameroon in the inset box, and expanded top right. Bottom: a map of Mbalmayo Reserve with the SRF site, and five other sites visited for fieldwork in Chapter 4 marked.

Climate

The region is sub-equatorial, and according to the Köppen nomenclature is classified as AWI (Trewartha, 1954), where 'W' indicates two rainy seasons separated by two dry seasons, and 'I' indicates that the mean temperature difference between the warmest and coldest months is less than 5 °C. The long-term (38 year) average rainfall for Mbalmayo varies between 1016 mm to 1990 mm, with a mean of 1522 mm, and is bimodal. The first rainy season extends from March to June, and the second from August to November (Figure 2.2). Air temperature varies by only 3°C through the year, with the warmest month February (25.2 °C) and the coolest July (22.5 °C). Relative humidity at Yaoundé Airport ranges from 73% to 84%. Further details can be found in Ngeh (1989).

Climate data were recorded during February to May 1994 by Grace *et al.* (unpublished data). Rainfall at the tower was lower than the Mbalmayo average for April and May, though no appreciable soil water deficit was experienced (Boyle, 1995). Mean temperature was 24.3 °C, and the vapour pressure of water in air remained close to the average value of 24.2 mbar, with a short period in late March (20th - 23rd) when it was drier, at 17 - 22 mbar. The lower temperatures in SRF compared to PRF appeared to explain the lower vapour pressure deficits experienced in the drier season. The mean value corresponds to a relative humidity of 74% and a vapour pressure deficit of 0.009 mol mol^{-1}.

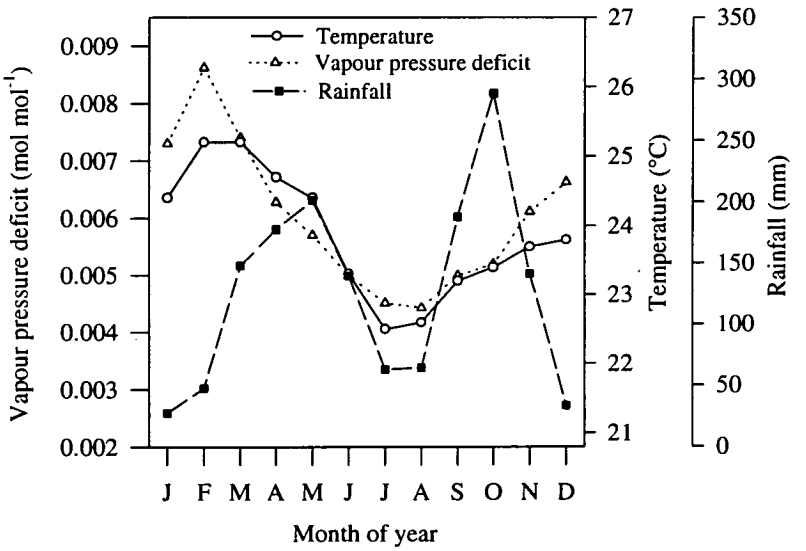

Figure 2.2. Annual climate data for SRF (1934-72 mean). Temperature and humidity data from Yaoundé airport, 60 km north of Mbalmayo Reserve. The rainfall data are for the Mbalmayo Region (Njib, 1987).

Geology, Geomorphology and Pedology

The Mbalmayo region belongs to the Mbalmayo-Bengbis-Ayos series of the Intermediate Pre-Cambrian Formation, which extends east to the Central African Republic. It is slightly metamorphic and formed of greenish schists, micaschists, and gneiss (Ngeh, 1989). The reserve is in the Nyong river midstream catchment area, with a level, undulating and rolling plateau surface approximately 650 m above sea level (Segalen, 1967).

The soil is designated as a yellow desaturated ferruginous sesquioxide by the Office de la Recherche Scientifique et Techniques Outre Mer (ORSTAM). This corresponds to an ultisol or oxisol (Soil Taxonomy, 1975; FAO). A detailed pedological study of the region by Sarlin (1968, cited in Foaham, 1982) distinguishes four main soil types. The following description is one of these and describes the general type found at the SRF site: 'highly weathered deep red or yellow, well drained, acid soils of low base status with generally excellent soil structure, loamy or clay texture'. Profiles taken by Ngeh (1989) in the reserve are consistent with this, describing a sandy clay near the surface (0 - 0.2 m) grading into a dark yellowish brown clay (0.2 -0.4 m) and then a yellowish brown clay (0.4 - 1.0 m) leading towards a gravelly structure or a hard laterile plinthite layer below 1.5 - 2.5 m (Table 2.1).

Vegetation

The climax semi-deciduous forest natural to Mbalmayo Reserve occupies an extensive area of the southern Cameroon plateau (Letouzey, 1985; Plate 2.2). It is variable across its range with the southern limit reaching the Atlantic and Djá forests, while to the north it abuts the foothills of the Adamawa plateau. In the north-west of the country, isolated patches may be found in the valleys.

Ngeh (1989) gives a species list typical for mature forest in the Mbalmayo Reserve. The dominant families are cited as Ulmaceae, Sterculiaceae and Combretaceae. The species list for the area close to the tower (Appendix E) is similar, though it indicates that Moraceae and Leguminoseae are also important in this part of the reserve. The vegetation within 0.7 km of the tower was a mosaic of mature and disturbed secondary forest with regenerating gaps left from the 1988-9 harvest. A few patches near the periphery were classified as flooded or plantation forest (Ministry for Forests, 1994, unpublished data; Lawson, 1995). This radius was also the approximate fetch for the eddy correlation measurements made from above the canopy as part of the TIGER 1&3 projects (Chapter 1).

Plate 2.2a&b. Photographs of SRF from the tower showing heterogeneity in canopy structure.

Table 2.1. Summary soil and vegetation descriptions for PRF and SRF. The data and descriptions are derived from Letouzey (1985), Pires & Prance (1985), Ngeh (1989), McWilliam *et al.* (1996), Hodnett *et al.* (1986), and this study. The soil nitrogen and organic carbon concentrations in PRF (A1 horizon) are obtained from Filho Amarelo *et al.* (1978; profiles 109 and 153, pages 332-334). n/a = data not available.

Feature	*PRF, Brazil*	*SRF, Cameroon*
Forest type	'Open', grading in places to 'dense'	Semi-deciduous
Mean height	33 m	36 m
Dominant families	Moraceae, Leguminoseae, Palmeae	Sterculiaceae, Ulmaceae, Leguminoseae
Soil type	Orthic acrisol	Ultisol or Oxisol
Surface texture	Sand	Sandy clay
Clay @ 0-0.5 m	4%	n/a
Sand @ 0-0.5 m	88%	n/a
Bulk density @ 0-0.5 m	1.38 Mg m^{-3}	n/a
Clay @ 0.5-1 m	24%	n/a
Sand @ 0.5-1 m	67%	n/a
Bulk density @ 0.5-1 m	1.38 Mg m^{-3}	n/a
Organic carbon	1.03% - 1.33%	1.83%
Nitrogen	0.1%	0.16%

3. Forest structure: biomass and leaf area

3.1 INTRODUCTION

The nature of the land - atmosphere interaction is determined to a large extent by how much vegetation there is. The structure and size of a forest canopy affects the physical environment, the flows of mass and energy within and above a canopy, and the stores among which matter may be transferrred. In order to scale gas exchange from leaf to canopy or further, structural information is required to quantify and drive the physiological source processes.

There exist few tropical moist forests for which the biomass, leaf area and structure are known. Furthermore most studies have concentrated on undisturbed forests only (*e.g.*, Odum 1970; Klinge *et al.*, 1975; Jordan & Uhl, 1978; Kato *et al.*, 1978; McWilliam *et al.*, 1993). Recently, the estimation of biomass has been made a little less challenging by the development of well tested regression techniques (*e.g.*, Brown *et al.*, 1989; Brown and Iverson, 1992; Deans *et al.*, 1996). Leaf area measurement methods have also been advanced with the application of image analysis to theory and practice developed over the last decade (*e.g.*, Lang *et al.*, 1985; Lang & Yeuqin, 1986; Lang, 1987; Norman & Campbell, 1991; Campbell and Norman, 1989). Furthermore, the interest in whole canopy ecophysiology and micrometeorology has precipitated the construction of infrastructure needed to access leaves throughout the canopy of a few of these remote forests (Nadkarni & Parker 1994).

This chapter presents biomass and leaf area estimates for SRF and PRF. The total biomass comprises above and below ground terms. Above the ground, it is divided further into branch, bole and leaf components. The leaf area and biomass of the whole canopy are also estimated separately, and the manner in which the composite canopy values vary with respect to height above the ground is considered. These primary structural features provide the basis for understanding the differences between the two forests, and for the calculation of their gas exchange characteristics. A complete inventory of species composition was not possible in this work, but a list of the species studied in Chapters 5, 6 and 7 is given in Appendix E.

3.2 METHODS

WOODY BIOMASS

Inventories were made at both the PRF and SRF sites in plots sited randomly within the 'flux footprint' of the above-canopy eddy covariance measurements being made as part of the NERC-TIGER programme (Grace *et al.*, 1995a; Grace *et al.*, unpublished). Since trees with a diameter at 1.3 m (d_{bh}) > 10 cm constitute ≥ 96% of total forest biomass in closed forests of the tropics (Brown & Lugo, 1984), d_{bh} was measured for all individuals with 10 cm as the prescribed lower limit. The variation of tree height (h) with d_{bh} was also estimated using a hypsometer for a sample of trees (51 trees in PRF; 85 trees in SRF) chosen to represent a wide range of d_{bh} values (0.03 m - 1.45 m in PRF; 0.05 m - 1.8 m in SRF). The choice of tree was random other than with respect to diameter class. A subsample of the h estimates were made of trees close to the micrometeorological tower whose height could be accurately gauged by climbing the tower, and were found to be correct to within 10% for h = 4 m - 35 m.

In Brazil, a 0.25 ha plot (50 m by 50 m) was marked out in 5 m intervals and the d_{bh} of each stem measured. In addition, the life form of each plant was noted (tree, palm or liana) and mapped together with the presence of rosettes of the dominant palm, *Maximiliana maripa* (Corre Serra) Drude (McWilliam *et al.*, 1996). Logistical circumstances prevented the use of identical procedures at SRF, where measurements were made by staff from the Ministry for Forests, Cameroon. Two separate 1 ha plots (250 m by 40 m) were marked out and all trees with d_{bh} > 0.1 m were located and counted. Data were collated in diameter classes rising in 10 cm increments from 0.1 - 0.2 m to 1.0 - 1.2 m. An estimate of standing and lying dead wood was also made for the SRF: stems or branches were measured for total length and mean diameter down to a minimum of 0.1 m.

Biomass was calculated using regressions obtained from two sources: Brown *et al.* (1989), and Deans *et al.*, (1996). Both require d_{bh} and h for the estimate. The Brown *et al.* formulation (Equation 3.1) is that given for moist tropical forest (*sensu* Holdridge, 1967) and refers to 'total above-ground biomass' (TAGB). The Deans regression (Equation 3.2) was obtained from trees harvested near the SRF site, in Cameroon during 1993 and refers to 'total biomass' (TB), that is, the sum of TAGB and the below-ground biomass, TBGB. The approximate ratio of TBGB : TAGB in the Deans data was 0.26; this is in agreement with unpublished data of Brown and Lugo (*personal communication*, D. Deans) and significantly larger than earlier estimates (Brown & Lugo, 1984; Nepstad *et al.*, 1994). The TAGB

values comprise branch and bole biomass; Equation 3.3 (D. Deans, *personal communication*) describes the regression used to estimate the ratio of stem and branch biomass. The d_{bh} of each tree in the PRF inventory, and the d_{bh} class midpoint (Gillespie *et al.*, 1992) from the SRF inventory, were used in the biomass estimates reported here.

Brown *et al.*	T_{ab}	$= \exp[-3.375 + 0.948 \ln(d_{bh}^2 h)]$	Equation 3.1
Deans	T_b	$= 0.52 + 0.0246\, d_{bh}^2 h$	Equation 3.2
Deans	B_{branch}	$= 0.23\, B_{bole} - 0.25$	Equation 3.3

where T_{ab} is TAGB in kg, T_b is TB in kg, B_{branch} is branch biomass in kg, and B_{bole} is bole biomass in kg; d_{bh} is in cm, and h is in m.

LEAF AREA AND BIOMASS

Estimates were made of the leaf area of the whole canopy, and of the vertical distribution of leaf area with height in the canopy. Destructive methods were not permitted in either reserve, so indirect measurements were made using photographs of the canopies.

Theory

Photographic methods of leaf area estimation rely on light acting as an infinitely thin rod-like probe. It is assumed to pass through vegetation where gaps exist and not where there are leaves. Leaves are assumed to be black and opaque. In the first procedures of this kind (Levy & Madden, 1933; Warren Wilson & Reeve, 1960; Warren Wilson, 1965), it was shown that the probability distribution of leaf contacts with a metal rod passing through a canopy of leaves positioned at random to the azimuth approximated the Poisson distribution, where the variance and mean are equal. If a rod is inserted into a canopy at a zenith angle i, the number of leaf contacts with the rod, N, is proportonal to the leaf area index of the vegetation (LAI, m^2 of leaf area *per* m^2 of ground area) such that:

$$N_i = u\, z\, K_i \qquad \text{Equation 3.4}$$

where z is the vertical distance from the top of the canopy, u is the leaf area density per unit volume of canopy, and K_i is an extinction coefficient defined by the inclination of leaves to the horizontal such that:

$$K_i = \sum_{j=1}^{Nj} g_j \cos\alpha_j \qquad \text{for } i \leq 90 - \alpha_j \qquad \text{Equation 3.5}$$

where g_j is the fraction of leaf area in leaf angle inclination class j, and cos α_j is the fraction of true leaf area inclined at an angle α_j to the horizontal that is projected in the direction of i. In effect, the product uz is equal to the LAI, L, and K_i is the fraction of true foliage area that is projected onto the horizontal (Norman & Campbell, 1991).

When applying this theory to light, the number of contact points cannot be measured, but the fraction of transmitted light can. The simplest condition of this type exists for horizontal leaves distributed randomly with respect to the azimuth on a horizontal plane. The probability, P, of a [light] probe passing through a gap is given exactly by the binomial expression

$$P = (1 - (A_l / A_s))^x \qquad \text{Equation 3.6}$$

where x identical leaves of area A_l are projected onto a horizontal surface A_s (Monsi & Saeki, 1953). If L is the leaf area per unit area of A_s,

$$L = x(A_l / A_s) \qquad \text{Equation 3.7}$$

and therefore: $$P = (1 - (L / x))^x \qquad \text{Equation 3.8}$$

For fixed L and A_l, Equation 3.7 shows that increasing the area of sample, A_s, increases x. In the limit, as $x \rightarrow \infty$, Equation 3.6 becomes the Poisson Law (as for the metal rod above), such that:

$$P = e^{-L} \qquad \text{or} \qquad L = -\ln P \qquad \text{Equation 3.9}$$

This result can now be combined with Equations 3.4 and 3.5 to give leaf area from the probability of a light probe passing through a canopy with leaves in the inclination class j:

$$LK_{ij} = -\ln P = N_{ij} \qquad \text{Equation 3.10}$$

Extending the argument to light passing through a canopy into an upward-facing hemispherical lens near ground level, P can be directly represented by τ, the transmitted fraction of incident light:

$$-\ln\tau = LK \qquad \text{Equation 3.11}$$

where K is the overall extinction coefficient for all angles of i and all leaf angle inclination classes. If different leaf angle inclination classes are considered for any given probe angle, i,

$$-\ln\tau_i = f_1 K_{i1} + f_2 K_{i2} + ... \qquad \text{Equation 3.12}$$

where f_j is the leaf area index in inclination class j, assuming azimuthal symmetry, a condition that is approximated by many canopies (Lemur, 1973; Ross, 1981; Lang & Yeuqin, 1986; Norman & Campbell, 1991). The LAI of a canopy may be calculated from suitably exposed hemispherical images looking skywards from the ground, by inverting this transmittance model for a range of incident zenith angles (Campbell and Norman, 1989). A simplified estimate of LAI has also been found to work well using the sum of the intercept and coefficent from a regression of contact number against zenith angle, i, in radians, for a range of zenith angles (Lang, 1987).

Techniques

Whole canopy LAI:

Hemispherical photographs were taken using a Nikon F camera with Nikkor 7.5 mm S3HP fisheye lens. The camera was mounted on a tripod at 0.5 m in PRF and 1.5 m in SRF. The greater height in SRF was chosen as a minimum to avoid overestimates of LAI resulting from the extensive litter and non-photosynthetic undergrowth that occurred at intervals in this disturbed secondary forest. The film used in PRF (1993) was a 35 mm monochrome Kodak TMX 100 ASA. In 1994, a high resolution colour image analysis system became available (Optimas 4.0 and 5.1) and the film type was changed to Kodachrome 200 ASA slide film. An extra advantage of the Kodachrome film is that it is processed using a standard procedure at one laboratory in the UK, so the images are comparable in quality and development.

Hemispherical photographs were taken during the first hour after dawn in conditions of even cloud cover, and diffuse light. In both forests account was taken of the horizontal heterogeneity in LAI by making measurements from many points on the ground: in PRF, 36 camera stations were marked out at 10 m intervals in the 0.25 ha plot; in SRF, 30 points were marked out at 10 m intervals along 150 m transects, directed along two randomly determined compass directions separated by more than 90°. To expose correctly for incident radiation, light readings were taken on the open sky by one person from above the canopy, standing on the micrometeorological tower. The camera operator on the ground took five photographs at each position, one at the 'correct' exposure, and two others bracketted at one and two f-stops either side of this. In the developed images, the optimal exposure was easily recognisable. For each photograph, the immobolised camera was remotely fired after levelling with a lens cap spirit level. The procedure at each point took approximately two minutes.

All photographs were analysed using the Optimas software linked to an LAI calculating routine coded by Dr P. van Gardingen of Edinburgh University. The technique constitutes three stages. Stage one requires the 35 mm image to be scanned at high resolution (850 - 1024 pixels *per* inch; Mikrotek Scanner). At this point, different filters can be used, and contrast, brightness, or exposure specified to improve the quality of the image. Quality is described as the best on-screen visual definition of leaf and non-leaf that most closely approximates the true image, which is simultaneously compared using an adjacent transparency projection system. In stage two, the range and number of zenith angles is chosen and the threshold procedure followed. In this latter method, the operator defines what shade of grey is allocated to 'black' (*i.e.*, no gap), and what is white. In stage three, the LAI is calculated by inverting the gap fraction signal.

Stages one and two permit a rational and consistent method of image ananlysis, but still include a small degree of subjective judgement. To minimise this, a range of scanning specifications were tried on test images to determine the optimal software set-up. Black and white scans were found to give the same results as colour scans, and so were favoured. For each set of photographs, a given set of scanning specifications was adhered to, and the threshold level held constant to within 3%. In stage three, all images were analysed for zenith angles from 10° to 80° (where 0° is vertically above the lens), divided up into six annuli. Zenith angles greater than 80° are poorly resolved by fish-eye lens. The image was then further divided up into azimuth angle classes, and analysed for gap fraction by zenith angle class. This method reduces underestimation of leaf area that may result from clumped (rather than perfectly random) leaf distributions. The inversion procedure used was the linear regression method of Lang (1987), where the contact number, κ, is calculated for each zenith angle

class, θ. The intercept (*a*) and coefficient (*b*) of a linear regression between κ and θ are then used to calculate *L* from:

$$\kappa = -\cos\theta \ln\tau(\theta) \qquad \text{Equation 3.13a}$$

$$L = 2(a+b) \qquad \text{Equation 3.13b}$$

Vertical distribution of LAI:

In Brazil, the vertical profile of LAI was estimated by taking hemispherical photographs at different heights (0 m, 8 m, 24 m and 32 m) up the micrometeorological tower. The camera was attached to a 3 m boom clamped to the tower, and remotely fired using an aluminium attachment and a length of cord. The exposure and analysis procedures described above were followed for these measurements. The difficulty with this technique is that the estimate at any point is subject to sampling error, as the spatial heterogeneity is high.

For the work in Cameroon a new method was devised, reminiscent of a semi-quantitative approach reported by MacArthur and MacArthur (1961). The heterogeneity of leaf area in the horizontal plane at each height must be accounted for in order to make a good estimate of the vertical profile in LAI. To do this, a tethered white meteorological balloon was filled with hydrogen and allowed to rise into the canopy at different heights above the ground at a known distance from the tower. A standard Nikon FE2 camera fitted with a Nikkor 300 mm lens was then positioned on the tower at each height and levelled using a tripod and spirit level. The objective was to measure the mean leaf area density between the lens and the balloon, and thus account for spatial heterogeneity in the vertical leaf area profile. Photographs were taken of the balloon using the camera light meter, and the bracketting procedure already described. Four profiles (north, south, east and west of the tower) were measured for a balloon raised to 4 m, 8 m, 16 m, 24 m and 40 m above the ground, over a 25 m path length from the tower. The balloon diameter was measured before and after taking the photographs (mean diameter was 0.64 m). It was necessary to use more than one balloon as a few burst during measurement; to avoid windy conditions and shadows on the target, photographs were taken early in the morning, as with the hemispherical images.

Gap fraction data were obtained using the Optimas software by restricting the analysed region of interest to the balloon target, seen as a flat white disc in the canopy (Plates 3.1a&b). Equation 3.11

was used to calculate the LAI by height after dividing the gap fraction term by the path length (25 m). Although the photographs were taken horizontally (rather than vertically), the theory given above can be applied to this situation by assuming that all light probes were perpendicular to the photographic image (*i.e.*, $i = 0$), and that the leaf angle distribution approximated that of a sphere (making $K = 0.5$). Since this value of K was uncertain, a check was made by scaling the $\ln\tau$ value at each level in each profile to the mean total LAI of the canopy estimated from hemispherical photographs. This proportionate scaling was possible as all images were taken over the same path length of 25 m.

Plate 3.1. Photographs of a balloon target taken horizontally from the micrometeorological tower at 4 m (left) and 20 m (right). The images were analysed to estimate the variation in leaf area density with height in the SRF canopy.

Leaf biomass

Freshly sampled leaves from different trees at different heights in the canopy of each forest were cored to produce 8 - 16 discs, using a leaf corer of internal diameter 16 mm (PRF) or 10 mm (SRF). The species chosen were those used for leaf respiration and photosynthesis measurements and are described in Chapters 6 and 7 respectively. Leaf material was dried to constant mass at 70° and the disc weights measured using a balance sensitive to 0.0001 g (Sauter Re1614, Albstadt, Switzerland). Further details of the analysis of leaf tissue are given in Chapters 6 and 7.

3.3 RESULTS

WOODY BIOMASS

Tree height and diameter

Brown *et al.* (1989) report a d_{bh} : h relationship in tropical forests of the form shown in Equation 3.13. However, a rectangular hyperbola (Equation 3.14) gave a better fit to the data from PRF (r^2 = 0.85 *vs* 0.80) and SRF (r^2 = 0.61 *vs* 0.50), and more accurately predicted tree height in the lower diameter classes. The d_{bh} : h relationships for each forest were rather similar, though the maximum fitted values for tree height were different (PRF = 50.0 m; SRF = 40.5 m. There were also differences in β for each forest (Table 3.1 and Figure 3.1). Neither of the fitted parameters were significantly different between SRF and PRF (data not shown). The spread of points at d_{bh} 0.2 m - 0.4 m was important in determining the shape of the rectangular hyperbola, especially for PRF.

Brown *et al.* (1989): $h = \exp(a + b \ln d_{bh})$ Equation 3.13

This study: $h = \frac{h_{max}\, \beta\, d_{bh}}{(h_{max} + \beta\, d_{bh})} + c$ Equation 3.14

Table 3.1. Fitted parameters to Equations 3.14 using d_{bh} and h data from PRF and SRF. The d_{bh} and h of the largest tree in each forest sample are given as a reference. Units are: h_{max}, d_{bh} and c in :m; β in m m^{-1}.

Forest	h_{max}	β	c	r^2	*Max* d_{bh}	*Max h*	*n*
PRF	50.0	175.1	0.12	0.85	1.45	42.0	51
SRF	40.5	240.0	0.00	0.61	1.80	37.0	85

Plot biomass and diameter class frequency distributions

The frequency distributions of d_{bh} classes for both sites showed a reverse-J shape typical of naturally regenerated forest (Figure 3.2). But significant differences between them were apparent. Most obvious was the very high frequency of trees of d_{bh} = 0.1 - 0.2 m in one of the SRF plots (Figure3.2b). Visually, this plot (Plot 1) was more disturbed than the second (Plot 2) and was dominated in places by the pioneer species, *Musanga cecropioides* R. Br..

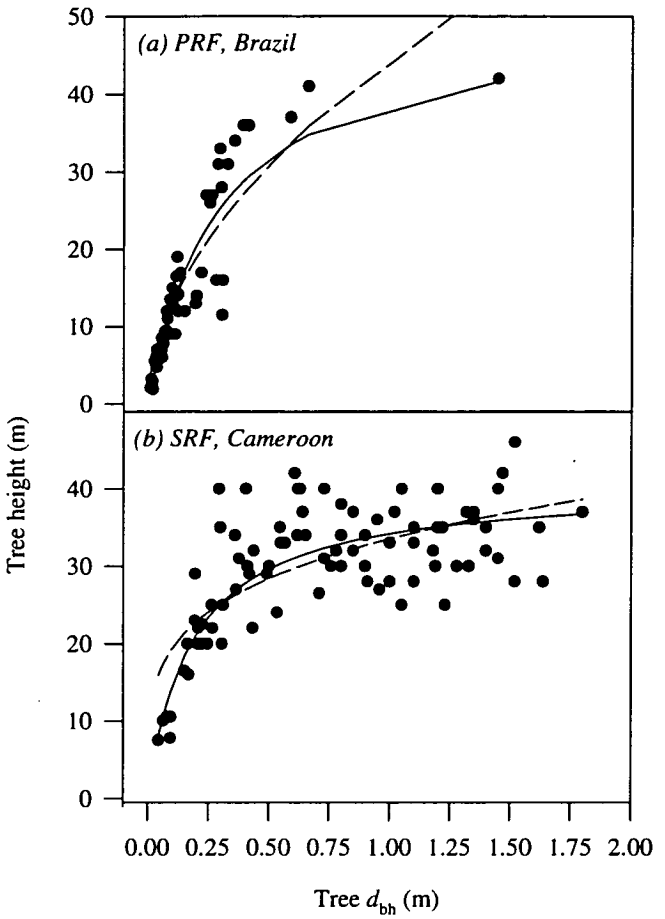

Figure 3.1. The variation in tree height, h, with diameter, d_{bh} in SRF and PRF. The two fitted functions refer to the Brown et al. formulation (Equation 3.13, dashed lines) and the rectangular hyperbola proposed in Equation 3.14 (solid lines). The greater number of large trees in SRF was the result of a larger sample obtained in Cameroon; only the trees in the 0.25 ha sample from PRF were measured in Brazil.

Plot 1 was not markedly different in the lowest d_{bh} class from PRF (Figure 3.2a), but both SRF plots showed a much lower abundance of individuals between d_{bh} = 0.2 m and 0.5 m than was found in PRF. Above d_{bh} = 0.55 m, there were very few trees present in SRF, and many size classes were empty. In PRF, several size classes for 0.55 m < d_{bh} < 1.75 m contained one or more individuals.

Table 3.2 shows the total and component biomass estimates for SRF and PRF. Inspection of Figures 3.2 and 3.3 reveals the presence of one very large tree in the PRF plot (d_{bh} = 1.75 m). This tree was excluded from the biomass values given in Table 3.2 as it increased TB from 300 t ha^{-1} to 400 t ha^{-1} (see Discussion). The mean total biomass (TB) of PRF was 300 t ha^{-1}, whilst that of SRF was 122 t ha^{-1}; 95% confidence limits (c.l.) = 16 t ha^{-1}. It was not possible to obtain a rigorous error for PRF,

although if pseudoreplication was practised, and the 0.25 ha plot divided into four equal quadrants of 0.0625 ha (625 m^2, spatially defined by the four compass points) that were then treated as individual sample estimates, then the TB estimate for PRF was: 277 t ha^{-1}; 95% c.l. = 48 t ha^{-1}).

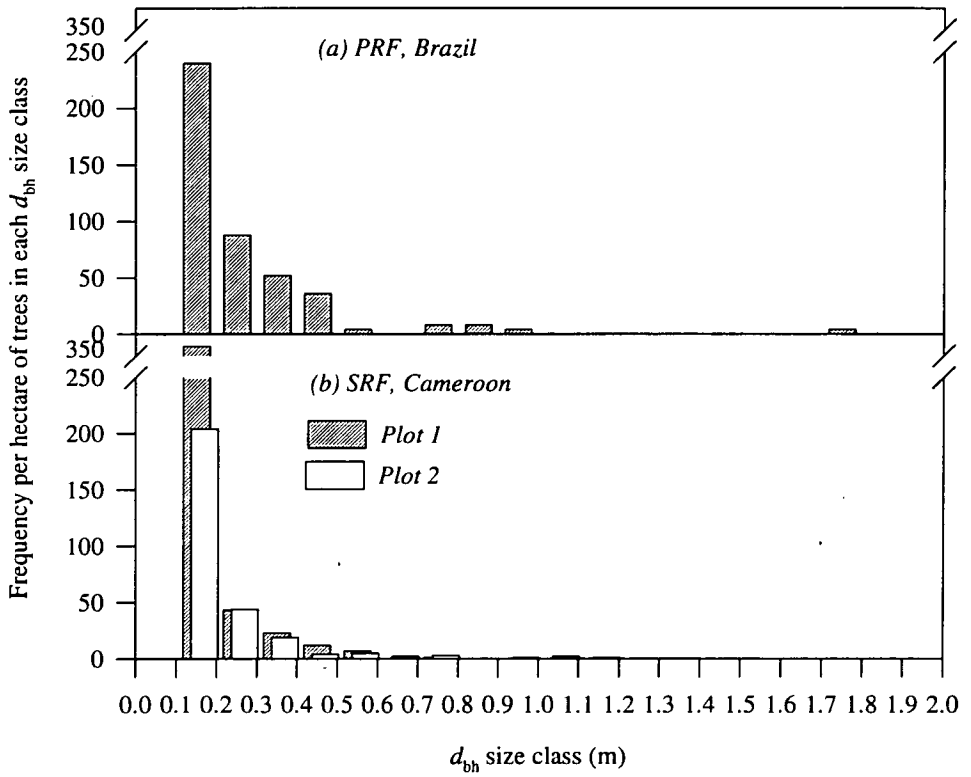

Figure 3.2. Frequency distributions *per* hectare of trees by d_{bh} class. Each d_{bh} class is defined as: 0.15 m (0.1 - 0.2 m), 0.25 m (0.2 - 0.3 m)... etc. In PRF, the data are scaled to 1 ha from the 0.25 ha inventory. In SRF, the data are for two 1 ha plots. Note the axis-breaks on the ordinates.

Within the TAGB component, tree boles comprised approximately 77%, and branches 23% of the total biomass in SRF and PRF. The distribution of biomass within different d_{bh} classes varied markedly between the two forests (Figure 3.3). In PRF, ignoring the largest tree, the majority of the biomass was found in trees of d_{bh} = 0.3 m - 0.9 m, with a peak at d_{bh} = 0.55 m. In SRF, the d_{bh} class with the maximum biomass was 0.15 m; above this diameter, the correlation between TB and d_{bh} was weak and roughly negative. The amount of standing or lying dead wood was only assessed in SRF. The mean density of wood in natural tropical forests of Africa is 0.5 (Reyes *et al.*, 1992). Assuming that the dead wood fraction had a density of 75% of this value, the mean dead wood biomass in SRF was 14.8 t ha^{-1}; 95% c.l. = 16 t ha^{-1}.

Data regarding the frequency of palms and lianas were not available for SRF, but were obtained in PRF. Palms were treated as trees in the biomass estimate for PRF; their frequency was 30 - 40 *per* hectare; mean d_{bh} = 0.16 m, with a d_{bh} range of 0.02 m - 0.35 m, most of which were less than 0.15 m. An additional regression was not sought to improve the estimate of the biomass contribution from this group; when treated as trees, their total exclusion only resulted in a reduction in TB of less than 10 t ha^{-1}. This reduction is likely to be an overestimate, and is well within the error for the whole forest.

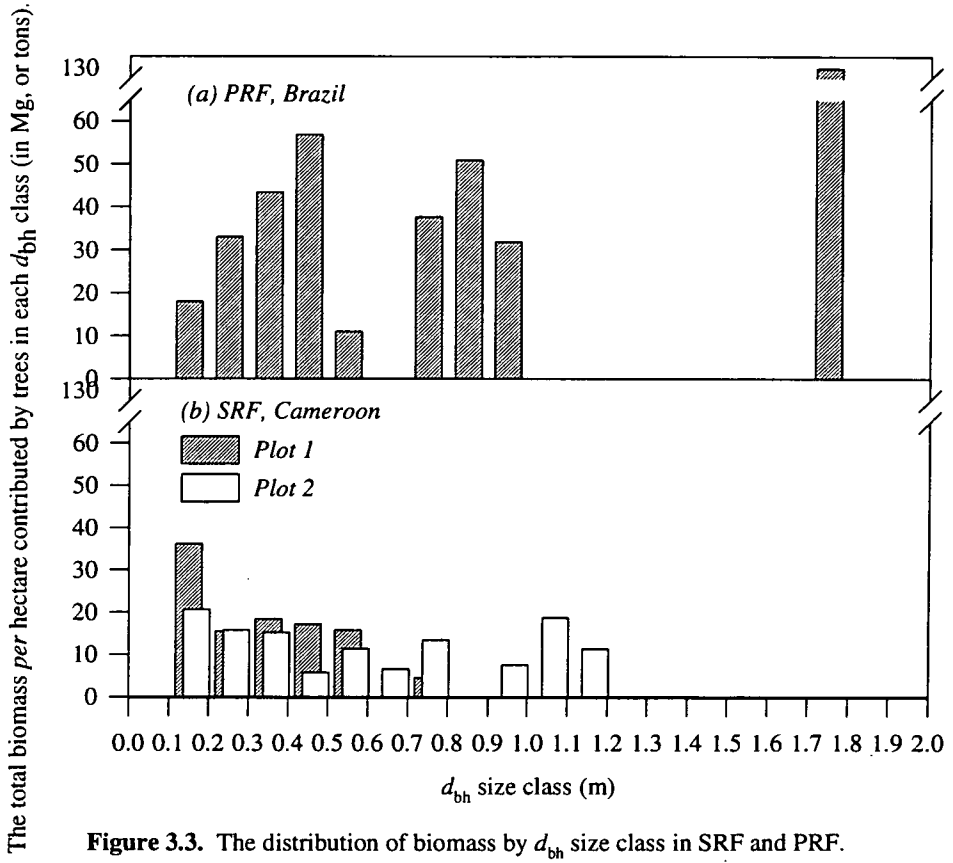

Figure 3.3. The distribution of biomass by d_{bh} size class in SRF and PRF. Note the axis-breaks on the ordinates.

Palm rosette numbers in PRF were relatively high (100 - 150 per hectare), but most of their biomass was associated with leaf area and measured using hemispherical photography. For the same reason, lianas were not included in the TB estimate; their frequency in PRF was 90 - 110 individuals *per* hectare; mean d_{bh} = 0.06 m and with a d_{bh} range of 0.03 m - 0.1 m.

Table 3.2. Estimates of total biomass (TB), total above-ground biomass (TAGB), total below-ground biomass (TBGB), branch biomass (B_{branch}), and bole biomass (B_{bole}) for PRF and SRF using the Equations of Brown *et al.* (1989) and Deans *et al.* (1996). Biomass is in t ha^{-1}; Area = the total inventoried area of each forest. Errors in parentheses are 95% confidence limits of means of the two 1 ha plot inventories in SRF; errors are not given for the derived values of B_{branch} and B_{bole}. TAGB estimates include leaf biomass values.

	PRF, BRAZIL			*SRF, CAMEROON*		
Component	*Brown et al.*	*Deans*	*Mean*	*Brown et al.*	*Deans*	*Mean*
TB	306.3	293.0	300.0	127.3 (12.8)	117.0 (18.4)	122.2
TBGB	79.6	76.1	77.9	33.1 (3.3)	30.4 (4.8)	31.8
TAGB	226.7	216.9	221.8	94.2 (9.4)	86.6 (9.4)	90.4
B_{bole}	176.6	168.1	172.4	71.8	67.0	69.4
B_{branch}	50.1	48.8	49.4	22.4	19.5	42.0
Area		0.25 ha			2.00 ha	

LEAF AREA AND BIOMASS

The mean whole-canopy LAI values were statistically similar for the two forests. PRF had a slightly lower leaf area than SRF, and the variance in LAI for PRF was smaller too: in PRF, LAI = 4.0; 95% c.l. = 0.7; and in SRF, LAI = 4.4, 95% c.l. = 0.9 (Figure 3.4). The maximum LAI measured for each forest was similar, but in SRF, the minimum value found was under 1.8, whilst in PRF it was 2.5.

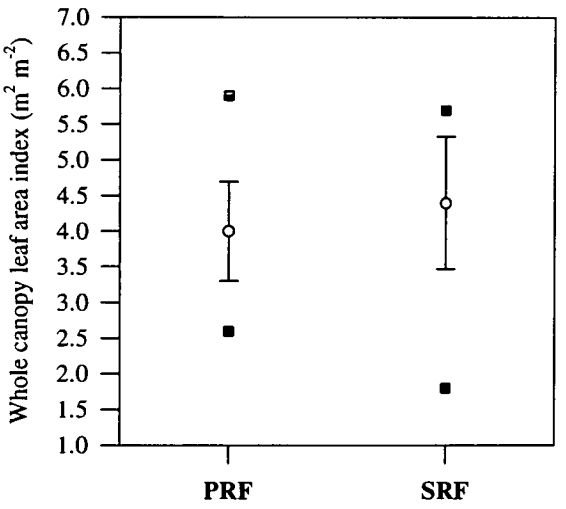

Figure 3.4. The leaf area index of the whole canopy of SRF and PRF. Error bars are 95% confidence limits of the mean (open circles); the squares are the maximum and minimum LAI measured in each forest.

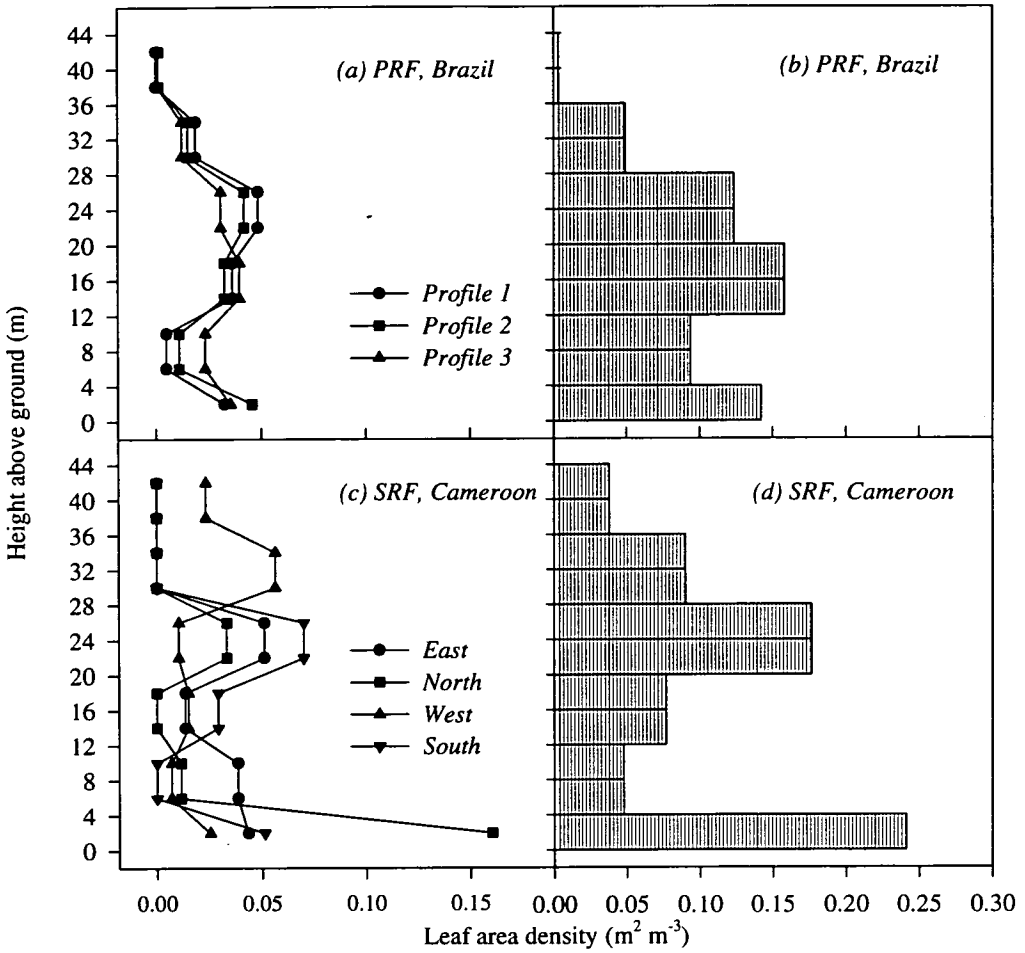

Figure 3.5a-d. The variation in leaf area density with height in SRF and PRF. Figures (a) and (c) show data normalised by $\ln\tau$ to permit comparison of the form of the profile; in order to distinguish data from different profiles, these are plotted as line graphs. Figures (b) and (d) show the averaged profiles scaled to give actual leaf area densities. The measurements were taken at six points, centred on 2 m, 8 m, 16 m, 24 m, 32 m and 40 m; this produced 5 layers of 8 m and the bottom layer of 4 m. In order to adequately compare different layers, each 8 m layer was divided into two equal 4 m layers. This procedure was followed in all four graphs The different profiles in PRF were obtained using gap fraction estimates or photographs; those in SRF were obtained using a novel photographic method (see text).

Comparing the vertical profiles in LAI for each forest was not straight-forward since the PRF hemispherical photographs represented a single point profile, whilst those from SRF were the average of four profiles, each accounting for horizontal heterogeneity in leaf area over a path length of 25 m. To improve the comparison, eye-estimated gap fraction data of the type formally obtained in Cameroon were used to obtain two extra profiles from PRF (Grace, unpublished data). Figure 3.5 shows the individual profiles, and the averaged profiles for each forest. The individual profiles (Figures 3.5a&c) are normalized to show the variation in shape among the different directions. Each profile may represent a different LAI specific to that area of the forest. The averaged profiles (Figure

3.5b&d) are scaled to the mean LAI for each forest. The PRF profiles were less variable than in SRF and indicate that, on average, there was less leaf area in the first 4 m in PRF than in SRF. The profile data from Cameroon were analysed further to test how robust the estimate of K in Equation 3.11 was. At $K = 0.5$ (a spherical leaf angle distribution, LAD), two of the profiles (S and W) were calculated to have an LAI ~4.4, whilst the remaining two (N and E profiles) gave LAI < 2.5 (Table 3.3).

Table 3.3. The total LAI of four measured profiles of the vertical distribution in LAI through the SRF canopy. N, S, E, and W refer to the compass directions of each profile, as measured from the micrometeorological tower. Calculated LAI is obtained using Equation 3.11, and assuming $K = 0.5$; LAI units are m^2 leaf m^{-2} ground area. The fractions of each profile with respect to the overall canopy LAI of 4.4 m^2 m^{-2} are also shown.

Profile direction	*S*	*W*	*N*	*E*
Estimated LAI	4.7	4.2	1.7	2.3
Fraction of mean LAI	1.06	0.95	0.39	0.52

Like LAI, specific leaf area (SLA, cm^2 g^{-1}) in each forest was also similar, with the largest values found near ground level and the highest at the top of the canopy (ranges in SLA: PRF = 80 - 200 cm^2 g^{-1}; SRF = 70 - 200 cm^2 g^{-1}). The vertical profiles in SLA are shown in Figure 3.6a and combined in Figure 3.6b with the average vertical profiles in LAI (Figure 3.5c&d) to show the variation in leaf biomass with height in SRF and PRF. As suggested by the LAI profiles, the foliar biomass in SRF was slightly greater than in PRF (3.4 *vs* 3.2 t h^{-1}). Leaf biomass rose with height to a maximum in both forests at sub canopy-top levels, between 20 m and 30 m, but was higher in SRF at ground level.

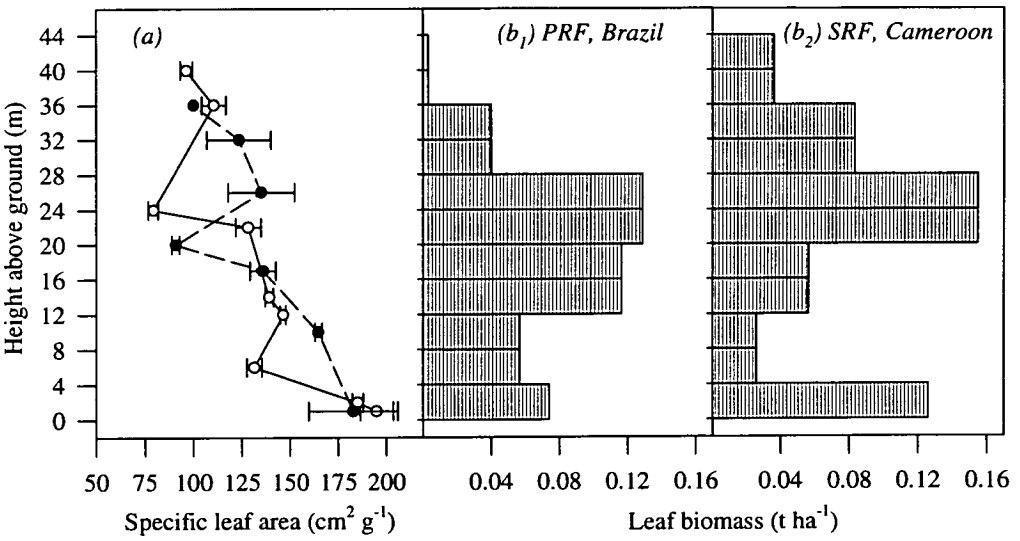

Figures 3.6a&b. In (a), the variation in specific leaf area with height in the canopies of PRF and SRF. Error bars are standard errors from means of 3 - 10 measurements. In ($b_{1\&2}$), the variation in leaf biomass with height in the canopies of SRF and PRF. The data are obtained by combining Figures 3.5 and 3.6a.

3.4 DISCUSSION

WOODY BIOMASS

Tree height and diameter

The rectangular hyperbola used for the d_{bh} : h relationship in this study fitted better to the observed data than the log-linear regression proposed by Brown *et al.* (1989). The main advantages accruing from this formulation were a smaller intercept (c in Equation 3.14 *vs* a in Equation 3.13), a more accurate estimation of h at intermediate d_{bh} and a [lower] maximum predicted h that was closer to the observed values (Figure 3.1). Also, a rectangular hyperbola can be fitted with respect to the rate of increase in h with d_{bh} before h reaches an asymptote. This feature may represent the biophysics of d_{bh} : h relationships more realistically than a log-linear function.

Despite these advantages, the fit to PRF data still under-estimated h at d_{bh} = 0.2 m - 0.4 m. The seven trees responsible for this (Figure 3.1), showed no pattern in species composition, so were not excluded from the dataset. With the omission of these seven values, the r^2 of the fitted model rose to 0.95.

The h_{max} value obtained for PRF (50 m) was greater than for SRF (40.5 m), and β was greater for SRF (220 mm^{-1}) than PRF (175 mm^{-1}). The tallest observed tree was also found in PRF (Figure 3.1), but the discrepancies in h_{max} and β are attributed to the spread and number of data points available to fit Equation 3.14 in each forest. Intrinsic differences in the d_{bh} : h relationship between SRF in SW Cameroon and PRF in SW Amazonia may or may not be reflected in these results.

Plot biomass and diameter class frequency distributions

Both forests showed reverse-J shaped d_{bh} class : frequency distributions, but they differed markedly in character (Figure 3.2). There were more large trees (d_{bh} > 0.55 m) and fewer trees in the smallest d_{bh} class (0.15 m) in PRF than SRF. This pattern reflects the logging history of the two forests (none known of in PRF; at least one harvest during 1989 in SRF). The observation of a relatively high frequency of *Musanga cecropioides*, a pioneer tree (*sensu* Swaine & Whitmore, 1988), in one plot in SRF confirmed the disturbed and regenerating status of this forest. Very few pioneers (mostly of the

genus *Cecropia*) were found in PRF, and generally only where tree-fall gaps had occurred. The large differences between Plots 1 and 2 in SRF (Figure 3.2) highlight the heterogeneous nature of this forest. The TB, TBGB and TAGB estimates obtained using the Brown *et al.* and Deans formulations were surprisingly similar for each forest. The Deans regression was more relevant to SRF as it was derived from trees of the same locality, whilst the Brown *et al.* formulation was derived from pan-tropical data. Their agreement suggests that the data in Table 3.2 are close to the true values. The overall TBGB values highlight the importance of woody biomass below ground level to overall forest biomass (*e.g.*, Nepstad *et al.*, 1994). In addition, the calculated ratio of B_{branch} : B_{bole} was 0.22 in both forests; this was very similar to the ratio (0.24) given by Kato *et al.* (1978) for a much larger forest in Malaysia. As the ratio obtained here was largely determined by the coefficient (0.23) in Equation 3.3, it would only change significantly for a forest in which most of the biomass was in trees of low d_{bh}.

The estimate in Table 3.2 for PRF biomass is in the lower range for forests of Amazonia and the tropics in general, but compares well with values for different forests in the same state, Rondônia (Martinelli, 1988, unpublished; Revilla Cardenas, 1986, cited in Fearnside *et al.*, 1993; Brown & Lugo, 1992). It also reflects the forest-type designation of '*floresta aberta, ombrofila*' (IBGE, 1993), and is in the most common biomass class obtained for moist forests of tropical America by Brown & Iverson (1992, Figure 1). Application to the PRF data of the d_{bh} : h relationship referred to above (with $r^2 = 0.95$) increased the TB estimate by only 5%. This gave further credence to the values in Tables 3.2 and 3.3. Not all authors publish TB values, but most forests can be compared using TAGB estimates. Table 3.4 gives a range for forests in Amazonia, together with values for rain forests of tropical Africa and Asia. As noted elsewhere (*e.g.*, Brown & Lugo, 1992; McWilliam *et al.*, 1993), South American undisturbed rain forests have a lower biomass than that of their Old World counterparts. To some extent, this is a consequence of lower stature: forests of S.E. Asia may commonly have h_{max} values near 60 m (Fölster *et al.*, 1976; Whitmore, 1984). The lower biomass may reflect factors peculiar to the region such as oligotrophic soils, forest age, history of land use, and climate (Brünig, 1983; Brown & Lugo, 1992).

The good agreement with reported biomass data for PRF suggests that the exclusion from the calculations of the single large tree in the PRF 0.25 ha plot was an appropiate measure. Over-estimates of forest biomass may have been reported in the past where small plots of this kind are extrapolated to larger scales. Bias can be introduced by the unwitting inclusion in a small plot of one or two large diameter trees (Brown & Lugo, 1992). This has also been considered a serious problem in temperate forests of the USA (McCune & Menges, 1986).

Table 3.4. TAGB estimates (t ha^{-1}) for moist forest in Amazonia and the tropics of Africa and Asia.

Forest location	*TAGB*	*Source*
Pasoh Forest, Malaysia	475	Kato *et al.*, 1978
Primary moist forest, Cameroon	279	Brown & Lugo, 1989
Manaus, Central Amazon, Brazil	275	McWilliam *et al.*, 1993
San Carlos de R. Negro, Venezuela, *terra firme*	234	Jordan & Uhl, 1978
Samuel Dam, Rondônia, Brazil '*broadleaf, open*'	328	Martinelli, 1988 in Fearnside *et al.*, 1993
Samuel Hydroelectric Reservoir, N. Rondônia, Brazil	285	Foster Brown *et al.*, 1995
Guapore district, Rondônia, Brazil	168	Brown & Lugo, 1992
Reserva Jarú, Rondônia, Brazil, '*aberta ombrofila*'	222	This study
Mbalmayo Reserve, Cameroon, '*secondary, disturbed*'	90	This study

There are fewer estimates of biomass for secondary or disturbed forest, and these vary with the nature of the definition of 'secondary forest'. Clearly, the TB values for SRF are lower than for PRF, as their histories are very different. TB and TAGB at the SRF site (Tables 3.2 and 3.4) fall within the reported range of 43 t ha^{-1} to 425 t ha^{-1} for secondary forests in the tropics (Brown & Lugo, 1992; Brown *et al.*, 1992; Honzak, 1996). The average density of the wood in SRF is likely to be different from undisturbed forest, so a further correction may be required for this site. An additional feature of SRF relevant to carbon balance estimates is the mass of dead wood present (15 t ha^{-1}; 95% c.l. 16 t ha^{-1}). This was greater than in PRF and presumably a consequence of harvesting (*personal observation*). An unknown amount of dead root biomass also accruing from the harvest in 1989 is likely to be present in SRF soil. This component could not be estimated as the harvest volume and previous forest condition are unknown.

LEAF AREA AND BIOMASS

LAI for the two forests was very similar (4.0 in PRF *vs* 4.4 in SRF; Figure 3.4). This result was surprising given the large difference in TAGB values. However, the difference can be explained by the high leaf area present near ground level in SRF (Figure 3.5). Informal field observations indicated that much of the ground level leaf area in SRF was not supported by trees, but herbaceous species, often of the Marantaceae family, *e.g.*, *Haumaniana danckelmaniana*. Consequently, the expected positive correlation between LAI and TAGB (*e.g.*, McWilliam *et al.*, 1993) did not operate here. The variation and range of LAI in SRF was greater than in PRF (95% c.l. of mean: 0.7 in PRF *vs* 0.95 in SRF; range: 2.6 - 5.9 in PRF *vs* 1.8 - 5.7 in SRF). Large gaps resulting from the harvest of 1989 in SRF explain the higher variability of leaf area in this canopy.

Leaf area changes very rapidly after disturbance in the humid tropics, making comparisons with SRF difficult. The mean LAI of PRF was lower than that reported for other forests of the Amazon Basin (5.1 - 7.5; McWilliam *et al.*, 1993), but was consistent with its relatively low TAGB, its forest-type designation (IBGE, 1993) and the relatively high abundance of palms. An independent estimate of LAI at the PRF site was made by Dr J. Roberts of the Institute of Hydrology, UK, using litter fall studies (*personal communication*); initial results gave an LAI of 4.0 - 4.5, in agreement with this study, though Roberts made an [untested] assumption of leaf longevity (1 year) in his calculations.

The vertical profiles in LAI for SRF were more variable than in PRF (Figure 3.5) and reflect the history of disturbance in SRF. The leaf area profiles from SRF are regarded as more reliable than those from PRF, as a formalized technique was used. To calculate LAI using the method used in Cameroon, an assumption was required either that $K = 0.5$ (Equation 3.11), or that $K \neq 0.5$, but remained constant with height (*i.e.*, proportionate scaling of $\ln\tau$ to the mean canopy LAI). To obtain a measure of LAI at a given height, it was necessary to view the target balloon horizontally. Consequently, it was not possible to circumvent assumptions regarding K by using a zenith angle of 57.3°, where all leaf angle distributions give a simliar extinction coefficient (Warren Wilson & Reeve, 1960; Campbell & Norman, 1989). For $K = 0.5$, the LAI for each profile was found to be ~4.4 for two profiles, and significantly less for the other two (Table 3.3). Field notes describing the vegetation close to the tower suggested that the LAI for the latter two profiles was much lower, so the values in Table 3.3 may reflect the true values; the assumption of a spherical LAD appeared satisfactory.

Although this method of measurement of the vertical profile in LAI is relatively inexpensive and rapid to use, it remains limited by the position of the tower, and the path length between the target and the camera. If the local canopy structure is not typical of the forest in general, the profiles will not be representative. The maximum usable path length is probably 30 m - 50 m, depending on leaf area density. This limits the estimate of horizontal heterogeneity in leaf area to the canopy radius of only 1 - 2 trees. These limitations are extremely difficult to overcome, even with highly expensive canopy scaffolding (Koike & Syahbuddin, 1993). The technique suggested here provides one answer to a challenging problem.

The profiles in SLA indicated for both forests that leaf thickness is greatest at the top of the canopy, and declines (SLA increases) in an approximately linear fashion, in negative correlation with height (Figure 3.6a). This pattern has been observed elsewhere in tropical forests (Odum, 1970; Yoda, 1974; Medina & Klinge, 1983; McWilliam *et al.*, 1993). The SLA values reported in these studies ranged

from 40 $cm^2 g^{-1}$ to 164 $cm^2 g^{-1}$. Average SLA values in tropical rain forest given by Schulze *et al.* (1994) range from 47 $cm^2 g^{-1}$ to 196 $cm^2 g^{-1}$. These data are similar to those found for SRF and PRF (range: 69 $cm^2 g^{-1}$ to 250 $cm^2 g^{-1}$), although the maximum measured values were a little higher in this study. The differences between forests probably reflect species differences, but the similarity in profile character is striking and likely to be linked to leaf physiology (see Chapters 6 and 7). The vertical profiles in leaf biomass (Figure 3.6b) underline the importance of leaves near the ground SRF.

3.5 CONCLUSIONS

Inventories were made in 0.25 ha of PRF and 2 ha of SRF. The minimum d_{bh} used was 0.1 m. Tree d_{bh} : h relationships were derived for each forest and used to estimate forest biomass from the regressions of Brown *et al.* (1989) and Deans *et al.*, 1996). The leaf area of each forest was measured indirectly using hemispherical photography, and the vertical distribution in leaf area was estimated using a new photographic technique.

The two forests differed structurally: SRF had a higher frequency of low d_{bh} trees, and few trees of high d_{bh}, whilst the reverse was true for PRF. The independent regressions of Brown *et al.* and Deans *et al.* gave very similar results, suggesting that the estimates obtained were close to the true values. The total biomass of PRF (300 t ha^{-1}) was greater than that of SRF (122 t ha^{-1}), but within the range of reported values for forests of Amazonia, and the state of Rondônia in particular. The total biomass of SRF was within the wide range of reported values for secondary forests in the tropics.

The total leaf area index of both forests was very similar (4.0 for PRF *vs* 4.4 for SRF). A significant proportion of the leaf area in SRF was supported by herbaceaous vegetation rather than trees. In both forests, the maximum leaf area was found between 20 m and 30 m above the ground. But the profiles differed significantly at ground level where in SRF leaf area was relatively high, whilst in PRF, it was low. The technique devised to estimate these profiles appeared to work reasonably well, and suggested that an assumption of a spherical leaf angle distribution may be satisfactory for such measurements when used in conjunction with ground-based hemispherical photographs. The specific leaf area was similar for both forests and was correlated negatively with height; the values were similar to, though the maxima a little higher than, those reported elsewhere for tropical rain forests (65 $cm^2 g^{-1}$ to 250 $cm^2 g^{-1}$). Total leaf biomass was similar for both forests (3.2 t ha^{-1} for PRF *vs* 3.4 t ha^{-1} for SRF), and less than that reported for other forests of higher biomass, in central Amazonia.

4. The flux of CO_2 from the forest floor

4.1 INTRODUCTION

The respiratory component of the terrestrial carbon cycle is dominated by the evolution of carbon dioxide from the soil (Bolin 1983; Houghton & Woodwell, 1979). Despite its importance, the magnitude of this flux remains poorly quantified, especially so in tropical regions (Singh & Gupta, 1977; Fung *et al.*, 1987; Raich & Schlesinger, 1992). In order to improve models of the carbon cycle is necessary to improve our understanding of the main sources of carbon dioxide in tropical forests, and how the principal underlying emission process, in soil, may change in concert with climatic variables (Townsend *et al.*, 1992; Gifford, 1994).

Carbon dioxide is produced in soils by the respiration of roots, bacteria, fungi, soil fauna, and by chemical oxidation of carbon compounds (Lundegårdh, 1927). The rate of transfer of CO_2 to the atmosphere is controlled by its rate of production, soil-atmosphere gradients in temperature and CO_2 concentration, soil physical properties, and turbulence-induced pressure fluctuations. The total flux of CO_2 from soil is a basic descriptor of metabolic activity in an ecosystem and the disentanglement of its component source processes has been an aim at site-specific scales (*e.g.*, Newton, 1923; Coleman, 1973a) and global scales (*e.g.*, Raich & Schlesinger, 1992). A further goal has been the characterisation of factors, such as soil moisture, composition and temperature, that determine respiration rates in soil (*e.g.*, Edwards, 1974; Ewel *et al.*, 1987).

The methods by which respiration in soil is assayed have changed as technology has improved; precise measurement of the phenomenon is not simple. Consequently a short discussion of measurement techniques and problems precedes the main body of this chapter. Emphasis is then given to the temperature response in soil CO_2 emissions. Soil composition factors are also included in the analysis for SRF. The spatial and temporal representation of CO_2 emissions from the forest floor as a whole is considered. Analysis is made of the effects of soil heterogeneity on how soil CO_2 emissions may be modelled, and improvements for future work are considered.

THE MEASUREMENT OF RESPIRATION IN SOIL

The measurement of CO_2 evolution from the soil began early in this century (*e.g.*, Neller, 1918). Several methodologies for field application have been devised, first following the ideas of Lundegårdh (1927) using alkali absorption techniques, and later using gas exchange methods (*e.g.*, Edwards, 1974; Verma, 1990). Reviews of these approaches can be found elsewhere (Schlesinger, 1977; Nakayama, 1990; Hutchinson and Livingston, 1993; Fang & Moncrieff, 1996). Detailed discussion here is restricted to those employed in this study, with the emphasis reflecting intensity of use.

Five main approaches have been taken for measurement of below-canopy soil CO_2 effluxes, three involving chambers sealed to the soil surface, one using eddy covariance and one using the CO_2 concentration profile method. The last of these, proposed by De Jong & Schappert (1972), differs from the other four in that efflux is not measured directly. Instead it is inferred from measurements of CO_2 concentration at different depths in the soil, together with respective estimates of gas diffusivity. The consequent benefit of avoiding the difficulties of surface flux measurement is offset by the requirement for an assumption of steady-state concentrations throughout the profile, and this approach is best followed in conjunction with other techniques.

The alkali absorption method operates whereby CO_2 released from the soil enclosed by a chamber is absorbed by hydroxide solution or soda-lime granules and measured by titration or weight gain. Although it is easy to employ in the field (*e.g.*, Coleman, 1973b), it suffers from errors accruing from incomplete absorption of evolved CO_2. These errors are likely to be larger at temperatures higher than 15 °C (Cropper *et al.*, 1985) even if more advanced methods are used (*e.g.*, Edwards, 1982).

The relatively recent availability of gas chromatographs and field-portable IRGAs has improved the estimation of soil CO_2 emissions using chambers and micrometeorological techniques (*e.g.*, Svensson, 1980; Parkinson, 1981; Keller *et al.* 1986; Norman *et al.* 1992). For this study three methods were used in conjunction with an IRGA: closed chamber, open chamber and eddy covariance. The chamber methods operate by sealing a chamber to the soil surface; they differ in that the closed chamber technique relies on the short-term spot measurement of the enrichment of CO_2 in air circulating within the chamber and IRGA *only*, whilst the open chamber technique requires ambient air to pass through and out of the measurement apparatus at a continuous flow rate. By contrast, eddy covariance makes no disturbance to the soil surface. Instead the vertical flux of CO_2 at a point is obtained by correlating instantaneous fluctuations of CO_2 concentration with vertical wind speed.

Methodological strengths and weaknesses

Chambers offer a relatively cheap approach but require care to avoid bias in measurement. Eddy covariance methods have the advantage of providing spatially integrated estimates, but are costly and require particular micrometeorological conditions. Furthermore, whilst the former approach measures the process(es) of CO_2 production from one compartment only (soil), the latter includes information about its transport and production within the trunk-space, as well.

Two categories of error using chamber methods can be identified: those arising from (a) physical or biological disturbances and (b) sample handling or computation of fluxes from concentration data (Hutchinson & Livingstone, 1993). The second of these is less relevant to the chamber methods employed in this study as the 'sample' was measured directly in the field, and the data obtained provided robust models for the computation of fluxes. Potential errors of the first type include: i) temperature anomalies resulting from covering the soil with a cuvette; ii) the effects of mean pressure differences between outside and inside the cuvette, or the damping of turbulence-induced high frequency surface pressure fluctuations; iii) internal concentration effects; iv) site disturbances such as soil compaction, root severance, disturbance of surface diffusion resistances upon collar emplacement, and the effects of rainfall on permanent installations.

Error types (i), (iii) and (iv) can be avoided with care, but type (ii) is strongly determined by the measurement method used. The open chamber approach is attractive as it allows continuous measurements to be made of soil CO_2 effluxes. But a major difficulty here has been the equalisation of the internal and external pressure whilst sucking or pushing ambient air through the system (Kanemasu *et al.* 1974), although recent advances have been made in this regard reducing pressure differences to below 0.1 Pa (Fang and Moncrieff, 1995; Rayment and Jarvis, 1996). A logistical challenge with this technique is the requirement for a satisfactory number of measurements to represent the mean properly. Soil CO_2 emissions are notoriously heterogeneous, varying by over 100% within 1m (Nakayama, 1990), and by season (Rochette *et al.*, 1991).

The closed IRGA method does not necessarily suffer from anomalous suction-induced fluxes of CO_2 associated with some open chamber techniques as air is circulated round the sealed chamber system by one pump. The short deployment time of the chamber during measurement also allows the heterogeneity in soil to be sampled widely, and is likely to avoid problems associated wth static

pressure fluctuations at the forest floor. Large turbulence events only rarely interrupt the low wind speeds at ground level in mature broadleaf forest (Odum *et al.*, 1970; Baldocchi & Meyers, 1991; Hutchinson & Livingston, 1993; Hanson *et al.*, 1993). But it is possible that such turbulent pumping can also aerate the soil and hence elevate oxidative processes over time (minutes or hours). Spot measurements are unlikely to disturb this hypothesised process, particularly if measurements are made during the night as well as the day, so that different conditions of turbulence are accounted for.

When comparing closed and open chamber systems, a balance should be met between the desire to understand the process(es) of soil CO_2 efflux, including the way environmental variables drive them, and the need for a good spatial estimate. These objectives are closely linked if predictive models are to be constructed, and hence the two methods are complementary.

Eddy covariance at 1 - 2 m above ground level offers a potential solution to the shortcomings of chamber methods if the objective is to quantify CO_2 fluxes passing from the soil into the canopy. The intruments sense wind speed and changes in temperature and gas concentration and the measurement is representative of a large (though variable) area, or 'flux footprint', making possible a good spatial estimate together with continuous data recording. No disturbance is made to the soil, so the effects of turbulence on respiratory processes can be assessed. Furthermore, a description of scalar transport is provided that may be important for the parameterisation of whole canopy transport models (Baldocchi & Meyers, 1991; Kruijt *et al.*, 1996). However some theoretical objections remain over its application below a canopy because of varying wind-flows near the ground, the difficulty of defining a vertical flux, and the presence of respiring plant material between the source (soil) and the sensors (Kaimal & Finnigan, 1994). The magnitude of the trunk-space source is small in comparison to the soil efflux, but where in-canopy eddy covariance has been shown to work effectively, only semi-continuous recording has been possible as the requirement of steady-state conditions can rarely be met during the hours around sunset (Baldocchi & Meyers, 1991).

4.2 METHODS

Three sites were visited in this study: in addition to the main PRF and SRF sites, it was also possible to take measurements in an open dry forest type in Central Brazil. This site, in the Reserva Aguas Emendades (15° 33' S, 47° 36' W); has an approximate LAI of 1 and a canopy height of 10 m. The vegetation is of the type cerrado *sensu stricto*, and is protected from fire. The soil is a red-yellow latisol, with a pH < 5. The annual rainfall is 1500 mm with a strong dry season from June to October, and the mean temperature is 22 °C (for further details, see: Miranda *et al.* 1996; IBAMA 1992). The nomenclature in this chapter remains the same for the rain forests, and cerrado is referred to as C.

CLOSED CHAMBER

This was the most intensively used technique. Efflux of CO_2 from the soil surface was measured by recording the accumulation of CO_2 in a chamber sealed to the soil surface and connected in closed circuit to an IRGA (Licor LI 6200; Licor Inc., Nebraska, USA), with a drying column containing magnesium perchlorate used for stabilising chamber air humidity. Soil CO_2 efflux, R, was calculated according to Equation 4.1, after correcting the IRGA for atmospheric pressure.

$$R\ (\mu mol\ m^{-2}\ s^{-1}) = \Delta[CO_2]_{ch}\ V_{ch} / (A_{ch}\ 0.0224) \qquad \text{Equation 4.1.}$$

where $\Delta[CO_2]$ is the change in concentration of CO_2 in chamber ($\mu mol\ mol^{-1}\ s^{-1}$), V_{ch} and A_{ch} are chamber volume (m^3) and enclosed ground surface area (m^2) respectively, and 0.0224 m^3 is the volume of one mole of gas at standard temperature and pressure.

The chamber was a perspex box, with drilled perspex sheet baffles behind the inlet and in front of the outlet. A small aperture at the side of the chamber (Plate 4.1) permitted venting to the atmosphere (by attachment of narrow bore tubing), or measurement of pressure differentials (by attachment of a digital manometer). The chamber was fitted into a narrow water trough attached to the perimeter of a steel collar inserted 1 - 2 cm into the soil. If the collar could not be inserted without minimal disturbance to the soil, damp sand was successfully used to seal the outside edges to the soil surface. The chamber was sealed to the collar by addition of water to the trough, carefully avoiding any spillage. The basal area of the whole unit was 0.042 m^2; the volume (depending somewhat on depth of collar insertion) was 0.0073 (± 0.0004) m^3.

After checking that chamber CO_2 concentration was close to or at ambient levels (380-600 μmol mol^{-1}, depending on time of day), measurements were made by logging data for 60 or 100 second intervals, using a five second time step, and then repeating the procedure. Data were subsequently checked for linearity of the CO_2 concentration time course over the observed increases of 30 - 60 μmol mol^{-1}. Measurements not fulfilling this stricture (approx. 10%) were discarded. In order to obtain time series data, a limited number of twenty-four hour measurements were made for individual points, or microsites, the collar being left in the soil for the whole of these periods.

Additional tests and observations were also carried out to explore possible errors. Initially, second readings were repeated at each microsite 10-20 minutes after the first to ensure that deployment of the collar had not caused an initial flush of CO_2 by disturbing diffusion resistances at the soil surface (Mosier, 1989); few sites behaved in this way. A collar was also left in the soil for seven days to identify any longer-term effects of chamber emplacement via biological disturbances such as fine root severance. In order to test for the effects of pressure differences between inside the chamber and out, a series of measurements were made with a narrow bore tube (15 cm long, 1.5 mm internal diameter) attached to the venting aperture. A digital manometer was also attached to the venting aperture. Finally, to investigate whether or not light at the bottom of the canopy might affect CO_2 evolution rates from the soil, a sheet of reflective plastic (Perifleur, UK) was used to compare dark and light conditions.

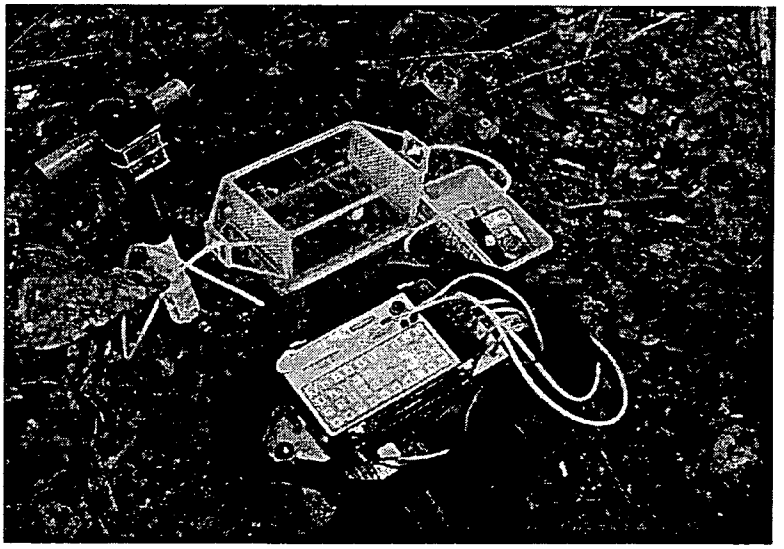

Plate 4.1. The closed chamber system used to measure soil CO_2 effluxes. The IRGA (foreground) is connected in a closed circuit to the chamber. A soil capacitance probe is also visible (left). The white plug on the chamber was the attachment point for the manometer or pressure venting tube.

Sampling of the forest floor was necessarily restricted to relatively flat patches of ground. Notwithstanding this, a wide range of microsites was chosen in an attempt to represent soil diversity with respect to distance from tree trunks, litter depth, and topography. In SRF, a more rigorous sampling strategy was logistically possible. Using the micrometeorological tower as a reference point, randomly positioned microsites were sampled in blocked areas concentric to the tower with radii as follows: 0 - 50 m, 50 - 100 m, 100 - 150 m, 150 - 300 m, and 300 - 500 m. These distances were within the flux footprint for the above-canopy eddy covariance measurements (Grace *et al.*, unpublished), allowing comparison with these data.

In Brazil, measurements were made during May and June 1993 for PRF and April and July 1993 for C. In Cameroon, in SRF, they were made at spaced intervals from December 1993 to May 1994; in addition four other soils were sampled in the area close to the main Mbalmayo Reserve site during April 1994. Three other secondary forest sites and one previously bulldozed site (Table 4.1) were visited in collaboration with Professor John Lawton of Imperial College, London.

Table 4.1. The sites where soil CO_2 emissions were measured in SRF, 1994. The localities are shown in Map 2.2, Chapter 2. An illness prevented collection of more data from sites 2 - 6.

Site	*Forest description*	*Map no.*	*n*
Main tower site, SRF	Secondary forest, logged 1989	SRF	178
Ebogo	Manually prepared forest, for plantation	1	6
Eboufek	Mature, secondary forest	2	6
Bilik	Very mature secondary forest	3	6
IITA Fallow	Field: recently burned fallow	4	6
Bulldozed	Field: bulldozed forest, planted trees	5	6

OPEN CHAMBER

The open chamber method was used for one microsite over a five day period during April 1994 in Cameroon, when equipment became available unexpectedly. A standard closed system cuvette was connected to a small pump system, air being drawn through the chamber at 1.0 l min^{-1} and delivered to a fast response IRGA (Licor LI 6262, Licor Inc., Nebraska, USA) calibrated for carbon dioxide and water vapour. Data were logged as the differential between ambient and chamber concentrations. Efflux values were calculated according to Equation 4.2, after correcting the IRGA for atmospheric pressure.

$$R\ (\mu mol\ m^{-2}\ s^{-1}) = \Delta[S]_{ch}\ F_{ch} / A_{ch} \qquad \text{Equation 4.2.}$$

where $\Delta[S]_{ch}$ is the difference in scalar concentration between air entering and leaving the chamber and F_{ch} is the molar flow rate through the chamber.

EDDY COVARIANCE

The Edisol eddy covariance system was erected at 1.5 m height above the forest floor using spare tower scaffolding, and data were logged for 48 hours between 7th and 9th May 1994, in SRF. The system has been described in detail elsewhere (Moncrieff *et al.*, 1996), and the precise set-up was as specified in Grace *et al.* (1995a), although particular care was taken to make sure the anemometer was vertical. The principle of the method is that fluxes of a scalar from a horizontally homogeneous surface, under steady-state conditions, can be calculated by the instantaneous correlation of fluctuations in vertical wind speed with scalar concentration (Verma, 1990). These entities are measured using a 3-dimensional sonic anemometer (Solent A1002R, Gill Instruments, Lymington, UK) and a fast response IRGA (Li6262, Licor, Nebraska, USA). Where the scalar in question is CO_2, Equation 3 can be used to represent this calculation:

$$F_C\ (\mu mol\ m^{-2}\ s^{-1}) = -\langle w'\ \rho_C' \rangle \qquad \text{Equation 4 3.}$$

where F_C is the CO_2 flux , w' and ρ_C' are instantaneous departures from the mean vertical wind speed and CO_2 concentration, calculated using a 200 s autoregressive moving average. By micrometeorological convention, the negative sign represents fluxes towards the surface (that is *from* the atmosphere) and the angle brackets denote time averaging. The Edisol software (Massheder & Moncrieff, 1995) corrects the measured fluxes for fluctuations in density (Webb *et al.*, 1980). To derive the vertical component of CO_2 fluxes from *above* a canopy the three-dimensional anemometer data are normally rotated three times to obtain zero $< w >$ (McCracken, 1993). Smooth wind-flow streamlines are not usually found *below* the canopy, so the Edisol software was adapted for this study to retain only the first rotation into the average wind direction (J. Massheder, *personal communication*), and reliance was placed on the vertical erection of the anemometer to derive zero $< w >$. Post-processing corrrections are usually employed to correct the data for non-ideal frequency responses in the system, such as attenuation of the signal down the sampling tube, mis-matched response times in the anemometer and gas analyser, and the underestimation of fluxes due to sensor

separation (Moore, 1986; Leuning & Moncrieff, 1990). However, turbulence conditions below a forest canopy are not necessarily representative of those above it (*e.g.*, McCracken, 1993), so the spectral models normally used to correct the data for signal loss resulting from differences in data aquisition by the anemometer and gas analyser (Kaimal *et al.*, 1972; Moore, 1986) were not used here.

Instead, the covariance in spectral density between *w'* and *t'* (the instantaneous departure from the mean temperature, *t*) was compared with that of *w'* and *c'*. An assumption was made that the *w't'* cospectrum for a given time period (*e.g.*, 30 minutes) represented the 'true' below-canopy cospectrum for this site, and that this could be used to correct the *w'c'* co-spectrum. The basis for such an assumption is that *w* and *t* were recorded at very high frequency (21 Hz) and the signal was not subject to errors such as 'smearing' caused by passage through tubing to the gas analyser. As a consequence, they were unlikely to require the corrections that *c* data demand. Comparing *w'c'* and *w't'* cospectra was not straightforward as attenuation in the *c* signal created differences in the normalised covariances between *w't'* and *w'c'*. At the minimum frequency (~0.01 Hz) there is likely to be no (or very little) signal loss with either species, so the covariances could be compared at this point. The fractional difference between the *w'c'* and *w't'* cospectral density at this minimum frequency was used to normalise the *w'c'* cospectrum with respect to the *w't'* cospectrum. The proportional difference between the overall flux signal in *c* and *w* was then calculated according to the difference between the integral under the new [retrieved, 'unattenuated'] *w'c'* cospectrum and that of the *w't'* cospectrum. This correction in signal was then applied in the final flux calculations.

The application of the eddy covariance technique near the forest floor remains experimental, though it has been successful elsewhere (*e.g.*, Baldocchi *et al.*, 1986). To my knowledge this was the first use of eddy covariance as a technique to measure soil CO_2 efflux in a tropical rain forest.

SOIL TEMPERATURE

With the closed chamber method soil temperature at 1cm depth was measured during the measurement of soil CO_2 efflux using a Cu-Cn thermocouple with an amplified output (sensitivity ± 0.2 °C). Soil temperature at 1 cm depth was also logged at other microsites, using a Campbell 21X micrologger (Campbell Scientific, Leicester, UK). The lag between changes in air and soil temperature, and the shaded environment of the forest floor, resulted in no detectable effect of chamber emplacement on soil surface temperature during measurement. In Cameroon the soil temperature profile was also

measured using a 25 cm probe (see Appendix A). The depths measured were litter, 1 cm, 2.5 cm, 5 cm, 10 cm and 25 cm. Four profiles were sampled during the field programme together with an extra profile measured in conjunction with the open chamber system.

SOIL COMPOSITION

Water volume fraction

Soil water volume fraction (WVF) was measured in SRF using a soil capacitance probe from the Institute of Hydrology, UK (IH). The instrument is a hand-held device based on the design of Dean *et al.* (1987) that exploits the high dielectric constant of water compared to that of dry soil (approximately 80 *vs* 4, at frequencies less than 1000 MHz) to detect small differences in soil water content.

The capacitance probe was site-calibrated for the SRF soil using augers designed to prevent compaction of the sampled soil, and gravimetric analysis was made using laboratory scales precise to 0.001g (Salter-AND FX-300, Salter, USA) and a drying-oven (Gallenkamp, UK) at the ODA/FMRP Research Station, Mbalmayo. The instrument was calibrated for soil WVFs between 0.18 and 0.35. Over this span, the response of the probe approximates a straight line (IH, unpublished literature). The regressions between capacitance and WVF were highly significant at 5 cm and 10 cm (see Appendix A for calibration details). Surface moisture levels were measured at both depths in the microsites where soil CO_2 efflux was measured (Table 4.2).

Table 4.2. The number of soil CO_2 efflux and water volume fraction (WVF) measurements obtained on different dates in Cameroon, 1993/4. One 'extra' measurement day was possible in 1993, denoted by day of year (345).

Date (day of year)	CO_2 *efflux*	*WVF at 5cm depth*	*WVF at 10cm depth*
345	33	--	--
52	34	17	17
71	30	31	31
104	57	57	57
135	24	18	18
Totals	178	123	123

Nutrient analysis

Soil samples were obtained from a subset of the soil respiration microsites in SRF. A total of 13 microsites were sampled to 5 cm and 10 cm using a 6 cm diameter auger; an illness prevented the collection of a larger dataset. Immediately after lifting the soil samples, all roots were carefully removed by hand using fine-tipped forceps, and then washed. Fine roots were separated from coarse roots using the criterion of a maximum fine root diameter of 2 mm (Ewel *et al.*, 1987). Dead roots were not removed and were treated as soil organic matter. To ascertain whether or not a root was alive it was twisted or bent and the tissue inspected. All roots and soil samples were oven dried at 70 °C to constant mass. The soil samples were analysed by the laboratory of the International Institute for Tropical Agriculture, in Yaoundé, Cameroon using the Kjeldahl method (Allen, 1974). The root samples were returned to the UK and analysed in Edinburgh using a standard wet digestion (Allen, 1974).

4.3 RESULTS

SOIL TEMPERATURE

The surface temperature rhythms for each vegetation type show an extending hysteresis with respect to the solar zenith in a progession from open dry forest (cerrado) to closed rain forest (Figure 4.1). The cerrado soil reached a maximum temperature of 22 °C at 1500 hours, whilst the rain forest sites attained maximum values of 23 - 24 °C nearer 1600 or 1700 hours. The amplitude of the temperature cycles differed as well: in cerrado, the diurnal temperature range was approximately 7 °C, whilst for rain forest it was 1-2 °C, except during *friagens* in PRF, or stormy weather. Furthermore, soil in the cerrado reached lower minima (~16 °C) than in the rain forests. The profile data from SRF typically showed temperature cycles to be damped and more strongly lagged with increasing depth down to 25 cm where the signal was very weak and daily weather regimes were only just observable (Figure 4.1d).

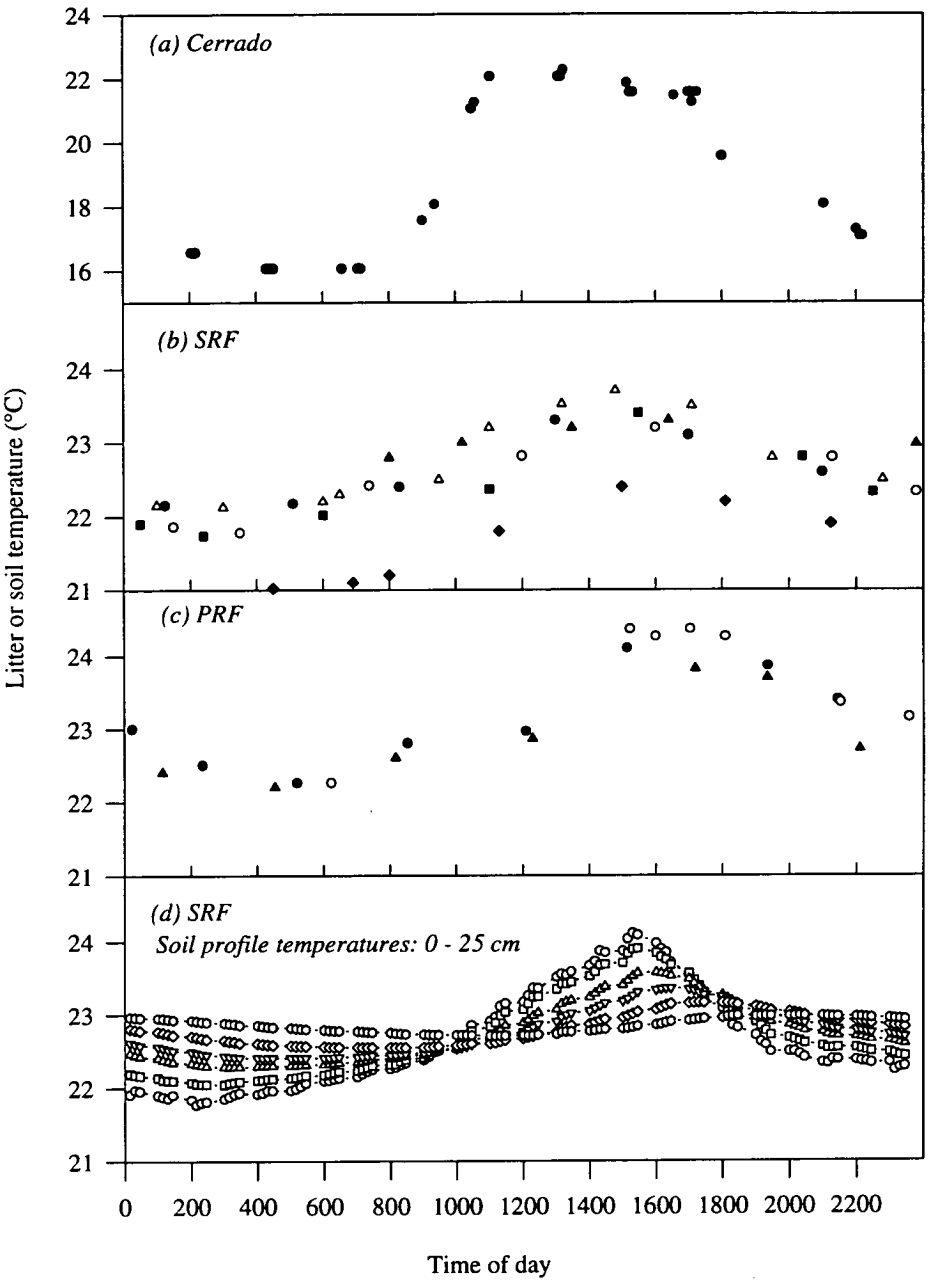

Figures 4.1a-d. Diurnal temperature at 1cm depth for: (a) C, (b) SRF (c) PRF. The different symbols in (a) - (c) represent different microsites. In (d) diurnal cycles are shown for litter and soil at 1cm, 2.5 cm, 5 cm, 10 cm & 25 cm. The time is local time: for PRF and cerrado local time is solar time; for SRF, local time is one hour ahead of solar time.

CLOSED CHAMBER MEASUREMENTS

Mean measured rates of CO_2 emission from soil were higher in rain forest than in cerrado, and higher in PRF than in SRF: PRF mean = 5.51 (± 0.13), n = 42, at 22.8 (± 0.1) °C; SRF mean = 4.60 (± 0.02), n = 178, at 22.5 (± 0.1) °C; C mean = 3.0 (± 0.07), n = 10, at 20.1 (± 0.5) °C, all effluxes in μmol m^{-2} s^{-1} with SE in parentheses Point variability was greatest in SRF (range = 10.5 - 2.6 μmol m^{-2} s^{-1}), and PRF was more variable than C (ranges = 7.1 - 4.0 μmol m^{-2} s^{-1} for PRF *vs* 3.8 - 2.2 μmol m^{-2} s^{-1} for C).

Table 4.2 summarises the CO_2 emissions from the five extra sites visited in SRF. The means and 95% confidence limits for each show that sites 1 - 4 were statistically indistinguishable and quite similar to the main SRF site, whilst the bulldozed site showed significantly lower CO_2 efflux rates and higher soil temperatures. Temperature-corrected data (assuming a Q_{10} of 2.0) grouped the three secondary forest sites as statistically different from the other two (p = 0.01, n = 2). The bulldozed soil was particularly heterogeneous, and appeared to have only a sparse layer of decomposing matter

Table 4.2. Soil temperature (at 1 cm, in °C) and CO_2 efflux rates (in μmol m^{-2} s^{-1}) from five extra sites in Mbalmayo Reserve, Cameroon. The data are not temperature corrected as temperature responses were unknown; 95% confidence intervals for each mean are given in parentheses CO_2 efflux units are. The map site numbers are as in Table 4.1 and Map 2.2.

Map site number / Site	*Temperature*	CO_2 *efflux*	*n*
(1) Secondary forest prepared for plantation	24.4 (0.1)	4.3 (0.6)	6
(2) Mature secondary forest	24.2 (0.2)	5.4 (0.7)	6
(3) Very mature secondary forest	23.6 (0.2)	4.8 (1.1)	6
(4) Fallow field, recently cut	27.3 (1.2)	4.7 (0.3)	6
(5) Bulldozed forest, replanted	30.8 (2.4)	2.4 (1.7)	6

The tests for possible biological or physical sources of measurement bias confirmed that the data from the closed chamber method were satisfactory. Pressure effects on CO_2 efflux rates were small and did not significantly affect measurement: differentials between inside and outside the chamber were not detectable during the short period of emplacement, and data obtained with and without a narrow-bore venting tube were virtually identical (Figure 4.2a). The seven day experiment where a collar was left in the ground confirmed indications from elsewhere (*e.g.*, Anderson *et al.*, 1983) that root severance leads to a gradual reduction in efflux rates (Figure 4.2b), and shading the chamber with a shroud did not affect efflux measurements, presumably because of the low light levels and little green vegetation on the forest floor (data not shown).

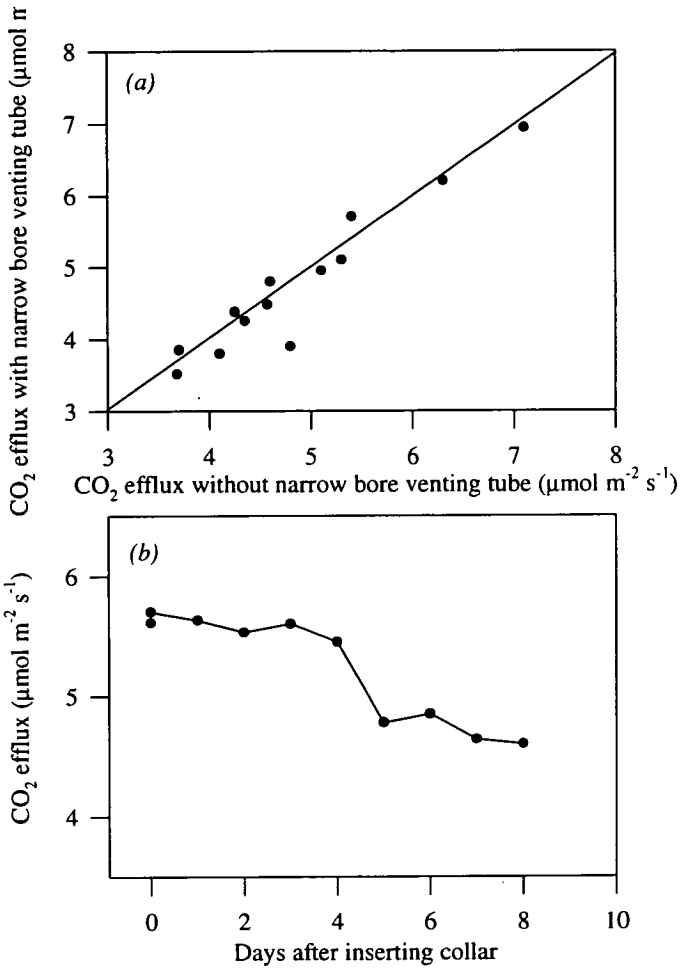

Figures 4.2a&b. In (a), CO_2 efflux from soil with and without a narrow bore vent; the data are not significantly different from a 1:1 relationship ($p < 0.01$). In (b), the medium-term effect of continuous chamber emplacement on soil CO_2 emissions.

Response to soil temperature

The twenty-four hour time series data for individual microsites indicated a strong relationship between temperature and CO_2 efflux. Figure 4.1 shows the diurnal temperature cycles as measured with CO_2 efflux; Figure 4.3 plots the respective efflux values against these same temperatures for each microsite. The efflux at each microsite was explained to a large extent by temperature, yielding r^2 values between 0.62 - 0.95, although inter-microsite variation was large for the rain forest soils. Regression statistics

could not be ascribed to these data as they do not fulfil the criterion of independence. There was no evidence for a diurnal cycle in soil respiration other than through the effect of temperature.

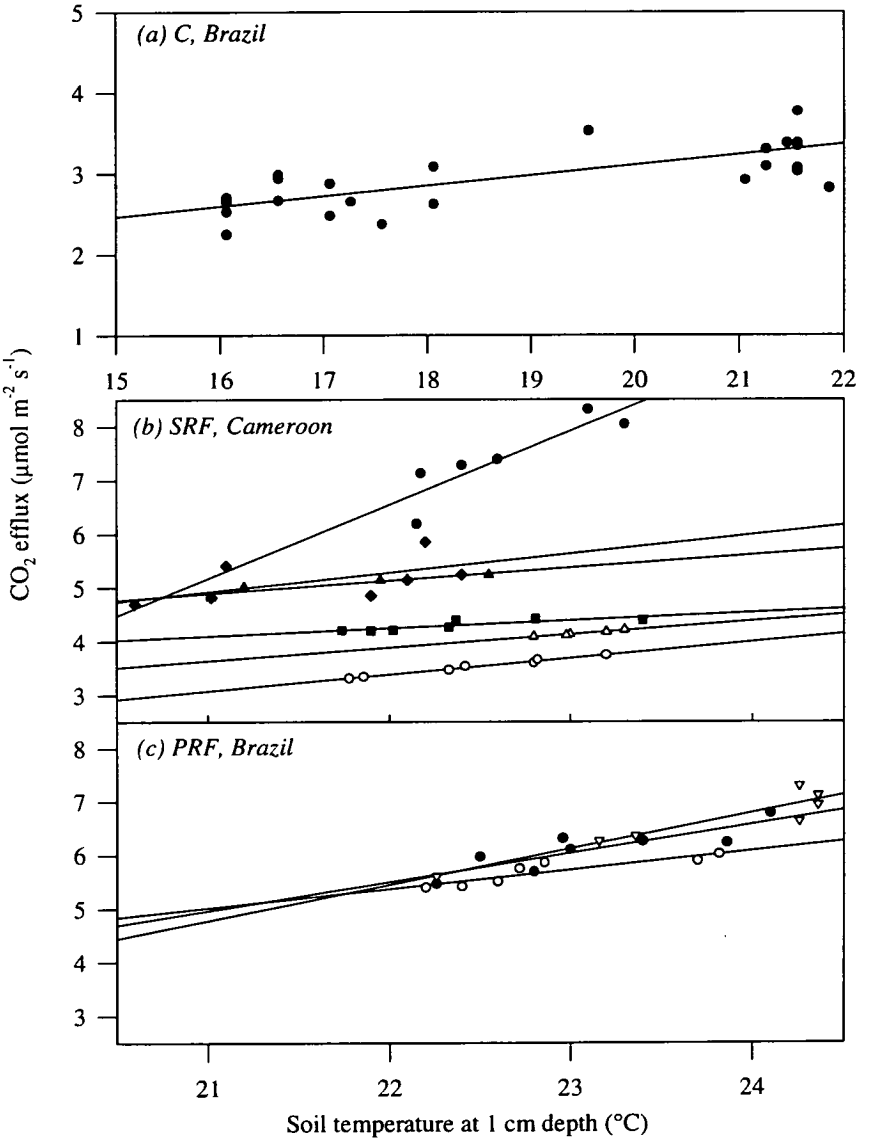

Figures 4.3a-c. Variation in CO_2 efflux with temperature at individual microsites in C, SRF and PRF. The efflux data are, respectively, the same microsites as given in Figure 4.1; different symbols denote different microsites. The regression lines are linear fits through data from individual microsites (*i.e.*, time series data).

The data from all the microsites (n = 42, 178 and 10 for PRF, SRF and C respectively) were fitted to an exponential temperature model, Equation 4.3:

$$R = R_0 \, e^{(kT)} \qquad \text{Equation 4.3i}$$

which can be rearranged to a linear relationship:

$$\ln R = \ln R_0 + kT \qquad \text{Equation 4.3ii}$$

where R = efflux in μmol CO_2 m^{-2} s^{-1} and T = temperature in °C. The Q_{10} value can be obtained from $\ln Q_{10} = 10k$.

The logarithmic function accounted for the variation in point emission rates to give highly significant regressions. Although the r^2 values were lower than 0.5, the fitted k values for the main datasets were similar to those obtained for individual microsites (Figures 4.3 & 4.4; Table 4.3). Arrhenius-type models (*e.g.*, Bridgham & Richardson, 1992; Lloyd & Taylor, 1994) were also applied to the data, but did not give improved fits, nor were the residuals spread more evenly about the predicted value (Figure 4.5). The temperature response functions in Table 4.3 were replotted on a linear scale in Figure 4.6 with the standard errors of prediction drawn in for SRF and PRF (Sokal & Rohlf, 1981). They emphasise the higher respiration rates in PRF than in SRF or C, and the larger Q_{10} value at 2.3 for PRF *vs* 1.9 for SRF and 1.6 for C. The R_0 and Q_{10} values were lowest in C.

Table 4.3. The regression data obtained from fitting the data in Figure 4.4 to Equation 4.3ii. The mean Q_{10} value for individual microsites from Figure 4.3 are also indicated, with the sample size appended; subscripts dictate the origin of Q_{10} values. The $^*Q_{10}$ value is for five of six microsites, as one site gave a very high Q_{10} of 7.5 (see Figure 4.3); including this microsite, mean Q_{10} = 2.4. Errors in parentheses are 95% confidence limits.

Forest site	R_o	k	p	$Q_{10Fig4.4}$	r^2	n	$Q_{10Fig4.3}$: n
C	1.32 (0.1)	0.044 (0.01)	0.08	1.6	0.33	10	1.6 : 1
SRF	1.09 (0.4)	0.063 (0.02)	0.001	1.9	0.06	178	1.9*: 5
PRF	0.81 (0.5)	0.083 (0.02)	0.003	2.3	0.21	42	2.3 : 3
PRF + Sept 1992	0.34 (0.5)	0.1 (0.02)	0.001	2.7	0.42	51	- -

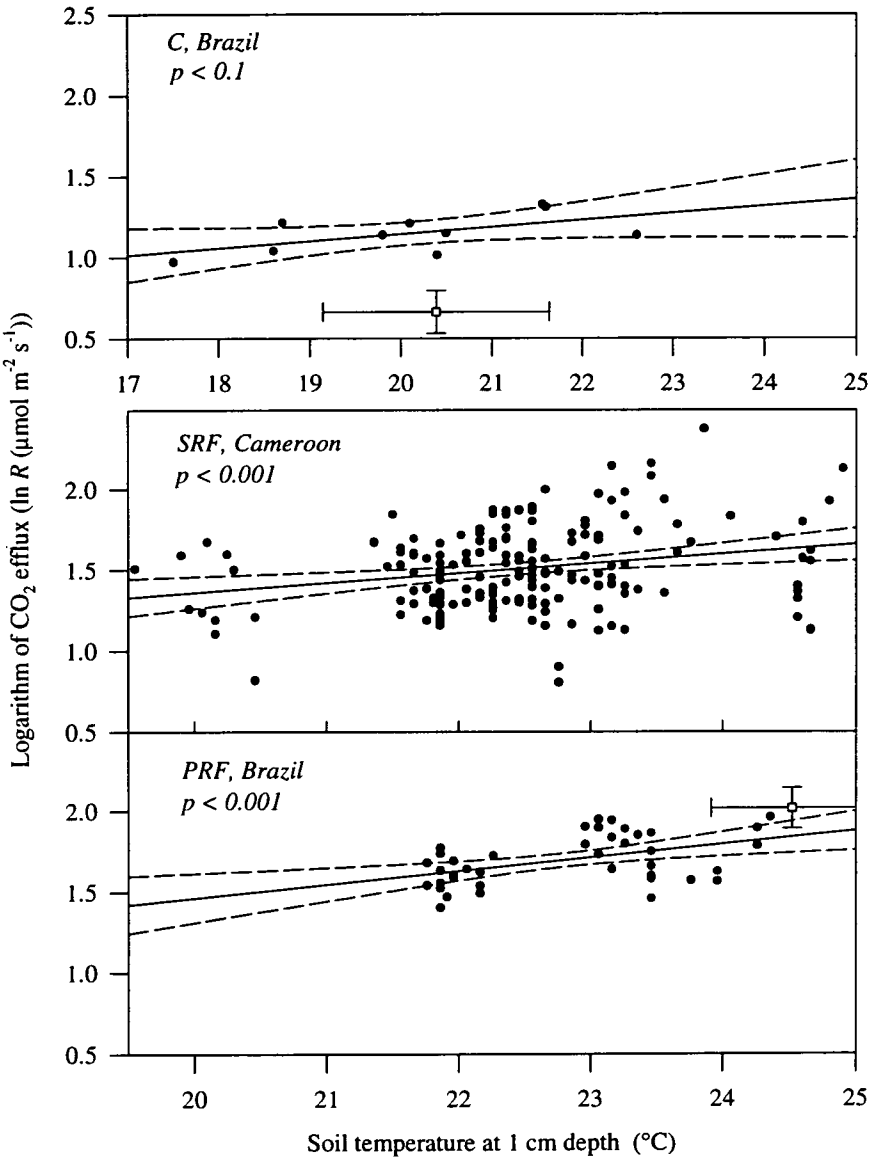

Figures 4.4a-c. Soil CO_2 efflux rates (spots) for all microsites measured in C, SRF and PRF, plotted as ln (R) *vs* temperature. The regression results are given in Table 4.3; confidence limits are 95%. The open squares in (a) and (c) are mean values, with 95% c.l. for dry season data from cerrado (July 1993; n = 8) and PRF (September 1992, n = 9, J. Grace, unpublished).

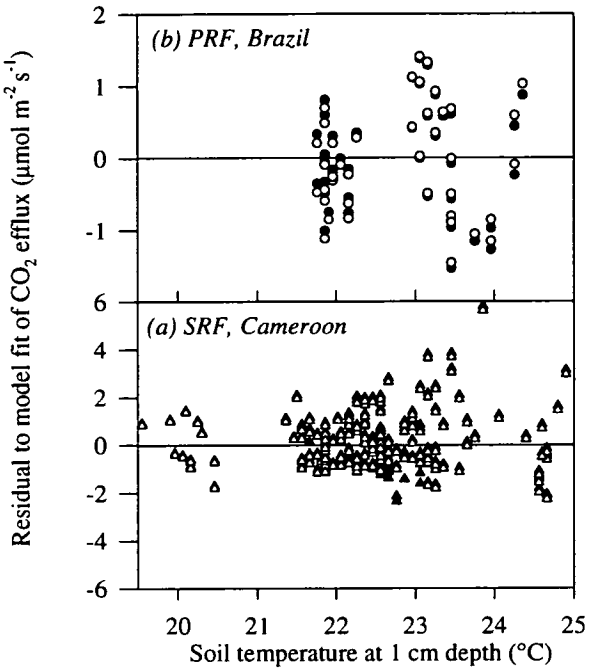

Figures 4.5 a&b. Residual plots for exponential and Arrhenius-type models fitted to data from SRF and PRF. The closed symbols respresent the exponential model and the open symbols the Arrhenius-type model.

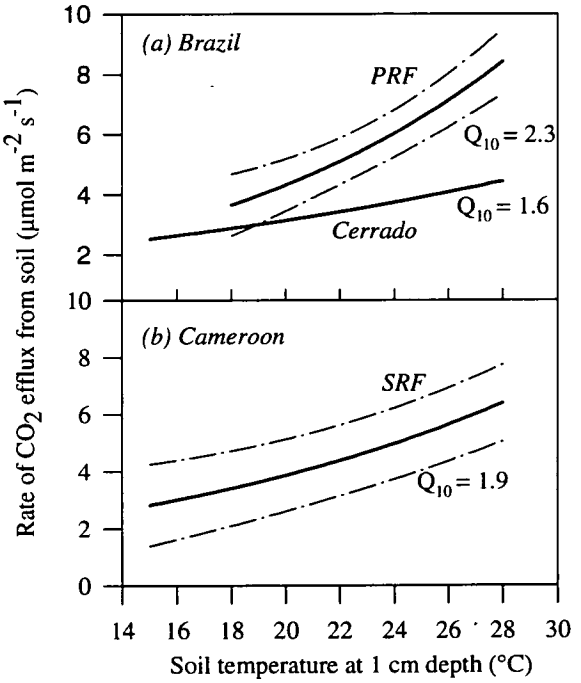

Figures 4.6a&b. Temperature response functions for CO_2 efflux in soil in C, SRF and PRF. The functions are fitted exponential models with the standard error of prediction intervals shown for SRF and PRF (Sokal & Rohlf, 1981).

Temporal and spatial representation of soil CO_2 emissions

Figure 4.4 also shows data obtained in C and PRF during a different time of year from the main dataset, the dry season (July 1993 for C, this work; and September 1992 for PRF (J. Grace, unpublished). The data were limited (C, n = 8; PRF, n= 9) but indicated a limitation in C during the dry season, whilst in PRF there was no apparent seasonality in soil effluxes: inclusion of the September 1992 data from PRF did not significantly change the regression obtained for the following wet season (Table 4.3). For SRF it was possible to get a better sample of temporal variation in respiration rates and a single factor analysis of variance revealed no significant between-date differences in fluxes from December 1993 to May 1994 (p = 0.8; n = 5).

Spatial heterogeneity was assessed in SRF via a single factor analysis of variance on temperature-corrected fluxes at different distances (0 to 500 m) from the tower: significant variance by distance was not observed (p = 0.6; n = 5; see Figure 4.7). The data from both SRF and PRF were further analysed by comparison with a normal distribution of soil CO_2 effluxes defined according to the mean and variance of each sample (Figures 8a&b, main plots). This was represented as the raw fluxes plotted against their expected probability of measurement, given in percentiles. Inset into both graphs is the same normal distribution plotted against expected frequency, but here the data (columns) were normalised to the mean observed soil temperature. In the main graph for PRF, the lack of deviation in observed fluxes from the expected distribution (the straight line) indicated a robust estimate of overall soil CO_2 emissions. For SRF (Figure 4.8b), the inset graph suggested some skew in the temperature-corrected data. This bias was a sampling problem also observed in the main graph, and resulted from the more heterogeneous soil at this site

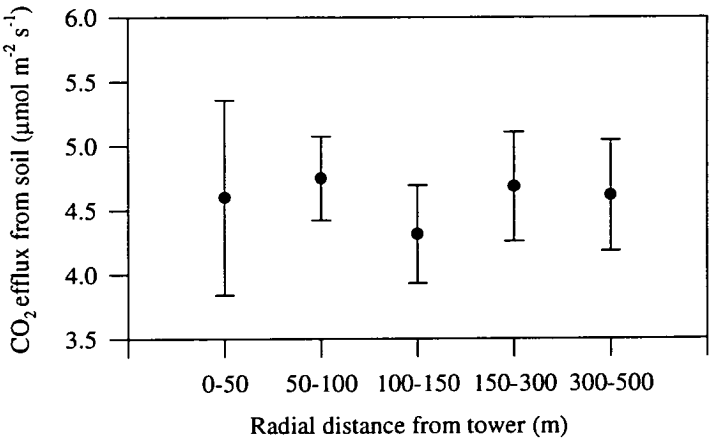

Figure 4.7. The variation in soil CO_2 efflux with distance from tower in SRF. The error bars are 95% confidence intervals about the mean.

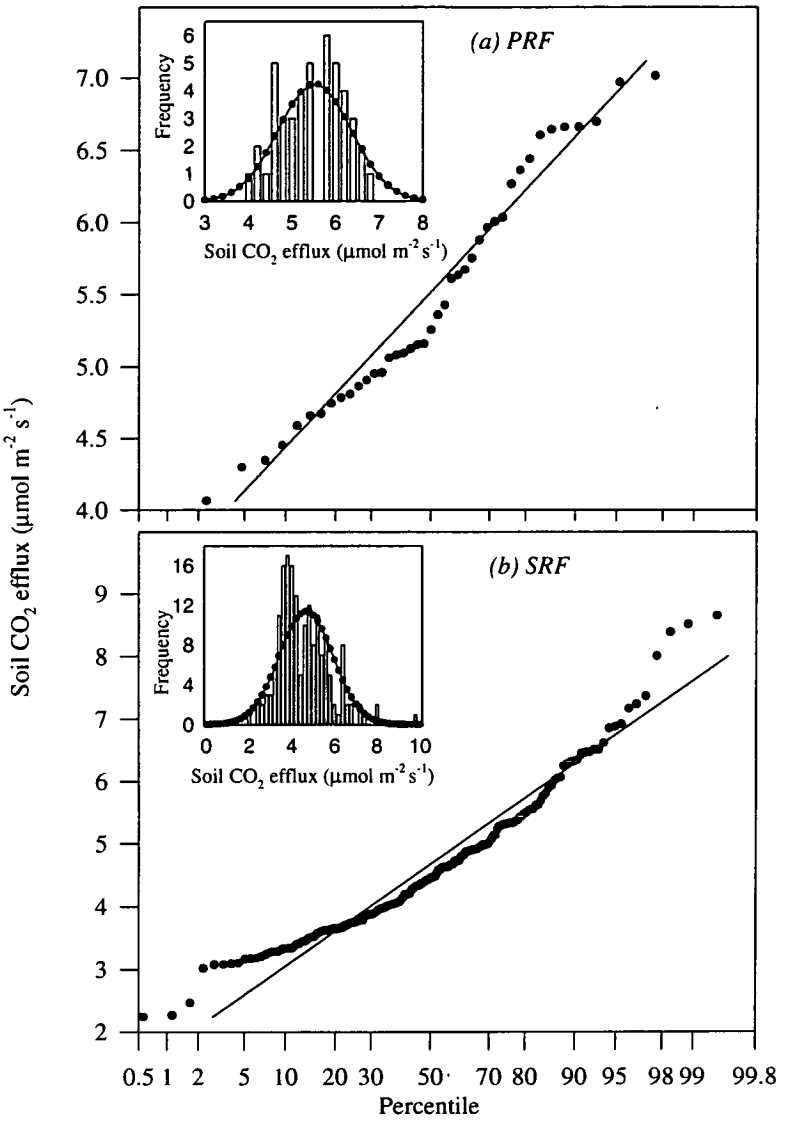

Figures 4.8a&b. Main graphs: CO_2 efflux plotted as percentiles of observed and expected distributions. Expected values are represented by the straight lines defined according to σ and mean of samples. The inset graphs are frequency distributions of temperature-corrected effluxes, with the normal distribution calculated from the sample σ and mean.

Response to soil moisture

The measurements from Brazil in C suggested that moisture limitation in respiration occurred during the dry season, but this did not happen in PRF (Figure 4.4). The data from SRF showed the surface 5 cm and 10 cm of the forest floor to become 15 - 30% wetter from February to May 1994, but the CO_2 efflux rates did not vary significantly over the same period (Figure 4.9). The storage of water in the soil profile was measured for both SRF and PRF (Hodnett *et al.*, 1996; S. Boyle, unpublished): it varied from 560 - 660 mm in SRF and 585 - 720 mm in PRF during the respective periods of fieldwork. The profile data from SRF correlated strongly with surface WVF for the same period (Figure 4.10). Making a crude assumption that water storage in the SRF soil profile affected CO_2 efflux rates in a similar way to the manner in which they were determined in PRF, the data further support the hypothesis that respiration was not moisture-limited in either rain forest.

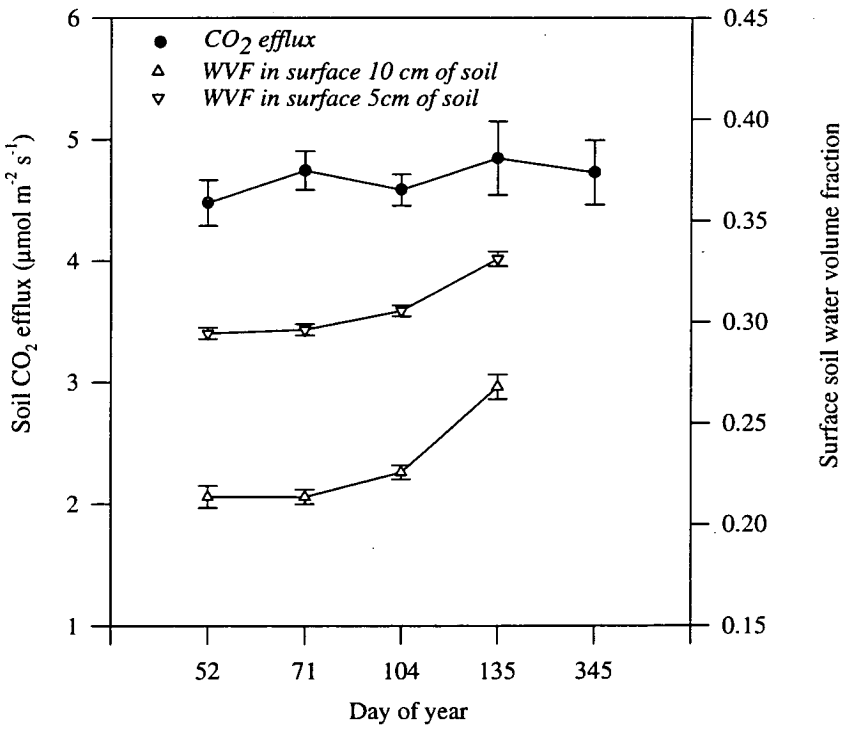

Figure 4.9. Water volume fraction in the surface 5 cm and 10 cm of the SRF soil and mean measured CO_2 efflux (±S.E.), normalised to the mean measured temperature for each period (21 - 23 °C), using the fitted R_0 in Equation 4.3ii. Note the non-linear scale for time.

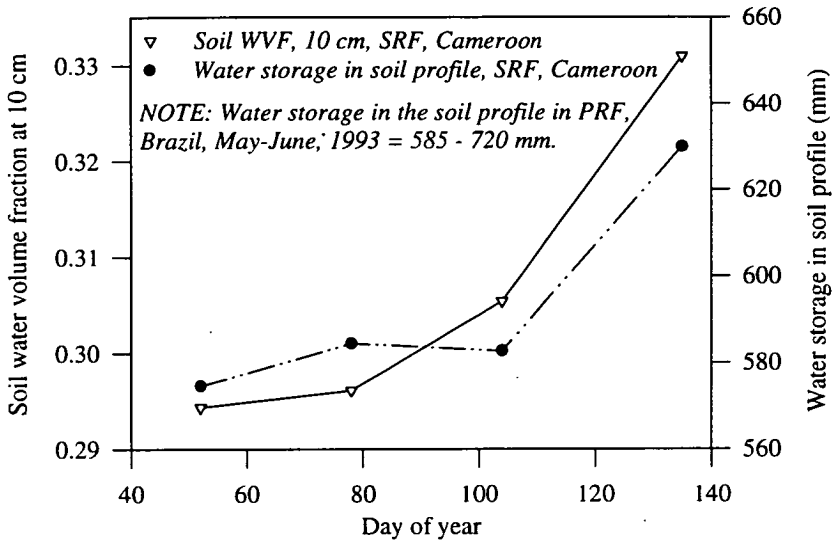

Figure 4.10. Soil surface (10 cm) and soil profile moisture levels in SRF, Cameroon, from February to May 1994. The soil profile storage for PRF during May - June 1993 is also shown in the key, for comparison. The spots represent profile storage data. Sources for soil profile water storage data: S. Boyle, *personal communication* (Cameroon) and Hodnett *et al.*, 1996 (Brazil).

Soil nutrients

In SRF, soil nitrogen concentrations ranged between 0.14 - 0.17 % dry mass and carbon concentrations between 1.6 - 2 % dry mass, the concentrations of both were higher in the top 5 cm. The CO_2 efflux rates obtained from each microsite correlated well with soil chemical composition. A non-linear regression model was fitted to these data (Equation 4.4), treating the carbon and nitrogen components as linear terms and the temperature component as an exponential, according to Table 4.3:

$$R = a[1.09\, e^{(0.063T)}] + b[N] + c[C] + d \qquad \text{Equation 4.4}$$

where R is in μmol m^{-2} s^{-1}, [N] and [C] are nutrient concentrations, and T is temperature in °C.

Despite the small size of the dataset an r^2 value of 0.82 in the top 10 cm and 0.72 in the top 5 cm was obtained (Figure 4.11; Table 4.5). There was no strong bias in the residuals for the overall model and CO_2 effluxes were predicted well across a large range of values (3.5 - 9.5 μmol CO_2 m^{-2} s^{-1}). However, carbon was the only significant variable in both 0 - 5 cm and 0 - 10 cm layers (Table 4.4b).

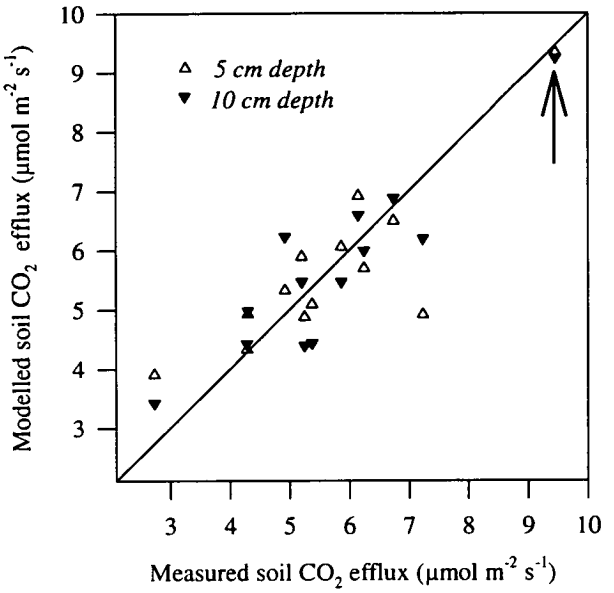

Figure 4.11. Measured *vs* modelled soil CO_2 efflux in SRF, Cameroon. A multiple regression of the form in Equation 4.4 was used to model the data. The regression statistics are given in Table 4.4. The arrow marks a microsite where the C:N ratio was 20 (see text).

Table 4.4a. Mean soil organic carbon and nitrogen concentrations (% by mass), SRF, Cameroon. 95% confidence limits are in parentheses.

Sample depth (cm)	*Organic carbon*	*Total nitrogen*	*n*
5	2.03 (± 0.39)	0.17 (± 0.02)	13
10	1.62 (± 0.23)	0.14 (± 0.02)	13

Table 4.4b. Regression results for the data in Figure 4.11 after fitting to Equation 4.4. The values in parentheses after each coefficient give the level of significance of each variable in the regression (*p*-value).

Depth	r^2	*p*	*a (p)*	*b (p)*	*c (p)*	*d (p)*	*n*
5 cm	0.72	0.007	-2.2 (0.3)	6.0 (0.5)	1.9 (0.01)	10.7 (0.2)	13
10 cm	0.82	0.001	-2.1 (0.3)	-2.9 (0.8)	3.95 (0.006)	9.3 (0.3)	13

Dry root mass in the surface layers was 3.9 (±0.6) t ha^{-1} and 8.9 (±1.7) t ha^{-1} at 0 - 5 cm and 0 - 10 cm respectively (data are means of 13 samples, with 95% confidence limits); fine roots (< 2mm) and coarse roots (>2 mm) constituted approximately half each of this total. Respiration was not significantly related to root density or root phosphorus concentration in either layer, but it was correlated with root nitrogen and potassium concentration for the 0 - 10 cm layer (Table 4.5).

Table 4.5. Root nitrogen, phosphorus and potassium concentrations in SRF, with 95% confidence limits in parentheses. The regression coefficients are given for the equation: $R = a$ [X] + b, where R is CO_2 efflux in μmol m^{-2} s^{-1} and [X] is concentration at 10 cm of root nitrogen or potassium in g m^{-2}; the coefficients, a and b have their p-values in parentheses after them. The regressions with root P were non-significant. The root data were obtained from the same microsites as the soil nutrient data.

Element	*g m^{-2} at 5 cm*	*g m^{-2} at 10 cm*	*p - value*	*a*	*b*	*n*
Nitrogen	5.49 (1.7)	10.29 (4.34)	0.1	0.097 (0.1)	4.6 (<0.001)	13
Phosphorus	0.02 (0.01)	0.06 (0.03)	--	--	--	13
Potassium	43.36 (8.9)	82.75 (31.5)	0.04	0.016 (0.04)	4.4 (<0.001)	13

OPEN CHAMBER MEASUREMENTS

Open chamber measurement was possible only in SRF. Figure 4.12 shows soil temperature (at 1 cm and 10 cm depth), with water vapour (H_20) and CO_2 fluxes from one microsite, logged from April 30th to May 5th, 1994. Rainfall events are shown as downward arrows. For two days prior to the first storm, both gaseous scalars showed diurnal traces with larger fluxes during the day than during the night. Evolution of CO_2 followed the soil temperature cycle with a lag of 15 and 120 minutes for soil temperature at 1 cm and 10 cm respectively, until it started to rain. At this point, efflux rates in the chamber increased dramatically, whilst soil temperature dropped. After the rain, the reverse happened, with the CO_2 efflux subsequently responding to temperature again, but at a rate below the previous levels. Notwithstanding further precipitation events, there was an apparent decrease in efflux over the five day period; a concurrent reduction in soil temperature at both depths could also be observed.

Data were used from before the first rainfall event to derive the temperature response of CO_2 and water vapour fluxes; the responses were a little noisy, reflecting the effects of static pressure fluctuations at the chamber inlet, but a there was a strong relationship (for CO_2, $R_0 = 0.98$; $k = 0.07$ [$Q_{10} = 2.2$]; $r^2 = 0.60$). The mean efflux rate was 5.8 μmol m^{-2} s^{-1}; this was higher than the mean rate for the rest of the SRF, but the temperature response for CO_2 efflux was close to that obtained using the closed chamber method ($k = 0.063$).

Soil temperature was logged from litter level down to 25 cm. After removing the lags in temperature at different depths, CO_2 efflux - soil temperature responses were determined for each level. The r^2 value from each regression was plotted against depth and the strongest relationship with temperature found at 10 cm (though only 10% more of the variation was explained by temperature variation at 10

cm than at 1 cm). Soil temperature at 25 cm explained as much as 65% of the variation in surface effluxes, indicating that an important 'source' of CO_2 production extended to at least this depth.

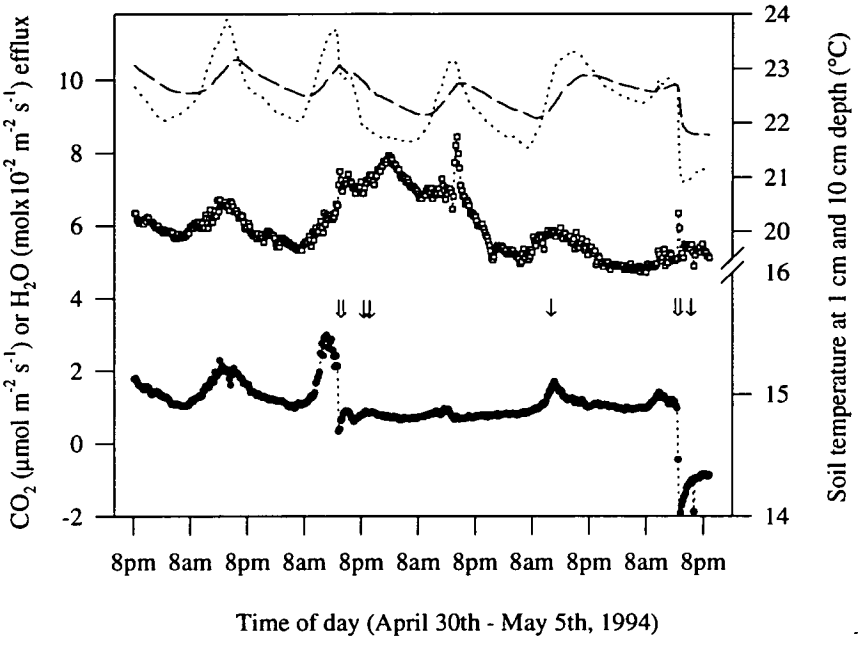

Figure 4.12. Open chamber system CO_2 and H_2O flux data for April 30th - May 5th, 1994, SRF, Cameroon. Also plotted on the graph are soil temperatures at 5 cm and 10 cm, and rainfall. **Key to graph:** CO_2 efflux:▪; H_2O flux: • ; Soil temperature at 1 cm: ···· ; at 10 cm: — ; Rainfall: downward arrows.

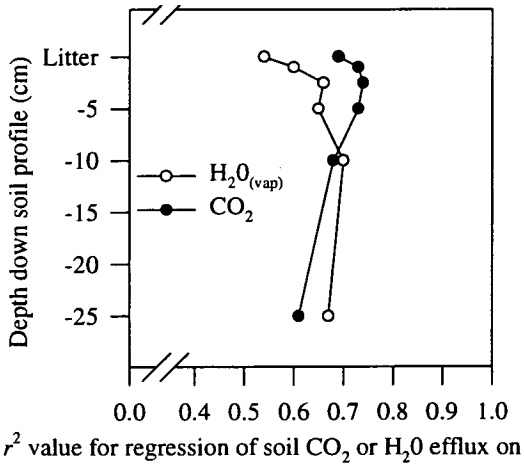

Figure 4.13. r^2 values for soil H_20 / CO_2 efflux - temperature regressions for temperature down the soil profile from litter to 25 cm. The data are from the open chamber system, SRF, Cameroon.

EDDY COVARIANCE MEASUREMENTS

Figures 4.14a and b show typical variance spectra for *w* (vertical component of wind speed) and *c* (CO_2 concentration), and covariance spectra for *w't'* and *w'c'*, with spectral cutoff frequencies occurring at approximately 1 - 2 Hz. These spectra were consistent from half hour to half hour, but distinct from the 'ideal' above-canopy spectra of Kaimal *et al.* (1972). However, the overall patterns of the *w'c'* and *w't'* cospectra were similar in shape, suggesting that the same sources and sinks were common to both scalars and this provided confidence in the use of the *w't'* cospectrum to retrieve the true signal in the attenuated *w'c'* cospectrum. The *w'c'* signal was found to be attenuated by 6 - 12%, with the corrections being most important in the frequency range 0.05 - 0.1 Hz (Figures 4.14b-d).

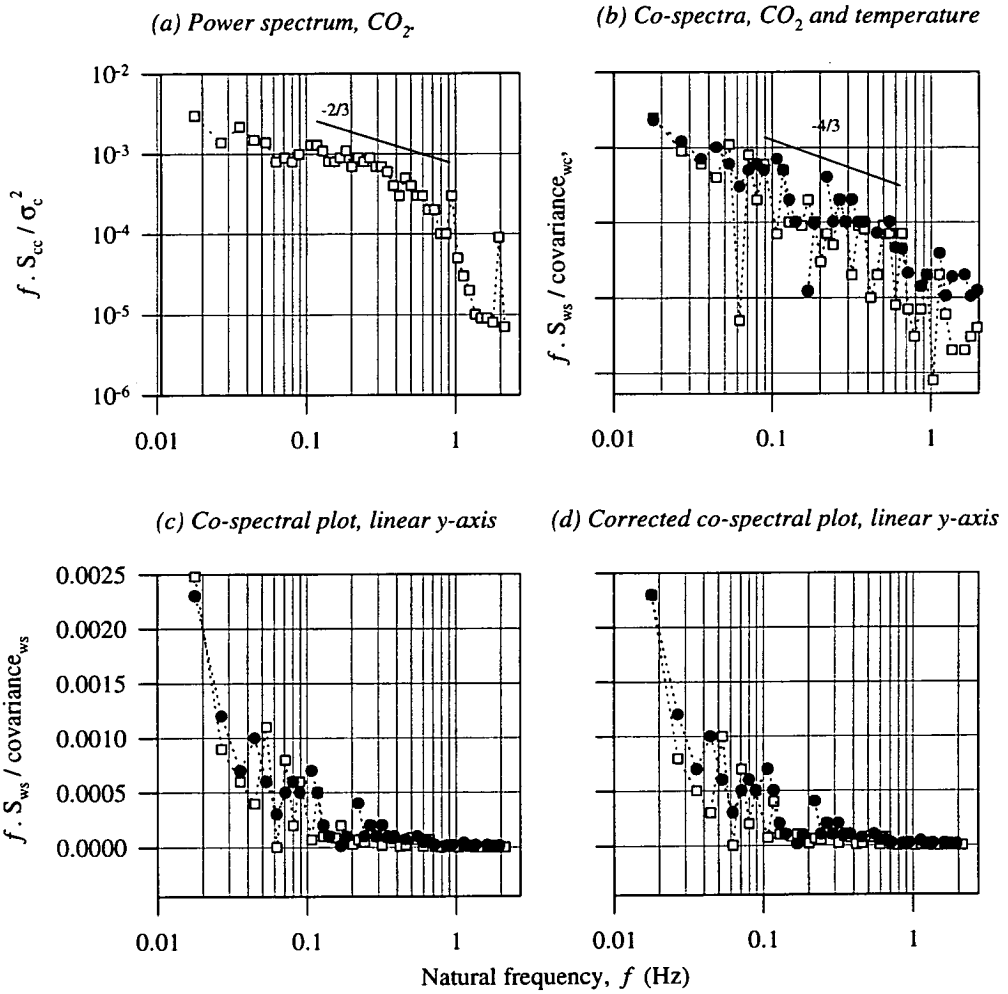

Figures 4.14a-d. Power and cospectral plots for CO_2 flux and temperature measured at 1.5 m, SRF, Cameroon. Figures 4.15a&b show power- and cospectral plots. Figures 4.15c&d show the correction applied to the *w'c'* cospectra (see text). The subscript 's' in (b) and (c) refers to either scalar, CO_2 or temperature. **Key to graphs:** open squares: CO_2; spots: temperature.

Figure 4.15a shows 30 minute CO_2 fluxes with chamber-derived model CO_2 effluxes for the same period (chamber *measurements* were not made between 7th and 9th May, because of an illness). The chamber-derived model was driven from above-canopy dry-bulb temperature measurements using the canopy-soil temperature algorithm described in Chapter 8 (page 143) and the fitted temperature response equation (Equation 4.3; Table 4.3). A diurnal pattern was not observed in the eddy covariance measurments, but the averaged efflux rate for the 48 hour measurement period was very similar to that obtained from the chamber-derived model (Table 4.6). As an additional check of this estimate, a further constraint was imposed upon the selection of data by defining 'steady-state conditions' as those half hour periods when 95% of the variation in CO_2 concentration was less than 5% of the mean CO_2 concentration. Most of the data that were removed were from the hours around dusk (1700 - 1900 hrs), as a result of low turbulence intensities in *w*. The mean efflux for this new dataset was the same as the mean efflux calculated from 30 min or 5 min intervals (4.3 $\mu molm^{-2} s^{-1}$).

The noise in the the 30 minute flux data may have resulted from limitations in the instruments, but it also reflected a turbulence regime below the canopy that was dominated by intermittent gusts penetrating through the whole vertical profile of the canopy (*e.g.*, Denmead & Bradley, 1985). The gusts carry momentum and scalars with them. Depending on the rhythmic frequency of these large eddies, the resulting flux calculations could have been big or small. These hypothesised low frequency eddies were tracked by shortening the interval period for flux calculation from 30 minutes to 10, 5, 3 and 1 minute intervals, and the data plotted against σ_w, the square root of the variance in *w*. The five minute fluxes were correlated more closely to σ_w than any other time interval, indicating that this was the dominant frequency of important turbulence events at 1.5 m above the ground (Figures 4.15b&c).

Table 4.6. Soil CO_2 effluxes measured using eddy covariance, in SRF. A comparison of the average upward flux rate of CO_2 at a height of 1.5 m with the soil CO_2 efflux rate for the same 48 hour period obtained using a chamber-derived model driven from soil temperature estimates. Three eddy covariance estimates are shown: (a) 30 minute fluxes; (b) 5 minute fluxes and (c) 30 minute fluxes using data selected for steady-state conditions (see paragraph above). Errors in parentheses are 95% confidence limits of the mean efflux for 48 hrs (30 minute estimates for the model data, 5 and 30 minute fluxes for eddy covariance data). All units are in $\mu mol\ m^{-2} s^{-1}$.

Estimate type	*Average Efflux Rate*
Chamber-derived model	4.5 (0.03)
a) 30 minute fluxes	4.3 (0.4)
b) 5 minute fluxes	4.3 (0.3)
c) Selected 30 minute fluxes	4.3 (0.4)

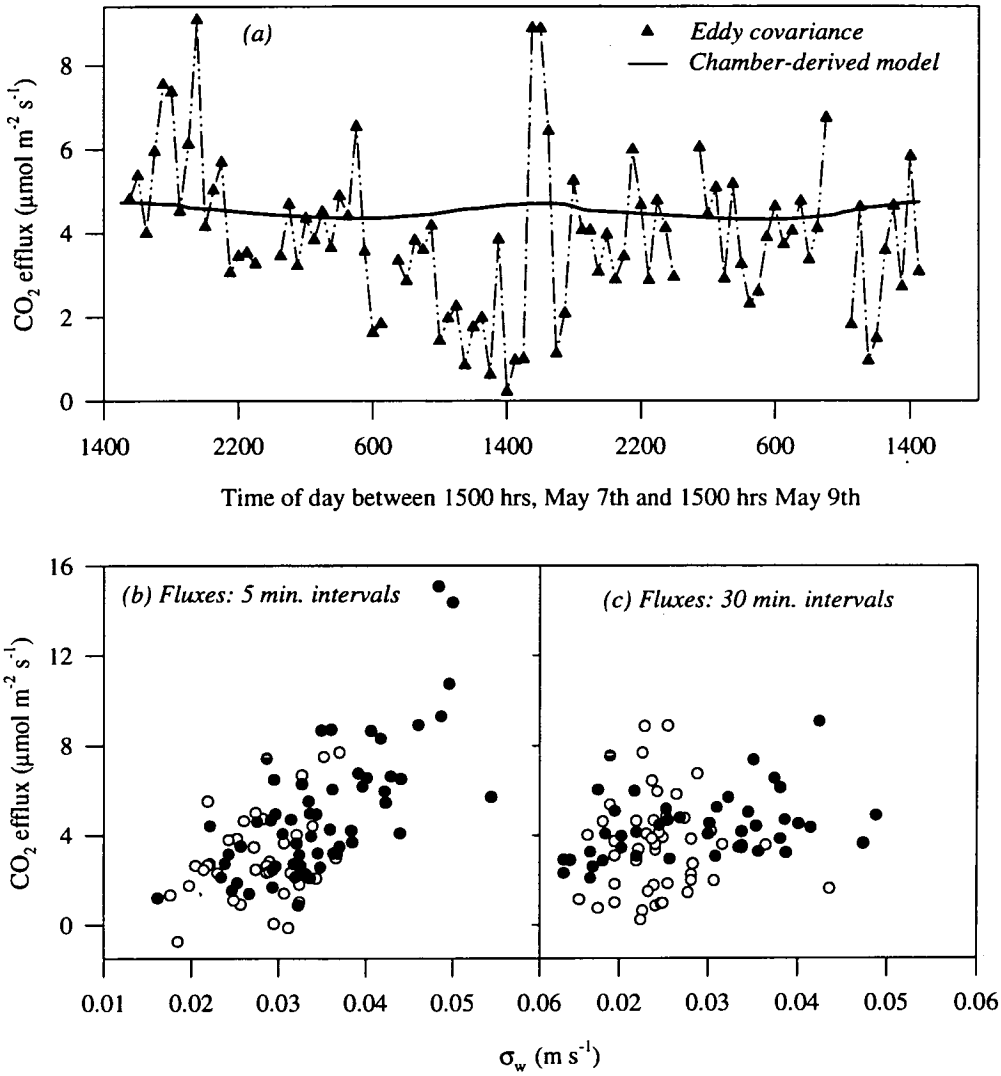

Figures 4.15a-c. In (a) is shown a time series plot of the eddy covariance data at 1.5 m, with the chamber-derived model. The measurement dates were 7th - 9th May 1994, SRF, Cameroon. In (b) and (c) the relationship between σ_w and CO_2 efflux: the closed symbols represent night-time fluxes (5 min fluxes: 1900 - 0100 hrs, day 127-128) and the open symbols daytime fluxes (5 min fluxes: 0900 - 1200, day 128). The 30 minute fluxes are for the full 48 hour measurement period.

4.4 DISCUSSION

SOIL TEMPERATURE

For all soils the maximum temperature occurred after the solar zenith, but in C this happened at 1400 hrs, whilst in SRF and PRF it took place nearer 1600 - 1700 hrs (Figure 4.1). This probably reflects the differing heat capacities of the three canopy types, which ranged from open dry forest to disturbed and undisturbed closed moist forest. The extra sites visited in Cameroon showed analogous characteristics where, during the day, field soils were up to 7 °C warmer than forest soils, a difference of three times the diurnal amplitude at the main SRF site (Table 4.2).

SIOL CO_2 EFFLUXESS

Overall differences among the forests

The CO_2 efflux rates obtained for C were consistent with previous studies for physiognomically similar vegetation types (Schulze, 1967; Raich & Schlesinger, 1992). Secondary rain forest data from the tropics are rare, and secondary forests are highly variable, although Raich (1983) reports similar values for a logged wet forest area on the Atlantic Slope in Costa Rica (4.4 *vs* 4.6 μmol m^{-2} s^{-1} for Cameroon), though the temperature reported by Raich was a little higher than in SRF (23 - 27 °C *vs* 22.5 °C in SRF). The rates for PRF were higher than some other estimates for Amazonian forest soils (*e.g.*, Medina *et al.*, 1980; Keller, 1986) but are similar to those of Fan *et al.* (1990), and assuming a soil temperature of 20 °C, those of Wofsy *et al.* (1988) for the Central Amazonian site, Reserva Ducke, near Manaus (4.5 *vs* 4.2 μmol m^{-2} s^{-1}). It is likely that the diversity of soil types across Amazonia (Jordan, 1985) will lead to a corresponding range of respiration rates in these soils. Metabolic activity in soil is maintained by above- and below-ground organic matter inputs. In the absence of such data, biomass and leaf area differences between the forest types can be used as surrogates to explain the observed variation, though given the low biomass in SRF (Chapter 3), the high efflux rate (4.5 μmol m^{-2} s^{-1}) may have reflected continued decomposition of below-ground biomass that was live prior to the harvest in 1989.

The variation among the extra sites in Cameroon was low within the group of secondary forests in Table 4.2. The fallow field showed higher rates of respiration than expected, perhaps reflecting the

recent cutting of the vegetation. Most striking was the bulldozed plot, where pre-planting treatment appeared to have removed most of the organic layer in the soil, leaving a very patchy and resource-poor environment. Consequently root and microbial respiration was low, despite higher temperatures.

Response to soil temperature

The well-defined temperature response for individual microsites (Figure 4.3; closed chamber method) contrasted with the apparent variation in this relationship observed with spot measurements from many microsites (Figure 4.4). The rain forests showed greater variation than did cerrado, suggesting more heterogeneous soil, but also reflecting the effect of temperature response on quantitatively higher effluxes. The higher variance in SRF data reflected disturbance in that forest; point variation in CO_2 emissions from soils is a common feature (Schlesinger, 1977; Singh & Gupta, 1977). The individual microsite data underlined the importance of temperature in determining relative changes in efflux rates. But the variability among microsites in Figure 4.3 also revealed differences in two features of this response: the intercept and slope (R_0 and k in Equation 4.1); these differences were averaged in the regressions in Figure 4.4.

It was desirable to determine whether an adequate sample of the natural variation in R, R_0 and k existed in the data. The estimate of R was tested in Figure 4.8 where observed data were compared with the experimentally determined Gaussian distribution for each sample. Overall the sample sizes were adequate, and rates closely followed a Gaussian distribution, though heterogeneity in SRF was visible. After correcting for temperature, inter-microsite differences in R_0 could be inspected (inset graphs, Figure 4.8). If soil chemical composition data had also been available to normalise all the observed microsite fluxes, a closer fit to the expected normal distribution would have been expected (*cf.* Figure 4.11). It was more difficult to directly assess variation in k, though it is reasonable to assume, other factors being equal, that the same features of the soil determining R_0 also determine k. Supporting this, the average k for individual microsites were close to those for the forest-wide datasets (Table 4.3).

The open chamber data agreed reasonably well with the closed chamber estimates for SRF ($R_0 = 0.98$, $k = 0.08$), though here, k was likely to be more reliable than R_0 as the chamber was not specifically designed for open path analysis. Two other features were significant. First, the data describe the effects of rainfall on CO_2 fluxes from soil: although the chamber created unnatural conditions by protecting the enclosed soil from rain, this artefact made clear the displacement of CO_2 from pores in the soil during and just after precipitation. It is possible that eddy covariance measurements could

detect this phenomenon. However, carbon dioxide in the soil would also go into solution during rain, and depending on soil pH and temperature, might be leached from the system. Estimates of dissolved CO_2 leached from forest ecosystems are rare, though Schlesinger & Melack (1981) suggest that 8.51 gC m^{-2} [of watershed] yr^{-1} flow out of the Amazon Basin.

Secondly, continuous data provide a means of remotely locating the primary temperature-sensitive source of CO_2 in the soil. Figure 4.13 implies that the top 10 cm, especially below 5 cm, was the site of maximum CO_2 production in the soil profile. Soil and litter may be drier at the surface, whilst decomposing matter may be most densely meshed between 5 and 10 cm, thus creating an environment where the greatest surface area of particulate metabolic substrate is present in favourable conditions of moisture and oxygen availability (White, 1987; Sorensen, 1981). A number of studies support a contention that the surface layer of tropical rain forest soil produces the greater proportion of total soil CO_2 (*e.g.*, Medina *et al.*, 1980; Luizao, 1987). However, although fine root density is highest near the surface (Cavelier, 1992), significant root mass (and therefore also root litter production) is known to exist deeper in SRF-type soils (Nepstad *et al.*, 1994), and what is seen in these data could merely represent the uppermost fraction of total soil CO_2 production, that changes with diurnal temperature.

The proportion of soil CO_2 production that responds to daily temperature fluctuations must be large in order to explain the observed termperature responses. By assuming that the temperature-varying fraction of soil has an efflux rate with a specific Q_{10}, it is possible to investigate what proportion of the original R_0 value (in Equation 4.3) is required to increase R, as observed for SRF, where a temperature change from 20 - 22 °C results in an increase from 3.9 to 4.4 μmol m^{-2} s^{-1} (Figure 4.6). Table 4.7 quantifies this approach for SRF using assumed Q_{10} values from 1.9 - 3.0: for an assumed Q_{10} of 2.0 (a realistic estimate of the 'pure' physiology (Amthor, 1989), 87% of total production responds to temperature, whilst 13% appears to be insulated from diurnal temperature cycles. The analysis supports the notion that the primary site of CO_2 production is near the surface, but is clearly simplified - without more data only limited account can be taken of the soil profile.

Table 4.7. Proportion of total soil CO_2 efflux that responds to daily temperature fluctuations assuming different Q_{10} values for this labile component and using the observed temperature response of soil CO_2 efflux for SRF. The Q_{10} range 1.9 - 3.0 is within that quoted by Singh & Gupta (1977).

Assumed Q_{10}	*R_o*	*Temp-labile fraction*	*Deep CO_2 fraction*
1.9 (observed)	1.09	1	0
2.0	0.95	0.87	0.13
2.5	0.58	0.53	0.47
3.0	0.39	0.36	0.64

Response to soil moisture

Whilst soil moisture is crucial to the prediction of soil efflux rates in many environments (Edwards, 1975; Cowing & McLean, 1982; Orchard & Cook, 1983; Norman *et al.*, 1992) it may not be necessary for rain forest (Figures 4.9 & 4.10). Above and below certain limits, soil moisture is thought to have no effect on respiration rate (Tesarova & Gloser, 1976); soil profile data obtained during the measurement period in both SRF and PRF, confirmed that there was no appreciable soil moisture deficit (S.Boyle, *personal communication*; Hodnett *et al.*, 1996), so it may be reasonable to assume that moisture levels were not limiting in either forest, though soil moisture deficits were experienced later on in the year at PRF (Hodnett *et al.*, 1996). Clearly annual data would be desirable to confirm this, though the similarity of the September 1992 data from PRF to those obtained during the measurements of May - June 1993 suggest that seasonal effects in that forest were slight.

Response to soil composition

Point-to-point differences in soil carbon and nitrogen explain the spatial heterogeneity frequently found in respiration in soil (Chapman, 1979), as also observed here (Figure 4.11). At a larger scale it may be expected that CO_2 effluxes from soils of different types may be predicted using characteristic data on root and soil chemical composition. This issue has been addressed with soil decomposition models such as CENTURY (Parton *et al.*, 1988) and the Rothamstead Model (Jenkinson, 1991). But in both cases the role of root respiration was not explicitly included. Carbon dioxide production by roots has been estimated at 5% to 70% of total soil efflux (*e.g.*, Singh & Gupta, 1977; Chapman, 1979; Ewel *et al.*, 1987), and is consequently important for estimates of total emission rates from soil. The significant relationship with root nitrogen and potassium in SRF was indicative of this relationship (Table 4.5), but root *production* estimates were not available for the site, and it is this process that may scale most clearly with CO_2 effluxes, not necessarily the standing crop (Nadelhoffer & Raich, 1992). The standing crop root biomass was slightly less than that for another semi-deciduous tropical forest, in Panama (9 ton ha^{-1}; Cavelier, 1992)

Table 4.4b indicates that the only significant variable in the regression used for Figure 4.11 was carbon - other nutrients did not limit respiration, whilst temperature did not explain well the inter-microsite differences (*cf.*, Figure 4.4). Severe carbon limitation in well watered soils is a common feature of the decomposition cycle (Ladd *et al.*, 1985). The regression was also re-expressed to include the C : N ratio as a fourth variable: in the 0 - 5 cm layer, the regression was highly significant

($p < 0.001$), C and the C : N ratio were both highly significant variables ($p < 001$), and the r^2 value rose from 0.82 to 0.87. All of the points in Figure 4.11, except one, represent C : N ratios of 10-15, suggesting that mineralisation was taking place (Carlyle, 1986). The microsite with the highest measured efflux rate also had a high organic carbon content (4.5%) and C : N ratio of 20 in the first 5 cm of soil; it is marked with an arrow in Figure 4.11. In these soil conditions, the large emissions might be explained by extra metabolic activity associated with a partial shift in microbial activity to immobilisation (*cf.* Jansson & Persson, 1982), or more simply, by hypothesising that the excess organic carbon was of a labile form and easily broken down, leading to high fungal, microbial and fine root respiration rates (Parton *et al.*, 1988; White, 1987).

Eddy covariance-derived data

When compared as a 48 hr average, the eddy-covariance flux estimates agreed well with the chamber-derived model data, even when data were strictly selected for steady state conditions (Table 4.6). The correction procedure probably worked because the *w't'* and *w'c'* co-spectra had peaks at the same frequency, though lower frequency spectral data would have confirmed this (Figure 4.14b). Despite this source of uncertainty and the error on individual spectral densities, the corrections were small, and the overall estimate was within ±15% of the chamber-derived value, the minimum error expected among point eddy covariance measurements (Moncrieff *et al.*, 1992). A general discrepancy between chamber-based fluxes and eddy covariance-based fluxes could also have been ascribed to the different areas of soil measured by the two methods. For within-canopy turbulence, the variance in the flux data was greater than for the even streamlines usually found above a canopy, as the flux footprint was only 50 - 100 m in radius from the sensors, and the 30 minute means were dominated by relatively few, irregularly spaced eddies (Figure 4.15a). Figures 4.15b&c show that the average frequency most closely associated with such eddies was of the order of five minutes.

A longer time-series than two days is needed if the turbulence-induced variance in the data is to be reduced. In particular, to detect a diurnal pattern, or enhanced effluxes resulting from oxygenation of the soil surface by gusts of wind, data for one or two weeks may be required to obtain an adequate mean. These results show that eddy covariance provided a good method in SRF by which to obtain area-averaged estimates of CO_2 effluxes passing from the soil into the canopy of a forest in certain situations. But, apart from their low capital cost, chamber techniques remain a necessity if process level data are required as well as fluxes.

MODELS OF CO_2 EVOLUTION FROM THE SOIL

A number of mathematical representations of empirical data on CO_2 flux from soils have been invoked in the past and are summarised by Fang & Moncrieff (1996). These range from linear to multiple variable polynomial functions. Polynomial models tend to predict efflux values well (*e.g.*, Grahammer *et al.*, 1991) but may be far removed from the underlying biology and physics. Applying such a function in a new or changed environment would probably not be successful.

In contrast, functions that have heuristic value are difficult to parameterise precisely. The clearest examples of this are found in attempts to include a soil moisture term (Howard & Howard, 1979; Bosatta, 1980). Soil moisture will influence respiration rates above and below certain thresholds (Tesarova & Gloser, 1976), and may simultaneously affect more than one parameter (Parker *et al.*, 1983). It is easier to include soil nutrient and root factors into such a model and this may prove useful for the general typing of soil CO_2 emissions.

However, for the rain forest soils in this study, an absence of moisture limitation directs the focus for a given field site to the temperature response. An exponential model, rather than a linear one, was chosen for these data, as the regression was better defined and the underlying physiology is non-linear (ap Rees *et al.*, 1988). Arrhenius-type models (*e.g.*, Bridgham & Richardson, 1992; Lloyd & Taylor, 1994) did not further improve the fit to the observed data (Figure 4.5). They are more mechanistically explicit, for example in parameterising the activation energy of 'respiration', but the complexity of respiration in soil does not lend itself to detailed functional interpretation from basic efflux data. This is because different decomposing and growing assemblages are found at different depths in soil. This is further overlaid by temperature regimes that exhibit variation in hysteresis and amplitude so that (assuming other soil physical properties and rainfall events were controlled for) different series of respiratory processes will suffer different levels of limitation reflecting local resource availability. Variations with temperature in Q_{10} or activation energy (Lloyd & Taylor, 1994) may result from this, though temperature variation in the rain forest soils studied here was not large enough to generate such phenomena. Composite soil CO_2 efflux rates will resist functional interpretation without more detailed profile data.

4.5 CONCLUSIONS

The flux of carbon dioxide from soil was measured in two rain forests, PRF and SRF, and an open dry tropical forest, cerrado. Efflux rates were higher in rain forest than dry forest, and higher in primary than secondary rain forest. Three methods were used to measure CO_2 emissions from the forest floor: closed chamber, open chamber and eddy covariance, and the results showed good agreement. The weaknesses and strengths of each approach were discussed: expediency dictates that chamber methods are likely to be used in the future, and may be preferred in some circumstances. In this case, a combination of closed and open chambers might be favoured in order to estimate well both the spatial heterogeneity and the processes of respiration in soil.

Soil CO_2 emissions in rain forest were sensitive to temperature, and correlated with soil nitrogen and soil organic carbon concentrations, but not to soil moisture. However, seasonal data from cerrado suggested that soil moisture deficits did limit respiration in this open forest type. There was little indication of seasonal differences in efflux rates from rain forest soils. The temperature sensitivity of soil CO_2 emissions was also shown to vary from point to point, and data from many microsites were used to obtain a robust, spatially integrated response function. An exponential model explained as much or more of the variability in the data than other potential functions; its suitability to represent soil CO_2 effluxes was discussed. Soil heterogeneity was observed in all soil types, rain forest showing greater variability than cerrado. For a given field site, this heterogeneity was explained well by soil composition. A non-linear regression model fitted well to soil composition and temperature data, and suggested that organic carbon was most strongly limiting decomposition processes. This approach could be used as a predictive tool for estimating total carbon dioxide efflux from different soil types.

5. The flux of CO_2 from woody tissue

5.1 INTRODUCTION

Respiration occurs in all living plant tissues. It comprises five main processes, namely glycolysis, the oxidative pentose phosphate pathway and the citric acid cycle followed by electron transport and oxidative phosphorylation. The operation of these primary metabolic reactions is coordinated to oxidise organic substrate, thereby generating high energy compounds (*e.g.*, ATP, NADH, NADPH) and carbon skeletons. These intermediate products may either be further oxidised or directly utilised for the biosynthesis of amino acids and organic acids (ap Rees, 1994). Two other types of respiration also exist, namely photorespiration and cyanide-resistant respiration, but they do not generate as much metabolic energy (Laties, 1982) and are not considered further here.

The main by-product of respiration is CO_2. This released by all cells, whereupon it may escape to the atmosphere, or be re-fixed by photosynthesis. The gas exchange of woody tissue is under-studied in comparison to that of leaves, particularly so in the tropics (Sprugel and Benecke, 1991). Autotrophic respiration may respresent 40% to 60% of gross photosynthesis in cool temperate forest (Linder, 1985); Sprugel and Benecke (1991) suggest that this estimate may rise to 90% for tropical forests, though, depending on root respiration rates, perhaps 50 - 60% is more likely (Singh & Gupta, 1977; Chapter 8). However, if above ground woody tissue respiration alone is considered, the estimate for tropical forest reduces to around 13% (Ryan *et al.*, 1994). The differences among these estimates represent an imperative for further research. Without more detailed knowledge it is not possible to answer apparently basic questions such as how the ratio of photosynthetic to respiring tissue changes with tree size, and to what degree respiration can limit forest production (Kira & Shidei, 1967; Ryan & Waring, 1992).

To answer such questions a mechanistic model of respiration in woody tissue is needed. This would provide the basis for identifying scalars suitable for estimating tree- and stand-scale respiration rates. Clearly temperature is one such scalar, but at a constant temperature, it is less clear whether surface area or [sapwood] volume describe CO_2 emissions from bark most accurately (Yoda *et al.*, 1965; Sprugel *et al.*, 1996). This is because CO_2 is produced by cambium and phloem cells near the outer surface of the stem but also by live parenchyma cells associated with the sapwood. If the stem is

growing, then the metabolic activity of the cambium and phloem cells will be high (Goodwin & Goddard, 1940); variable growth rates in similarly sized woody sections will confound efforts to identify the main source of respiration.

To overcome these problems it is useful to divide respiration into two main components - construction respiration (R_c), required to build new tissue, and maintenance respiration (R_m), required to sustain current tissue by protein replacement, membrane repair and the maintenance of ion gradients (Johansson, 1933, Penning de Vries, 1975; Lambers *et al.*, 1983; Amthor, 1989; Sprugel & Benecke, 1991). This distinction, embodied in the functional model (McCree, 1970; Thornley, 1970, 1977), can be expressed as follows for a whole plant:

$$R = m\,W + g\,(\Delta W / \Delta t) \qquad \text{Equation 5.1}$$

where R is total plant respiration, W is plant mass, $\Delta W / \Delta t$ is the plant growth rate, g is the cost of producing a unit of tissue, and m is the cost of maintaining a unit of tissue. Thus, the first term refers to R_m and the second to R_c.

In this view, R_m is a basal metabolic requirement that is sensitive to temperature and dependent on the live biomass, whilst R_c can be calculated simply as the biochemical *cost* of constructing new tissue, a cost that is independent of temperature (Penning de Vries *et al.*, 1975; McDermitt & Loomis, 1981). This separation of R_m and R_c implies, though not explicitly, that the processes for each are different. They are not. Both are driven by the same *respiratory* pathways, and respond to the same environmental variables, particularly temperature. The heuristic value of this distinction is not disputed here, but when separating R_m from R_c it should be remembered that the CO_2 is being released by the same biochemical processes.

The functional model has also suffered from the criticism that it does not address certain metabolic details. Various reported formulations for g (*e.g.*, Lambers *et al.*, 1983) describe additional respiration demands associated with growth, such as photosynthate transport costs (so-called 'maintenance for growth'). More seriously, variation in R_m and R_c between and within different tissues make it difficult to define g and m precisely for whole trees (Chung & Barnes, 1977; Szaniawski & Kielkiewicz, 1982; Brooks *et al.*, 1991; Sprugel *et al.*, 1996). Despite these shortcomings, the model provides a general framework for analysing respiratory costs that confers advantages outweighing most of the disadvantages.

Two further processes affecting CO_2 efflux rates from wood are the transport of CO_2 in the transpiration stream and the re-fixation of CO_2 by photosynthetic chlorenchyma present in the cortex. Corticular photosynthesis can reduce net efflux rates of CO_2 by up to 80% in temperate species (Foote & Schaedle, 1976; Linder & Troeng, 1980), but this will be strongly affected by the photon flux density incident on chloroplasts below the bark. Schaedle (1975) estimated as a broad average that 15% of external light penetrates the periderm, so it is not clear how much re-fixation will take place within a dense forest canopy.

The possible transport of respired CO_2 within sap was recognised over sixty years ago (Boysen-Jensen, 1933, cited in Sprugel *et al.*, 1996), and remains a confounding factor in woody tissue respiration measurements (*e.g.*, Ryan, 1990). Carbon dioxide produced by roots and microbes in the soil and by respiring plant tissue may be carried in sap to other tissues. This can result in stem CO_2 efflux rates that are above or below the source production rate (*e.g.*, Negisi, 1972; Sprugel, 1990; Martin *et al.*, 1994). By carrying carbon to the leaves, sap flow has also been shown, using isotopic labeling, to act as a source of assimilate (Vapaavouri & Pelkonen, 1985). This phenomenon will generate errors in cuvette-based photosynthesis measurements.

In a study of CO_2 transport in the transpiration stream, effluxes of CO_2 from excised woody sections whose sap flow was experimentally controlled using a pump responded negatively to increased flow rates (Negisi, 1979). However, Negisi did not specify the sap CO_2 concentration, making the interpretation of the results rather difficult. A more direct approach would be to measure CO_2 concentration in sap, but this has rarely been done for trees. Chase (1934, cited in Kramer & Kozlowski, 1960) estimated CO_2 concentration to vary up to 10% in air spaces in poplar sapwood, whilst Hari *et al.* (1991) obtained estimates varying from 20 - 30,000 ppm for *Chamaecyparis obtusa*. Hari *et al.* used Henry's Law (Stumm & Morgan, 1981) to convert these figures to sap CO_2 concentration. Assuming typical transpiration and photosynthesis rates, they concluded that internal CO_2 transport could supply carbon representing 2 to 9% of total leaf photosythesis. However, the authors did not appear to measure sap pH or temperature (both are required by Henry's Law), and their samples were obtained from drilled holes, apparently without maintaining atmospheric pressure within the sample chamber. The consequent measurements may have been contaminated by atmospheric air and tissue wounding, or affected by pressure differences in the gas samples.

The work in this chapter addresses process-level questions relating to woody tissue respiration, with a view to using this information for scaling up estimates to the stand level in Chapter 7. The following questions were addressed:

1) The temperature response of CO_2 effluxes from woody tissue.
2) The relative importance of construction and maintenance respiration components, and how these affect the relationship between CO_2 efflux and stem or branch diameter. The hypothesis that 'CO_2 efflux scales with surface area and volume according to an alternating dominance defined by the diameter of the woody section' was investigated. The extent of corticular photosynthesis in bark was considered briefly.
3) The proportion of photosynthesis accounted for by dissolved CO_2 in sap was quantified.

All the measurements were made in PRF, Brazil and SRF, Cameroon. A longer field period in Cameroon made possible more detailed measurements.

5.2 METHODS

INTRODUCTION

Carbon dioxide efflux from woody tissue was measured in PRF and SRF. Bark surface and bark sub-surface temperatures were measured at both sites, for individual trees. Shielded and unshielded bark temperatures were also measured through the vertical profile of the forest canopy by embedding thermocouples in the bark surface on upper and lower sides of branches, and in stems. In Cameroon, it was possible to make a more extensive study investigating woody tissue respiration in relation to stem growth and the occurrence of stem photosynthesis. All species identifications were carried out by botanists employed from national herbaria of Brazil and Cameroon. Where possible, fertile specimens of each species were deposited in the herbaria in Belém (Brazil) and Yaoundé (Cameroon). Experimental work devised and practised in Edinburgh to study the interaction of the transpiration stream with woody tissue CO_2 efflux was also extended to two tree species in Cameroon.

MEASUREMENT SYSTEMS AND CHAMBERS

Measurements of carbon dioxide efflux from woody tissue were made from trees in PRF, during May and June 1993, and in Cameroon, in SRF, from February to May 1994. Two measurement methods were used in this work: closed and open chamber infra-red gas analysis. The principle of operation was the same as for the respective soil CO_2 efflux systems described in Chapter 4.

Chambers

Chambers were constructed from perspex. Two designs were used: one (type A) to encircle the narrower stems (diameter < 10 cm) using a split cylinder; and one (type B) made to be adpressed against the bark surface of larger stems (diameter > 10 cm) sealing a rectangular area of bark from ambient air. In all cases neoprene gaskets were used to seal chambers to the bark. Type A cylinders were used on stems of different diameter by varying the thickness of the end gaskets wrapped around the section of wood under study. Adequate mixing of air in the chamber was achieved by minimising chamber volume and placing inlet and outlet nozzles on opposite sides of the measured wood section (Plate 5.1). A small fan was inserted into the back wall of the type B chambers to provide mixing; to make a better seal against the bark on larger stems, two layers of neoprene (low density laid down on high density) were used as gaskets (Plate 5.2). Chambers were sealed to stems and branches using elasticated cord and nylon cable ties. Type A chambers were 8 - 15 cm in length and 80 - 250 cm^3 in volume; Type B chambers were 15 cm x 6 cm, and including the fan, 400- 500 cm^3 in volume.

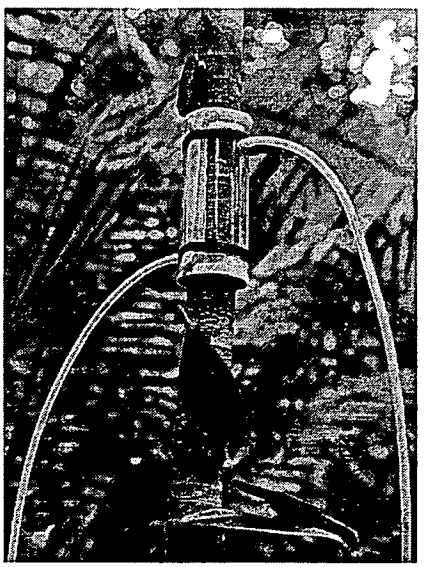

Plate 5.1. A type A chamber used to measure the efflux of CO_2 from woody stems and branches. The non-wood volume was reduced to a minimum, and the chamber connected to the IRGA.

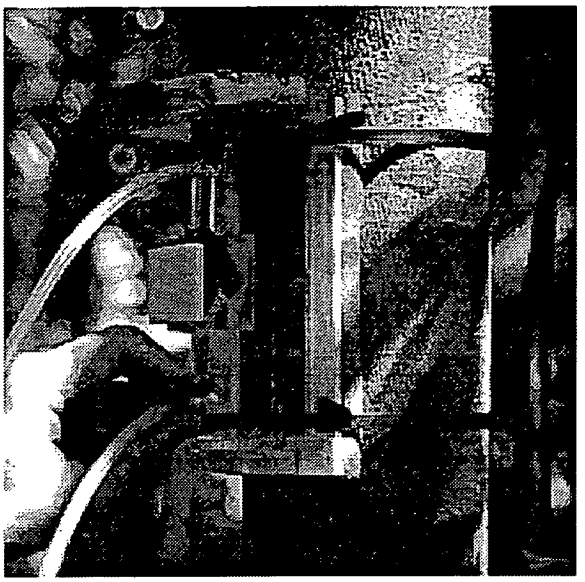

Plate 5.2. A type B chamber used to measure CO_2 effluxes from woody tissue. A fan was used to mix the air passing between the tube in/outlet.

Closed chamber measurements

Chambers were sealed to bark and attached in a closed circuit to an IRGA (LI 6200, Licor, Nebraska, USA). In order to minimise any possible leaks, chamber CO_2 concentration was drawn down to a point below ambient concentrations (360-450 ppm, depending on time of day) and allowed to rise an approximately equal amount above ambient. Measurements were made by logging data for 60 second intervals, using a five second time step, and then repeating the procedure. Data were subsequently checked for linearity of the time course of CO_2 concentration. Measurements not fulfilling this stricture (less than 5%) were discarded. Bark surface temperature was measured inside the chambers using a Cu-constantan thermocouple with an amplified output. Means of the repeated measurements were used as spot values, and recorded together with the diameter of the woody section enclosed by the chamber. Diameters were recorded as the average of four measures at the top and bottom of the section (measurement precision 0.1 mm, vernier calipers, RS, UK); woody sections were treated as cone frustra. It was not possible also to measure sapwood volumes in the woody sections.

For both forests, an initial experiment was set up with chambers permanently attached to stems for 24 hours. Ambient air was continuously passed through all chambers at ±1.5 l dm^{-3}, except during CO_2 efflux measurements that were taken at intervals throughout the 24 hours. Subsequently, a wide range of species and stem, or branch sizes, were sampled as spot measurements in order to represent

emissions of CO_2 for the stand as a whole (Table 5.1). In Cameroon a longer study was possible. For each tree, dendrometer bands were attached to ten trees of differing size. Efflux rates of CO_2 from bark were measured for all trees on three dates between February and May 1995. In this way any [seasonal] changes in respiration rates could be detected. Where possible up to 10 individuals of the same species were sampled in this way. The only four species found in suitable abundance were: *Musanga cecropioides* (a pioneer species, *sensu* Swaine and Whitmore, 1988; Anon., 1987), *Distemonanthus benthaminanus* (a climax forest species, *sensu* Swaine and Whitmore, 1988; Anon., 1987), *Triplochiton scleroxylon* and *Trema orientalis* (Table 5.1).

Open chamber measurements

An open path IRGA was available for the Cameroon field campaign (LCA2, ADC, Hoddesdon, UK). This was connected in series to a cuvette and air was drawn in by a mass-flow controlled air supply unit (MASU, ADC, Hoddesdon, UK) at 350-500 cm^3 min^{-1}. Before entering the cuvette, ambient air was passed through a 2 dm^3 buffer chamber; and before entry into the optical bench of the analyser it was dried (using a column of silica gel) to allow for cross-sensitivity to water vapour in this instrument. The drying agent was changed regularly and the IRGA re-calibrated every two days. Bark surface temperature inside the chamber was measured using a Cu-constantan thermocouple, and all data were stored in a Campbell 21X datalogger (Campbell Scientific, Leicester, UK) as 15 minute averages of readings sensed every second. Continuous data were recorded for three *Musanga cecropioides*, two *Distemonanthus benthaminanus* and one *Trema orientalis*.

This equipment was also used to examined the radial temperature profile across the stem, and its relation to stem respiration. Cu-constantan thermocouples were positioned at the bark surface, 1 cm and 5cm depth (holes drilled were ~1 mm diameter), and the CO_2 efflux recorded with temperature for 48 hours during 1st and 2nd May, 1994. In a further experiment, cortical photosynthesis was investigated in *Trema orientalis* on stem tissue near ground level, and in *Musanga cecropioides,* on branch tissue at 20 m height (accessed from the micrometeorological tower). Chambers were set up as above, with a PPFD sensor placed immediately above the cuvette, normal to the [vertical] plane of the stem. Data were recorded for two days and then a sheet of black-backed silver polyurethane (Peritherm, Perifleur, UK) was taped round the equipment, with the silver side outwards to prevent entry of any light, and a further two days' data were logged. Only limited measurements of this kind were possible because of an illness; the analysed results are in Table B1 (Appendix B) and are referred to in the Discussion.

THE RELATIONSHIPS BETWEEN CO_2 EFFLUX RATE, T, D_w, R_c AND R_m

The temperature response in CO_2 efflux rates

The temperature response of CO_2 effluxes from wood were fitted to an exponential equation using least-squares non-linear regression:

$$R_r = R_o e^{(k T)} \qquad \text{Equation 5.2}$$

where R_r is the raw efflux rate (μmol m^{-2} s^{-1}), R_o is the theoretical efflux rate at 0 °C, T is temperature (°C) and k is a coefficient determining the Q_{10}, the relative change in reaction rate with a change of 10 °C such that $\ln Q_{10} = 10k$. Efflux rates were normalised to 25 °C (R_t) for subsequent analysis and initially investigated in relation to woody section surface area and volume.

The calculation of R_m and R_c

The growth data from SRF were used to estimate R_c and R_m from R_t by two separate methods:

Method 1: The increase in wood volume under the chamber was calculated from growth measurements between February and May 1994. The specific gravity of each species (Reyes, *et al.*, 1992) was then used to obtain the dry mass of new wood. Where specific gravity data were unavailable (only three species), a value of 0.5 g cm^3 was assumed. The amount of carbon per gram of dry wood was then assumed to be 50% of the ash free dry mass (Edwards *et al.*, 1980; Griffiths, 1993). Ash free dry mass was taken as 99.3% of dry mass (Ryan *et al.*, 1994).

Penning de Vries (1975) estimated a metabolic construction requirement of 0.43 g CO_2 per gram of new woody tissue. This is likely to be a minimum as it excludes any extra growth-related processes, though experimental determinations show good agreement at 0.46 (Benecke, quoted in Sprugel and Benecke, 1991) and 0.47 (Ledig *et al.*, 1976). Taking the average of these, and converting to grams of carbon expended per gram of new wood, a figure of 0.124 g g^{-1} was reached. Recalculating for the carbon in one gram of wood gave a final requirement of 0.248 g carbon to be respired for one gram of

carbon to be constructed. Using these calculations, R_c was converted to standard units (μmol CO_2 m^{-2} s^{-1}) and subtracted from R_t to give R_m, the maintenance respiration rate.

Method 2: Initial stem diameters (D_w) and growth measurements were used to obtain the relative growth rates (RGR) for each tree. An empirical regression between the natural logarithms of D_w and R_t was used to normalise R_t for each tree to the average diameter of all trees with zero or positive growth patterns (Figure 5.6; Table 5.4). This efflux rate, R_{td} ,was plotted against RGR, and the regression between them extended back to the ordinate (RGR = 0) in order to determine the mean rate at zero growth, that is, R_m. R_c was calulated as the difference between the mean R_{td} and R_m.

A functional interpretation of the D_w - R_m relationship

The R_m values derived using 'Method 1' were fitted to Equation 5.3 in order to address point (2) in the Introduction where it was hypothesised that both surface area and volume determine efflux rates from woody tissue. The key features of this curve were thought to reflect the varying dominance of surface area (a linear function of D_w) and volume (a quadratic function of D_w) in determining R_m: at low D_w, R_m was approximately constant, and at larger diameters R_m increased to the [approximate] square of D_w until an asymptote was reached, after which R_m was constant with D_w. The results of this analysis were compared with correlations between R_r and the radial temperature profile of a *Trema orientalis* stem (see 'Open chamber measurements' above).

$$R_m = a + b\,[1 + \exp(c + d \log D_w)] \qquad \text{Equation 5.3}$$

where a is minimum value at low D_w, and b, c and d are fitted constants.

DETECTION OF DISSOLVED CO_2 IN THE TRANSPIRATION STREAM

Sap rising in a tree stem contains dissolved CO_2; air in the sapwood was assumed to be in equilibrium with this dissolved CO_2. Sapwood CO_2 concentration was measured using a system designed and tested in Edinburgh in collaboration with P. Levy, of Edinburgh University. Two 50 cm^3 cuvettes were constructed and sealed with 'Blu-tac' mastic to the stems of birch (*Betula pendula*) and oak (*Quercus petraea*) trees in Scotland, and *Musanga cecropioides* and *Distemonanthus benthamianus* trees in Cameroon. Each chamber had an aperture through which 2 - 5 cm^3 samples could be removed

with a closeable syringe. A second aperture, open to the atmosphere, was attached to a polyurethane bag which behaved rather like a lung by inflating inside the chamber as a sample was removed, thus preventing pressure changes developing in the sample or the chamber. Chambers were left in position for up to 9 days to allow full equilibration between CO_2 in air in the sapwood and the chamber air. Silicon grease was smeared around the bark within a 2 cm radius of the chambers to inhibit CO_2 diffusion out of the chamber. Samples were removed approximately once a day and injected into an IRGA operating as a closed system (LI 6200, Licor, Nebraska, USA). To avoid over-pressuring the analyser, the plunger was withdrawn to its original position after injecting and allowing 10 seconds for mixing. The concentration of the sample was calculated as:

$$[CO_2]_s = \{(V_g + V_s) / V_s\} \times \{d[CO_2] + [CO_2]_i\} \qquad \text{Equation 5.4}$$

where $[CO_2]_s$ is sample CO_2 concentration, V_g is system volume, V_s is sample volume, $d[CO_2]$ is the difference between the initial system CO_2 concentration, $[CO_2]_i$, and the final CO_2 concentration.

To obtain the concentration of CO_2 dissolved in water in the sap ($[CO_2^*]$), Henry's Law, (Stumm and Morgan, 1981) was applied to the data. In Cameroon, pH was measured by pressing pH paper against freshly revealed sapwood, and temperature was measured with a Cu-constantan thermocouple. For birch, pH was estimated and air temperature was taken from a nearby weather station. The concentration of CO_2 in sap is very sensitive to pH and slightly less so to temperature, making the estimate of birch sap pH quite important.

Henry's Law: $$[CO_2^*] = pCO_2 K_H(T)\left[1 + \frac{K_1(T)}{[H+]} + \frac{K_1(T)K_2(T)}{[H+]^2}\right] \qquad \text{Equation 5.5}$$

where $[CO_2^*]$ is the concentration of all forms of CO_2 dissolved in water,

pCO_2 is the partial pressure of CO_2 in air,

$K_H(T)$ is Henry's constant for CO_2,

and $K_1(T)$ and $K_2(T)$ are dissociation constants for carbonate ions.

The derived $[CO_2^*]$ in *Betula pendula*, *Musanga cecropioides* and *Distemonanthus benthanmianus* was examined in relation to measured transpiration and photosynthesis rates for each species, and the importance of sap-derived CO_2 to photosynthesis considered.

Table 5.1. The species and families of all trees measured for CO_2 efflux from woody tissue during fieldwork in PRF, Brazil (May-June, 1993) and SRF, Cameroon (February-May, 1994).

(1) PRF, BRAZIL

Family	*Species*	*n*
Anacardiaceae	*Astronium lecointei* Ducke	1
Annonaceae	*Xylopia* sp	5
Arecaceae	*Orbigynia speciosa*	3
Chrysobalanaceae	*Licania* sp	1
Euphorbiaceae	*Hironima* sp	1
Lauraceae	*Ocotea* cf *caudata* (Nees.) Mez	1
Lecythidaceae	*Bertolettia* sp	1
Leguminoseae; Caes	*Sclerolobium* sp	3
Meliaceae	*Guarea kunthii* A. juss.	2
Meliaceae	*Trichilia quadrijuga* H.B.K.	1
Moraceae	*Cecropia ficilifolia* Snethl.	1
Moraceae	*Cecropia sciadophylla* Mart.	3
Moraceae	*Naucleopsis glabra* Spr. ex Baill	2
Moraceae	*Naucleopsis krunnii* (Standl) C.C. Berg.	5
Moraceae	*Pseudomeldia* sp.	1
Moraceae	*Sorocea guilleminiana* Grand.	1
Moraceae	*Trymatococcus amazonicus* Poepp et Endl.	2
Myristicaceae	*Virola calophylla* Warb.	4
Myristicaceae	*Virola michelii* Hackel	2
Sterculiaceae	*Sterculia pruriens* (Aubl.) Schum	6
Sterculiaceae	*Theobroma microcarpum* Mart.	21
Sterculiaceae	Unknown	2
Violaceae	*Rinorea pubiflora* (Benth.) Spreng.	1

(2) SRF, CAMEROON

Family	*Species*	*n*
Annonaceae	*Xylopia etiopica*	2
Asteraceae	*Vernonia conferta*	1
Burseraceae	*Santira trimera* (Oliv.) Aubr.	1
Combretaceae	*Terminalia superba* Engl. & Diels	2
Leguminoseae; Caes	*Distemonanthus benthamianus* Baill.	7
Leguminoseae; Pap.	*Ptercarpus soyauxii* Taub.	1
Icacinaceae	*Desmostachys tenuifolius*	1
Irvingaceae	*Desbordesia glaucescens* (Engl.) Van Tiegh.	1
Irvingaceae	*Kainedoxa gabonensis* Pierre ex Engl. var oblongifolia	1
Moraceae	*Musanga cecropoides* R.Br.	10
Myristicaceae	*Coelocaryon preussi* Warburg	1
Ochnaceae	*Lophira alata* Banks ex Gaertn.f.	2
Olacaceae	*Panda oleosa* Pierre	1
Sterculieaceae	*Triplochiton scleroxylon* K. Schum.	7
Ulmaceae	*Celtis mildbraedi* Engl.	7
Ulmaceae	*Trema orientalis* (Linn.) Bl.	10
Verbenaceae	*Vitex grandifolia*	1

5.3 RESULTS

WOODY TISSUE TEMPERATURE

Bark temperature measurements showed a typical diurnal cycle (Figures 5.1a&b). Canopy-top bark temperatures, whilst highest during the zenith, were also lower at night than those lower down. In the lower-canopy, temperatures were less extreme and lagged behind those higher up by up to three hours. Maximum temperatures were higher in PRF than SRF (42 °C *vs* 34 °C). The profile was also deeper: maximum temperature differences between upper and lower canopy in PRF were 15 - 20 °C, whilst in SRF they were rarely more than 10°C. The PRF forest was subject to episodic '*friagens*' which were associated with cooler southerly winds and reduced daytime maxima of up to 20°C, though minimum temperatures were changed by less than 5 °C. The end of a *friagem* can be observed at the start of the graph in Figure 5.1a.

Shielded (lower side of twig) and unshielded (upper side of twig) temperatures changed in approximate synchrony with each other, although unshielded values were ± 0.5 °C higher than shielded ones, and up to 1.5 °C higher during maxima. A radial temperature profile within the stem of *Trema orientalis* is shown in Figure 5.1c; the expected hysteresis and damping between surface and internal temperatures (1 cm and 5 cm depth) is visible.

CO_2 EFFLUXES FROM WOODY TISSUE

The temperature response of woody tissue respiration

Time series measurements made using the closed chamber system on individual trees over 24 hours indicated that CO_2 efflux from wood was strongly related to temperature (Figures 5.2a-d). Measurements using Type B chambers made at different points around the circumference of a stem were statistically indistinguishable. The gradients and zero-intercepts in Figure 5.2c&d represent k and R_0 respectively; different trees exhibited fairly similar k values, but different R_0 values (Table 5.2).

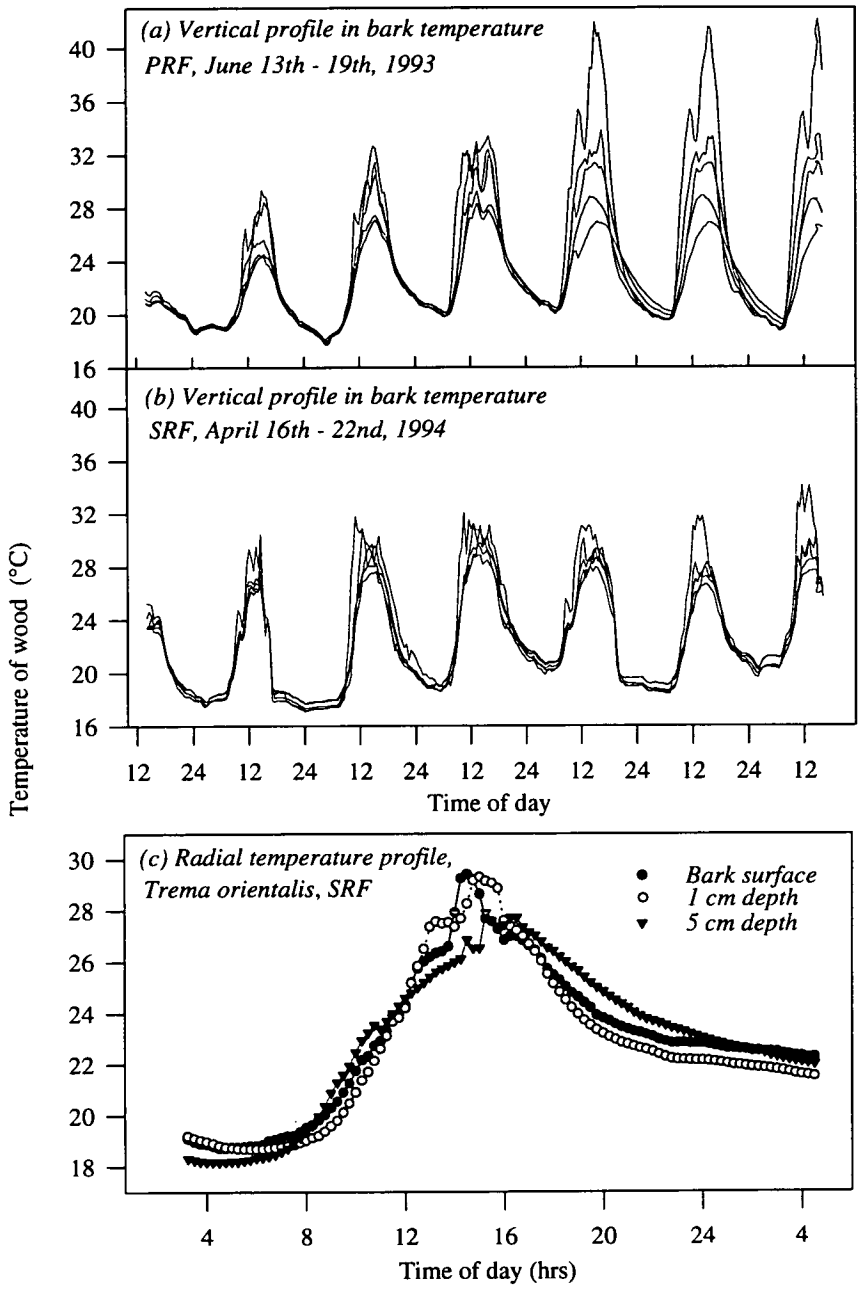

Figures 5.1a-c. Typical woody tissue temperature profiles. In (a) & (b), the vertical profile in bark surface temperature through the canopy in PRF and SRF. The positions in the canopy that each trace represents can be identified during the maxima, where from top to bottom the lines represent temperature at 36m, 20m, 15m, 10m, & 3m for PRF; 40 m, 30 m, 20 m, 12 m and 8 m in Cameroon. In (c), the radial temperatur profile through the vertical stem of a *T. orientalis.* tree of diameter 13.6 cm in SRF, 1st - 2nd May, 1994.

Table 5.2. Parameters fitted to Equation 5.2 using time series CO_2 efflux measurements made on individual trees. Data from Brazil collected during May - June 1993, and from Cameroon during February - May 1994 using the closed chamber system. Units: D_w in m and R_o in μmol m^{-2} s^{-1}.

BRAZIL					CAMEROON				
Tree	D_w	R_o	k	n	*Tree*	D_w	R_o	k	n
N. krunnii.	0.04	0.03	0.087	1	*M. cecropiodes.*	0.34	1.17	0.043	1
Pseudomeldia sp.	0.10	0.06	0.073	1	*X. etiopica*	0.25	0.41	0.037	1
T. microcarpum.	0.02	0.05	0.059	1	*T. orientalis*	0.14	0.41	0.045	1
V. michelii	0.40	0.27	0.056	1	*V. conferta*	0.05	0.22	0.060	1
N. krunnii.	0.05	0.08	0.040	1	*D. benthamianus*	0.23	0.96	0.045	1
T. amazonicus	0.24	0.23	0.065	1	--	--	--	--	--
Mean	0.14	0.12	0.062	6	Mean	0.20	0.63	0.046	5

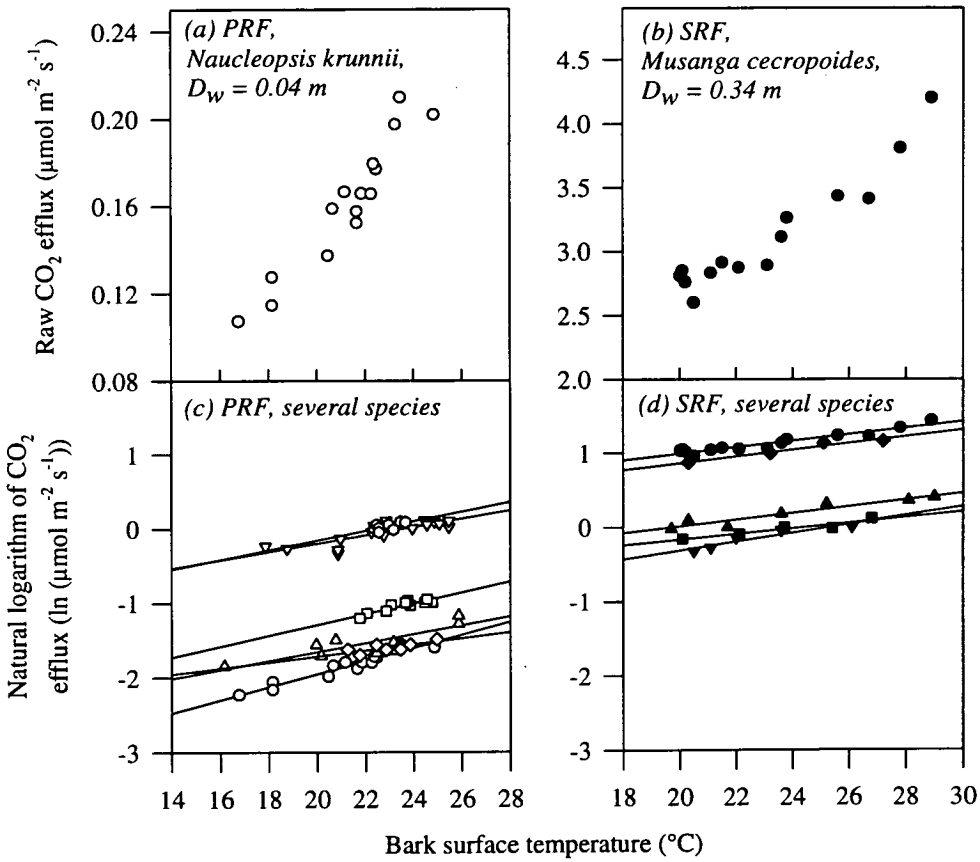

Figures 5.2a-d. Temperature response of CO_2 efflux from woody tissue in PRF, Brazil and SRF, Cameroon. All measurements were made with a closed chamber system. In (a) and (b) are raw data for one tree from each forest. In (c) and (d) are data for several trees (represented by different symbols), plotted as a linear function of ln (CO_2 efflux).

In Cameroon, continuous data were also obtained using an open chamber system. Temperature and CO_2 efflux data are shown in Figure 5.3 for a *Musanga cecropioides* and a *Distemonanthus benthamianus*. A comparison between the two measurement methods (Figure 5.4) showed good agreement among R_t values. Data obtained with the open system were also analysed using Equation 5.2. The parameters were close to those found using the closed IRGA system (Tables 5.2 & 5.3).

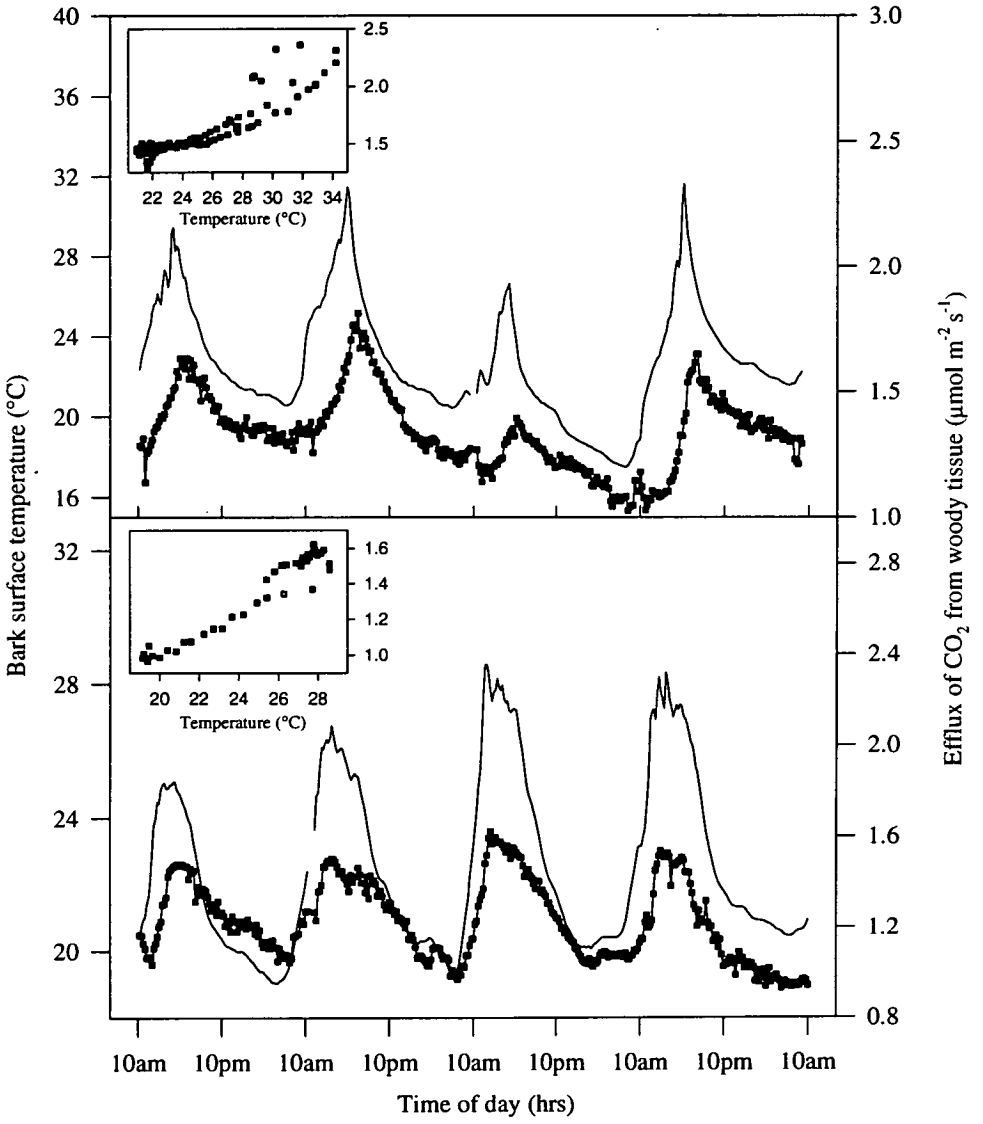

Figures 5.3a&b. Continuously recorded woody tissue temperature and CO_2 efflux from (a) *Distemonanthus benthamianus* (14th-18th March, 1994) and (b) *Musanga cecropoides* (14th-18th April, 1994). The inset graphs show temperature responses for (a) 6am - 5pm, 15th March and for (b) 6am - 5pm, 15th April. The breaks in the traces are when the IRGA was being re-calibrated. Squares = CO_2 efflux.

Table 5.3. Parameters fitted to Equation 5.2 using continuous CO_2 efflux and temperature data collected during February - May 1994, in SRF, Cameroon. Bark temperatures inside and outside the chamber did not differ by more than 3 °C during these measurements. The *M. cecropiodes** reading was taken at 24 m, from a branch. n = number days of measurement. Those trees marked with $^{\varphi}$ are also found in Table 5.2.

Tree species	D_w	R_o	k	n
M. cecropiodes .	0.05	0.42	0.038	12
M. cecropiodes $^{\varphi}$	0.34	0.72	0.044	10
T. orientalis$^{\varphi}$	0.14	0.46	0.040	5
D. benthamianus.$^{\varphi}$	0.23	0.71	0.047	4
D. benthamianus.	0.02	0.24	0.040	4
*M. cecropiodes.**	0.04	0.48	0.036	3
Mean for all species	0.16	0.51	0.042	--

Overall, the data suggest that the sensitivity of woody tissue CO_2 emissions to temperature was higher in PRF (Q_{10} = 1.8; k = 0.062) than in SRF (Q_{10} = 1.6; k = 0.044), though the R_0 values were higher in SRF (0.1 - 0.2 μmol m^{-2} s^{-1} in PRF vs 0.5 - 0.6 μmol m^{-2} s^{-1} in SRF).

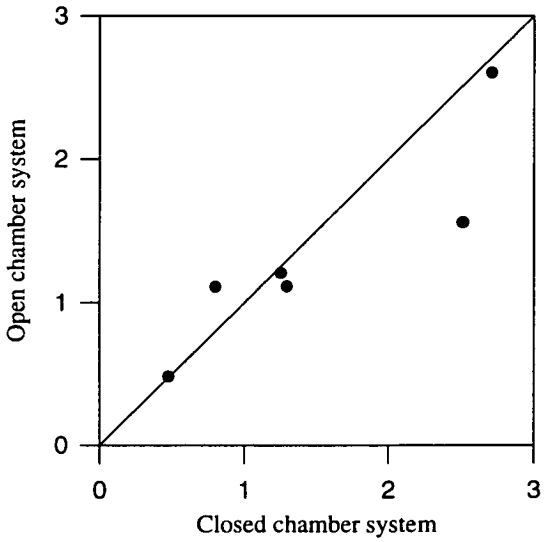

Figure 5.4. A comparison of the closed and open chamber systems used to measure CO_2 efflux from 5 tree species in SRF, Cameroon. All units are in μ mol m^{-2} s^{-1}. The 1:1 line is shown; a regression of the ordinate upon the abcissa, passing through the origin did not distinguish the measurements from this line: gradient = 1.1with 95% confidence limits = 0.3; p = 0.01; n = 5.

The effect of cortical photosynthesis on R_t estimates

It was only possible to make a few measurements to test the effect of cortical photosynthesis on respiration, by correlation with PPFD or placing a shroud over the stem. The data tentatively indicated that there was a small reduction (~2%) in R_t due to photsynthesis in the cortex of some woody species, but not others (Table B1, Appendix B). More data are needed to evaluate further these results.

THE RELATIONSHIPS BETWEEN R_t, D_w, R_c AND R_m

Woody tissue CO_2 efflux rates in PRF ranged from 0.1 to 3.3 μmol m^{-2} s^{-1} for D_w between 0.1 and 1.4 m. In SRF, the efflux rates were higher: 0.2 to 5.2 μmol m^{-2} s^{-1} for D_w between 0.002 and 0.6 m. R_t was plotted against diameter and expressed either on an area or volume basis (μmol m^{-2} s^{-1} or μmol m^{-3} s^{-1}; Figures 5.5a-d). Surface area did not predict CO_2 emissions well at $D_w > 0.1$ m (otherwise efflux would have been constant with D_w). The volume based description was hyperbolic but the relationship a little noisy. However, if the data were transformed to natural logarithms, highly significant regressions ($p < 0.001$) were obtained between D_w and R_t (Figures 5.6a&b; Table 5.4).

Table 5.4. Linear regression results for plots of R_t *vs* D_w for PRF and SRF. The form of the equation is $\ln R_t = a + b \ln D_w$. The values in parentheses are 95% confidence limits.

Forest	*a*	*b*	r^2	*p*	*n*
PRF, Brazil	1.56 (0.3)	0.40 (0.12)	0.62	< 0.001	51
SRF, Cameroon	1.65 (0.3)	0.60 (0.13)	0.46	< 0.001	50

The calculation of R_m and R_c

Efflux rates of carbon dioxide from each tree did not change significantly between February and May 1994, suggesting an approximately constant growth pattern during this time. Seventy-five percent of the trees grew by a detectable margin (minimum = 0.002 m girth); the remaining 25% showed no growth, or a very small reduction (less than 0.002 m girth) possibly attributable to a temporary low water status. R_c was calculated for each tree using 'Method 1', whilst R_m was obtained from the regression intercept on the ordinate of Figure 5.7, using 'Method 2'. The calculations using either technique produced a similar answer, and suggested that R_m constituted approximately 80% of total respiraton during the measurement period (Table 5.5).

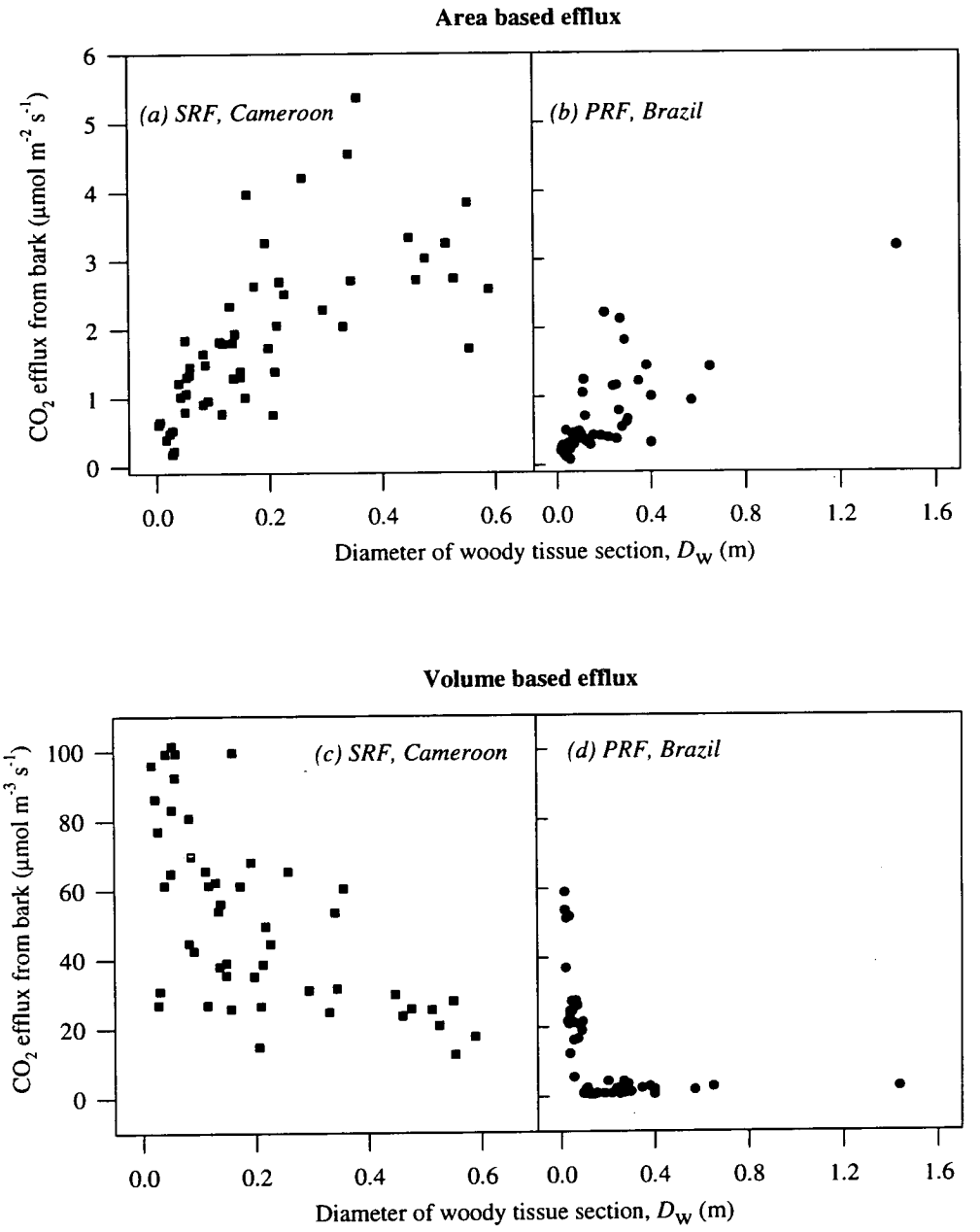

Figures 5.5a-d. Efflux of CO_2 from woody tissue in SRF, Cameroon (squares) and PRF, Brazil (spots). Efflux is not a straight forward function of volume or surface area; see text. Figures (a) and (b) show efflux expressed on an area basis; Figures (c) & (d) show efflux expressed on a volume basis.

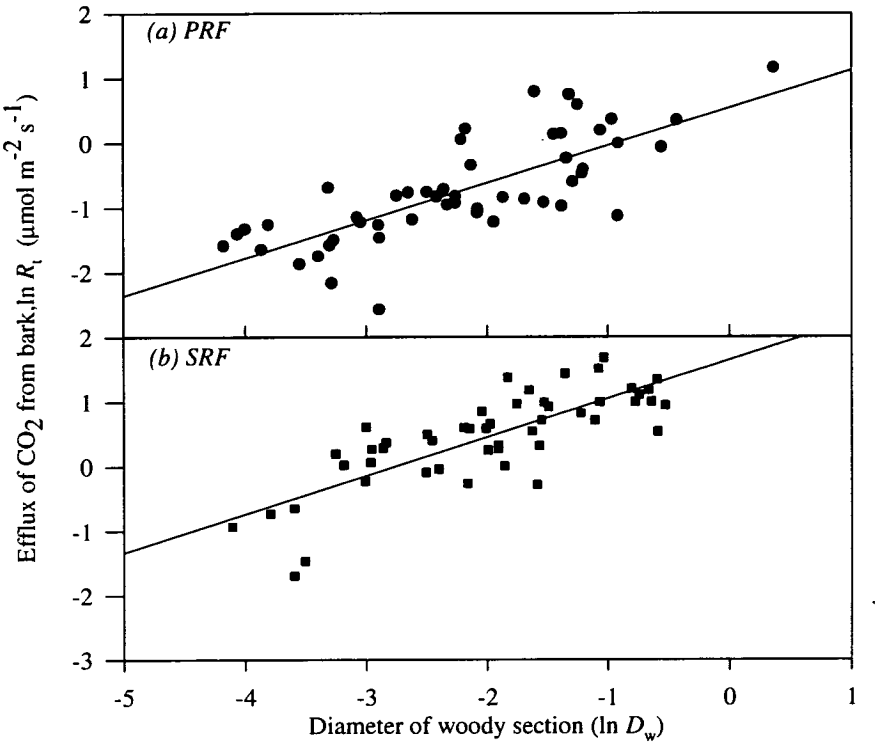

Figure 5.6a&b. Efflux of CO_2, R_t, from woody tissue in SRF, Cameroon (squares) and PRF, Brazil (spots). Both diameter and efflux are expressed as natural logarithms.

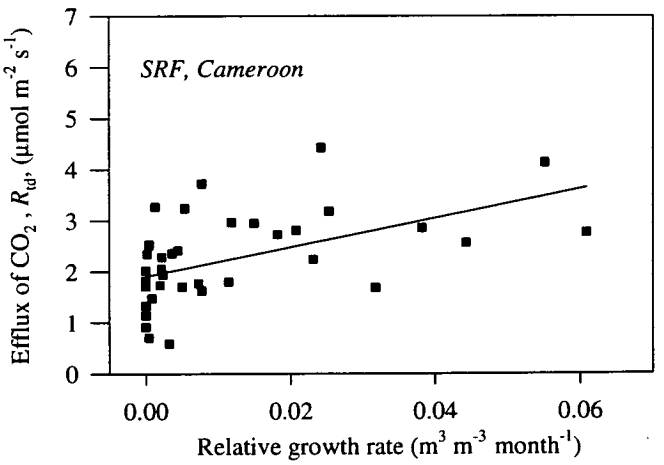

Figure 5.7. Relative growth rates of trees in SRF, Cameroon *vs* R_{td}. The efflux rate on the ordinate is normalised according to the mean diameter using the results in Table 5.4, and corrected to 25 °C (see text). The regression line shown is highly significant ($p < 0.001$; $r^2 = 0.34$; $n = 38$; with the three highest R_{td} values removed, the $r^2 = 0.48$). One month is defined as 30 days.

Table 5.5. A comparison of the mean relative contributions of R_m and R_c to total respiration rates for trees in SRF. The R_t value for method 1 = mean R_t and for method 2 = mean R_{td}; the units for R_t are μmol m^{-2} s^{-1}. Standard errors are in parentheses. See Methods section for explanation of 'Methods 1 and 2'.

Calculation of R_c or R_m	R_t	% R_m	% R_c	*n*
Method 1	2.0 (0.7)	84 (8)	15 (8)	38
Method 2	2.2 (0.6)	80 (7)	20 (7)	38

A functional interpretation of the D_w - R_m relationship

Figure 5.5 strongly suggested that surface area or volume were not good individual scalars upon which solely to base estimates of woody tissue CO_2 efflux for trees in SRF and PRF. When R_m and R_t were plotted against D_w for the SRF data, the increased scatter in R_t attributable to R_c was revealed (Figure 5.8a). The same plot is also shown for four individual species: *Musanga cecropioides*, *Distemonanthus benthamianus*, *Trema orientalis* and *Triplochiton scleroxylon* (Figures 5.8b-e). The functionally based Equation 5.4 fitted better to the R_m values, with an r^2 of 0.66, than did the empirical logarithmic regression model to the R_t values, which gave an r^2 of 0.46 (Figure 5.9; Tables 5.4 & 5.6). An exceptionally good fit to Equation 5.4 was obtained for *M. cecropiodes* (r^2 = 0.95), though the relationships for the other three species were less good (regression results not shown). Although there was some noise in Figure 5.9, a curve similar to the theoretical one inset on this graph could be clearly discerned. At smaller diameters, the flat section of the curve was very small, but at higher D_w, R_m increased with the approximate square of D_w until a saturation point was reached, after which R_m increased slowly. At the smallest diameters (*e.g.*, twigs of D_w = 1 - 5 mm) the relationship broke down as the proportion of living tissue rises very rapidly with reducing D_w. In SRF, twigs of 2 mm and 5 mm gave efflux rates of 0.65 and 0.61 μmol m^{-2} s^{-1} (or 460 and 800 μmol m^{-3} s^{-1}; compare Figure 5.5).

Table 5.6. Parameters for Equation 5.4 fitted to R_m and D_w values SRF.

	a	*b*	*c*	*d*	r^2	*n*
Fitted value	-0.23	0.23	-10.39	0.41	0.66	50

The relative dominance of surface area or volume in determining respiration was also investigated using continuously logged CO_2 efflux data with measurements of the radial profile in stem temperature (surface, 1 cm, and 5 cm). Temperatures at greater depths showed decreasing lags with respect to CO_2 efflux. After removal of the lags, an exponential temperature response (Equation 5.2) was fitted to the data. Temperature at all three depths explained over 90% of the variation in measured CO_2 efflux,

indicating that the temperature-sensitive contribution from the cells near the surface was rather similar to that from the sapwood volume (Table 5.6 & Figure 5.1c). Dendrometer measurements on this tree had shown very little growth, indicating that this result fitted the function in Figure 5.9, where at D_w = 0.136 m, the R_t and R_m values were in Stage **2** of the graph where both surface area and volume are important in determining total efflux rates (Figure 5.9).

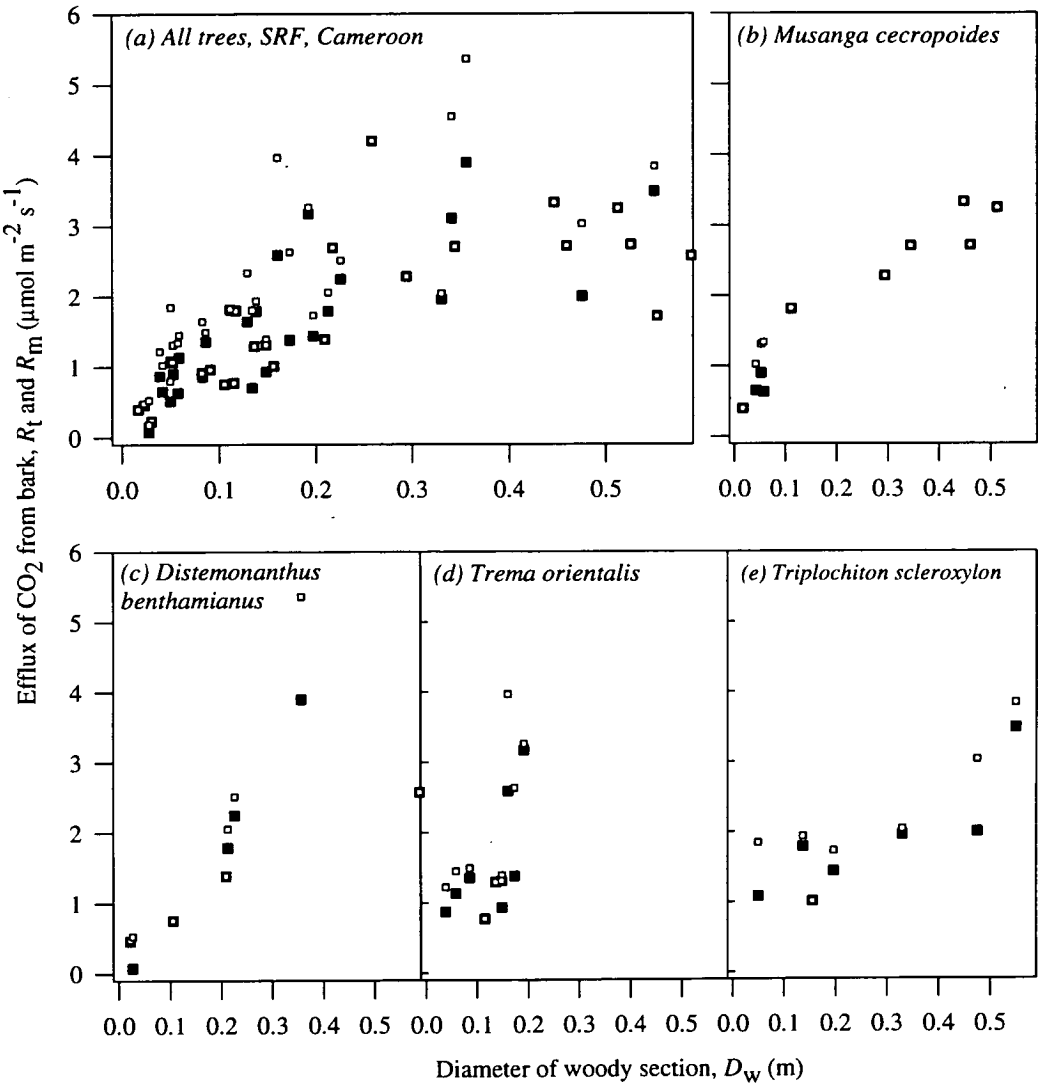

Figures 5.8a-e. R_m (closed symbols) and R_t (open symbols) *vs* D_w for trees in SRF, Cameroon. In (a) is the pattern for all the data; in (b) - (e) are the data for four species for which there were several trees available. Where R_c was zero, the open square (R_t) is nested inside the closed square (R_m).

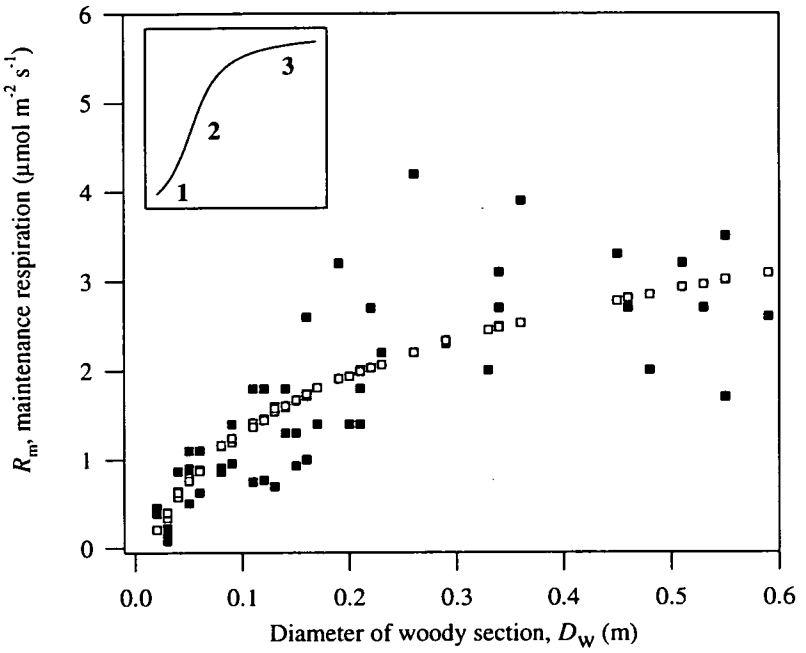

Figure 5.9. Calculated maintenance respiration (R_m) for trees in SRF, Cameroon. The inset graph shows an idealised pattern with three stages (see text). The closed symbols are the fitted model ($r^2 = 0.66$) according to Equation 5.3, page 78.

Table 5.6. The lag times between temperature and CO_2 effluxes for a *Trema orientalis* tree in Cameroon at 3 depths into the stem. The r^2 values for the [de-lagged] temperature response function at each depth are also shown. Stem radius was 6.8 cm; $R_t = 1.3$ µmol m^{-2} s^{-1}.

Depth in stem (cm)	*Lag time for CO_2 efflux*	*r^2 for temp. response*
Surface	45 min	0.92
1 cm	30 min	0.92
5 cm	0 - 15 min	0.93

DISSOLVED CO_2 IN THE TRANSPIRATION STREAM

Chamber concentrations on the birch and oak trees reached an asymptote within one to two days of sealing the chambers to the trees (Figure 5.10). This maximum value was higher for wounded bark tissue, and lower when in the light (when the shroud was removed). The approximate equilibrium concentration for birch was measured at 30,000 ppm. For the *Musanga cecropioides* and

Distemonanthus benthamianus trees in Cameroon, equilibrium values ranged from 92,000 to 30,000 ppm. Using Henry's Law, the calculated concentration of CO_2 in sap, [CO_2*] ranged between 3 mmol dm^{-3} H_20 in *Betula pendula* to a maximum of 11 mmol dm^{-3} H_20 in *Musanga cecropioides* (Table 5.7).

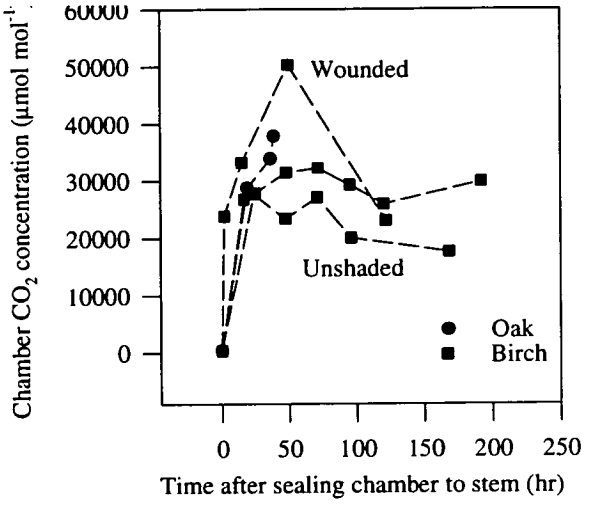

Figure 5.10. The increase in chamber CO_2 concentration with time. An equilibrium value of approx. 30,000 µmol mol^{-1} was reached after 24 hours. This value was lower in the unshaded chamber and higher when holes were drilled, apparently inducing wound respiration. These data were collected jointly with P. Levy.

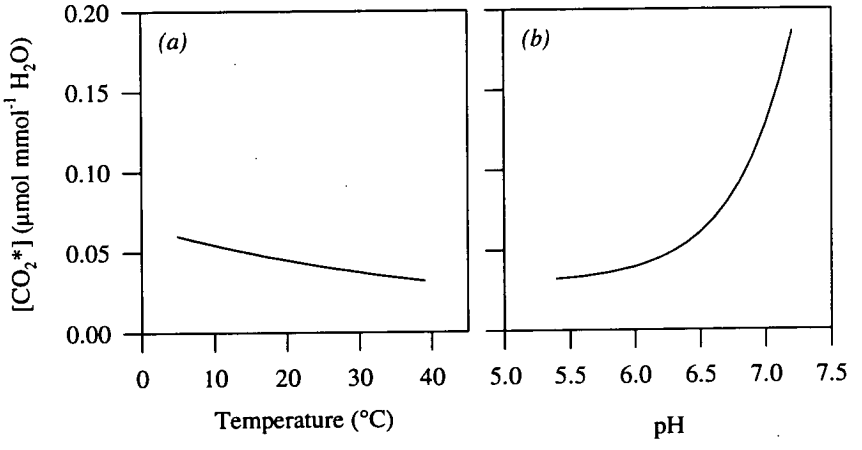

Figure 5.11. The effect of temperature and pH on [CO_2*], the concentration of all products of CO_2 dissolved in water. The data were calculated using Henry's Law (Equation 5.5) assuming that the water in the sap was in equilibrium with air at 30, 000 ppm CO_2 with a pH of 6.4 (a) and at 10°C (b). At both pH = 6.4 and 10 °C, the calculated value = 0.054 µmol CO_2 $mmol^{-1}$ H_20, or 3.02 mmol CO_2 dm^{-3} H_20.

Table 5.7. Sap CO_2 concentrations (in mmol dm^{-3}) in temperate and tropical trees. Temperature (°C) and pH values are also appended. Chamber [CO_2] is in µmol mol^{-1}. Values are means with 95% confidence limits in parentheses for pH and temperature, and the effects of these as calculated to produce [CO_2*].

Species	*Sap pH*	*Bark temp.*	*Chamber [CO_2]*	*[CO_2*]*	*n*
Betula pendula	6.4	10.0	30,000	3.02	1
M. cecropiodes	6.78 (0.2)	25.9 (2.0)	84,600 (5800)	11.01 (-4.97)	4
D. benthamianus	5.25 (0.17)	25.2 (1.9)	31,700 (1800)	1.21 (-0.17)	4

Using measured transpiration and photosynthesis rates for *B. pendula* in Scotland and *M. cecropiodes* or *D. benthamianus* in Cameroon, potential sap-sourced refixation was calculated to represent up to 30% of photosynthesis as measured using a cuvette, though estimated mean values were in the order of 1 - 10% (Table 5.8). The rate of re-fixation would have been greater at high sap pH and sap flow rates, and at lower temperatures (Figures 5.11a&b).

Table 5.8. Sap CO_2 refixation for *B. pendula* in Central Scotland and *M. cecropiodes* and *D. benthamianus* in SRF, Cameroon. A_l is a leaf typical photosynthesis rate, in µmol m^{-2} s^{-1}; *E* is a typical transipiration rate, in mmol m^{-2} s^{-1}; refixation rates are in µmol m^{-2} s^{-1}, temperature in °C. The errors in parentheses are 95% confidence limits for pH and temperature; for maximum and minimum refixation, the values were calculated using the ranges of values for A_l, *E*, pH and temperature. Typical photosynthesis and transpiration rates for *B. pendula* were provided by A. Rey (*personal communication*); for the trees in Cameroon the data are taken from Chapter 7. For comparison, an estimate for an arid-zone shrub from Niger, *Combretum micranthum*, is included (Levy, 1995).

Species	A_l	*E*	*pH*	*Temperature*	*Refixation rate*	*Refixation as % of A_l*
B. pendula	10	3	6.4	10.0	0.163	1.9
M. cecropiodes	4 - 14	1 - 4	6.78 (0.2)	25.9 (2.0)	0.129 - 1.225	5.4 (31 - 9)
D. benthamianus	4 - 14	1 - 4	5.25 (0.17)	25.2 (1.9)	0.019 - 0.101	0.6 (2.5 - 0.1)
C. micranthum	4.3	3.1	7	34	0.290	6.9

5.4 DISCUSSION

WOODY TISSUE TEMPERATURE AND THE RESPONSE IN CO_2 EFFLUX

Woody tissue temperature

The lower night-time bark temperatures at the canopy-top were probably a result of radiative cooling in both SRF and PRF. The two forests were distinguished by the higher maxima in PRF and deeper

daytime temperature profiles (Figure 5.1a&b). These differences probably reflected the more broken canopy in the secondary forest. Canopy gaps adjacent to the tower in Cameroon permitted light to penetrate to the forest floor at a several solar angles, creating a rather different temperature regime to that found in the closed canopy in Brazil.

The temperature response in CO_2 efflux

Assuming for the moment that other transport processes, such as sap flow, do not interact with diffusion of CO_2 through the bark, it is possible to model the temperature sensitivity of CO_2 production in wood. Without detailed biochemical data, many complex reaction series models reduce to behaving like an Arrhenius or an exponential function (Johnson & Thornley, 1985). The former is sometimes preferred as it encourages mechanistic rigour by requiring an activation energy (E) to be fitted to the data. However, this equation remains semi-empirical: in a reaction chain, activation energies may differ from one step to the next making an overall estimate of E uninformative. With an eye to parsimony, the simpler exponential function (Equation 5.2) was used here since the fit to the data was as good as or better than with the Arrhenius equation.

The fitted exponential temperature responses for both forests showed more variation among species in the value of R_o than k (Tables 5.2&5.3; Figures 5.2&5.3). Variation in R_o reflected differences in size, growth regimen and species, whilst k was likely to be more conservative as it refers to the biochemical processes of respiration. However there existed a general difference in temperature sensitivity between PRF and SRF: k was higher in the former (0.062; Q_{10} = 1.8 in PRF *vs* 0.044; Q_{10} = 1.6 in SRF). Possible causes for this discrepancy include differences between the forests in the rate of delivery of substrate to respiring cells, or removal of carbon dioxide from cells in the transpiration stream. The disturbed nature of the forest in Cameroon provides a basis for these hypotheses, but unfortunately they could not be addressed with these data. The Q_{10} values in both SRF and PRF were lower than the often-quoted general value of 2 (*e.g.*, Linder & Troeng, 1981; Butler & Landsberg, 1981). Q_{10} values may be reduced at higher temperatures (Hulett, 1956; Ninomiya & Hozumi, 1981), although the results here are within the range of reported values from other woody species (Q_{10} = 1.4 - 3.4; Hagihara & Hozumi, 1981).

THE RELATIONSHIPS BETWEEN R_t, D_w, R_c, AND R_m

The logarithmic relationship between D_w and R_t was strong for both forests, and though apparently similar (Figures 5.6a&b), the regressions were significantly different (Table 5.4). The broadly higher efflux rates found in SRF were hard to explain, though soil nutrient status and differences in growth regimen during the measurement period were probably responsible. At the stand level, variation among species was probably less important. The regressions in Table 5.4 required the assumption that the growth patterns in the sample of measured trees accurately represented the forest as a whole. In the absence of more detailed information, they provide an empirical basis for predicting R_t from D_w, but may be biased. Using a more functional approach, the physiological processes controlling the exchange of CO_2 in woody tissue can be split into respiration and cortical photosynthesis. The small dataset from SRF tentatively suggested that cortical photosynthesis may not cause large reductions in total efflux rates. To analyse R_t further, its respiratory components needed to be distinguished. Since data on sapwood volumes by species were not available, R_m was separated from R_c using the growth measurements from SRF.

The two estimates of R_m suggested that maintenance constituted the greater proportion (~80%) of total respiration (Table 5.5). This agreement was encouraging given the wide range of species, growth rates and stem sizes sampled. Between-species comparisons of R_m and R_c could not be made because of the range of growth rates, and the limited sample sizes. The proportionate contribution of R_c to R_t in SRF was very similar to that found for a mature rain forest species, *Minquarita guianensis*, in Costa Rica (R_c = 25% of R_t; Ryan *et al.*, 1994) though less than for a fast growing species in the same study (*Simarouba amara*, R_c = 46% of R_t). Few other comparative data exist for tropical trees, although Paembonan *et al.* (1991) reported an annual R_c of 21% for *Chamaecyparis obtusa*. The values obtained in this study point either to rather low growth rates or high maintenance costs. Without data for a full year it is difficult to choose, though recovery from previous logging disturbance (Chapter 2) could explain low growth rates for this secondary forest.

Area or volume based expressions of woody tissue respiration (Figure 5.5a-d) indicated that the source of CO_2 production in wood partly resided just below the bark (*viz*: the cambium and phloem cells) and partly the live volume (*viz*: the sapwood parenchyma); the ratio depended on D_w. To account for this R_m was expressed as a function of D_w according to Equation 5.4 and gave a better fit than was obtained using the logarithmic relationship between D_w and R_t (Tables 5.4 & 5.6). The variation that was unaccounted for by the fitted model can probably be ascribed to error because of the sample size and the assumptions made in calculating R_c. In particular, it is likely that different trees effect different

construction conversion efficiencies that reflect local resource transport needs and species-specific chemical defence strategies (Amthor, 1989). The single conversion efficiency used here smoothed out this detail. The R_m values at low D_w did not fit the curve so well, but relatively high twig respiration rates are quite common (Sprugel *et al.*, 1996) and may not be important at the stand scale. A functional interpretation of the relationship for larger woody sections identifies three stages, based on Figure 5.9:

1 $D_w < 0.03$ m. Surface area (SA) to volume (V) ratio dominated by SA.

2 0.03 m < D_w < 0.3 m. SA:V ratio becomes increasingly dominated by V as sapwood volume and associated living parenchyma cell numbers increase (*cf.* Table 5.6).

3 $D_w > 0.3$ m. Sapwood volume and associated living cells have reached a maximum. Continuing growth requires that the trunk expands radially, increasing the total SA of the tree, but CO_2 efflux on an area basis does not increase as the volume of living cells below any given point remains constant.

The stage transitions are not switches, they are gradual. Furthermore, the suggested 'break point' for stage **3** of 0.3 m is an estimate averaging for a large number of species; the true value for each species may vary significantly. If growing conditions differ greatly, intra-specific variation is also possible (Lehto & Grace, 1994). At D_w values greater than in stage **3**, sapwood volume increases very slowly as the leaf area of the tree (or branch) is hypothesised to reach an asymptote. Well accepted models of water transport within trees suggest that leaf area dictates sapwood volume on a supply/demand basis (Shinozaki *et al.*, 1964; Cannell & Dewar, 1994). In this view, as growth proceeds, the increase in leaf area will eventually stop, resulting in the sapwood volume of the tree also reaching a maximum (Friend, 1993), and hence causing the curve in Figure 5.9 to flatten. When Equation 5.4 was also applied to D_w:R_m data from four individual species in SRF (Figures 5.8b-e), it fitted well for *Musanga cecropioides*. The relatively simple architecture of *M. cecropiodes* probably contributed to a tightly constrained leaf area to sapwood volume ratio that would explain the high r^2 (0.95) in this species. The weaker fit in the other species may have been improved with larger sample sizes.

The preceding logic paves the way for a potential method of modelling whole-tree R_m using sapwood volumes: the same cross-sectional area of sapwood in the trunk is merely split up into branches in real crowns, and might be considered as a single column of cells the height of the tree. However this approach, which differs from the less accurate method of considering sapwood volumes in the bole only (*e.g.*, Ryan, 1989, 1990; Sprugel, 1990), would not account for the R_m of phloem and cambium

cells around the circumference of the separate branches in a real crown. Unfortunately data to test these hypotheses in tropical forest, where branches may constitute 20% of total above-ground biomass (Kato *et al.*, 1978; Chapter 3), is not readily available, though it may be so in the future (D. Deans, *personal communication*; *cf.* Ryan *et al.*, 1994)

Woody tissue respiration is not a simple function of surface area as has sometimes been assumed (*e.g.*, Whittaker & Woodwell, 1967; Landsberg, 1986). Above-ground woody tissue R_m for a forest stand may be estimated using a function of the form in Equation 5.4, given sufficient structural information. For an annual estimate of R_t, additional information is needed to account for annual forest growth, and hence R_c. Clearly more data are needed in these areas for tropical forests if precise values are required; more general estimates may be made using empirical models.

DISSOLVED CO_2 IN THE TRANSPIRATION STREAM

Measurements of both respiration and photosynthesis contain an implicit assumption that measured changes in CO_2 concentration within the chamber equate with all the activity in the enclosed leaf or woody stem. This experiment was designed to address the effect on such measurements of a high flux of CO_2 from the transpiration stream, originating from respiration in other parts of the plant.

The 'equilibrium' gas concentrations of CO_2 measured inside the purpose-built chamber were higher than the estimates of Hari *et al.* (1991), especially for the tropical trees (Figure 5.10; Table 5.7). Raven & Farquhar (1989) present data for pH and CO_2 in a gas phase equilibrium with xylem exudate for *Phaseolus vulgaris* that also show CO_2 concentrations of 20 - 30,000 ppm and a sap pH of 5.6 - 6.1, which are in line with the birch data. The sap CO_2 concentrations in Table 5.7 were within the range of other values obtained using isotope tracer techniques: 0.8 mmol dm^{-3} and 3 - 16 mmol m^{-3} (Marshall *et al.*, 1994) for mistletoe, and 22 mmol dm^{-3} found for *Juniperus osteosperma* (Marshall & Ehleringer, 1990).

Carbon dioxide present in the sap may diffuse outwards through the stem, or be re-fixed, primarily by leaf photosynthesis. The re-fixation rates estimated in Table 5.8 suggest a mean of 1 - 10%, though the maximum value for *Musanga cecropioides* was 30%. These data are in approximate agreement with an estimate for the arid-zone tropical shrub, *Combretum micranthum* (6.9%; Levy, 1995). In the case of *Musanga cecropioides*, the high re-fixation rate is of some speculative interest given the very fast growth rate of this species. High levels of dissolved inorganic carbon similar to those measured

here have been associated with markedly increased biomass production in *Salix* (Bergquist, 1964; Pelkonen *et al.*, 1985; Vapaavuori & Pelkonen 1985; Vuorinen *et al.*, 1989). If this phenomenon is real, and occurs in *M. cecropoides*, high sap pH may be maintained to facilitate fast growth.

The interaction of sap CO_2 concentration with cuvette-based measurements is more difficult to account for in measurements of woody tissue effluxes. It introduces an unknown bias and may hinder attempts to separate maintenance and growth respiration, especially at high sap flow rates. Similarly, the underestimate inherent in photosynthesis calculations is likely to introduce error into models formulated using cuvette-derived data that estimate total fluxes for a single component of a forest ecosystem. However, the problem does not extend to overall carbon budget estimates as 'losses' in the measurement of one component may be balanced by gains in another. This holds true for both cuvette and eddy-covariance techniques.

5.5 CONCLUSIONS

Effluxes of CO_2 from woody tissue were measured on 24 tree species in PRF, Brazil and 17 tree species in SRF, Cameroon. Total efflux rates ranged between 0.2 and 5.2 μmol m^{-2} s^{-1}. The temperature responses for CO_2 efflux were lower for secondary forest (Q_{10} = 1.6) than for primary forest (Q_{10} = 1.8); both figures are within the range reported in the literature. Using growth measurements, maintenance respiration rates were calculated to constitute approximately 80% of total woody tissue respiration for SRF. A functional relationship between R_m and D_w was developed to take in to account the differential dominance of surface area and volume components contributing to R_m. This model explained 66% of the variation in the data for all species and 95% of the variation for one species, *Musanga cecropioides*. An empirical, logarithmic model linking D_w and R_t was also presented for data from Brazil and Cameroon. The model for each forest, though not functionally based, explained 62% and 42% respectively of the variation in the data.

Sap CO_2 concentration was measured in trees in Scotland and Cameroon. This CO_2 interacts with the fluxes of CO_2 to and from trees and can therefore affect the calculation of respiration and photosynthetic parameters obtained from flux measurements. The measured sap CO_2 concentrations were calculated to lead to underestimates of up to 30% of cuvette-derived photosynthetic rates, though the range 1 - 10% may be more common. These values were particularly sensitive to sap pH, transpiration rates and temperature.

6. Respiration in leaves at night

6.1 INTRODUCTION

The respiration of foliage in the dark consumes carbohydrate resources in order to fuel cellular metabolism. Energy and metabolites released in respiration are divided in their destinations among: tissue construction processes, maintenance and repair of existing biomass, particularly proteins, the transport of metabolites, and the upkeep of cellular ion gradients (Amthor, 1989). At an ecosystem level, the annual carbon cost of foliage respiration, as a fraction of total assimilation, has been estimated in temperate forests to range from 9% for a twenty-year old *Pinus sylvestris* L. stand (Linder & Axelsson, 1982; Linder, 1985) to 21% in a *Pinus contorta* Dougl. stand (Benecke & Nordmeyer, 1982). Few data are available for the tropics, although Yoda (1983) estimated leaf respiration to constitute approximately 50% of total above-ground biomass respiration, a value that we will see agrees with the up-scaled estimates for the present work (Figure 8.8).

Whilst photosynthesis is relatively well understood (*e.g.*, Farquhar & von Caemmerer, 1982; Field & Mooney, 1986), respiratory leaf physiology has received less attention. Given the important role played by leaf respiration in the forest carbon cycle, further research is needed to model adequately respiratory CO_2 fluxes from foliage. In particular, maintenance requirements for leaves are not well parameterised. There already exist methods by which the carbon cost of leaf synthesis can be estimated using foliar elemental composition, organic nitrogen, or ash-free carbon content (McDermitt & Loomis, 1981; Williams *et al.*, 1987; Vertregt & Penning de Vries, 1987), but there is no model in general use for predicting leaf maintenance requirements.

The link between respiration rate and tissue nitrogen content has been known for over forty years (James, 1953). Similarly, carbohydrate levels have also been correlated with respiration rates (*e.g.*, Baysdorfer *et al.*, 1987), though fewer studies have looked at other leaf tissue elements in this context. The focus on nitrogen is unsurprising since most organic nitrogen in leaves is in protein, and 60% of maintenance respiration goes towards protein repair and replacement (Penning de Vries, 1975). Indeed, linear relationships between nitrogen and respiration in leaves have been found in many studies (*e.g.*, Kawahara *et al.*, 1976; Waring *et al.*, 1985). However it is not always the case that total nitrogen concentrations represent accurately the nitrogen that is the subject of maintenance activities.

Free amino acids, or nitrogen buried in structural molecules, may not reflect the metabolic status of a cell, and may thereby introduce noise into any relationship between respiration and nitrogen concentration (McCree, 1983; *c.f.* Aber *et al.*, 1989; Brooks *et al.*, 1991; Ryan, 1994). It is possible that the introduction of phosporus into a model predicting leaf respiration may help to account for some of the variance. A general model of this kind is especially attractive given the connection then possible between models of other processes limited by nitrogen and phosphorus, such as photosynthesis (Field & Mooney; 1986; Reich *et al.*, 1994) and litter decomposition (Parton *et al.*, 1988; Carlyle, 1986)

The dark respiration of leaves measured during the daytime, and after correction for temperature, has been shown elsewhere to be 40% higher than that measured during the night (Hubbard *et al.*, 1995), which suggests it is important to make measurements overnight. In this study, foliar respiration was measured in PRF and SRF. The initial focus of the work was to record the night-time characteristics of leaf respiration throughout the canopy of tropical forest, and to parameterise the temperature response of this process. The hypothesis was then tested that variability in respiration among leaves of different species and at different heights would collapse onto a single relationship governed by temperature and leaf chemical composition.

6.2 METHODS

LEAF RESPIRATION AND NUTRIENT ANALYSIS

Respiration measurements were made by placing leaves in a photosynthesis leaf chamber (Licor, Nebraska, USA) attached in a closed circuit to an IRGA (Licor 6200, Licor, Nebraska, USA). Measurements were made at ambient temperature and humidity during the night. Leaf temperature was measured using the proprietory leaf chamber thermocouple. Access to leaves through the vertical profile of the canopy was obtained using the micrometeorological tower at each site.

In order to measure maintenance respiration (R_m), measurements were made on fully expanded (but not apparently senescing) leaves from different species. Leaves at different heights in the canopies of PRF and SRF were accessed from a micrometeorological tower (Table 6.1) and measured at intervals throughout the night. In Brazil, measurements were made on the nights of 25th May and 4th June,

1993, and in Cameroon on the 11th and 22nd March 1994. Immediately after the final measurement was taken, most of the measured leaves were removed. In a few cases in SRF, leaves were also being used for the measurement of photosynthesis; these were removed after a delay of a maximum of 5 days. In the field laboratory, leaf area measurement was not possible, so leaves were carefully flattened and photocopied. Leaf area was measured using a pre-calibrated Delta-T leaf area meter (Delta-T Devices Ltd, Cambridge, UK) upon return to Edinburgh. A leaf corer was used to obtain 10 - 20 discs of known area (diameter = 16 mm, Brazil; 10 mm, Cameroon) from each fresh sample. All leaf material was then oven-dried at 70 °C to constant mass. Specific leaf area determinations were made using a precision balance (Sauter Re1614, Albstadt, Switzerland; maximum sensitivity = 0.0001g). Leaf total nitrogen and phosphorus concentrations were determined using a standard wet digestion (Allen, 1974) in Edinburgh (leaves from Cameroon). The leaves from Brazil were analysed at ANU, Canberra for soluble sugars, starch, total non-starch carbohydrate, leaf nitrogen and leaf phosphorus concentrations. In total, approximately 35 leaves were measured from each forest; those from PRF were grouped by species before nutrient assays were done, whilst those from SRF were treated individually where possible.

Table 6.1. Species and height (m) in canopy of leaves measured for respiration during the night in Brazil (1993) and Cameroon (1994). Each species was identified by botanists from national herbaria in Belém (Brazil) and Yaoundé (Cameroon); specimen samples were deposited in the respective herbaria. The / marks denote leaves found at more than one height. *h* is height, in m.

BRAZIL			CAMEROON		
Species	*Family*	*h*	*Species*	*Family*	*h.*
Maximiliana maripa (Corre Serra) Drude	Palmae	1	*Hypsodelphis violacea* (Ridl.) M-Redh.	Marantaceae	1
Naucleopsis krunni (Standl) C.C. Berg	Moraceae	1	*Dichapetalum sp.*	Dichapetalaceae	1
Theobroma microcarpum Mart.	Sterculiaceae	1	*Afromomum giganteum* (Oliv. & Harb.) K. Schum.	Zingiberaceae	1
Erythroxylum c.f.*macrophyllum* Cav.	Erythroxylaceae	3	*Trichilia sp.*	Meliaceae	1
Leonia glycicarpa Ruiz	Violaceae	10/16	*Musanga cecropioides* R.Br.	Moraceae	1/22 -26
Derris pterocarpa (DC) Killip	Leguminseae (Papilionoideae)	20	*Haumania dankelmaniana* M-Redh.	Marantaceae	3
Protium polybotrium (Turcz) Engl.	Burseraceae	20	*Staudtia stipitata* Warb.	Myristicaceae	7
Inga sp. (*nobilis* or *capitata*)	Leguminoseae (Mimosoideae)	26/32	*Celtis adolfi-friderici* Engl.	Ulmaceae	12/14
Strychnos amazonicus Krukoff	Loganaceae	30/32	*Amphimas pterocarpoides* Harms.	Leguminoseae (Caesalpiniaceae)	36/40
Cedrela odorata L.	Meliaceae	36			

6.3 RESULTS

LEAF TEMPERATURES

Leaf temperature in both forests declined over the nocturnal cycle. Leaves at the top of the canopy commenced the night at higher temperatures and cooled to lower temperatures by morning in comparison to those near ground level. The main difference between the two forests was in the greater decoupling of leaves at ground level in PRF over those in SRF. This resulted in steeper and more closely defined pre-dawn temperature gradients in Brazil (Figure 6.1). The absolute temperatures were similar for both forests, though the range was greater for SRF (25 - 18 °C) than for PRF (25 - 21 °C); if measurements had been made during a *friagem* period in Brazil the PRF minimum would have been lower.

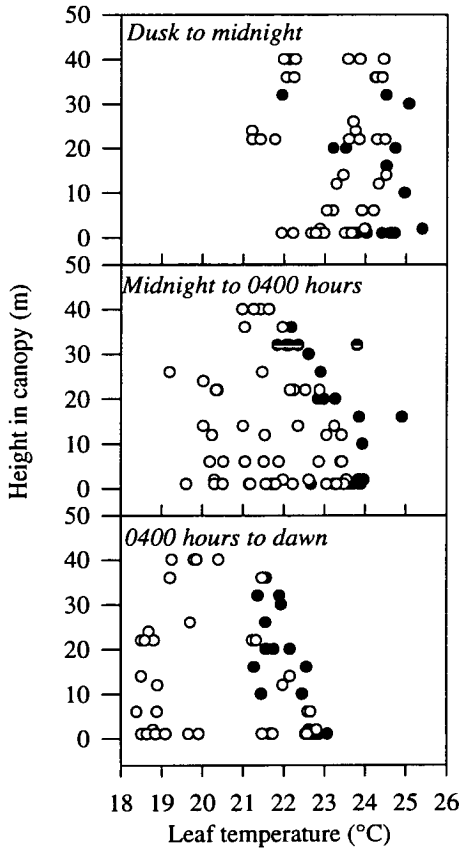

Figure 6.1. Leaf temperature during the night through the vertical profile of the canopy in SRF (open circles), and PRF (spots). The measurement dates were May/June, 1993 (PRF) and March, 1994 (SRF).

LEAF RESPIRATION RATES

Figures 6.2a-d show nocturnal cycles in raw leaf temperatures and respiration rates for two species from Brazil and two from Cameroon. The traces for *C. adolfi-friderici* and *L. glycicarpa*reveal a pre-dawn rise in respiration that changes in counterpoint to leaf temperature, whilst *A. ptercarpoides* and *N. krunnii* show a pre-dawn drop in leaf respiration. This reduction is greater than would be expected given the measured foliar cooling, and assuming a Q_{10} of 2.0. Patterns of this sort in pre-dawn leaf respiration were not consistent with species or height. In contrast, for measurements made before 0100 hrs, the temperature response of all leaves was more similar, with Q_{10} values around two. Some variation in the measured Q_{10} values occurred probably as a result of the very small temperature ranges from which they were obtained (Table 6.2.). A few of the species enumerated in Table 6.1 are not represented in Table 6.2 as in these cases insufficient measurements were made before 0100 hrs to calculate a temperature response.

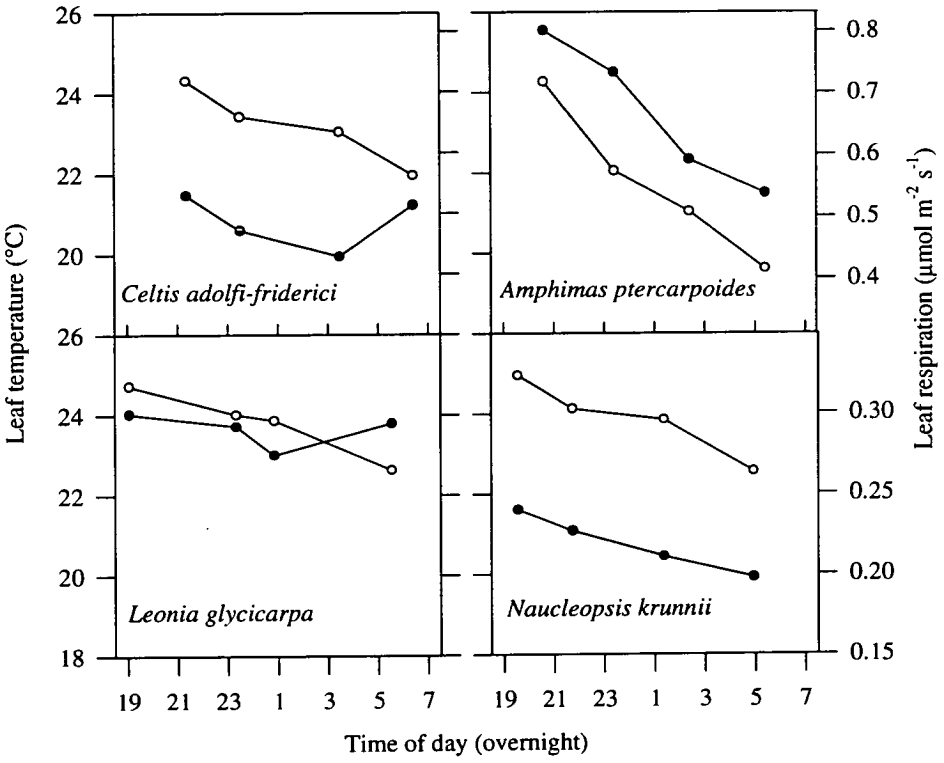

Figure 6.2a-d. Night-time traces in leaf temperature and respiration for two species from SRF (a) and (b) and PRF (c) & (d). The spots are leaf respiration and the open circles are leaf temperature

All leaf respiration rates were normalised to 22 °C using a Q_{10} of 2.0, and compared by height in the canopy (Figure 6.3). The patterns for SRF and PRF are rather similar: CO_2 effluxes remained constant up to 10 m, followed by a steep rise between 10 m and 20 m to maxima at 25 m (SRF) and 30 m (Brazil). Both canopies were divided into five strata (0-5 m; 5-15 m; 15-25 m; 25-30 m and 30-40 m) and the composite respiration rates compared. Leaf respiration at 22 °C was significantly larger ($p <$ 0.01 for each stratum) in the secondary forest in Cameroon than in the primary forest in Brazil.

Table 6.2. Estimated temperature responses in leaf respiration before 0100 hrs from SRF and PRF. The all species value is the mean, with the 95% confidence in parentheses.

PRF		SRF	
Species	Q_{10}	*Species*	Q_{10}
Maximiliana maripa	1.5	*Amphimas ptercarpoides*	1.8
Theobroma microcarpum	2.1	*Musanga cecropoides*	1.6
Naucleopsis krunnii	2.9	*Afromomum giganteum*	2.1
Inga sp.	1.7	*Staudtia stipitata*	3.1
Leonia glycicarpa	1.9	*Hypsodelphis violacea*	1.7
Derris pterocarpa	4.1	*Celtis adolphi-friderici*	1.9
All species	2.3 (1.7)	All species	2.0 (0.9)

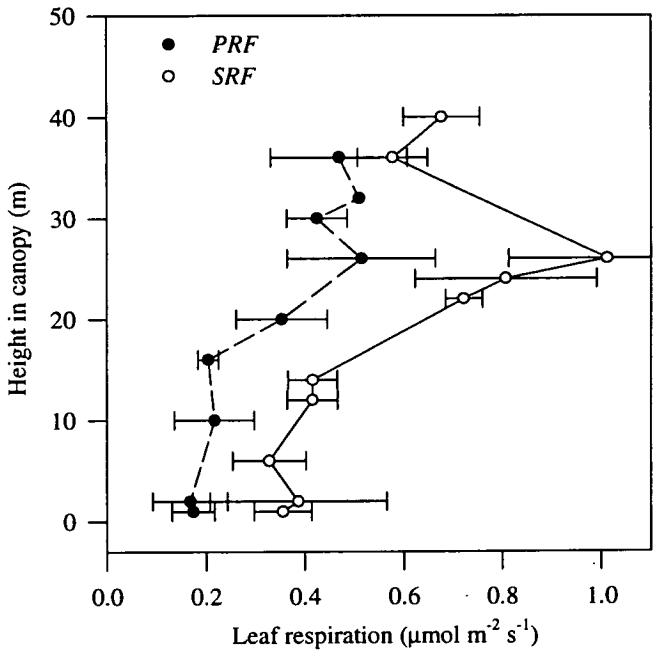

Figures 6.3a&b. Variation in night-time leaf respiration (leaf area basis) with height in SRF and PRF. The error bars are 95% confidence; n = 1 - 3 in PRF and 2 - 4 in SRF. Respiration rates are normalised to 22 °C.

Data were not processed as an analysis of variance by species and height, since most species occurred once only, at only one level. Among the exceptions to this, only one species, *Musanga cecropioides* in Cameroon, had a sufficient vertical separation between samples to show a significant difference in respiration rate between heights (respiration = 0.44 μmol m^{-2} s^{-1} at ground level [at 21.2 °C] and 0.80 μmol m^{-2} s^{-1} at 24 m [at 22.3 °C]; $p < 0.001$). In Brazil, at ground level, the palm *M. maripa* gave a significantly lower respiration rate ($p < 0.05$) than the other two species measured. In Cameroon, also at ground level, *H. violacea* and *Dichapetalum sp.* were grouped, with significantly lower leaf respiration rates ($p < 0.05$) than the other three species at this height, *A. giganteum, Trichilia sp.*, and *M. cecropioides.* In PRF, near the top of the canopy, comparisons were possible between *P. polybotrium.* and *D. pterocarpa* at 20 m, and between *Inga sp* and *S. amazonicus* at 30 m. For both, the latter of each pair was a liana species and showed significantly higher respiration rates ($p < 0.05$).

VARIATION IN LEAF RESPIRATION WITH NUTRIENT CONCENTRATION

The patterns in Figure 6.3 could have resulted from differences in leaf structure or nutrient concentration, or both. Figure 6.4 indicates that the varation in R_m with height, as expressed on an area basis, was strongly related to leaf thickness (specific leaf area, SLA; see also Figure 3.6). The variation with height in leaf nitrogen (N_{leaf}) and phosphorus (P_{leaf}) in the canopies of PRF and SRF was examined (Figures 6.5a-d). At the bottom level (first 2 m) there there was some variation among leaves, but above this the area-based nutrient content increased with height, with a larger relative change for N_{leaf}. Mass-based N_{leaf} and P_{leaf} did not show a clear gradient with height; when they were related to R_m (as g C g^{-1}) a significant correlation was found only with the P_{leaf} data for PRF (Figures 6.6a-d; Table 6.3). The nutrient concentrations in SRF were higher than in PRF, particularly so for P_{leaf}. The relationship between N_{leaf} and R_m was dissected further by reference to a molar ratio, R_m:N_{leaf} (μmol C s^{-1} [mol N]$^{-1}$). The molar R_m:N_{leaf} ratio was larger at greater heights: leaves at the top of the canopy in both forests appeared to respire at a faster rate *per* unit nitrogen than those at the bottom, though significant differences in R_m:N_{leaf} were only found between some heights (Table 6.4).

In the absence of a strong mass-based R_m - leaf nutrient relationships, regressions of R_m on N_{leaf} and P_{leaf} were calculated on an area basis (Figures 6.7a-d & Table 6.5a); only the regression for N_{leaf} in PRF was non-significant ($p = 0.06$). The intercepts for the overall N_{leaf} and P_{leaf} regressions were not significantly different from zero at the 95% level. R_m was also related to N_{leaf} and P_{leaf} in a multiple linear regression (Table 6.5b). Measured leaf respiration rates agreed well with modelled rates using this function (Figure 6.8; in SRF, $p < 0.001$, $r^2 = 0.68$; in PRF, $p < 0.01$, $r^2 = 0.66$). The intercept was

only significantly different from zero (95% level) for SRF and not for PRF (Table 6.5b). In addition, nitrogen was not a significant variable for the multiple regression in PRF, though phosphorus was ($p > 0.8$ *vs* $p < 0.001$). From the data available, R_m measured in PRF did not appear to scale with leaf carbohydrate concentrations(Figure 6.9).

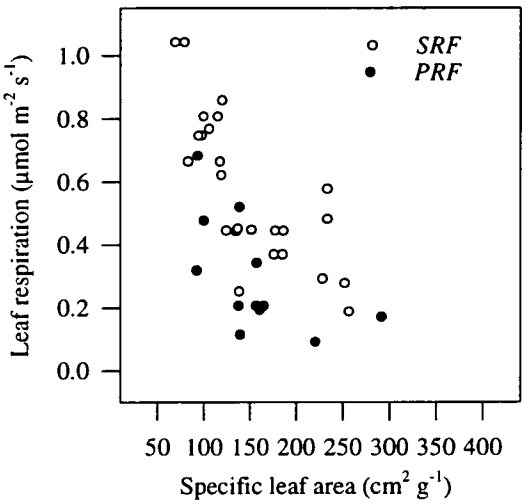

Figure 6.4. The variation in leaf respiration rate with specific leaf area (SLA) in SRF and PRF.

Table 6.3. Results for mass-based single regressions between R_m and P_{leaf}, where R_m is in g C g^{-1} s^{-1} and P_{leaf} is in g g^{1}. Errors in parentheses are 95% confidence limits. The data are for PRF, PRF + SRF and SRF..

Forest	*Element*	*Intercept*	*Co-efficient*	*p - value*	r^2	*n*
PRF	P	2.1 x 10^{-9} (3x10^{-8})	1.0 x 10^{-4} (8x10^{-5})	0.02	0.47	12
SRF	P	7.3 x 10^{-8} (4x10^{-8})	1.4 x 10^{-5} (3x10^{-5})	0.33	0.04	25

Table 6.4. R_m:N_{leaf} ratio in μmol C s^{-1} [mol N_{leaf}]$^{-1}$ at different heights in the canopies of SRF and PRF. Errors in parentheses are the 95% confidence limits.

Ht(m)	*SRF: R_m:N_{leaf}*	*n*	*PRF: R_m:N_{leaf}*	*n*
36-40	4.17 (0.33)	4	4.71 (0.52)	2
22-26	5.45 (0.66)	7	2.57 (1.19)	2
12-14	3.31 (0.44)	3	1.61 (0.35)	2
7	3.54 (1.89)	2	--	--
2	4.60 (0.67)	2	2.44	1
1	2.59 (0.73)	4	1.43 (0.35)	3

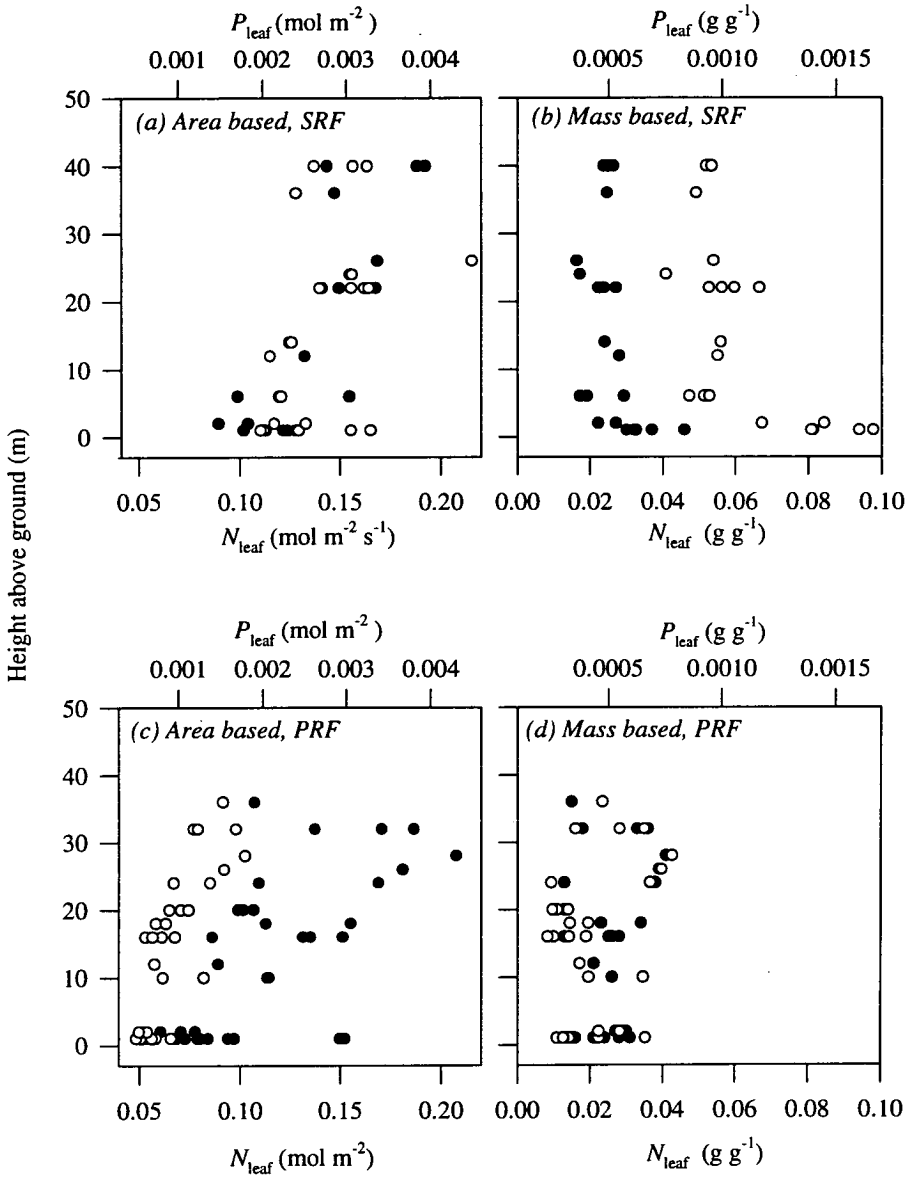

Figures 6.5a-d. Variation in N_{leaf} and P_{leaf} with height in the canopy for SRF and PRF. Data are expressed on an area and mass basis; the nitrogen data are spots and the phosphorus data are open circles.

Table 6.5a. Results for area-based single regressions between R_m and N_{leaf} or P_{leaf}, where R_m is in μmol m^{-2} s^{-1} and N_{leaf} or P_{leaf} are in mol m^{-2}. Errors in parentheses are 95% confidence limits. The data are for SRF and PRF.

Forest	*Element*	*Intercept*	*Co-efficient*	*p - value*	r^2	*n*
SRF	N	-0.25 (0.37)	6.04 (2.70)	< 0.001	0.52	22
SRF	P	-0.25 (0.34)	306.9 (123)	< 0.001	0.57	22
PRF	N	-0.02 (0.35)	2.59 (2.8)	0.06	0.30	12
PRF	P	-0.09 (0.21)	397.1(199)	0.001	0.66	12

Table 6.5b. Results for the area-based multiple regressions between R_m and N_{leaf} and P_{leaf}, where R_m is in μmol m^{-2} s^{-1} and N_{leaf} and P_{leaf} are in mol m^{-2}. Errors in parentheses are 95% confidence limits. The form of the relationship between respiration and nutrient content is $R_m = aN_{leaf} + bP_{leaf} + c$. The data are for SRF and PRF.

Forest	*a*	*b*	*c*	*p - value*	r^2	*n*
SRF	0.247(0.09))	205.7(65.8	-0.45 (0.17)	< 0.001	0.68	22
PRF	-0.243 (2.9)	414 (298)	-0.08 (0.2)	0.007	0.66	12

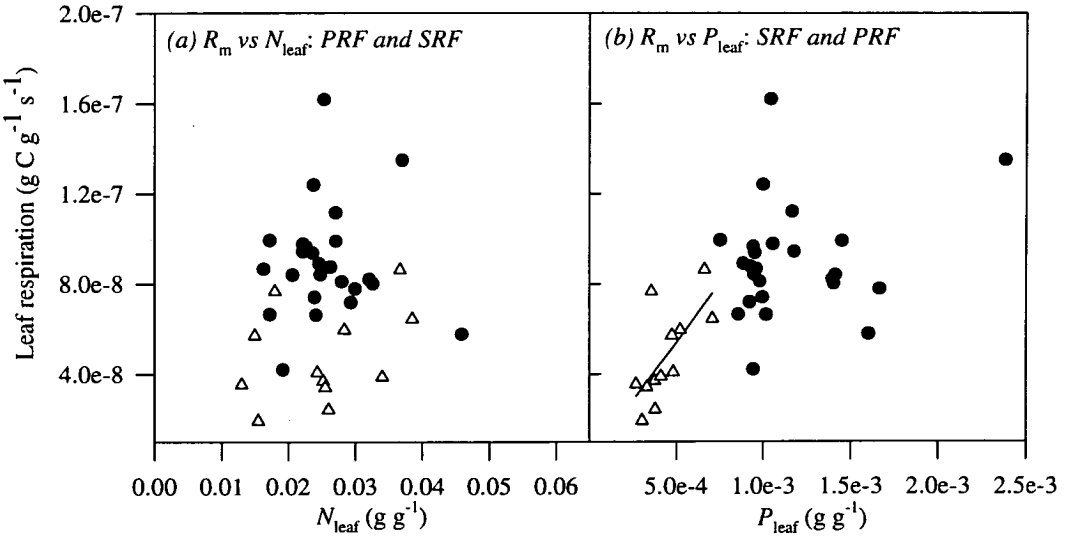

Figures 6.6a&b. The variation in leaf respiration with (a) N_{leaf} and (b) P_{leaf} as expressed on a mass basis. The PRF data are the open triangles and the SRF data are the spots. The regression line is plotted for R_m *vs* P_{leaf} from PRF ($p < 0.05$); the remaining plots show no significant correlation.

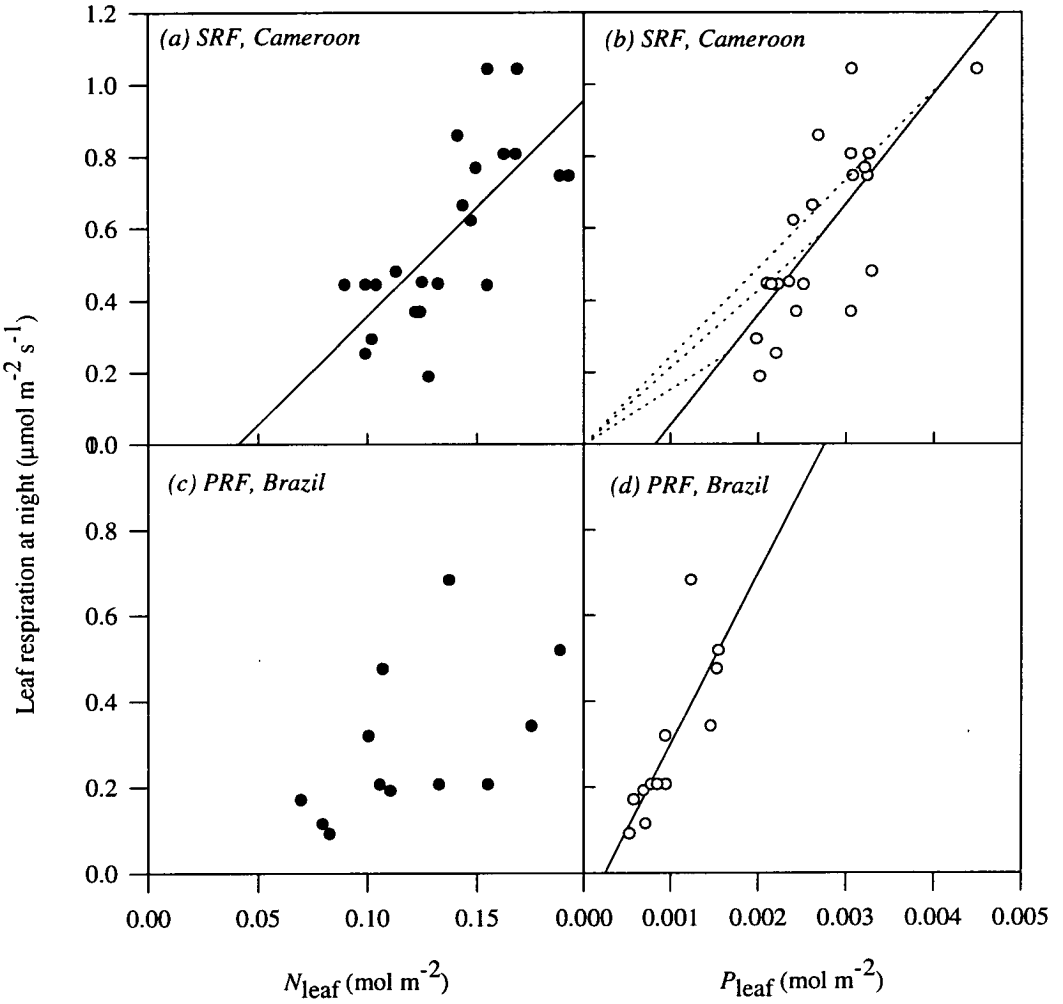

Figure 6.7a-d. The variation in leaf respiration with N_{leaf} and P_{leaf}, expressed on an area basis. The nitrogen data are spots and the phosphorus data open circles. In (a) and (b), data from SRF refer to individual leaves; in (c) and (d), data from PRF are species averages at each height (n = 4 - 16). The data in plot (c) showed no significant correlation, so no line has been drawn; the regression results for all the graphs are given in Table 6.5a. The dashed lines on (b) represent R_m:N_{leaf} ratios at differents heights (see Discussion)

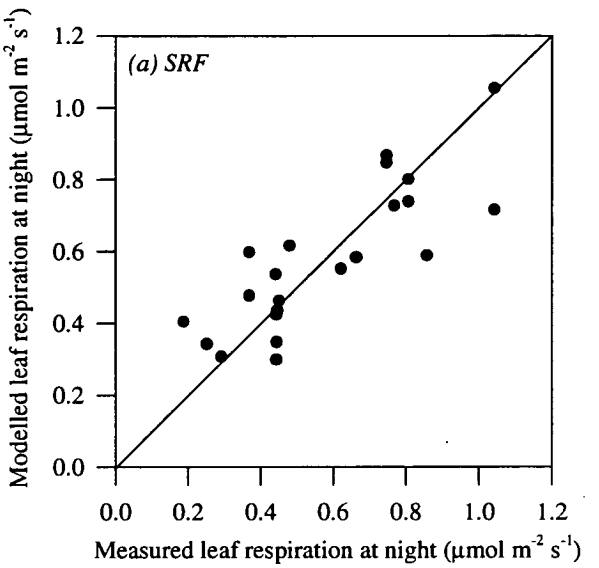

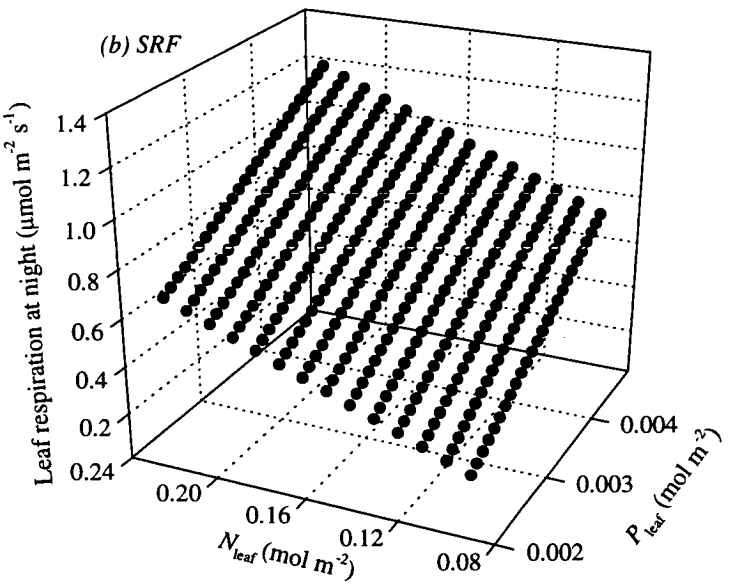

Figures 6.8a&b. The multiple regression of R_m on N_{leaf} and P_{leaf} in SRF. The PRF multiple regression is not shown as it was not significantly better than with P_{leaf} alone (see text). Figure (a) shows measured *vs* modelled leaf respiration for SRF and Figure (b) shows the model results for P_{leaf} and N_{leaf} over their measured physiological ranges The r^2 value for the SRF model is 0.68.

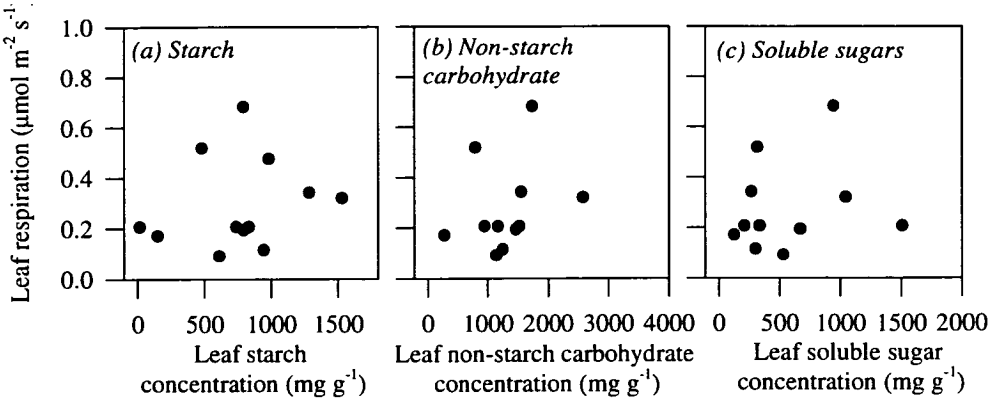

Figure 6.9a-c. The variation in leaf respiration at night in PRF with the concentration of different leaf carbohydrates. No significant correlations were found.

6.4 DISCUSSION

Leaf respiration rates tend to be low, and consequently even measurements using a closed IRGA system, as used here, may be made near the limits of instrument sensitivity, thereby introducing noise into the data. However, most measured chamber - atmosphere CO_2 differentials were 15 - 50 times the sensitivity of the Licor 6200 IRGA, suggesting that the data were unlikely to have been swamped by random instrument error.

The lower temperatures of leaves during the night the near the ground in SRF may have resulted from better coupling than in PRF because of the more open canopy structure; also stable meteorological conditions during the night were more prevalent in PRF (Grace *et al.*, 1995a; Grace *et al.*, unpublished). Leaf respiration was determined by leaf temperature in a fairly regular manner before the pre-dawn period; Q_{10} values were in the region of two, as found elsewhere (Amthor, 1989; Ryan, 1991). The larger temperature ranges experienced in Cameroon reduced the variability in calculated Q_{10} values by comparison to those from Brazil.

Leaves exhibited inconsistent patterns of pre-dawn respiration. The two extremes of this behaviour were seen as increases in respiration against the prevailing temperature regime, or greater decreases than than expected given the rate of foliar cooling (Figure 6.2). The former condition might be explained by reference to entrained physiological rhythms generating elevated metabolic rates just before dawn in preparation for photosynthesis, though there is little experimental evidence for this

phenomenon. The latter condition implies that the factors determining the respiration rate changed at the end of the night from temperature and oxygen availability to carbohydrate supply. Measurements of excised leaf sections have shown that soluble sugar levels do not limit night respiration in some temperate trees (Collier *et al.*, 1992), though the period of darkness during that study was approximately 17% less than that of the two tropical rain forests studied. Furthermore, the tropical forest temperatures here were higher by 4 - 8 °C than those for the temperate trees.

There are almost no data on the variation in leaf respiration rates through the vertical profile of tropical forest canopies. What physiological information there is usually extends only to photosynthetic parameters (Roberts *et al.*, 1990; Koch *et al.*, 1994; McWilliam *et al.*, 1996). In this study, respiration rates in leaves at a given height were consistently higher in SRF than in PRF (Figure 6.3). As all the measured leaves were fully expanded, this represents a difference in foliar maintenance respiration rates (R_m; in $\mu mol^{-2} s^{-1}$) between the forests.

Variation in R_m is likely to result from differences in physiology engendered by prevailing light and nutrient availability. Amthor (1994) defines R_m as a function of canopy leaf nitrogen content, N_{leaf}, and three physical states relating to temperature, ambient CO_2 concentration and incident photon flux density. For individual species, there is evidence that R_m increases linearly with N_{leaf} (Kawahara *et al.*, 1976; Jones *et al.*, 1978; Irving & Silsbury, 1987), though Byrd *et al.* (1992) did not find a relationship. Since 50 - 60% of maintenance respiration is attributed to protein turnover (Penning de Vries, 1975), an R_m - N_{leaf} correlation might be expected, though if a large proportion of N_{leaf} is in the form of free amino acids rather than protein, then departures from the relationship are possible. Photoynthetic capacity is also related to N_{leaf} (Field & Mooney, 1986), so it is possible that carbohydrate synthesis during the preceding light period may further determine R_m values (Byrd *et al.*, 1992; Azcon-Bieto & Osmond, 1983; Ryan, 1994) though the effect may be slight.

Leaf nutrient and physiological data have been expressed in the literature on both a mass and area basis (*e.g.*, Reich & Walters, 1994; Reich *et al.*, 1994; Evans, 1989). In both SRF and PRF, R_m varied on an area basis with nutrient concentration, height, and accordingly by leaf thickness (*cf.* Figure 3.6; Figures 6.3 - 6.5, 6.7). But any trends were generally non-significant when values were expressed on a leaf mass basis (Figures 6.5 & 6.6). The P_{leaf} data for PRF were an exception to this (Table 6.3) and highlighted a distinguishing feature of the leaves there (see discussion below). The R_m ($gC\ g^{-1}$) *vs* N_{leaf} ($g\ g^{-1}$) relationship was particularly weak (Figure 6.5), a result contrasting with that of Ryan (1994). His regression for 14 boreal and subalpine tree species was forced through the origin (apparently

without justification), and showed variation within and among species about the fitted line, although the relationship was significant. However, the range of Ryan's N_{leaf} values was large (0.005 - 0.04 g g^{-1}). It is possible that a wider range of N_{leaf} in the samples for my study would have changed the result, but incorporation of N_{leaf} data from PRF with SRF did not generate a significant relationship.

Alternatively, it may be that R_m is not precisely related in a universal way to N_{leaf} on a mass basis. Leaves at the top of the canopy appeared to respire at a faster rate for a given nitrogen concentration than those lower down (Table 6.4). This suggested that either respiration in these leaves was more 'nitrogen-efficient' or that a greater percentage of N_{leaf} was involved in respiratory processes. The latter hypothesis is more reasonable since leaves at the top of the tower were thicker, and so contained less structural nitrogen relative to 'metabolic' nitrogen than the thinner leaves near the ground.

R_m:N_{leaf} molar ratios have been reported for data from crops, ryegrass, boreal trees and subalpine trees (Table 6.6). The R_m:N_{leaf} ratio in leaves in the upper canopy for SRF and PRF was approximately double the values obtained elsewhere; since the non-tropical values were normalised to 10 °C, this discrepancy is most directly explained by the difference in temperature at which the data were obtained, assuming a Q_{10} of two. Further variation among the estimates may result from R_m and Q_{10} values varying slightly between 10 and 22 °C (Amthor 1984; Ryan, 1994; Amthor, 1994).

Differences in the R_m:N_{leaf} ratio between 'sun' and 'shade' leaves were not significant in boreal and subalpine species (Ryan, 1994). Using height as a surrogate for the light environment, Table 6.4 suggested a decline in R_m:N_{leaf} from 'sun' leaves (top) to 'shade' leaves (ground) in both PRF and SRF. Variation in the pattern partly reflected species differeces, but it is possible that this variation also reflected the different average radiation flux experienced by the individual leaves that were sampled. The high R_m:N_{leaf} at 2 m in SRF indirectly supports this, given the canopy gaps present at this site. Assuming a close linkage between photosynthesis and respiration, these data are consistent with a theory of optimal nitrogen allocation within a forest canopy (*e.g.*, Sellers *et al.*, 1992; Schulze *et al.*, 1994) and assuming an additional term to account for differences in total leaf nitrogen because of differences in structure among leaves.

Table 6.6. The R_m:N_{leaf} ratio expressed as μmol C s^{-1} [mol N_{leaf}]$^{-1}$ for SRF and PRF (upper canopy leaves), crops, ryegrass, boreal trees and subalpine trees and shrubs.

Vegetation type	R_m:N_{leaf}	*Temperature*	*Source*
Crops and 'wild-land tissues'	1.48	10 °C	Ryan 1991
Ryegrass	2.26	10 °C	Jones *et al.*, 1978
Boreal/Subalpine trees	2.26	10 °C	Ryan 1994
Tropical rain forest (SRF)	4.15	22 °C	This study
Tropical rain forest (PRF)	4.71	22 °C	This study

The area based R_m - leaf nutrient relationships in PRF and SRF produced significant regressions for each forest. The high r^2 value of 0.68 for the multiple regression of R_m on N_{leaf} and P_{leaf} in SRF suggested that it is a reasonable predictor of leaf respiration for that forest (Figure 6.8). The residuals for both the N and P coefficients (not shown) were not skewed, adding strength to the predictive capacity of the model across the full range of N_{leaf} and P_{leaf}. However, N_{leaf} was not a significant variable in the multiple regression of R_m on N_{leaf} and P_{leaf} for PRF. N_{leaf} and P_{leaf} values for the primary forest in Brazil were lower than in SRF. The difference was most marked with P_{leaf} which in Cameroon was almost double the levels found in Brazil (700 - 2000 μmol m^{-2} in Brazil, *vs* 2-4000 μmol m^{-2} in Cameroon). The differences in P_{leaf}, rather than N_{leaf}, explain the overall variation in R_m observed between SRF and PRF; this is supported by the significant regressions between R_m and P_{leaf} in PRF on either a mass or area basis, but the non-significant relationships with N_{leaf} (Tables 6.3 & 6.5a). The data suggest that P_{leaf} determined [was limiting] leaf respiration in PRF, whilst in SRF both N_{leaf} and P_{leaf} determined respiration. Low phosphorous availability in PRF, a common feature of Amazonian soils (Stark & Jordan, 1978; Nadkarni, 1981) could have been the cause of this discrepancy.

The intercepts on the ordinates of the respiration - leaf nutrient relationships in Figure 6.7 are also of interest. They are not significantly different from zero, a result consistent with the frequent assumption that the regression crosses the origin (*e.g.*, Jones *et al.*, 1978; Ryan, 1994). But the data for SRF still suggest that a proportion of N_{leaf} and P_{leaf} was not related to the respiration rate. At zero CO_2 efflux, N_{leaf} was predicted to be 0.04 mol m^{-2} and P_{leaf} to be 0.0008 mol m^{-2}. The significant intercept for the multiple regression of R_m on N_{leaf} and P_{leaf} in SRF ($p < 0.001$; Table 6.5b) also supports the existence of these intercepts. If they accurately reflect cellular metabolism, then they give an estimate of the average quantity of canopy leaf N or P that is decoupled from respiration. This protein is likely to be required for non-respiratory metabolism, or for structural proteins with low turnover rates, though it may also be in the form of free amino acids that do not have recurrent maintenance costs.

The R_m:N_{leaf} ratios in Table 6.4 indicated that the proportion of structural to total nitrogen is lower nearer the ground; this can also be seen in the example of Figure 6.7b where dotted lines drawn from the origin to the regression line at different R_m values represent the R_m:N_{leaf} ratio at different heights (where R_m is used to denote height, *c.f.*, Figure 6.3). Removal of [structural] leaf N and P that is not involved in photosynthetic or respiratory metabolism from total N_{leaf} and P_{leaf} values could improve models that seek to treat canopies as a single 'big-leaf' (Kull & Jarvis, 1995).

6.5 CONCLUSION

Leaf respiration (R_m) was measured on leaves from a range of species throughout the vertical profile of PRF in Brazil, and SRF in Cameroon. A gradient in foliar respiration was observed rising from 0.2 - 0.4 μmol m^{-2} s^{-1} at ground level to 0.7 - 1.2 μmol m^{-2} s^{-1} at the canopy-top. Inconsistent patterns of pre-dawn respiration were observed among all species, although before 0100 hrs, the temperature response of most leaves approximated a Q_{10} of two. The highest respiration rates were found in a liana species, *Strychnos amazonicus*, in Brazil, and in a pioneer tree species, *Musanga cecropioides*, in Cameroon. In the latter species, R_m varied significantly with height in the canopy.

Leaf respiration on an area basis was strongly related to SLA and foliar chemical composition. For each forest, a model incorporating both N_{leaf} and P_{leaf} was found to explain 68% (SRF) and 66% (PRF) of the variation in CO_2 effluxes, irrespective of height or species. Both R_m and P_{leaf} at each height in the forest canopy in Cameroon were approximately double that found in Brazil. By contrast, N_{leaf} did not explain the difference in R_m between the two forests. A possible method for separating foliar protein ascribed to respiration from that involved in other metabolic and structural functions was proposed using the relationships between leaf R_m and N_{leaf} and P_{leaf}.

On a mass basis leaf respiration rate was poorly related to N_{leaf} and only significantly related ($p = 0.02$) to P_{leaf} in PRF. It is possible that R_m does not respond in a general way to N_{leaf} on a mass basis. The data were also expressed as the molar ratio between R_m and N_{leaf}, and compared with values from different temperate vegetation types. The molar R_m:N_{leaf} ratio in these environments was found to be consistent with the values for 'sun' leaves in SRF and PRF, after allowing for differences in acclimated leaf temperatures, and was reduced in leaves found in deep shade near the ground. The molar R_m:N_{leaf} ratio integrates the effects of SLA on nutrient - respiration relationships, but variation among leaves

may remain reflecting relative nutrient allocation to different cellular functions, which in turn may depend on the radiation environment of the leaves. These findings may provide the basis for a general model of leaf respiration applicable in a wide range of environments, although systems where nitrogen or phosphorus are not limiting may add complexity (Ryan, 1994). The prospect of a general model is attractive as it bridges this and other processes also determined by tissue nutrient levels, such as photosynthesis (Field & Mooney, 1986; Evans, 1989), and microbial decompostion processes in the soil, where carbon and nitrogen concentrations dictate the balance between immobilization and mineralisation (Melillo *et al.*, 1982; Carlyle, 1986; White, 1987).

7. Photosynthetic leaf gas exchange

7.1 INTRODUCTION

Photosynthesis constitutes the largest single flux of carbon between vegetation and the atmosphere (Raich & Schlesinger, 1992). In forests this may be measured at the whole canopy level using eddy covariance techniques (Baldocchi *et al.*, 1988), or at the leaf level, using portable IRGA's and suitably designed leaf gas exchange chambers. The advantage of the latter approach is that it provides physiological data relating to one component of the ecosystem, and permits comparison by position in the canopy and species. Such information is vital for understanding leaf physiology, for modelling ecosystem gas exchange, and ultimately for the validation of larger scale vegetation - atmosphere models. In tropical forests, there is a dearth of information on photosynthesis, and even less on the pattern of gas exchange through the vertical profile of the canopy (McWilliam *et al.*, 1996).

Photosynthetic physiology is complex, and is driven by a suite of primary environmental variables, the most important being incident photon flux density (Q), temperature, and the water vapour pressure deficit (D) of ambient air. These factors affect leaf biochemistry, and gas diffusion parameters such as stomatal conductance to water vapour and carbon dioxide (g_s). But they do not limit photosynthesis independently (Jones, 1992): unless controlled for in a laboratory, they can covary, making net g_s and leaf photosynthesis (A_l) rates contingent upon these covarying interactions. Models of photosynthesis are made to account for this phenomenon by fitting observed data to non-linear equations that incorporate the form of the response in A_l and g_s to each environmental variable, as it is currently understood at the physiological and biochemical level.

Gas exchange data from leaves throughout the vertical profile of the canopy of SRF were obtained in March 1994. It was possible to analyse these data using two approaches. The phenomenological model of Reed *et al.* (1976) and Jarvis *et al.* (1985) drives A_l according to observed responses in photosynthetic parameters to the physical environment. The model of Farquhar & von Caemmerer, (1982) incorporates these responses but interprets them according to the biochemistry of photosynthesis. It consequently has the advantage of allowing analysis of the effect of changes in ambient CO_2 concentration on photosynthesis. This model was fitted to the measurements from SRF. In order to constrain the possible set of fitting parameters within acceptable bounds, and where

reasonable, certain biochemical values were assumed from the literature (*e.g.*, the Michaelis-Menten constants for carboxylation (K_c) and oxygenation (K_o) by ribulose-1,5-bisphosphate carboxylase-oxygenase, Rubisco).

The physical environment in a tropical forest changes markedly from the canopy top to the forest floor (Lemon *et al.*, 1970). Different species, with different physiognomies and physiologies, are commonly found at different heights. This variation must be accounted for when modelling the gas exchange behaviour of a whole canopy. Two approaches present themselves: the 'splitters' choice, where physiological and environmental detail at every level is described (*e.g.*, MAESTRO, Wang & Jarvis, 1990); and the 'lumpers' approach where the canopy is accredited composite gas exchange characteristics and treated as a single 'big-leaf' (*e.g.*, Grace *et al.*, 1995a). The latter approach requires that photosynthetic capacity is distributed with height according to the local physical environment (irrespective of, though potentially covarying with, species composition). Leaf nitrogen and phosphorus are good indicators of photosynthetic capacity (Field & Mooney, 1986; Evans, 1989, Brooks, 1986). The allocation of leaf nitrogen with height in some mono-specific stands is in proportion to absorbed irradiance (Field, 1983; Evans, 1993). This is consistent with models of optimal carbon gain (Field 1988; Schulze *et al.*, 1994). Under the assumption that such a distribution also occurs in mixed species forests, the condition of optimality (Farquhar, 1989) has been used to scale from leaf to canopy in the construction of composite gas exchange models for use at larger scales (*e.g.*, Sellers *et al.*, 1992). Leaf nutrient data and photosynthetic parameters are reported here with a view to comparing lumped and split canopy photosynthesis models in Chapter 8.

MODELLING PHOTOSYNTHESIS

A_l is predicted from Q, C_a and temperature, with additional calculated or assumed parameters. Those used or referred to in this chapter are listed below:

A_l is the rate of net photosynthesis by individual leaves (μmol m^{-2} s^{-1})

C_a is the ambient concentration of CO_2 (μmol mol^{-1}),

C_c is the concentration of CO_2 in the chloroplast (μmol mol^{-1}),

C_i is the internal concentration of CO_2 in the intercellular spaces at the surface of the cell walls in the leaf (μmol mol^{-1}),

C_{st} is the concentration of CO_2 at the site of evaporation within the sub-stomatal cavity (μmol mol^{-1}).

$E_{c/o/v/j}$ are the Arrhenius activation energies for K_c, K_o, V_{max} and J_{max} respectively (kJ mol^{-1})

g_s is the stomatal conductance to H_20 (mmol m^{-2} s^{-1})

g_c is the stomatal conductance to CO_2 (mmol m^{-2} s^{-1}),

g_i is an internal conductance from the sub-stomatal cavity to the sites of carboxylation within the chloroplasts (mmol m^{-2} s^{-1}),

H_J/S_J are fitting parameters affecting J_{max} at low and high temperatures (J mol^{-1} & kJ mol^{-1}),

K_c is the Michaelis-Menten constant for carboxylation by Rubisco (μmol mol^{-1}),

K_o is the Michaelis-Menten constant for oxygenation by Rubisco (mol mol^{-1})

Γ^* is the leaf CO_2 compensation concentration in the absence of dark respiration (μmol mol^{-1}),

pO is the ambient concentration of oxygen (mol mol^{-1}),

$\boldsymbol{R}$ is the universal gas constant (8.314 J mol^{-1} K^{-1}),

R_d is the daytime leaf respiration rate at $Q = 0$ (μmol m^{-2} s^{-1}),

Q is photon flux density of incident photosynthetically active radiation (μmol quanta m^{-2} s^{-1}),

T_l is leaf temperature (°C or, as T_{lK},in K).

The Farquhar & von Caemmerer (1982) model

A_l is calculated as the minimum of Rubisco limited (A_v) and electron transport limited (A_j) assimilation (Farquhar *et al.*, 1980; Farquhar & von Caemmerer, 1982).

Rubisco limited assimilation:

$$A_v = \frac{V_{max}(Cc - \Gamma^*)}{(Kc[1 + pO/Ko] + Cc)} - R_d \qquad \text{Equation 7.1}$$

where V_{max} is the maximum rate of carboxylation, and the Arrhenius-type temperature sensitivities for V_{max}, K_c and K_o are defined relative to their rates at 25 °C as given below:

$$V_{max} = V_{max25} \exp\left[\frac{E_v}{298.2\,\boldsymbol{R}}\left(1 - \frac{298.2}{T_{lk}}\right)\right] \qquad \text{Equation 7.2a}$$

$$K_c = K_{c25} \exp\left[\frac{E_c}{298.2\,R}\left(1-\frac{298.2}{T_{lk}}\right)\right]$$ Equation 7.2b

$$K_o = K_{o25} \exp\left[\frac{E_o}{298.2\,R}\left(1-\frac{298.2}{T_{lk}}\right)\right]$$ Equation 7.2c

The compensation concentration of CO_2 in the absence of dark respiration is Γ^*. It differs from Γ used in some other formulations since the latter incorporates a [variable] amount of CO_2 evolution (respiration) other than photorespiration, and is consequently a slightly poorer indicator of the ratio of carboxylation to oxygenation in chloroplastic Rubisco (Brooks & Farquhar, 1985).

Electron transport limited assimilation:

$$A_J = \frac{J}{4}\left(\frac{C_c-\Gamma^*}{C_c+2\Gamma^*}\right) - R_d$$ Equation 7.3

where J is the rate of electron transport defined by the maximum rate of electron transport, J_{max} (*i.e.*, at saturating Q), the irradiance, I_2, absorbed by photosystem II, and θ a convexity factor varying from 0 (a rectangular hyperbola) to 1 (a Blackman response curve, two straight lines), according to Farquhar & Wong (1984). Implicit in the formulation of A_j is the assumption that four electrons generate sufficient ATP and NADPH for the regeneration of ribulose bisphosphate, RuBP, in the Calvin cycle (Farquhar & von Caemmerer, 1982).

$$J = \frac{I_2+J_{max}-\sqrt{\left(I_2+J_{max}\right)^2-4\theta\,I_2 J_{max}}}{2\theta}$$ Equation 7.4

$$I_2 = Q\,\frac{\left[(1-f)(1-r-t)\right]}{2}$$ Equation 7.5

where f corrects for the spectral imbalance of light (Evans 1987), r and t are the canopy reflectance and transmittance of the incident photosynthetically active radiation, Q.

$$J_{max} = J_{max25} \frac{\exp\left[\frac{(T_{lk}/298.2 - 1)E_j}{RT_{lk}}\right]\left[1+\exp\left(\frac{298.2Sj - H_j}{298.2R}\right)\right]}{1+\exp\left[\frac{S_j T_{lk} - H_j}{R T_{lk}}\right]}$$ Equation 7.6

Leaf respiration, R_d, and the compensation concentration, Γ^*:

Leaf respiration, R_d, is temperature sensitive according to an exponential relationship, but a constraint by $Q > 10$ μmol m^{-2} s^{-1} is also included (Brooks & Farquhar, 1985; Lloyd *et al.*, 1995b):

$$R_{do} = R_o e^{(kT)}$$ Equation 7.7a

At $Q < 10$ μmol m^{-2} s^{-1}, $R_d = R_{do}$ Equation 7.7b

At $Q > 10$ μmol m^{-2} s^{-1}, $R_d = R_{do}[0.5 - 0.05 \ln(Q)]$ Equation 7.7c

where k defines the Q_{10} of leaf respiration according to: $Q_{10} = e^{(10k)}$.
The temperature sensitivity of Γ^* follows the description by Brooks & Farquhar (1985), but uses an intercept more recently reported by von Caemmerer *et al.* (1994).

$$\Gamma^* = [38.6 + 1.68(T_l - 25) + 0.012(T_l - 25)^2]$$ Equation 7.8

Stomatal conductance:

In order to effectively predict A_l, a stomatal conductance model must also be derived. Two commonly used general formulations are the Jarvis (1976) model and the Ball *et al.* (1987) model. The latter type predicts g_s using relative humidity (h) at the leaf surface, and the correlation between A_l and g_s. However h is defined according to T, and fitting a photosynthesis model using observed A_l for g_s as well as predicted A_l may introduce circular correlations.

To avoid these difficulties, a Jarvis-type model was chosen. This formulation prescribes the stomatal response to water (g_s) to different environmental variables (Q, D, T, leaf water potential, φ, *etc*) in a multiplicative non-linear model, and assumes that the separate functions do not interact. This

approach has been successful in a number of studies at the leaf (Lohammar *et al.*, 1980) and canopy level (Shuttleworth, 1989; Lloyd *et al.*, 1995b).

$$g_s = gq(Q).\ gd(D).\ gt(T).\ gp(\varphi)....$$ Equation 7.9

and according to the difference in diffusivity between CO_2 and H_20,

$$g_c = g_s / 1.6$$ Equation 7.10

The original model (Jarvis, 1976) proposed that: the response to Q follows a rectangular hyperbola, saturating at high Q; the respone to D is linear with a negative slope; and the response to T is bell-shaped with a maximum, minimum and optimum temperature. Various manipulations have been made to the original form, particularly in the response to D (*e.g.*, Leverenz, 1981; Leuning, 1995), which is more commonly represented as an hyperbolic relationship. The specific manipulations used to fit g_s here are described in the Results and Discussion.

C_c can now be estimated from A_l and g_s, according to Equation 7.11:

$$C_c = C_a - \frac{A_l}{g}$$ Equation 7.11

where g is the series sum of conductance to CO_2 diffusion across the stomatal pores (g_c) and the internal conductance from the sub-stomatal cavity to the sites of carboxylation in the chloroplasts (g_i), estimated from the literature (von Caemmerer & Evans, 1991; Lloyd *et al.*, 1995b). In this way A_l can be solved by combining Equations 7.1, 7.3 and 7.11, and the analytical solutions allowing A_l to be calculated from V, J, g_i, g_c, Q, T, and R_d (Lloyd *et al.*, 1995a) are given in Appendix C.

7.2 METHODS

Leaf gas exchange data were obtained using an LCA3 IRGA (ADC, Hoddesdon, UK) with a proprietry leaf chamber, and a PLC(N) designed for broadleaf species (ADC, Hoddesdon, UK). The leaf chamber and IRGA operate as an open gas exchange system and are described in Appendix C. Measurements were made on seven species accessed at different heights from the micrometeorological tower, and also at ground level (Table 7.2). The data were obtained in SRF, Cameroon, for the period 16th to 28th March 1994, when the equipment was available.

Table 71. Tree and shrub species measured for leaf gas exchange parameters in SRF, Cameroon, March 1994. Canopy position was used to provide a qualitative description of the prevailing light environment of each species; gaps above species in lower strata were over one sector of the sky. Not all individuals on the ground were next to the tower.

Species	*Family*	*Life form*	*Ht. (m)*	*Canopy position*
Amphimas pterocarpoides Harms	Fabaceae - Caes.	Tree	40	Top
Musanga cecropioides R.Br.	Moraceae	Tree	26	Top, large gap
Celtis adolfi-friderici Engl.	Ulmaceae	Tree	8	Middle
Staudtia stipitata Warb.	Myristicaceae	Tree	6	Middle
Haumaniana danckelmaniana M-Redh.	Maranthaceae	Herb	0 - 1.5	Ground
Megaphrynium macrostachyum	Maranthaceae	Herb	0 - 1.5	Ground, large gap
Trichilia sp.	Meliaceae	Tree	0 - 1.5	Ground, understorey

The IRGA was calibrated every morning using a pre-calibrated gas source; the PLC sensors were also calibrated and then checked up to four times during a measurement day. Temperature sensors were compared with a pre-calibrated thermocouple and the relative humidity sensors were calibrated using a water vapour generator (Licor 610, Licor, Nebraska, USA). The latter usually required slight re-adjustment during the course of a day. Where a constant environment was needed for calibration, the PLC was placed in an insulated box situated in the shade.

Data were obtained using two methods: (a) spot measurements, whereby leaves were placed in the chamber at their natural angle of inclination, the humidity and carbon dioxide levels allowed to stabilise before storage of the data; and (b) sequential shading, whereby leaves were exposed to full sunlight, a reading taken as in (a), and a neutral density filter placed over the chamber before taking a subsequent reading. In the latter technique, Q was sequentially reduced to zero (*i.e.*, to give dark respiration). To make the spot measurements (type a) as representative as possible of ambient conditions they were taken relatively quickly (within 45 - 90 seconds of sealing the leaf in the chamber) to minimise any error accruing from stomata responding to the new environment within the chamber. For each species, two leaves were tagged and measured repeatedly; in addition, a larger

number of leaves were measured to provide an estimate for the whole tree. After the measurement period was complete, leaves were harvested, samples taken for specific leaf area determination (leaf disc diameter = 10 mm), and the tissue dried to constant mass at 70 °C. Leaf nitrogen and phosphorus concentrations were determined on these leaves in Edinburgh, using a standard wet digestion (Allen, 1974).

Gas exchange data were downloaded from the LCA3 to a portable computer. Software errors in the LCA3 can sometimes occur in the measurement of leaf temperature. Consequently gas exchange parameters were re-calculated using leaf tempeature derived from solving the energy balance, and atmospheric pressure, as measured using a site-calibrated aneroid barometer. The main equations used are found in Field *et al.* (1989), Jones (1992) and the ADC manual (ADC, 1990). Models of stomatal conductance and photosynthesis were fitted to observed A_l and g_s using the relevant driving environmental variables. Models were fitted by minimising the error sum of squares using non-linear regressions (SPSS, *v.* 5.01, SPSS Inc., USA). The procedure followed was to obtain initial parameter estimates from previous, simpler analyses, or if not possible in the first place, from the literature. Constraints were only applied when the natural bounds of a parameter could be reliably estimated (*e.g.*, minimum values greater than zero). Residual analysis of the fitted functions was used to detect skew in the predicted data. In fitting the Farquhar & von Caemmerer model to the data, a number of values had to be assumed as the variance in the measurements was too great to estimate all the features of the photosynthetic biochemistry, such as the embedded temperature coefficients. Table 7.2 lists the assumed parameters, their values and their sources.

Table 7.2. Parameters assumed when fitting the Farquhar & Caemmerer (1982) model.

Parameter	*Value*	*Units*	*Source*
E_c	59.4	kJ mol^{-1}	Harley *et al.* (1986)
E_o	36.0	kJ mol^{-1}	Harley *et al.* (1986)
E_v	53.0	kJ mol^{-1}	Kirschbaum & Farquhar (1984)
E_i	41.0	kJ mol^{-1}	Lloyd *et al.* (1995b)
H_i	220.3	kJ mol^{-1}	Lloyd et al (1995a)
S_i	0.71	kJ K^{-1} mol^{-1}	Lloyd et al (1995a)
K_c	258	μmol mol^{-1}	von Caemmerer *et al.* (1994)
K_o	0.171	mol mol^{-1}	von Caemmerer *et al.* (1994)
Γ* intercept	38.6	μmol mol^{-1}	von Caemmerer *et al.* (1994)
$1 - r - t$	0.85	--	Lloyd et al (1995a)
f	0.12	--	Evans (1987)
pO	0.21	mol mol^{-1}	--

7.3 RESULTS AND DISCUSSION

GENERAL CHARACTERISTICS OF STOMATAL CONDUCTANCE AND PHOTOSYNTHESIS RATES

A_l reduced in all species from high rates at 0900 hrs - 1100 hrs to a minimum near sunset (Figure 7.1). In general, leaves at the top of the canopy exhibited higher assimilation rates than those at ground level. Assimilation near the ground, in *Trichilia*, peaked nearer 1200 hrs. Differences in the timing of maximum A_l probably reflected more the daily radiation regime as dictated by the broken canopy above (*c.f.* Table 7.1), rather than changes in D (data not shown). A_{max} declined with height (Table 7.4).

Analogous plots for g_s (Figure 7.2) showed stomatal conductance to be highest before 1200 hrs in all species, and to drop throughout the day. The trees highest in the canopy did not show the highest g_s, perhaps as a result of leaf water stress. The species with the largest value was a herb (*Megaphrynium macrostachyum*; maximum $g_s \approx 1000$ mmol m^{-2} s^{-1}). The large entire leaves of such a species are likely to be associated with lower leaf boundary conductuances and have been found elsewhere to show high g_s values, in excess of 1200 mmol m^{-2} s^{-1} (Whitehead *et al.*, 1981; Grace *et al.*, 1981; Grace, 1983). In *Amphimas*, at the canopy-top, g_s dropped rapidly after the morning high, as expected in conditions where D increases the most rapidly (Roberts, 1990; Table 7.3 for maximum observed D values).

The gas exchange rates observed in Cameroon were similar to those found elsewhere for undisturbed tropical forests (*e.g.*, Koyama, 1981; Grace *et al.*, 1982; Pearcy, 1987), though maximum g_s values were greater than those found by Koch *et al.* (1994) in a 'dense wet lowland forest', in Cameroon (0.4 mol H_20 m^{-2} s^{-1}) . The few reported data on vertical profiles (Roberts *et al.*, 1990; McWilliam *et al.*, 1996) show maximum rates in the morning declining over the day, as found here.

STOMATAL CONDUCTANCE

The multiplicative model for g_s excluded leaf water potential, as this was not measured (unpublished data from elsewhere suggest that leaf water potential does not affect g_s; G. Jackson, *personal communication*). Stomatal conductance was strongly determined by the response to D (Figure 7.3a). Variation with Q showed a typical asymptotic curve but there was noise in the relationship caused by other factors, such as D (Figure 7.3d). g_s showed only a weak response to T_l; constraints were met, or optimal temperatures could not be found during the fitting process. Temperature covaries wth D in

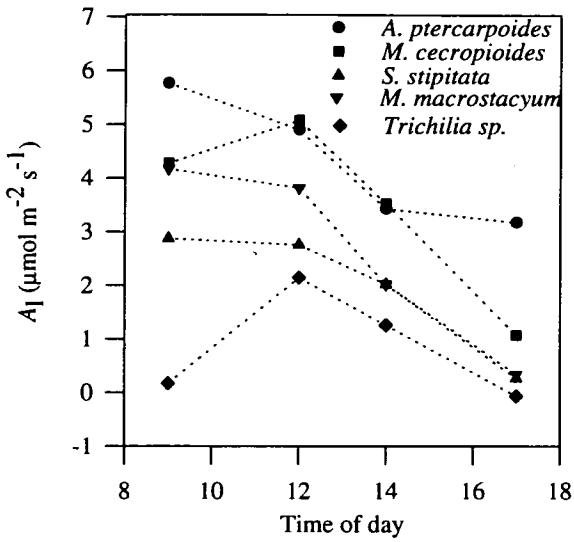

Figure 7.1. Diurnal patterns in photosynthesis in five of the trees in SRF. The values are means of all observations.

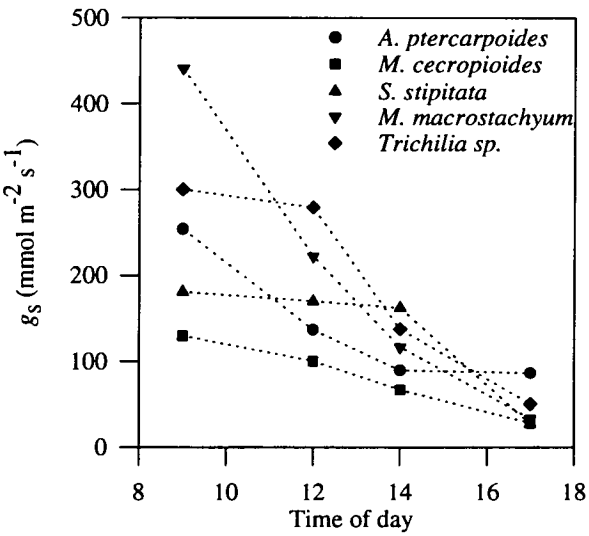

Figure 7.2. Diurnal patterns in stomatal conductance in five of the trees in SRF. The values are means of all observations.

field conditions (Figure 7.3b), and after correcting observed g_s for T_l, D and Q, (normalised to T_l = 30 °C, D = 0.015 mol mol^{-1} and Q = 300 μmol m^{-2} s^{-1}), a faintly peaked signal could be seen (Figure 7.3c). But the density of points at different temperatures prevented any improvement in the fit with T_l.

Consequently, only D and Q were used in the final model. The form of the fitted Q response is described below. Several forms of the response to D were tried: a best fit was found using a hyperbolic function (Equation 7.13b, below). The response of stomata to D remains incompletely understood, indeed one author has suggested that the response is to evaporation rather than D (Monteith, 1995). The hyberbolic function in Equation 7.13b, initially propsed by Lohammar *et al.*, (1980), has been shown to be identical to treating g_s as a linear function of evaporation (Leuning, 1995). A second, more complex g_{sD} function was also devised (Equation 7.13a, below) which predicted g_s well. However, this improved the overall fit to the observed data in one species only, *Musanga cecropioides*, so was not used further.

[*Response to D:* $g_{sD} = \left[\exp\left(\frac{D}{a}\right)b\right] + cD$ NOT USED Equation 7.13a]

Response to D: $g_{sD} = [1 + D / D_0]^{-1}$ Equation 7.13b

Response to Q: $g_{sQ} = \frac{g_{smax}\,\alpha_g\left(Q + g_d/\alpha_g\right)}{\left(g_{smax} + \alpha_g\left(Q + g_d/\alpha_g\right)\right)}$ Equation 7.14

Overall: $g_{sp} = g_{sQ} + g_{sD} \times 1000$ Equation 7.15

where Q is photon flux denstiy, g_{smax} is maximum g_s at infinite Q; α_g is the initial slope of the g_s - Q response, g_d is g_s at $Q = 0$; D is the water vapour pressure deficit in mol mol^{-1}, D_0 is a fitted constant and g_{sp} is the predicted g_s, in mmol H_2O m^{-2} s^{-1}. The results for different species are shown in Table 7.3 and Figure 7.3e. The r^2 values for whole trees were higher than for individual leaves (data not shown) mainly because more data were available for whole trees and a wider range of D and Q values were recorded. The residual variation in the model fits derive from three main sources: systematic and random error, incomplete stomatal responses (see below), and biological variation among leaves. The generally even spread of residuals indicated that there was little systematic error in g_{sp} (Figure 7.3; data are for *Amphimas ptercarpoides*). There is little skew in any of the variables driving stomatal conductance, though a small tendency was observed for the overall model to slightly underpredict at high g_s (Figure 7.4a) The wide, though even, spread in residuals at low D was primarily an artefact - at low D, g_s is likely to be large, so that a random error of the same proportion will be numerically larger than at high D.

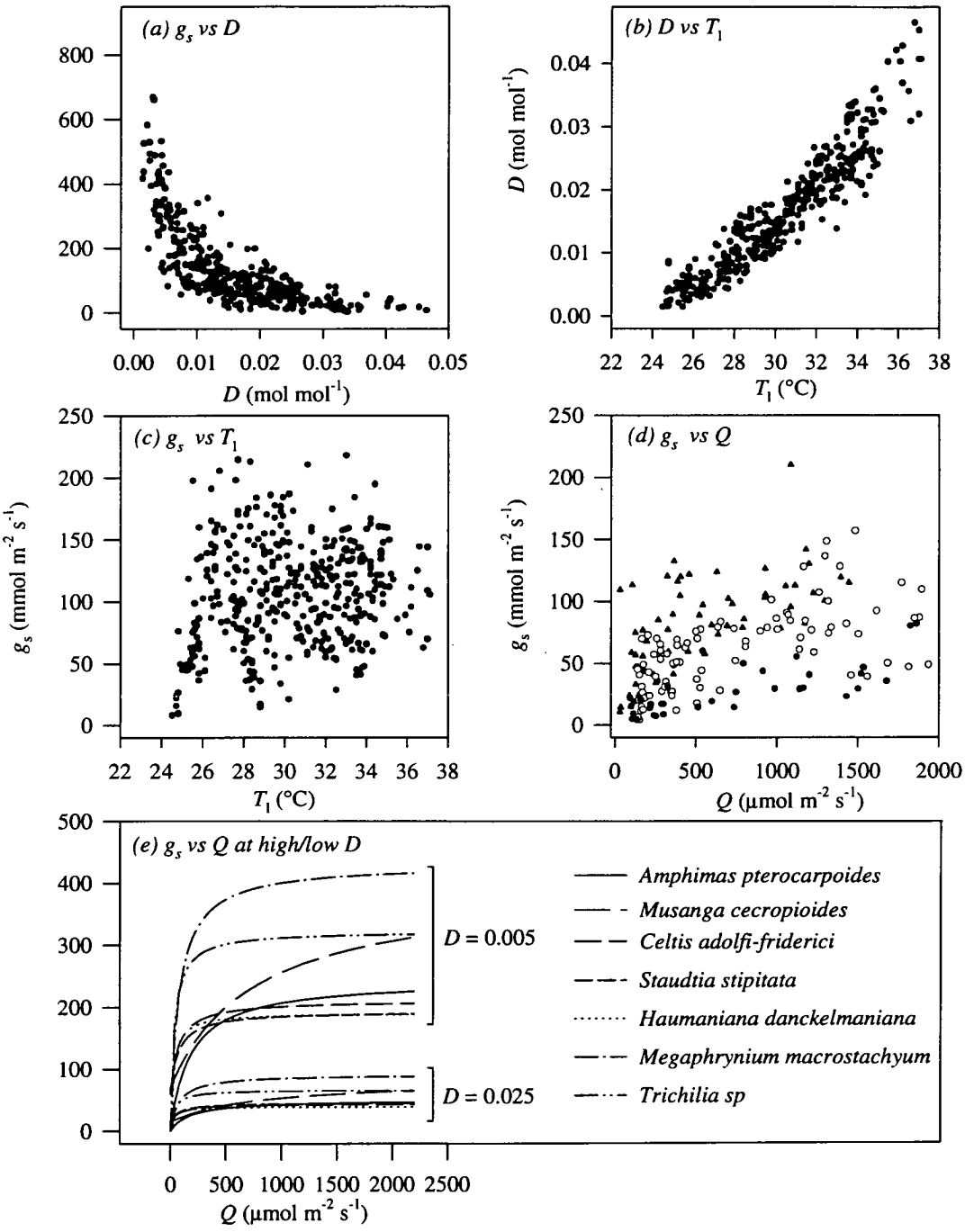

Figures 7.3a-e. Environmental variables correlated with g_s. (a) shows g_s *vs* D; (b) shows the covariation of with D with T_l; (c) shows the residual variation in g_s after correcting for Q and D; (d) shows variation in g_s with Q at $0.02 > D > 0.01$ (filled triangles); $0.03 > D > 0.02$ (open circles) and $0.04 > D > 0.03$ (filled squares). The data are for *Amphimas pterocarpoides.* Figure (e) shows the fitted g_s response to Q at D = 0.005 and 0.025 for all seven species. All D units are in mol mol^{-1}.

Errors resulting from incomplete stomatal responses were probably most closely linked to temperature effects. When a leaf was placed in the chamber, it entered a slightly changed environment. In particular, the temperature of the cuvette was 0 - 5 °C warmer than the air temperature. The response in chloroplasts to Q occurs within seconds, but stomata respond to changes such as a temperature increase more slowly, over the course of minutes. It is possible that some of the measurements were not made quickly enough to avoid this acclimation, resulting in an error term, though this did not appear to be systematic. The final source of error, biological variation, was accounted for by using a large sample size. For all species the sample size was quite big, though only one part of the tree was accessible, so some leaves may have been measured more than once, making the effective sample size a little smaller than the n value in Table 7.3.

Table 7.3. The fitted parameter values for all species, SRF. The data were fitted to Equation 7.15. D_0 is a fitted constant; g_{smax} is in mol m^{-2} s^{-1}; α_g is in mol mol^{-1}; g_d is in mol m^{-2} s^{-1} , D is in mol mol^{-1}. † represents the parameter constraint. The asymptotic 95% confidence limits are given in parentheses for the fitted parameters. Max D is the maximum D value observed for each species.

Species	D_0	g_{smax}	α_g	g_d	r^2	n	*Max D*
A. pterocarpoides	$2.1x10^{-4}$	5.4	0.032	0	0.82	408	0.046
	($0.6x10^{-4}$)	(2.2)	(0.016)	--			
M. cecropioides	$2.6x10^{-4}$	8.0†	0.01	1.7	0.60	197	0.042
	($1.0x10^{-4}$)	--	(0.01)	(1.2)			
C. adolfi-friderici	2.7x10-4	4.1	0.08	0	0.83	163	0.039
	(1.5x10-4)	(2.0)	(0.008)	--			
S. stipitata	$1.2x10^{-3}$	1.0	0.041	0	0.70	104	0.029
	($7x10^{-4}$)	(0.6)	(0.06)	--			
H. danckelmaniana	$2.2x10^{-4}$	4.53	0.163	0	0.86	101	0.029
	($2.0x10^{-4}$)	(3.5)	(0.15)	--			
M. macrostachyum	$3.8x10^{-4}$	6.2	0.08	0	0.87	69	0.034
	($1.6x10^{-4}$)	--	(0.05)	--			
Trichilia sp.	$2.1x10^{-4}$	8†	0.24	0	0.75	66	0.021
	($3x10^{-4}$)	--	(0.4)	--			

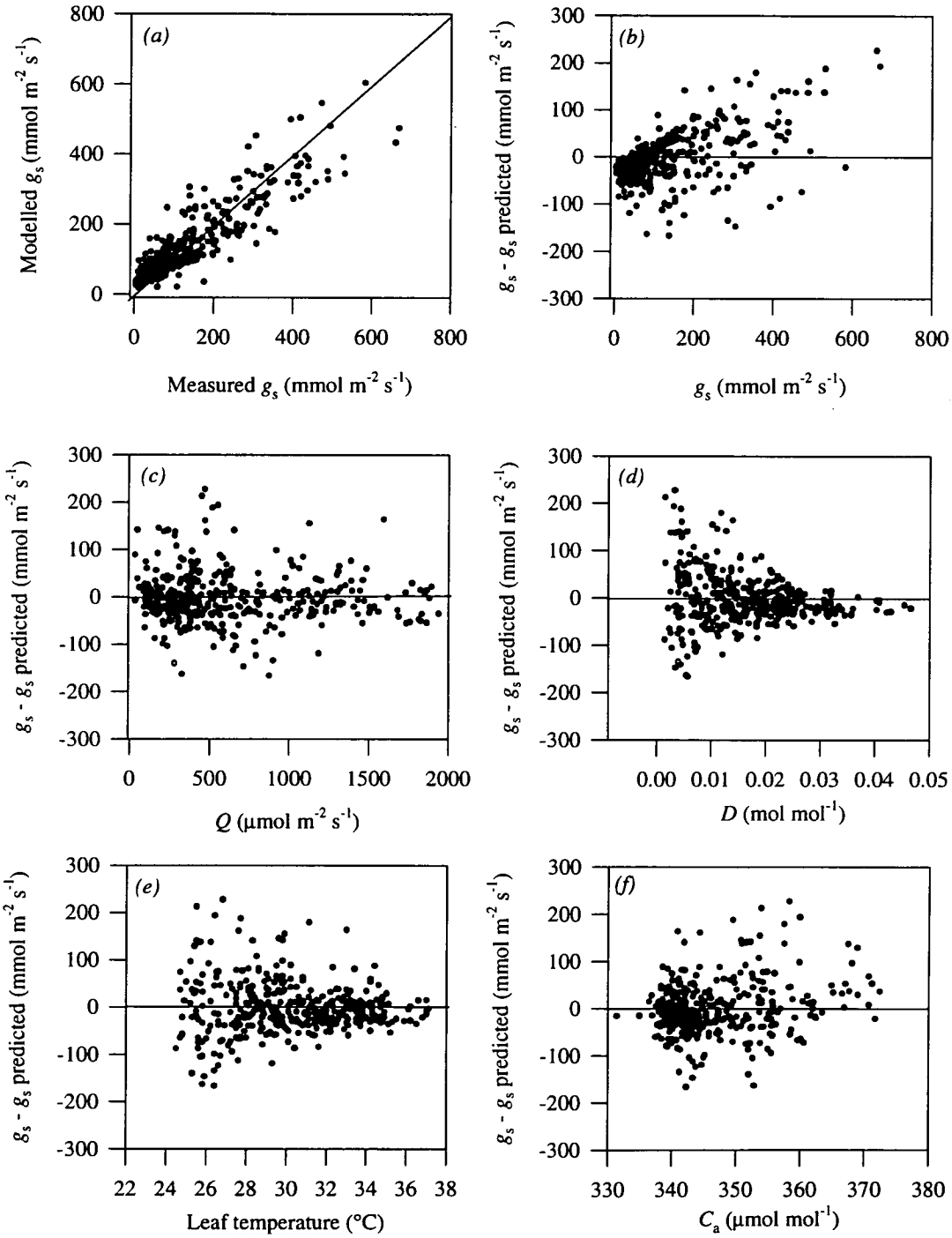

Figures 7.4a-f. g_s model results. Figure a compare modelled with measured g_s, the line shown is the 1:1 line. Figures (b) - (f) are residual plots of g_s - $g_{s\ predicted}$ *vs* g_s, Q, D, T_l, and C_a. The data are for *Amphimas ptercarpoides*.

PHOTOSYNTHESIS

Dark respiration rates and light response curves

In an initial examination of the data, a rectangular hyperbola was fitted to data from all the species (Table 7.4). The basic model used was a light response curve, as described by Equation 7.16:

Photosynthetic light response: $$A_l = \frac{A_{max}\,\alpha\,Q}{(A_{max} + \alpha\,Q)} - R_d \qquad \text{Equation 7.16.}$$

where A_l is leaf assimilation rate, A_{max} is leaf assimilation rate at maximum Q in μmol CO_2 m^{-2} s^{-1}, Q is photon flux density in μmol quanta m^{-2} s^{-1}, α is the maximum light use (quantum) efficiency in μmol CO_2 mol $quanta^{-1}$, and R_d is dark respiration in μmol CO_2 m^{-2} s^{-1}.

The R_{d0} values obtained by shrouding the leaves to simulate Q = 0, and the R_d values obtained using Equation 7.16 are in approximate agreement, though there was considerable variation in the shrouded leaf data. These values are greater than the night-time leaf respiration rates found in Chapter 6, though the temperatures during day were higher. Daytime dark respiration at 15 °C of *Pinus strobus* leaves was greater by 40% than respiration at the same temperature during the night (Hubbard *et al.*, 1995).

The patterns through the vertical profile of the canopy in α and A_{max} are also of note. From canopy top to bottom, α increased from 0.04 to 0.06, whilst A_{max} declined from 14 to 6 μmol m^{-2} s^{-1} (Figure 7.5a, inset). This may be explained by hypothesising that leaves lower down in the canopy harvest light more efficiently than those higher up, but are not able to maintain such high maximum photosynthetic rates. Alternatively, it may be that α is a biophysical constant, and the variation in Figure 7.5a may reflect the effect on *observed* quantum efficiencies of within-leaf light gradients in leaves of different thickness (*c.f.* variation in SLA with height, Chapter 3). However, not all the species behaved in the same way; this was especially apparent at ground level where very different α and A_{max} values were encountered. The variation was partly a species effect, but also reflected the open canopy of the SRF site. Some individuals at ground level were not homogenously shaded by the canopy above (Table 7.1), and exhibited characteristics found in leaves higher up. *Megaphynrium macrostachyum* appeared

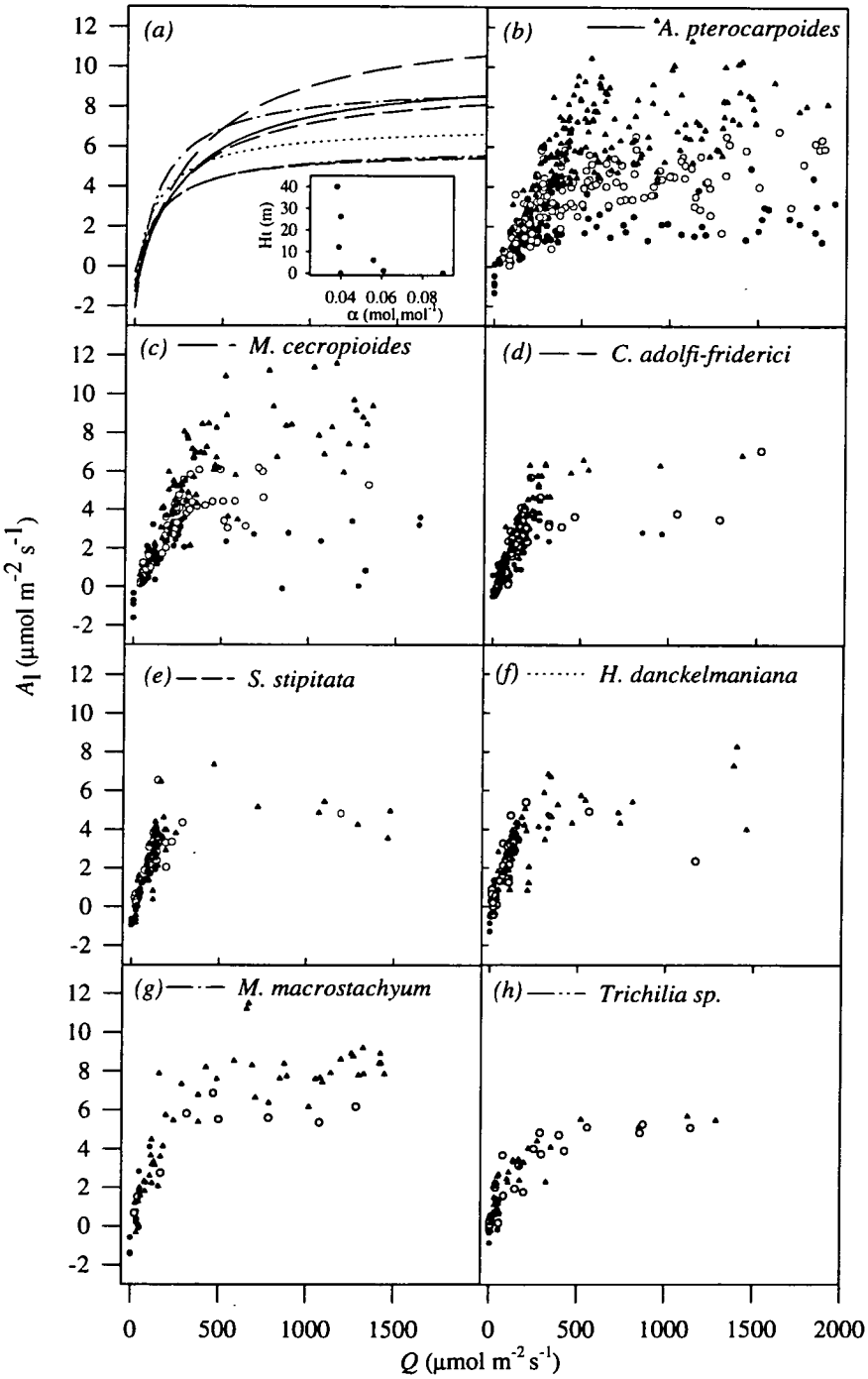

Figures 7.5a-h. Leaf photosynthetic light responses in SRF. In (a) are fitted curves to the data in each of (b)-(h), using Equation 7.16; the inset plot is the variation in α with height (see text). The data in (b)-(h) are for the 7 species in Table 7.1. A_l is coded in (b)-(h) by g_s: $g_s > 100$ (triangles); $50 < g_s < 100$ (open circles) and $g_s < 50$ (spots). g_s units are mmol m^{-2} s^{-1}.

to have a very high quantum efficency ($\alpha = 0.09$). A second feature of these data is the low r^2 values for the highest two trees, *Amphimas* and *Musanga*. For both, the $A_l : Q$ response showed much greater variation than for the other species (Figures 7.5b-h). These trees also experienced greater maximum D, as would be expected at the top of the canopy (Table 7.3). Incorporation of a stomatal conductance term in the prediction of A_l could account for this variation.

Table 7.4. Parameter estimates obtained from fitting Equation 7.16 to $A_l : Q$ data for all species. Height in m; the units for A_{max}, α and R_d are as described for Equation 7.16; mean R_{d0} values (in μmol m^{-2} s^{-1}) are the mean of 2 - 5 measurements on the same leaf shrouded to complete darkness.

Species	*Height*	A_{max}	α	R_d	*Mean* R_{d0}	r^2	*n*
A. ptercarpoides	40	11.0	0.038	1.1	1.0	0.41	408
M. cecropioides	26	13.9	0.040	1.3	1.1	0.56	197
C. adolfi-friderici	8	10.3	0.039	0.9	0.02	0.81	163
S. stipitata	6	6..8	0.056	0.9	0.9	0.79	104
H. danckelmaniana	1	7.8	0.061	0.7	0.8	0.84	101
M. macrostachyum	0	11.3	0.09	2.1	1.1	0.85	69
Trichilia sp	0	6.3	0.04	0.3	0.2	0.86	66

The Farquhar & von Caemmerer photosynthesis model

The $A_l : Q$ plots in Figures 7.5b-h give assimilation for each species coded by stomatal conductance to show how the $A_l : Q$ response varies with g_s. The Farquhar & von Caemmerer model was fitted to the measurements and incorporated this variation to give improved fits, particularly for *Amphimas* and *Musanga* (Table 7.5). In the residual plots, as found for g_s, there was no significant skew, suggesting that little extra variation could be accounted for with these variables (Figure 7.6b-h; data for *Celtis* are shown, other species behaved similarly). Species lower in the canopy showed quite high convexities (θ) for the light response portion of the model (Table 7.5; Figures 7.5d-h). This is consistent with photosynthesis saturating at lower Q in these leaves, as noted in Table 7.4.

The estimates in Table 7.5 for J_{max} and V_{max} are in the lower range of those given by Harley *et al.* (1992) for cotton plants grown in non-limiting laboratory growing conditions, but are similar to or slightly greater than those obtained by Anten *et al.* (1996) for a tropical tree, *Tetrorchidium jrubrivenium*. The estimate for g_i, the stomatal conductance from the sub-stomatal cavities to the sites of carboxylation in the chloroplasts, gave best fits at 0.65 mol m^{-2} s^{-1}, a figure similar to previous estimates (Caemmerer & Evans, 1991; Lloyd et al, 1995b). Fitting temperature optima did not improve the r^2 values shown in Table 7.5, and as found for the g_s model (Figure 7.3c), the variability in the data obscured the temperature signal; constraints were often reached in the fitting process, so

fixed values estimated from the literature were used (Table 7.2). There was no unbiased way of refining the dataset, so further fits for optimal temperature parameters were not attempted.

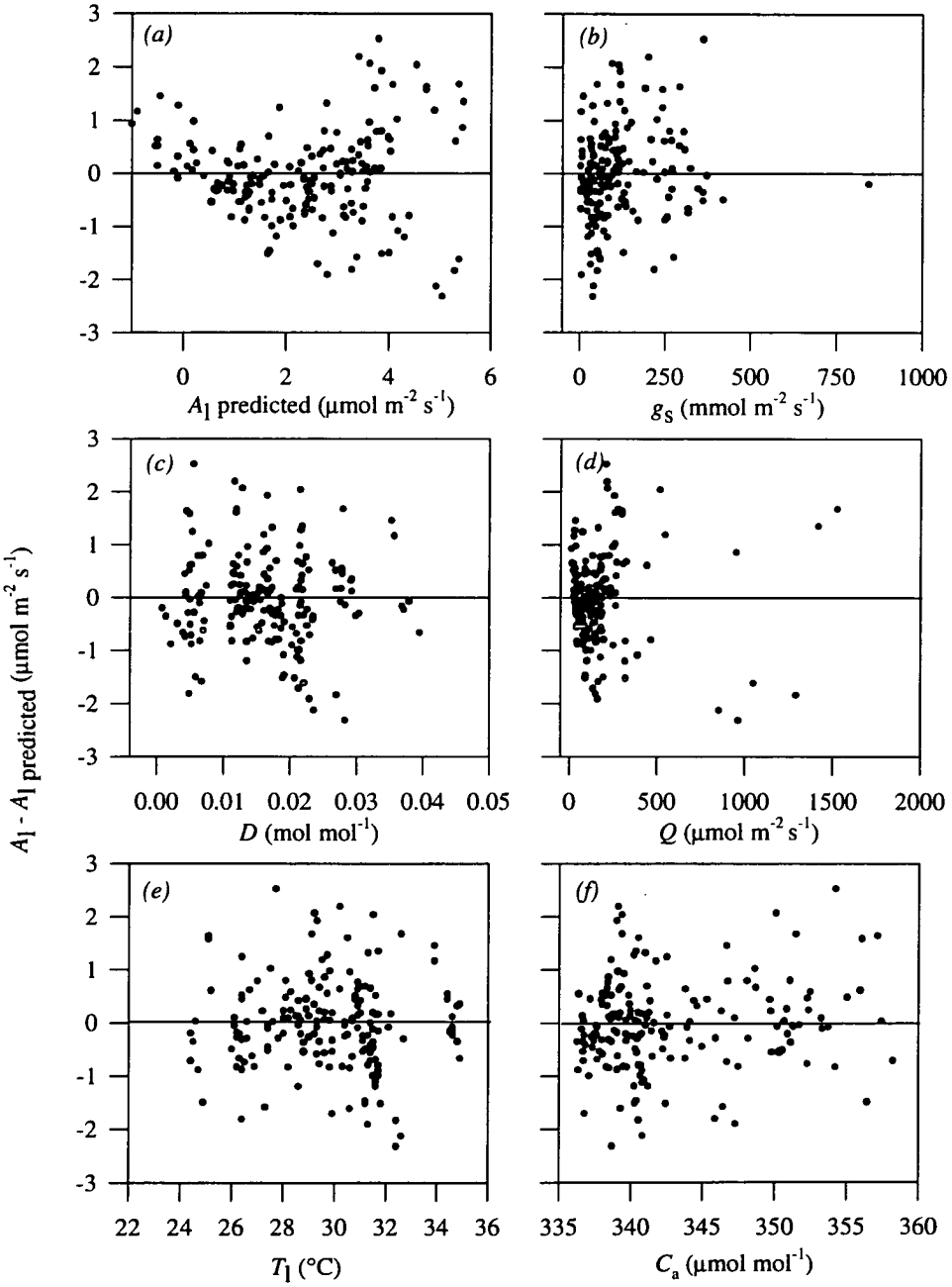

Figures 7.6a-f. The Farquhar photosynthesis model results. All plots are residual plots of $A_{l\ observed}$ - $A_{l\ predicted}$, *vs* g_s, D, Q, T_l and C_a. The data are for *Celtis adolfi-friderici*.

Table 7.5. Parameter estimates for Equations 7.2a and 7.6 after fitting to all species in SRF. Ht. is height in m; J_{max}, V_{max}, and R_d are in μmol m^{-2} s^{-1}; θ is a coefficient defining the shape of the non-rectangular hyperbola in Equation 7.4; the best fit value for g_i was 0.65 mol m^{-2} s^{-1}. In parentheses are asymptotic 95% confidence limits.

Species	*Ht*	J_{max}	V_{max}	R_d	θ	r^2	*n*
A. ptercarpoides	40	83 (6)	37 (6)	1.8 (0.3)	10^{-5}	0.78	408
M. cecropioides	26	106 (10)	49 (7)	1.6 (0.3)	10^{-6}	0.82	197
C. adolfi-friderici	8	58 (5)	26 (5)	0.8 (0.1)	10^{-6}	0.84	163
S. stipitata	6	41 (4)	30 (1)	0.65 (0.2)	0.5	0.83	104
H. danckelmaniana	1	43 (4)	33 (2)	0.48 (0.3)	0.4	0.82	101
M. macrostachyum	0	66 (5)	59 (3)	1.0 (0.5)	0.4	0.88	69
Trichilia sp	0	40 (5)	37 (1)	0.31 (0.2)	10^{-5}	0.84	66

Photosynthetic characteristics of leaves through the vertical profile of the forest canopy

In general, the leaves exhibited higher V_{max}, J_{max} and R_d values at the canopy-top, and lower values nearer the ground; scatter visible at ground level in Figures 7.7a-d probably reflect the broken canopy in SRF where the radiation regime was very different for *Trichilia sp.* (in understorey shade) and *H. danckelmaniana* (in a gap). The differences in response to C_c between V_{max} and J_{max} describe the relative allocation in leaves to light capture and carboxylation, and thus provide a way of addressing the extent of light-acclimation in the SRF canopy. Measurements of leaf nitrogen and phosphorus permit an indirect approach, where variation in photosynthetic parameters could be related to leaf nutrient content (*c.f.*, Field, 1983; Schulze *et al.*, 1994). Figures 7.8a-h show variation in N_{leaf} and P_{leaf} with V_{max}, J_{max}, R_d and A_{max}; each regression is significant (Table 7.6). Together they suggest that a degree of photosynthetic acclimation to the light environment occurs, and provide limited support for proposals of an optimal nitrogen distribution in 'big-leaf' canopies (*e.g.*, Sellers *et al.*, 1992). The question of mass or area based expressions of gas exchange and leaf composition (see Chapter 6) is also relevant here. The poor relationship with height in N_{leaf} and P_{leaf} on a mass basis (Figure 6.5) suggests that nutrient concentration by mass does not necessarily reflect photosynthetic capacity. The role of non-photosynthetic nitrogen and phosphorus in determining these values requires further study.

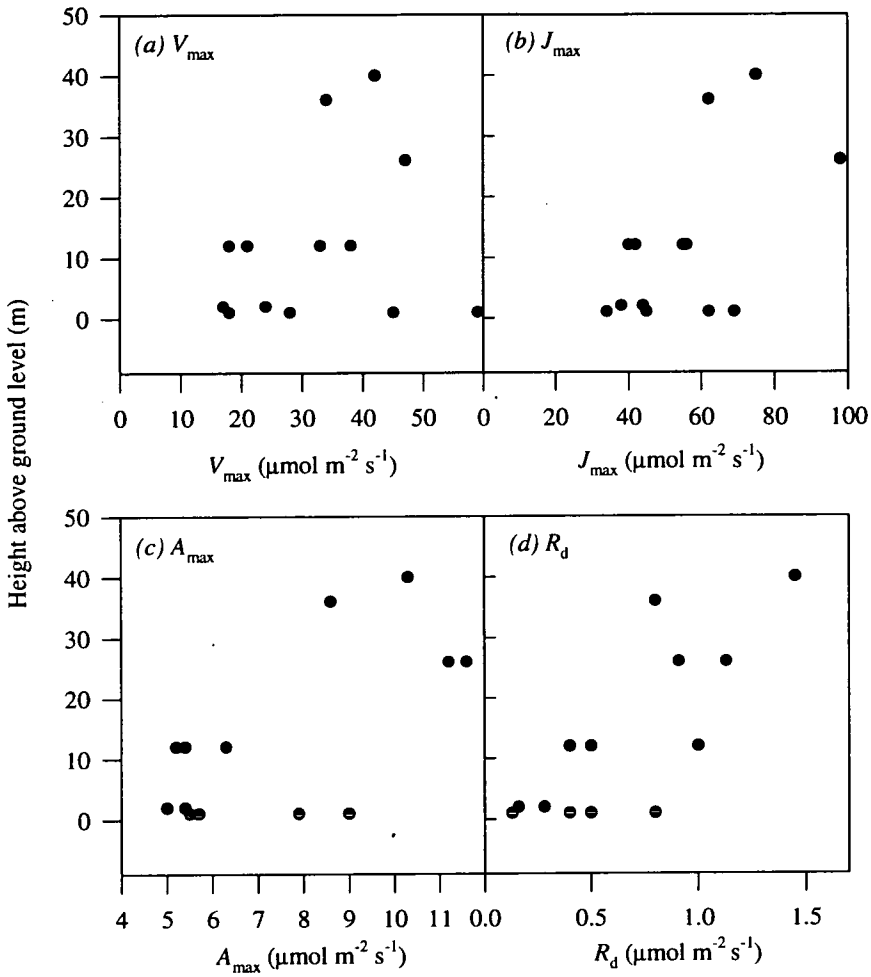

Figures 7.7a-c. Variation in the fitted photosynthetic parameters with height in the canopy of SRF. Figures (a)-(d) show V_{max}, J_{max}, A_{max} and R_d respectively. The data are from individual leaves (two per species).

Table 7.6. Regression results for the N_{leaf}/ P_{leaf} plots shown in Figures 7.8a-h, fitted using the relationship: $Y_1 = a.\ X_1 + b$, where X_1 is V_{max}, J_{max}, R_d or A_{max} in μmol m^{-2} s^{-1}, and X_1 is N_{leaf} or P_{leaf} in mol m^{-2}. The estimates were obtained from independent leaf estimates only. If the average values were used for each species, the regression results were almost identical, but not all were significant because only seven independent points could be used.

Parameter	*N/P*	*a*	*b*	r^2	*p*	*n*	*[X] at $Y_1 = 0$*
V_{max}	N	475	-25.9	0.39	0.02	14	0.055
J_{max}	N	760	-39.3	0.50	0.008	14	0.052
R_d	N	12.1	-0.95	0.57	0.001	14	0.08
A_{max}	N	78.5	-2.98	0.67	0.0004	14	0.038
V_{max}	P	33620	-46.2	0.47	0.01	14	0.0014
J_{max}	P	48270	-56	0.48	0.006	14	0.0012
R_d	P	680	-1.1	0.52	0.003	14	0.0016
A_{max}	P	4320	-3.54	0.56	0.002	14	0.0008

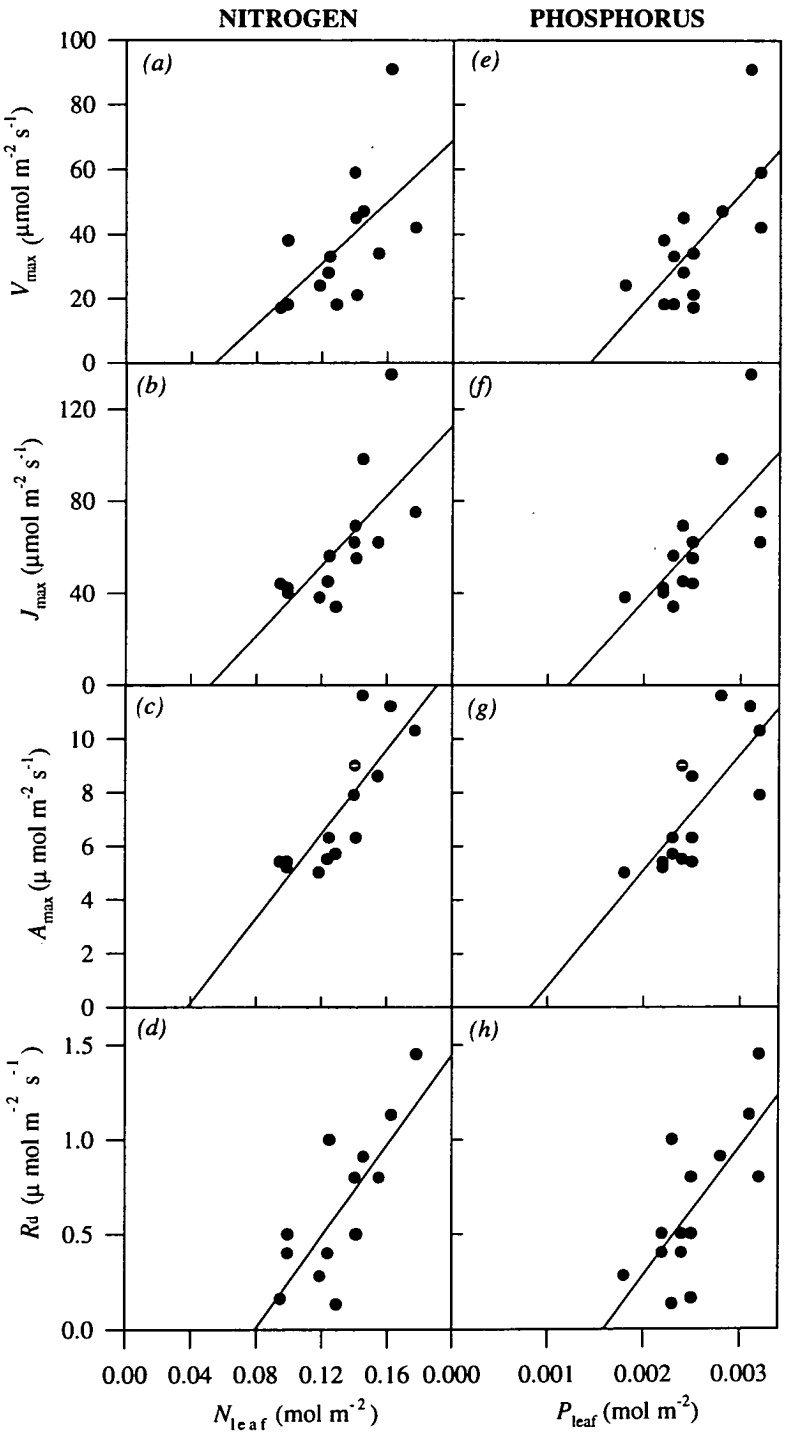

Figures 7.8a-h. Variation in the fitted photosynthetic parameters with N_{leaf} and P_{leaf}. In (a)-(h) respectively are: V_{max}, J_{max}, A_{max} and R_d. All regressions are significant ($p < 0.05$; see Table 7.6). The data are from individual leaves (two per species).

Comparison of N_{leaf} / P_{leaf} with leaf respiration (Chapter 6) and photosynthetic parameters

The regression for each photosynthetic parameter in Figure 7.8 parameterises N_{leaf} and P_{leaf} in the enzymes required for respiration and photosynthesis. Each has a negative intercept on the ordinate; at X_1 = zero, the graphs represent N_{leaf} and P_{leaf} that is not actively involved in photosynthetic metabolism. As in section 6.3, these intercepts are non-significantly different from zero (p = 0.05 - 0.06, except for R_d where $p < 0.05$). But the multiple linear regression between X_1 and leaf nitrogen and phosphorus is highly significant ($p < 0.001$; p(intercept) < 0.01; p(N coefficient) < 0.01; p(P coefficient) < 0.1), suggesting that the intercepts on the single element regressions are not artefacts. The residual N and P defined by these intercepts may be found in structural, or storage compounds that do not have high turnover rates. If the mean is taken of N_{leaf} and P_{leaf} at zero V_{max}, J_{max}, R_d and A_{max}, (Table 7.6) the values are very similar to those obtained for the same average 'low turnover' N_{leaf} and P_{leaf} in section 6.3, obtained from night-time leaf respiration data: N_{leaf} = 0.05 *vs* 0.04 mol m^{-2} and P_{leaf} = 0.001 *vs* 0.0008 mol m^{-2} (the data given second are derived using night-time leaf respiration rates, section 6.3).

Reich *et al.* (1994) quote A_{max} : N_{leaf} correlations for Amazon tree species from terra firme forest (*e.g.*, *Licania heteromorpha*) and tall caatinga forest (*e.g.*, *Caraipa heterocarpa*) in Brazil that are very close to the data in Table 7.6. On the other hand Harley *et al.* (1992) give data for cotton for a V_{max} : N_{leaf} relationship that is close, and a J_{max} : N_{leaf} relationship that is greater than these (at N_{leaf} = 0.11 mol m^{-2}, predicted V_{max} = 45 *vs* 37 and predicted J_{max} = 70 *vs* 142; units μmol m^{-2} s^{-1}, Harley *et al.* data given second). The differences may be real, or may reflect the effect of laboratory *vs* field measurement conditions. Figure 7.9 describes the variation in A_{max} with N_{leaf} and P_{leaf} for SRF in Cameroon; the response slope shows that, over the natural range in leaf nutrient composition, A_{max} is more sensitive to N_{leaf} than P_{leaf}, though both variables are significant. Further data of this type from nutrient limited and non-limited environments should illuminate the relative roles played by N and P in determining maximum leaf photosythesis and respiration rates. As with leaf respiration in Chapter 6, the separation from total leaf nutrient concentrations of N_{leaf} and P_{leaf} that is decoupled from leaf photosynthesis, may improve models seeking to treat canopies as a 'big-leaf' (Kull & Jarvis, 1996).

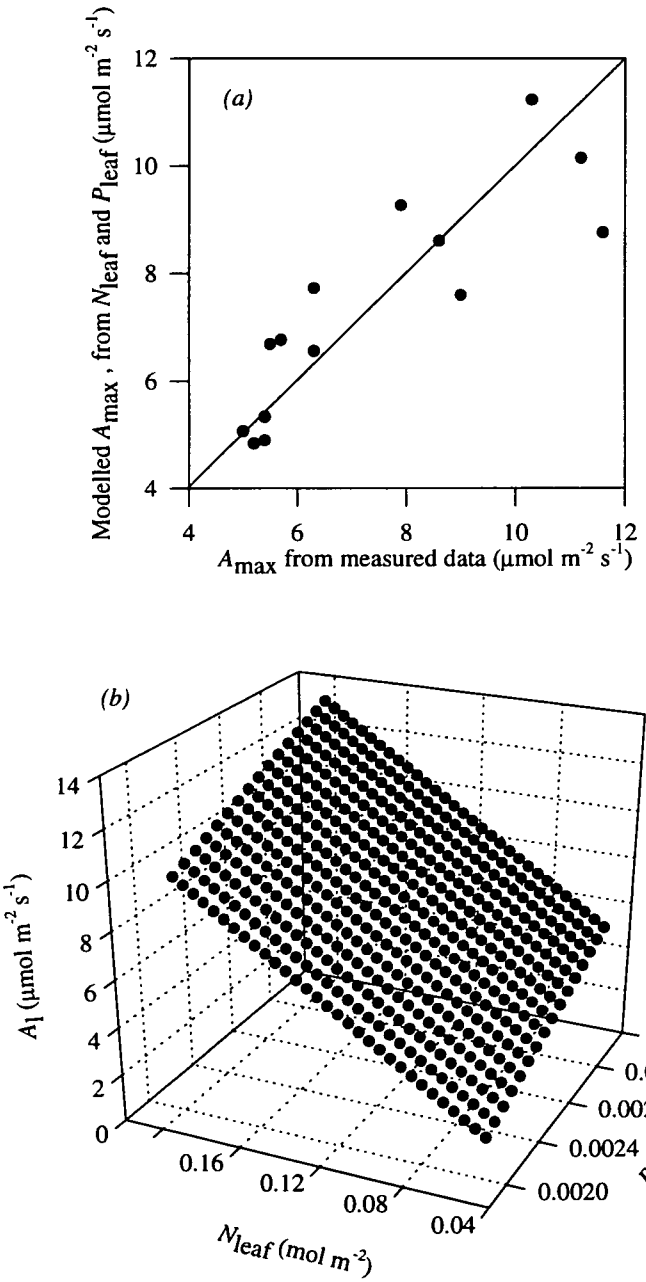

Figure 7.9a&b. The A_{max} : N_{leaf} and P_{leaf} relationship for SRF. In (a) is plotted measured *vs* modelled A_{max}, and (b) shows the model results for N_{leaf} and P_{leaf} over their measured physiological ranges. The r^2 value for the model is 0.74.

7.4 CONCLUSIONS

Leaf gas exchange was measured on leaves through the vertical profile of SRF, in March 1994. Diurnal patterns in stomatal conductance were similar to other tropical forests: g_s reached a maximum (100 - 400 mmol m^{-s} s^{-1}) in the early morning, between 0800 hrs and 1000 hrs, and declined over the day. Stomatal conductance was higher in some species (*e.g.*, *Megaphrynium macrostachyum*) near the forest floor, partly as a result of lower *D*, especially in the case of large leaves. Photosynthetic rates were also highest in the morning (2 - 7 μmol m^{-2} s^{-1}), though A_l tended to peak later in the day (0900 - 1200 hrs) in response to increasing radiation. Maximal rates of photosynthesis were a little higher than in an undisturbed forest in Cameroon (Koch *et al.*, 1994), though the mean values were rather similar to those from other tropical rain forests (Roberts *et al.*, 1990; McWilliam, 1996 [PRF site]).

An initial analysis of the light response in A_l showed A_{max} and α to decline with height in the canopy. The pattern with height exhibited variation which was attributed to the light environment consequent upon the irregular canopy cover in this secondary forest, particularly at the forest floor. A multiplicative model (*sensu* Jarvis) was fitted to the g_s data, whilst a biochemical model (*sensu* Farquhar) was fitted to the photosynthesis data. Both models fitted with r^2 values between 0.7 and 0.9 for most species. In particular, the two species highest in the canopy (*Musanga cecropioides* and *Amphimas distemonanthus*) showed A_l rates that were strongly affected by g_s; this variation was incorporated by the photosynthesis model but not by a simple light response model.

The variation in photosynthetic parameters with height in the canopy was related to leaf nutrient concentrations. There was a strong relationship between A_l and N_{leaf} or P_{leaf} on an area basis, which was partly a function of specific leaf area. The relative allocation of nitrogen and phosphorus to photosynthesising enzymes with respect to the leaf nutrient : A_l relationship requires further research.

8. Forest - atmosphere gas exchange

8.1 INTRODUCTION

The gas exchange behaviour of a forest stand can be modelled using component-level or whole-ecosystem data. The objective here is two-fold: first, to test how well understood are small- and larger-scale processes and the links between them, and secondly to make estimates of gas exchange for situations when measurement is not possible.

In this chapter, two canopy photosynthesis models are developed for estimating the carbon balance of SRF. To retrieve net forest gas exchange rates, the models are linked to respiration estimates and tested against eddy covariance observations. In the first, a multilayer model is developed by marshalling data from Chapters 2 - 7, and scaling organ-level physiological measurements to the whole forest. In the second, eddy covariance measurements are used to calibrate a photosynthesis model by assuming that the canopy behaves as a 'big-leaf'. This approach has some theoretical basis (Farquhar, 1989; Sellers *et al.*, 1992; Evans, 1993b), but has not been fully tested. The work presented here is the first attempt I am aware of that compares a big-leaf approach with up-scaled leaf photosynthesis and concurrent eddy covariance measurements for tropical forest. A big-leaf model of this sort has been presented elsewhere for PRF (Lloyd *et al.*, 1995a) and an annual carbon balance estimate made for the site (Grace *et al.*, 1995b). The respiration component of CO_2 exchange in PRF is also presented in this chapter, and considered along with the models for SRF in the context of climatic changes in temperature, radiation and carbon dioxide concentration.

8.2 METHODS

OVERVIEW

The two models for SRF are represented in Diagram 8.1. Canopy photosynthesis is calculated using parameters derived (i) from leaf-level chamber measurements at different heights in the canopy, given

in Chapter 7 (this is referred to as the multilayer model) and (ii) canopy-level measurements made using the eddy covariance technique, given in this chapter (this is referred to as the big-leaf model). For the multilayer model, photosynthesis at each level is scaled according to the vertical profile in leaf area density (Figure 3.5). Respiration is treated as the component sum of CO_2 efflux from soil, wood and leaves, and is calculated from the parameters derived in Chapters 3, 4, 5, and 6. Respiration is combined with photosynthesis in both models to yield the net canopy assimilation rate. Both photosynthesis and respiration are driven using above-canopy weather station climate data; in-canopy climate variables are derived from these data using empirical models. The model outputs are analysed by comparison with the eddy covariance measurements in SRF (Grace *et al.*, unpublished). For PRF, component-summed respiration is estimated and presented in the context of a big-leaf model for this forest (Lloyd *et al.*, 1995b).

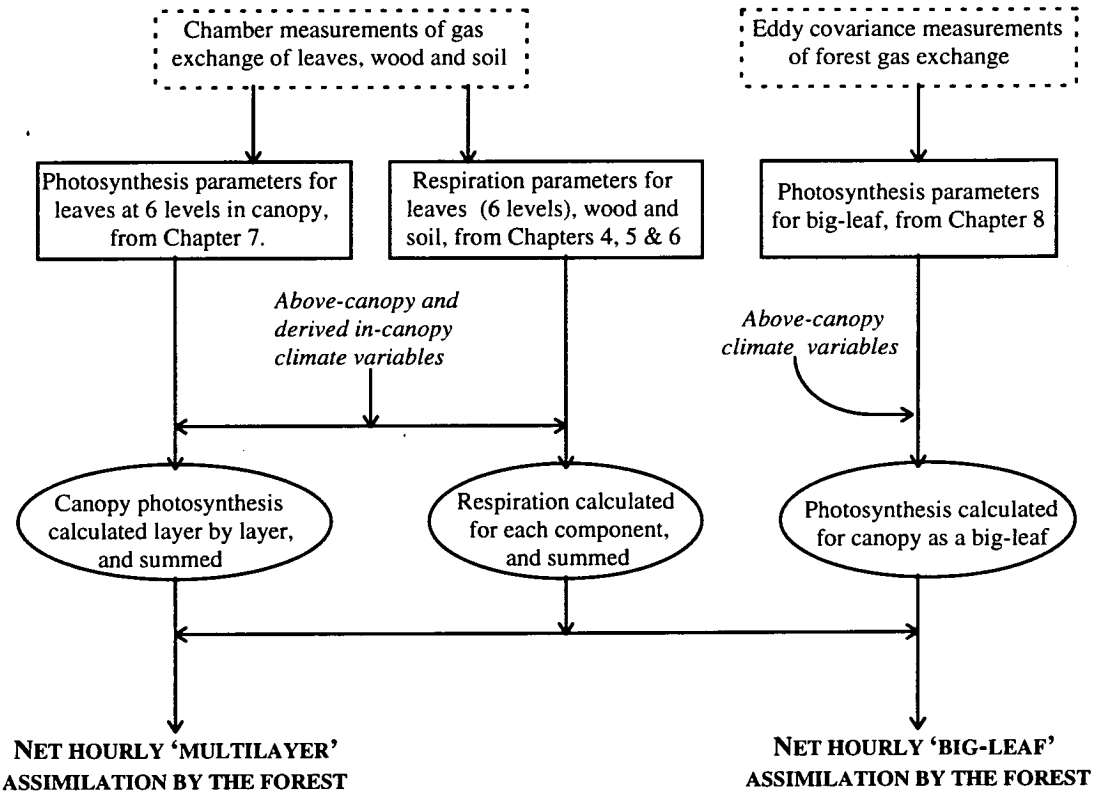

Diagram 8.1 A description of how forest gas exchange in SRF is estimated using the multilayer and big-leaf models. Gas exchange measurements are in broken-line boxes; parameters in solid-line boxes; driving environmental variables in italics; model calculations in elipses; and model outputs are in bold capitals. For respiration, in-canopy climate data are used to drive leaf respiration, whilst soil and woody tissue temperatures at different heights are driven using the above-canopy measurements.

MEASUREMENT AND ESTIMATION OF THE DRIVING ENVIRONMENTAL VARIABLES

Each measured variable (temperature, humidity, CO_2) was related to the reference above-canopy weather station measurements in order to provide hourly estimates. The procedures used for this are described below.

Temperature

Continuously measured tissue temperature, T_t, and soil temperatures, T_s, (see Chapters 4 & 5) were empirically related to above-canopy dry bulb temperatures, T_c, obtained from the weather station. In the case of woody tissue, the measured temperature at each height was taken as the mean of 'shielded' (underside of branch), and 'unshielded' (top side of branch) readings. For soil, the reference depth used was 1 cm, chosen to match that used for the measurement of CO_2 efflux from soil. Where it was necessary to introduce a time lag between the solar zenith and localised maxima, a polynomial function was fitted to the data that included a time component, as shown in Equation 8.1. This was important for soil temperatures which tended to peak between 1600 hours and 1700 hours.

Form of fitted equation used to predict T_t and T_s from T_c:

$$T_{pred} = (\cos(t + a))\, b + cT_c + dT_c^2 + e \qquad \text{Equation 8.1}$$

where T_{pred} is predicted tissue or soil temperature, t is time in radians (where midday = π rads) and a - e are fitted constants. If a satisfactory model could be obtained using fewer fitted constants, this approach was favoured.

In Brazil and Cameroon, woody tissue temperature was logged at six heights by embedding Co-Cn thermocouples into the bark surface (Chapter 5). Night-time leaf temperatures were measured as part of the leaf respiration measurements made in both forests, though only in SRF were daytime leaf temperatures obtained, as part of the photosynthesis measurements (Chapters 6 & 7). Also available in the larger dataset from Cameroon (Grace *et al.*, unpublished) were a sequence of air temperature profiles obtained between 9th and 28th of March, 1994 by Dr J. Lloyd of ANU, Canberra. Other variables measured in the canopy profile were the ambient water vapour pressure deficit and ambient CO_2 concentration. Temperature and water vapour were recorded at four heights (1 m, 15 m, 33 m and 46 m) using psychrometers, and CO_2 concentrations were recorded at six heights (1 m, 7 m, 15 m,

22 m, 33 m and 46 m) by pumping air from each sampling point through Decabon tubing to an infra-red gas analyser.

Soil temperature at 1 cm depth was measured for each CO_2 efflux measurement microsite, and was also continuously recorded (Chapter 4). In SRF, soil temperature profiles were obtained at several sites. The continuous temperature records were fitted to Equation 8.1, and the extent to which they were representative of spatial variation over the forest floor was assessed by comparison with the spot measurements obtained from the microsites at which CO_2 efflux was measured.

Water vapour pressure deficit and carbon dioxide concentration

Water vapour pressure deficits (D) and CO_2 concentrations (C_a) were measured throughout the vertical profile of the SRF canopy during measurement of photosynthesis, and on a continuous basis as part of the profile dataset. Longer term measurements were made of D and C_a above the canopy (denoted D_c and C_{ac}) using the weather station and the eddy covariance equipment (Grace *et al.*, unpublished). As with temperature, empirical relationships between D or C_a at any given height in the canopy and that obtaining above the canopy were derived. The variation in D with height was modelled as a simple first or second order function of D_c, whilst with C_a, variation in the shape of the profile according to time of day was incorporated into the expression driven by C_{ac}.

Radiation flux

The photosynthetically active photon flux density (Q, in μmol quanta m^{-2} s^{-1}) was measured at six heights in the canopy (44 m, 24 m, 16 m, 8 m, 4 m, and 1 m) during a 14 day period from April 28th to May 12th 1994 (Grace *et al.*, unpublished). The ratio of above-canopy solar radiation to Q was determined, and logarithmic radiation profiles derived for hours of the day with similar profile shapes. The equation used to relate Q at any given height, Q_h, with Q_c above the canopy was:

$$Q_h = \exp[\, a_t (h\, b + c)] \qquad \text{Equation 8.2}$$

where a_t is the ratio between measured and expected Q_c at the time t, and b and c are fitted constants, and Q_h is Q at height h (m). Expected Q_c is obtained from the linear regression between $\ln Q$ and h for each time period, t.

MEASUREMENT AND PROCESSING OF ABOVE-CANOPY EDDY COVARIANCE DATA

The Edinburgh University eddy covariance system, Edisol, was erected at 46m above the ground. The components and operation of the equipment are described in detail elsewhere (Moncrieff *et al.*, 1996). Likewise, the processing of raw data to reveal above canopy fluxes of the different scalars of interest is given in the same publication. Raw fluxes were corrected by J. McIntyre, Edinburgh University, for density fluctuations and attenuation of the signal down the tube (Webb *et al.*, 1980; Leuning & Moncrieff, 1990), and for sensor separation (Moore, 1986). Although some of the high frequency signal was lost through smearing effects in the sampling tube, this was recovered using transfer functions derived by comparison of the data with an 'ideal' co-spectral density function (Kaimal *et al.*, 1972). Uncertainty in the flux measurement is estimated at ±15 - 20% using this method (Baldocchi *et al.*, 1988; Moncrieff *et al.*, 1992).

Barring a few small gaps, a record of the net exchange of CO_2 between the forest and the atmosphere, F_n, was logged from 3rd March to 6th May 1994. Similarly, net fluxes of heat and water vapour were also obtained (Grace *et al.*, unpublished). Standard climatological variables were recorded during this period using instrumentation provided by Edinburgh University and the Institute of Hydrology (Campbell Scientific Ltd, UK, and Didcot Instruments, UK). The data were measured at the same height to give hourly means of solar radiation, net radiation, aspirated wet and dry bulb temperature, vapour pressure deficit, and rainfall.

In an initial analysis of the CO_2 profile data (J. Lloyd, unpublished), spline curves were fitted for each half hour, and the difference between successive intervals calculated to give the change in storage of CO_2 in the canopy space ($M\mathrm{d}C_a / \mathrm{d}t$). When subtracted from the net ecosystem exchange, the net assimilation of CO_2 by the ecosystem, F_{eco}, can be calculated using Equation 8.3 (Grace *et al.*, 1995b).

$$F_n = F_{eco} + M\mathrm{d}C_a / \mathrm{d}t \qquad \text{Equation 8.3}$$

The measured water vapour fluxes were used to calculate canopy stomatal resistance to water vapour, r_s, and by extension, to CO_2 (Jarvis, 1976). Data were derived at hourly intervals by first calculating the aerodynamic resistance, r_a, (Equation 8.4), and then inverting the Penman-Monteith equation (Equation 8.5) to give r_s:

$$r_a = \left(\frac{u}{u_*^2}\right) + \frac{1}{ku_*}\left[\ln\left(\frac{z_{0M}}{z_{0H}}\right) + \psi_M - \psi_H\right] \qquad \text{Equation 8.4}$$

where r_a is aerodynamic resistance in s m^{-1}, u is the mean horizontal wind speed in m s^{-1}; u^* is friction velocity in m s^{-1}; and k is von Karman's constant (~ 0.41). The term $\ln(z_{oM} / z_{oH})$, taken as 1.5 (Garratt, 1992), corrects for the differences in the sites of the sources and sinks, transport resistances and transfer mechanisms between momentum and heat or mass. The last terms, ψ_M and ψ_H, are the integral diabatic correction factors for heat and momentum (Paulson, 1970); the formulae for their calculation are given in Appendix D.

$$r_s = \frac{\left(E\lambda s\, r_a - sR_n r_a - \rho_a c_p D\right)}{E\lambda\gamma} \qquad \text{Equation 8.5}$$

where r_s is the stomatal resistance in s m^{-1}; E is the flux of water vapour in mmol m^{-2} s^{-1}; λ is the latent heat of vapourisation of water vapour in J g^{-1}; γ is the psychrometer 'constant' in Pa K^{-1}; s is the rate of change of the saturation vapour pressure with temperature in Pa K^{-1}; R_n is the net radiation in W m^{-2}; ρ_a is the density of dry air in kg m^{-3}; and c_p is specific heat of dry air in J kg^{-1} K^{-1}.

The resistances represented by r_a and r_s may be converted into molar conductances which are used elsewhere in this thesis by application of Equation 8.6.

$$g_s = \frac{P}{(RTr_s)} \qquad \text{Equation 8.6}$$

where g_s is stomatal conductance in mmol m^{-2} s^{-1}; P is pressure in kPa; and R is the universal gas constant (8.314 J mol^{-1} K^{-1}). The formulae used for the calculation of λ, s, ρ_a, γ and e_s, the saturation water vapour pressure, are given in Appendix D. The values were corrected for the average ambient pressure of 930 mbar.

MODELLING RESPIRATION AND ASSIMILATION

Respiration (PRF and SRF)

Spatially robust estimates of the amount of physiologically active tissue are required for stand-scale calculations of respiration. In the case of wood and foliage, detail in the vertical dimension is needed to correctly estimate the effect of a diurnally changing temperature profile on respiring tissue at different heights. For above-ground biomass, spatial estimates were obtained using the data presented in Chapter 3.

The temperature responses for soil efflux were taken from Chapter 4 (Equation 4.3), and night-time leaf respiration characteristics were taken from Chapter 6 and combined with the vertical profile in LAI (Figure 3.5) to give summed foliar respiration for total LAIs of 4 (PRF) and 4.4 (SRF). Errors in the calculated leaf respiration rates were obtained by varying the total LAI for each forest according to the upper and lower 95% confidence limits of the measured values shown in Figure 3.4.

Woody tissue respiration was calculated for individual trees, and separately for boles and branches. Fluxes of CO_2 from boles were calculated according to the d_{bh} and height of each stem by estimating the frequency of 50 cm long woody sections of different diameters and applying Equation 5.3 to each section. The temperature sensitivities for respiration used Equation 5.2 and were taken from Table 5.2. A conic function was used to describe the variation in stem diameter with height. Data on branch respiration are very sparse, though branch tissue is generally more active than stem tissue (Sprugel *et al.*, 1994). Table 3.2 showed that branch biomass was approximately 20% of stem biomass. Allowing for a higher ratio of active : inactive biomass, branch respiration was estimated at 40% of stem respiration. In SRF, the fluxes of CO_2 from rotting dead wood were calculated by assuming each decaying log was of the diameter and length given in the inventory described in Chapter 3, and applying Equations 5.2 and 5.3. The total uncertainty in the flux of CO_2 from woody tissue was difficult to calculate. In SRF an error was derived for effluxes from boles and dead wood by comparing the two 1 ha plot inventories. This was not possible in PRF and so a maximum error was ascribed by applying that derived for SRF.

Total canopy respiration, R_t, was calculated at hourly intervals using the sum of the wood and soil components during daylight hours, and the sum of the wood, soil, and leaf components during the night.

Photosynthesis (SRF)

Multilayer model:

The measured leaf-level parameters given in Tables 7.3 and 7.5 were assumed to represent accurately the average properties of foliage at each of the six heights in the canopy (1 m, 7 m, 15 m, 22 m, 33 m, and 46 m). Photosynthetic parameters for ground level vegetation were highly variable in SRF (Table 7.5). This was accounted for by assuming that 15% of the vegetation at ground level exhibited characteristics similar to gap-dwelling herbs of the genera *Megaphrynium* and *Haumanaiana*, whilst the remaining 85% behaved in a similar way to the understorey leaves of *Trichilia*.

Using measured or simulated values, stomatal conductance and assimilation at each level was predicted at hourly intervals using Q, T, C_a, and D to drive Equations 7.1, 7.3 and 7.15. Whole canopy fixation, F_{cm}, was obtained by scaling the photosynthetic rate to the LAI measured at each height (Chapter 3). During the hours of darkness ($Q = 0$), measured leaf respiration rates were used in favour of the R_d values fitted to the photosynthetic measurements. The net modelled ecosytem exchange, F_{ecom} was then calculated for this composite model by subtracting R_t from F_{cm}.

Big leaf model:

The big leaf model was parameterised using F_{eco} values (Equation 8.3) corrected for respiration, R_t, to give the total canopy assimilation, F_c, according to Equation 8.7:

$$F_c = F_{eco} + R_t \qquad \text{Equation 8.7}$$

However, high quality data were required for the fitting procedure (Grace *et al.*, 1995a), as the aim was to parameterise the photosynthetic physiology of the canopy rather than a mixture of the photosynthetic process and several micrometeorological processes that may have been occurring simultaneously. Examples of the latter include: conditions when the radiation field was changing rapidly; when the aerodynamic conductance was very low; when the leaves were wet; situations where the fetch was affected by a nearby settlement; and periods of exceptional CO_2 fluxes from the canopy in the early morning resulting from turbulent flushing events. F_c data during these conditions were filtered out to give a selected dataset, F_{cs}. A parsimonious approach was followed in the selection of data so as to minimise any possible bias so caused.

The F_{cs} data were analysed using the same techniques described for individual leaves in Chapter 7. A Jarvis-type model (1976) was fitted to canopy [stomatal] conductances (Equation 7.15), and a Farquhar & von Caemmerer model (1982) was fitted to the assimilation data, using Equations 7.1 and 7.3. The resulting parameters were then used to model as a big-leaf the total canopy assimilation, F_{cb},. Hourly weather station data were used to run the simulations. Net modelled fluxes of carbon dioxide were obtained by removing R_t from F_{cb} at hourly intervals to reveal the ecosystem exchange, F_{ecob}.

The performance of each model was examined with respect to the eddy covariance measurements. Their response to changes in major climatic parameters (temperature; radiation, carbon dioxide concentration) was also discussed.

LIST OF SYMBOLS USED IN THIS CHAPTER

Basic climate variables:

C_a, C_{ac}	CO_2 concentration of air (μmol mol^{-1}). C_{ac} refers to above-canopy C_a.
D, D_c	Water vapour pressure deficit of air (mol mol^{-1}). D_c refers to above-canopy D.
Q, Q_c	Photosynthetically active photon flux density (μmol quanta m^{-2} s^{-1}). Q_c refers to above-canopy Q.
R_n	Net radiation (W m^{-2}).
T_t, T_s, T_{pred}, T_c	Temperature (°C). The subscripts t, s, pred and c refer respectively to tissue, soil, p redicted and above-canopy temperatures.
u	Mean horizontal wind speed (m s^{-1}).

Fluxes, conductances and resistances:

E	Flux of water vapour between forest canopy and the atmosphere (mmol m^{-2} s^{-1}).
F_n / $_c$ *etc*	CO_2 flux between the forest stand and the atmosphere, or ecosystem exchange (units in μmol m^{-2} s^{-1}). The subscripts n, c, cs, eco, ecom and ecob refer repectively to: net measured fluxes, canopy photosynthesis (corrected for respiration terms from soil and wood), selected dataset of canopy photosynthesis, storage corrected [biotic] fluxes, and modelled net fluxes using the multilayer and big-leaf models.
g_s / $_{sc}$ *etc*	Stomatal conductance to water vapour (mmol m^{-2} s^{-1}). The subscripts s, sc, scm and scb refer respectively to leaf-level conductance, canopy conductance, and modelled canopy conductance using the multilayer and big-leaf models.
r_a	[Canopy] aerodynamic resistance (s m^{-1}).

r_s	[Canopy] stomatal resistance to water vapour (s m^{-1}).
R_t	Total forest respiration - CO_2 efflux from soil + wood + leaves (mmol m^{-2} s^{-1})
g_a	[Canopy] aerodynamic conductance (mmol m^{-2} s^{-1})

Aerodynamic variables:

u^*	Friction velocity (m s^{-1}).
ψ_M , ψ_H	Adiabatic correction factors for momentum and heat respectively (Paulson, 1970).
z_{oM} , z_{oH}	Roughness length for momentum and heat respectively. z_{oH} also represents the roughness length for H_20 and CO_2 in this treatment (m).

Constants or known variables:

c_p	Specific heat of dry air (J kg^{-1} K^{-1}).
γ	Psychrometer 'constant' (Pa K^{-1}).
k	von Karman's constant (~ 0.41).
λ	Latent heat of vapourisation of water vapour (J g^{-1}).
P	Pressure in (kPa).
R	Universal gas constant (8.314 J mol^{-1} K^{-1}).
ρ_a	Density of dry air (kg m^{-3}).
s	Rate of change of the saturation vapour pressure with temperature (Pa K^{-1}).

8.3 RESULTS

DRIVING ENVIRONMENTAL VARIABLES

Temperature (PRF and SRF), water vapour pressure deficit (SRF) and radiation (SRF)

Figure 8.1 shows a comparison between predicted and observed soil temperatures in PRF and SRF. The modelled soil temperatures agree well with the measured data. The amplitude in soil temperature was 1 - 3 °C for both forests. The functions relating T_c to wood or air temperature at different heights in the canopy fitted to the observed data with good accuracy, giving r^2 values of 0.9 - 0.98 (Appendix D). The variations in wood temperature with height were shown in Figures 5.1a and b; typical air

temperature profiles for SRF are shown in Figure 8.2a. In general, wood temperatures were slightly higher in PRF during the day (28 - 40 °C in PRF *vs* 28 - 33 °C in SRF) but similar in both forests during the night (18 - 21 °C for PRF and SRF).

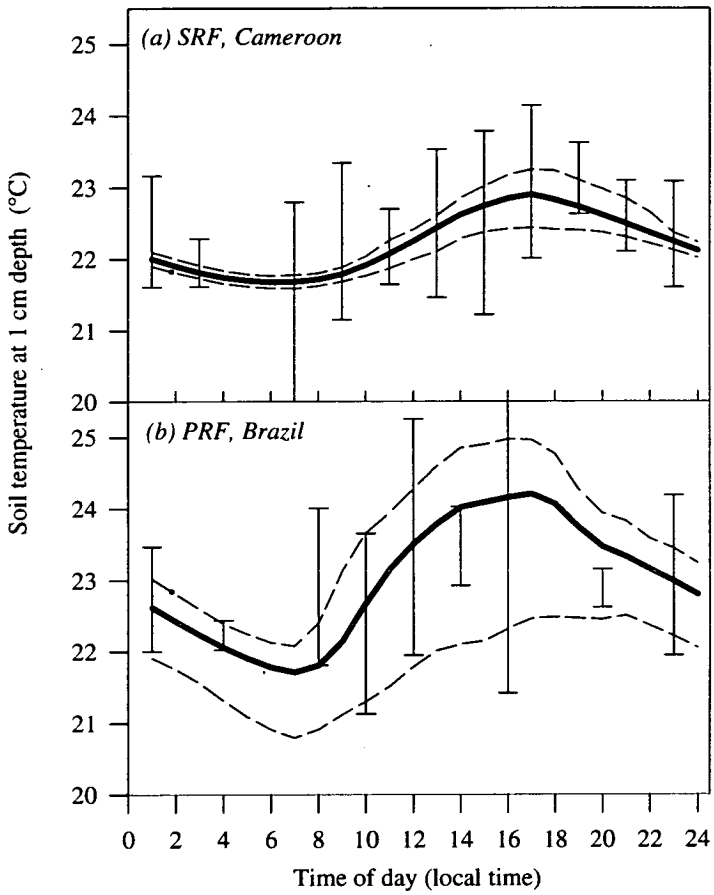

Figure 8.1. Modelled and measured soil temperature at 1 cm depth for SRF and PRF. Thick lines = mean estimated value; broken lines = maximum and minimum estimated values; vertical lines = 95% confidence limits of all measurements of individual microsites used for soil efflux measurement (n = 178 and 42 for SRF and PRF respectively). The modelled values used for the comparison are averages for each measurement period.

The vertical profile in D for SRF could also be described accurately by simple regression models driven from D_c (Appendix D). Typical profiles are shown in Figure 8.2b; the water vapour pressure deficit varied from close to zero during the night to maximum values of 0.025 mol mol^{-1} during the early afternoon.

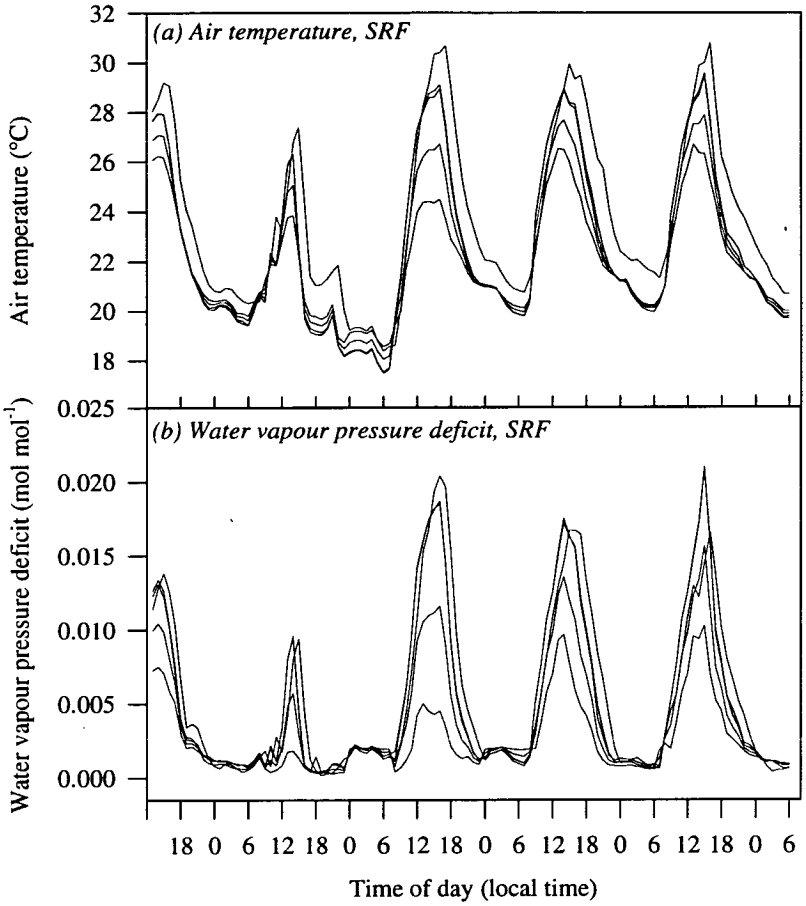

Figure 8.2a&b. Profiles of air temperature and water vapour pressure deficit in SRF, from 8th to 13th March, 1994. The measurement heights are 46 m, 24 m, 16 m 8 m and 1 m above the ground. The data were collected by J. Lloyd (ANU, Canberra).

Figure 8.3a shows measured Q from April 28th to May 3rd.. Midday values above the canopy rose to 1600 - 1800 μmol m^{-2} s^{-1}, whilst those nearer the canopy floor reached 70 - 200 μmol m^{-2} s^{-1}. The nature of the extinction curve varied with time of day, but in all cases could be linearised with respect to height using a ln$Q$ transformation. Following linearisation, quantitatively similar Q profiles were encountered for three groupings of hours representing: the early morning and evening (0600 - 0700 hrs, 1800 hrs) the middle morning and late afternoon (0800 - 0900 hrs, 1600 - 1700 hrs), and the middle hours of the day (1000 - 1500 hrs). Linear regressions were fitted to these data and gave r^2 values of 0.8 - 0.9 (Appendix D). Simulated values were obtained by scaling the fitted profile to the measured radiation above the canopy recorded by the weather station. Figures 8.3b-d show sample plots of measured *vs* modelled Q at 45 m, 8 m and 1 m above the ground for 28th April to 3rd May.

Higher in the canopy, the agreement was good, whilst nearer the ground the relationship was a little noisier. Where modelled values were in error they tended to slightly overestimate the measured data. However, none of the plots was significantly different from a 1:1 line at the 95% confidence level.

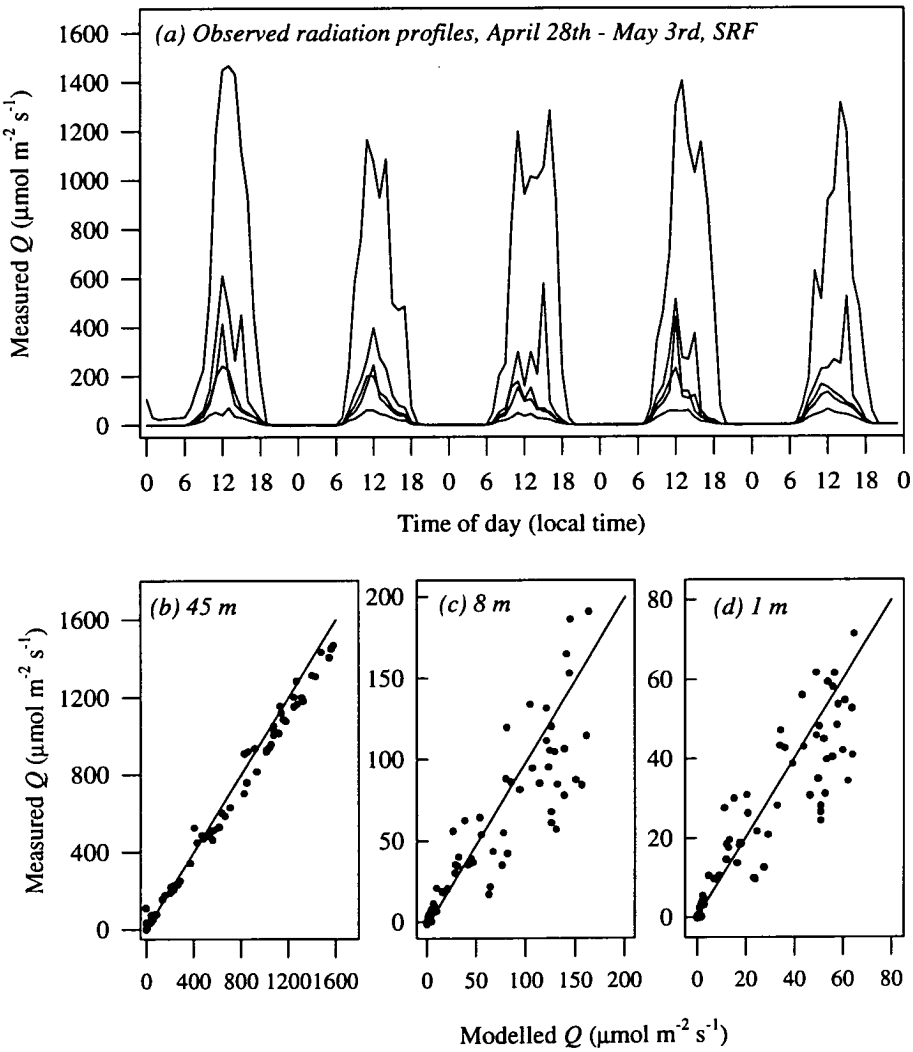

Figure 8.3a-d. In (a) are shown observed profiles in Q for 28th April to 3rd May, 1994, in SRF. Data are plotted from 45 m, 24 m, 16 m, 8 m and 1 m above the ground. In (b) - (d), measured *vs* modelled data are shown for the same dates, at three of the levels: 45 m, 8 m and 1m, with 1:1 lines drawn in. The measurements were made by Grace *et al.* (unpublished).

Carbon dioxide concentrations (SRF)

The mean profile of CO_2 concentration varied during the day. In the early morning, average concentrations throughout the canopy were greater than 400 μmol mol^{-1} and near ground level this increased sharply to 450 - 500 μmol mol^{-1}. During the middle of the day, increased turbulence created an almost vertical profile between the canopy-top (C_{ac}) and the 7 m level, with C_{ac} values dropping to around 360 μmol mol^{-1}. Below 7 m, mean C_a was proportionately greater than C_{ac}, this proportion differing hourly. Towards the end of the day overall concentrations began to rise, and a through-canopy gradient in C_a was generated again, with C_{ac} reaching a mean value of 380 μmol mol^{-1} by 1900 hrs (Figure 8.4a).

These patterns were used to model empirically the in-canopy CO_2 concentrations. For the hours during the middle of the day, a vertical profile from C_{ac} to C_a at 7 m (taken as a mean difference of less than 2 μmol mol^{-1} between C_{ac} and C_a at 7m) was assumed. The remaining hours at the start and end of the day were simulated individually by using the mean linear gradient in the profile from C_{ac} to C_a at 7m. For each daylight hour, C_a at 1 m was estimated as a fixed multiple of C_a at 7 m. This method permitted the estimation of C_a within the canopy for all hours when C_{ac} was measured using the eddy covariance equipment. Appendix D gives the fitted functions describing these gradients, and lists the mean hourly fractional increase in C_a from 7 m to 1 m. Measured *vs* modelled C_a values are plotted in Figure 8.4b-d for 36 m, 8 m and 1 m above ground level. None of the plots was significantly different from a 1:1 identity at the 95% confidence level.

EDDY COVARIANCE AND CANOPY STORAGE (SRF)

The aerodynamic properties of the SRF canopy were similar to those found elsewhere in tropical forests. Figures 8.5a and b indicate the relationships between wind speed (u), friction velocity (u^*), and the aerodynamic conductance (g_a) to heat, CO_2 and water vapour. For u^*, the response to wind speed was linear with a gradient of 0.19 and an intercept statistically identical to zero. Aerodynamic conductance was also a linear function of wind speed, with maximum values of g_a reaching ~4 mol m^{-2} s^{-1}. Higher values of g_a were observed during the day than night. g_a (note Equation 8.6 for $r_a \leftrightarrow g_a$ interconversion) was sensitive to the value used for the term $\ln(z_{oM} / z_{oH})$ in Equation 8.4; the value considered most likely by Garratt (1992) is 1.5, and was used here. Variation in $\ln(z_{oM} / z_{oH})$ generates differences in the calculated values for r_s, the canopy resistance to water vapour, but despite this

caveat, canopy g_s showed diurnal patterns that were coherent with the other measured micrometeorological variables (Figure 8.6).

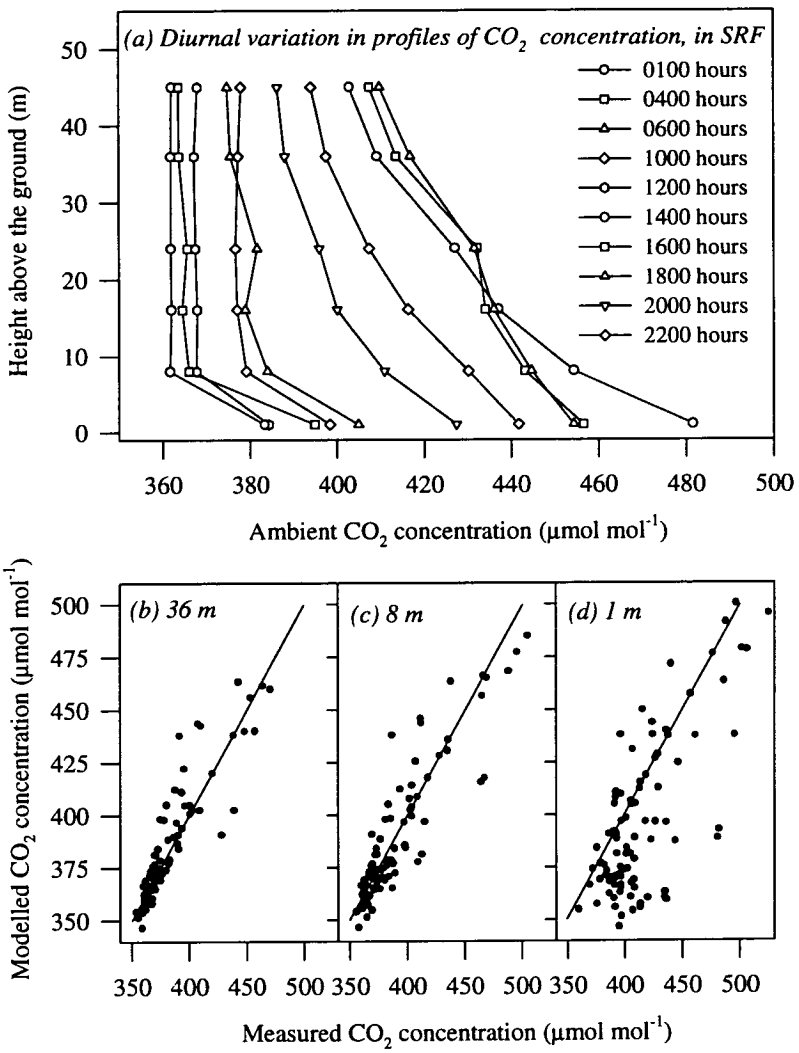

Figure 8.4a-d. In (a) are shown the mean vertical profiles in CO_2 concentration through the canopy in SRF. The measurements in (a) are from 9th - 15 th March, 1994, and were made by J. Lloyd (ANU, Canberra). Figures (b) - (d) show the plots of measured *vs* modelled data from three heights: 36 m, 8 m, and 1 m, with 1:1 lines.

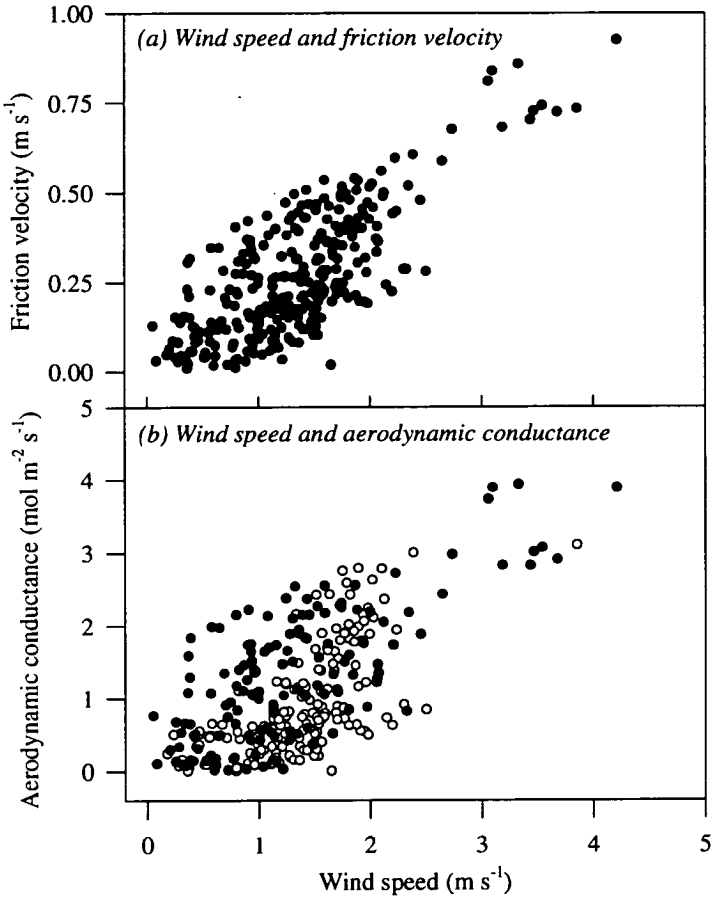

Figure 8.5a&b. The relationships between wind speed and (a) friction velocity and (b) aerodynamic conductance in the SRF canopy. In (b), the spots are during unstable conditions, and the open circles are during stable conditions. Data were derived from eddy covariance measurements made by Grace *et al.* between 8th March and 13th March, 1994.

Using the spline-curve fitting procedure, the night-time canopy storage values were found to be extremely variable and will be analysed further (J. Lloyd, *personal communication*). However, during the day, storage was typically low and could be calculated using standard techniques, making possible the estimation of F_{eco}.

The sequence of panels in Figure 8.6 shows typical meteorological, canopy conductance, F_n, canopy storage and F_{eco} data, obtained from March 17th, 1994. Micrometeorological convention requires that negative signs denote mass gain by the canopy (downward flux of gases from the atmosphere). In this presentation however, the physiologist's approach of using positive signs for assimilation is retained in order to make clear the subsequent big-leaf modelling procedures that employ the same equations as

were used for individual leaves in Chapter 7. During the day, Q rose to a maximum of 1700 μmol m^{-2} s^{-1} at 1200 hrs, and the same pattern was mimicked by transpiration. Plotted below these traces are temperature, g_s and D. The vapour pressure deficit rose during the day to reach a peak of 0.02 mol mol^{-1} around 1500 - 1600 hrs, whilst g_s commenced the day at maximum values of 0.8 mol m^{-2} s^{-1}, dropping sharply by mid-morning and then falling more gradually. Lower values of g_s coincided with D. The increase visible in g_s at 1600 hrs was also reflected in the transpiration and assimilation records. The storage term during the day was largest in the early morning, as CO_2 was both vented from, and assimilated by, the canopy. After 0900 hrs, the canopy became further coupled to the airflow above, reducing the storage term, and making F_c and F_{eco} rather similar. Net assimilation rates increased rapidly in the morning and reached a peak of 15 - 16 μmol m^{-2} s^{-1} between 10 am and 1 pm, tailing off in the afternoon in response to the reductions in g_s and Q. The canopy reached a carbon compensation point at 1700 - 1800 hours, after which it returned to being a net source for CO_2 during the night.

Canopy physiology

The period when all measurements were in progress, from which g_s, F_c and F_{eco} could be directly calculated was limited to March 9th - March 22nd. After discounting night-time values, and a period on day 72 when weather station data were not recorded, a total of 225 data points were available. Selection for measurements that could be used for the modelling of canopy photosynthesis excluded 176 points, leaving a core of 46 high quality measurements, or approximately 21% of the original total.

Figure 8.7a shows the light response characteristics of the selected F_{eco} data. Photosynthetic assimilation was approximated a linear function of Q up to 800 μmol m^{-2} s^{-1}, and above that the response began to saturate. A linear regression was fitted to the data for $0 < Q < 800$ μmol m^{-2} s^{-1} to determine the initial characteristics of the light response curve. The quantum requirement was approximately 40 (±7) photons per mole of fixed CO_2; and the apparent dark respiration of the system was 5.8 (±1.5) μmol m^{-2} s^{-1}; errors are 95% confidence limits, $n = 28$. After removal of R_t from each F_{eco} value to give F_{cs}, the data also show that maximal canopy photosynthesis reached 20 - 25 μmol m^{-2} s^{-1}, though light saturated rates were modulated by stomatal conductance (data not shown). Stomatal conductance itself varied as a function of D and Q (Figure 8.7b), and the sensitivity of conductance to D was improved by using canopy ('leaf')-to-air vapour pressure deficits obtained from an analytical

solution of the energy balance to yield leaf temperature given by Jones (1992, Equation 9.5). Figure 8.7b indicates a positive correlation between g_{sc} and Q, and a negative correlation with D. However, there were a few (marked by a triangle on Figure 8.7b) unexpectedly high g_{sc} values associated with high D values. The individual responses in g_{sc} to Q and D are shown in Figures 8.7c&d.

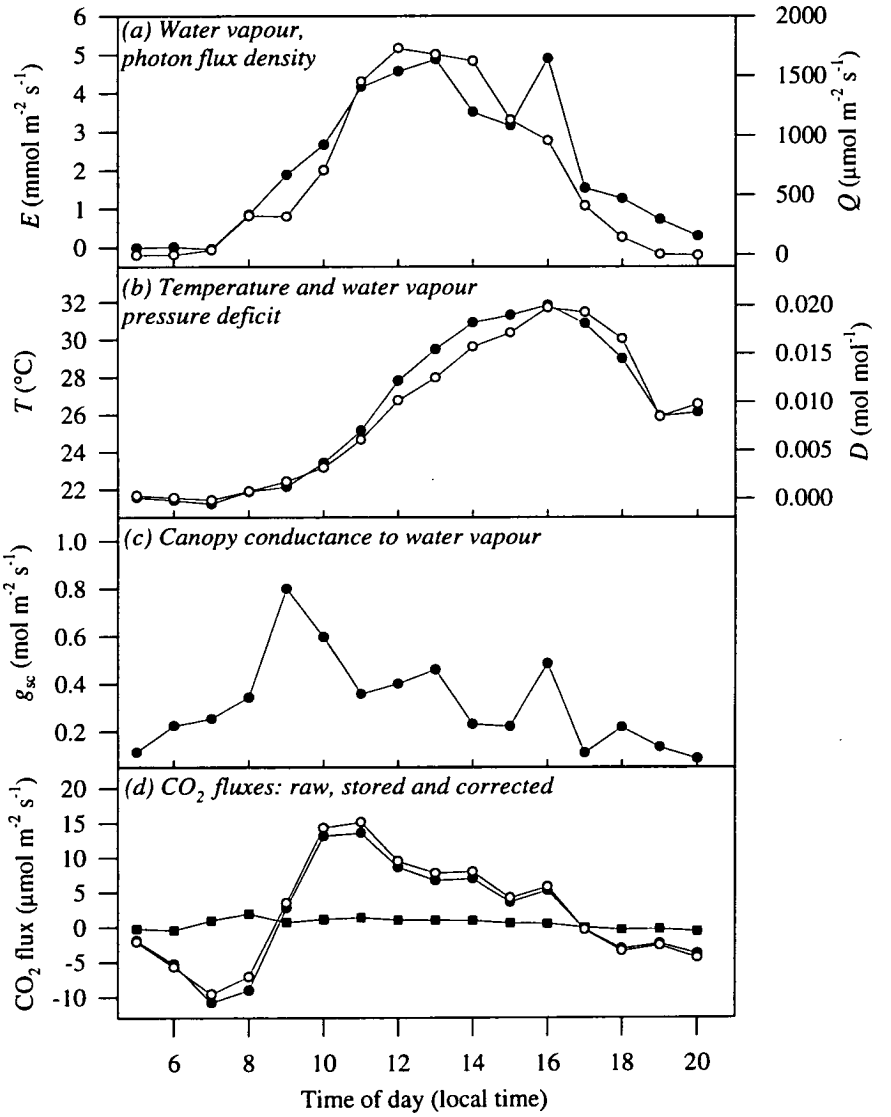

Figure 8.6a-d. Fluxes over SRF of radiation, water vapour, and CO_2 on 17th March, 1994. In (a) incident radiation (PPFD - open circles) and water vapour flux (spots); in (b) temperature (spots) and water vapour pressure deficit (open circles); in (c) canopy [stomatal] conductance; and in (d) CO_2 fluxes: squares = changes in storage, spots = raw measurements, and open circles = raw flux corrected for storage. The measurements were made available by Grace *et al.*.

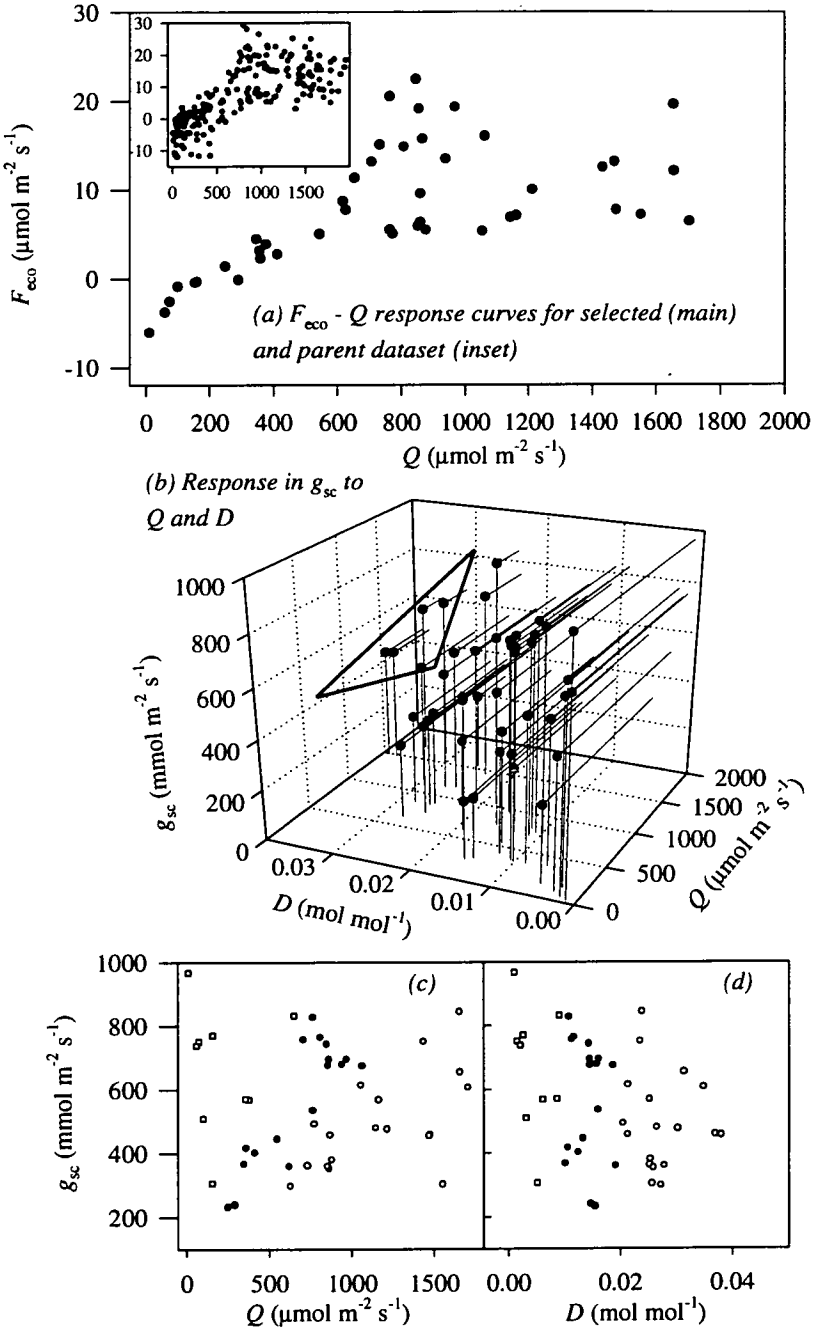

Figure 8.7a-c. In (a), the response in storage-corrected CO_2 flux (F_{eco}) to Q. The main chart shows the selected data used for modelling; the inset shows the parent dataset. In (b), the response surface in g_{sc} to Q and D. The triangle encloses points with high g_{sc} at high D, thought to result from contamination of the H_20 flux signal (see text). The individual responses in g_{sc} to D and Q are shown in (c) and (d): the data are separated by bands of D from 0-0.1(squares), 0.01-0.02(spots), >0.02(circles). Units = molmol^{-1}. F_{eco} data from J. Lloyd (ANU, Canberra).

MODELLING RESPIRATION AND PHOTOSYNTHESIS

Respiration (PRF and SRF)

The CO_2 efflux from each component of the forest in PRF and SRF varied with temperature. Maximum values were experienced during the night as a result of the extra contribution from leaves, though the peak efflux rates from soil and wood were between 1600 and 1700 hrs, in synchrony with the afternoon peak in biomass and soil temperature. Figure 8.8 describes the daily cycle in R_t for SRF in Cameroon; the pattern for PRF was similar. The disjuncture between night and day is shown to emphasise the additional contribution from leaves, by assuming respiration only occurs when darkness falls; in the model results (Figure 8.12c), a smoother transition is incorporated where the photosynthesis equations predict partial assimilation or respiration at dawn and dusk. Inset on Figure 8.8 are pie charts that indicate the proportional contribution to R_t from the leaves, wood and soil in both PRF and SRF. The largest component of R_t was the soil which comprised over 75% of total respiratory fluxes in both forests. Typical night-time (~1800 hrs - 0600 hrs) values for R_t in PRF were 7.1 μmol m^{-2} s^{-1}, and in SRF, 6.3 μmol m^{-2} s^{-1}. Although the efflux from soil was greater in PRF, leaf respiration rates were higher in SRF, making the two overall R_t estimates rather similar.

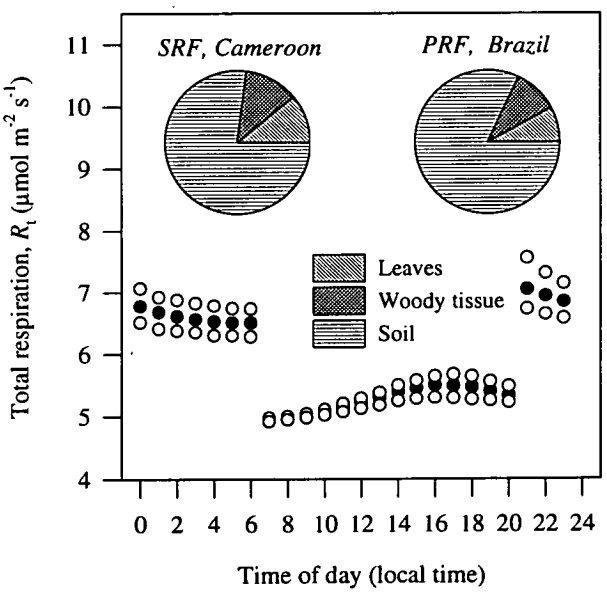

Figure 8.8. Total respiration. In the main graph the diurnal cycle in R_t is shown for SRF. The night - day difference is exaggerated (see text). The inset pie-charts show the proportional contribution made to night-time respiration by each component of the forest.

A direct comparison between R_t and the eddy covariance measurements can only be made during the night, as day-time data are confounded with assimilation. Two comparisons were possible for PRF, and one for SRF. For both forests, the intercept was estimated on the ordinate of the light response curve for the selected F_{eco} values (Figure 8.7a for SRF; Figure 8 in Grace *et al.*, 1995a for PRF). The second comparison required night data for F_{eco}, and is given here for PRF. Table 8.1 shows that the comparisons generally indicate good agreement among the different types of estimates. The largest discrepancy was found between F_{eco} for PRF and the component-derived R_t estimate, but they were not significantly different. Uncertainty regarding the error for R_t is acknowledged and reflected the difficulty in sampling the spatial heterogeneity in the soil and the above-ground biomass .

Table 8.1 Comparison of canopy respiration rates at night as measured using (1) eddy covariance (a = measured during night; b = intercept on Q : F_{eco} graph using the selected F_{eco} datasets), and (2) component summation from chamber measurements. Errors are in parentheses. Standard errors are given for (1a); n = 44 in PRF and (1b); n = 16 in PRF and 28 in SRF; those for soil CO_2 efflux in (2) are standard errors of prediction from the regressions in Figure 4.5; the errors for leaf and woody tissue respiration in (2) are derived as explained in the Methods. Eddy covariance data were provided by Grace *et al.* (1995a & unpublished); n/a = not available.

	BRAZIL			CAMEROON		
Component	*Eddy c. (1a)*	*Eddy c. (1b)*	*Chamber (2)*	*Eddy c. (1a)*	*Eddy c. (1b)*	*Chamber (2)*
Leaves	---	---	1.0 (0.1)	---	---	1.2 (0.2)
Wood	---	---	0.7 (0.2)	---	---	0.6 (0.2)
Soil	---	---	5.5 (0.7)	---	---	4.5 (0.7)
Total	6.6 (0.25)	6.54 (1.0)	7.1 (1.1)	n/a	5.8 (0.9)	6.3 (1.2)

Using measured above-canopy temperature to drive the respiration models at hourly intervals, R_t was estimated for one year in PRF (1992 - 1993, weather station data supplied by ABRACOS), and for days 67 - 113 of 1994 in SRF. The total efflux of CO_2 during the year 1992-3 in PRF was 23.2 ton C ha^{-1}; in SRF the 46 day total was 2.8 ton C ha^{-1}, which if extrapolated directly to 365 days would give a corresponding figure of 21 ton C ha^{-1} yr^{-1}.

Stomatal conductance (SRF)

Big-leaf model:

Stomatal conductance measurements obtained from the selected F_{eco} dataset were fitted to Equation 7.15. When the separate responses to D and Q were combined in the model, an r^2 of 0.65 was obtained (Figure 8.9). The residual plots in Figures 8.9a-f show two features. First they indicate that there was little skew in the model across the normal range of meteorological variables. And secondly,

they show that the normal range all variables was represented. The fitted values for Equation 7.15 and its components were: D_o = 0.007; g_{smax} = 8 mol m^{-2} s^{-1}; α_g = 0.002 mol mol^{-1}, g_d = 0.67 mol m^{-2} s^{-1}. The calculation of stomatal conductance was driven from weather data to yield canopy conductance estimates (g_{scb}).

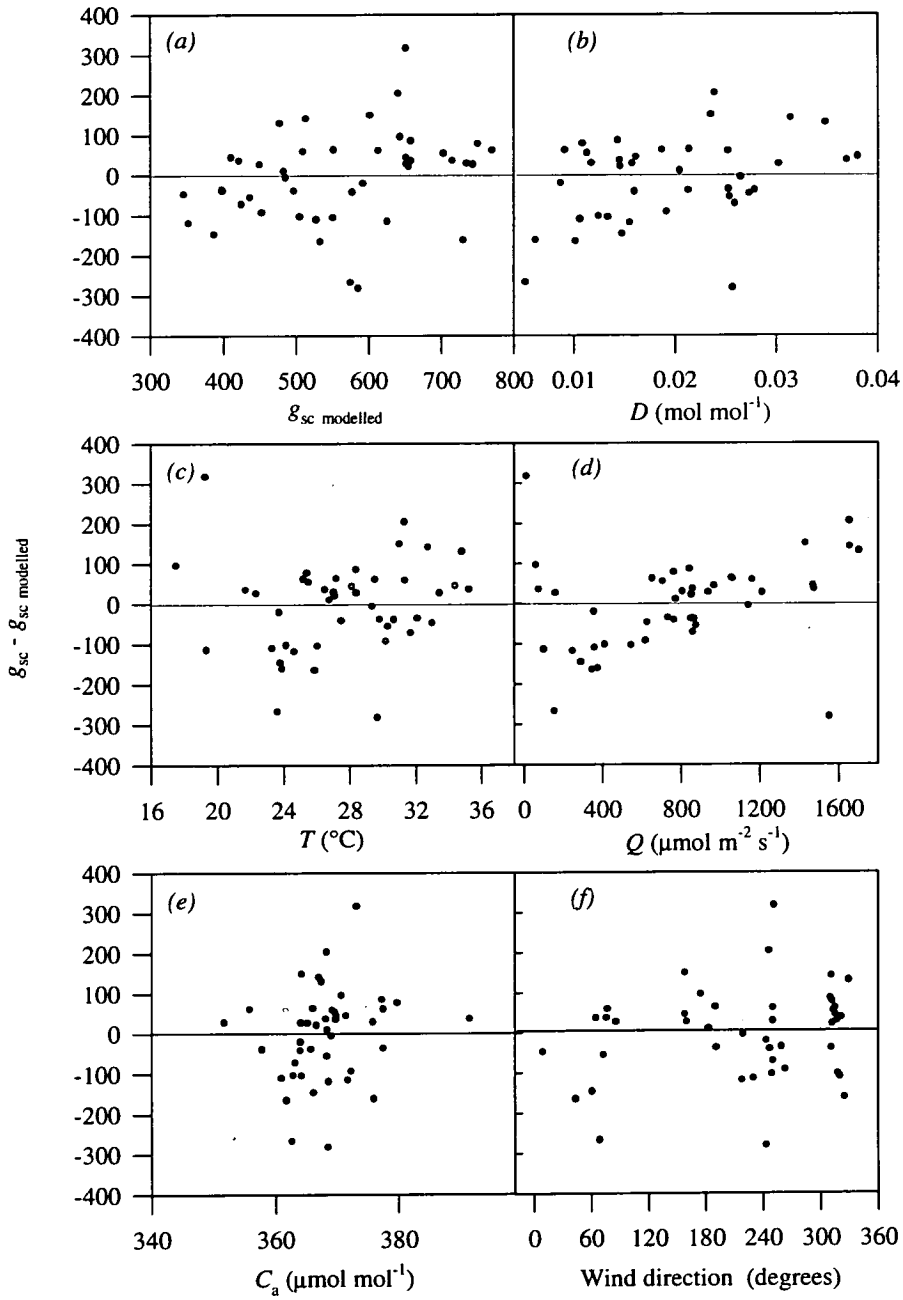

Figures 8.9a-f. Canopy stomatal conductance (big-leaf) model results. All graphs plot the residuals as g_{sc} - $g_{sc\ modelled}$ *vs* each of g_{sc}, D, T, Q, C_a, and wind direction respectively.

Multilayer model:

The daily patterns in stomatal conductance, vapour pressure deficit and radiation in SRF (Figures 8.10a&b) show diurnal leaf gas exchange traces for three of the six layers within the canopy: the bottom, middle and top. These results compared well with the measured values of g_s (Figure 7.2).

For leaf-level g_s, maximal values of 100 - 500 mmol m^{-2} s^{-1} occurred at the start of the day (0800 hrs to 1000 hrs) and decreased towards minima of less than 100 mmol m^{-2} s^{-1} near sunset. The rate of decrease in g_s tended to reduce after 1500 hrs. On some days (*e.g.*, second day in Figure 8.10c), g_s at one or two heights increased in response to reduced D; this phenomenon was not marked in the mean *measured* conductances (Chapter 7), though a tendency in *Amphimas* to maintain g_s levels after 1500 hours can be discerned (Figure 7.2b). These values were scaled according to the vertical profile in LAI to give g_{scm} estimates.

Figure 8.10d compares measured and modelled stomatal conductance for the whole canopy. The traces follow similar patterns with high morning values (400 - 1000 mmol m^{-2} s^{-1}) dropping from 1100 hrs onwards down to 100 - 200 mmol m^{-2} s^{-1} near sunset. However there are discrepancies. Most obvious is the difference in smoothness between the measured g_{sc} and the modelled g_{scm} and g_{scb} (though the *mean* g_{sc} approximated closely the modelled values). The modelled stomatal conductances differed mainly in that g_{scm} was more responsive than g_{scb} to changes in the driving variables, particularly D: the morning peak in g_{scm} was larger than the respective g_{scb} on both days when D was lower. Concurrent peaks were also observed in the g_{sc} trace. Overall, the multilayer model estimated g_{sc} well in some instances but overestimated it in others, whilst the big leaf model tended to slightly underestimate g_{sc}.

Photosynthesis and net assimilation (SRF)

For both assimilation models the above stomatal conductance simulations were used to drive the equations of photosynthesis together with the weather data. Gross [canopy] photosynthesis estimates were then combined with gross respiration to resolve the net modelled canopy assimilation rate.

Big leaf model:

The leaf photosynthesis model (Equations 7.1 and 7.3) were fitted to the F_{cb} values in Figure 8.7a and gave an r^2 of 0.61 for the photosynthesis model. The residual plots in Figure 8.11a-f show that the

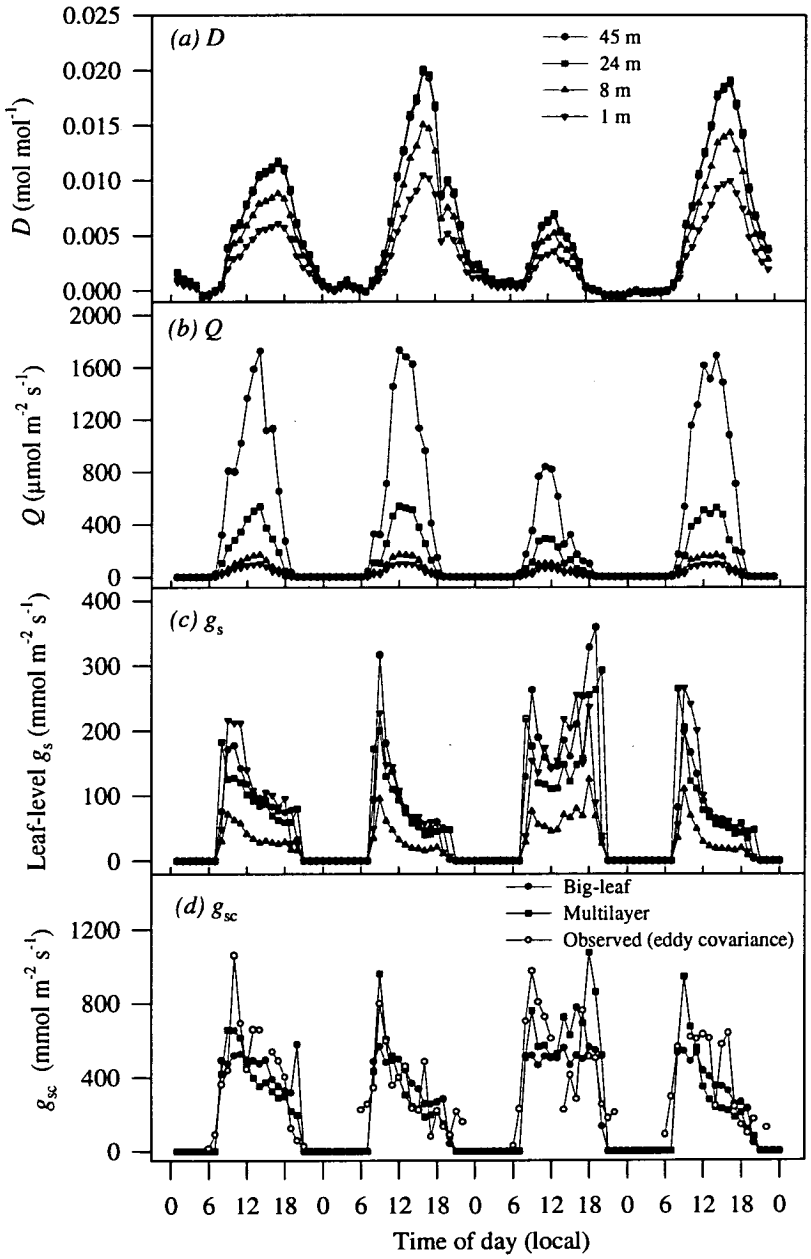

Figures 8.10a-d. Stomatal conductance in SRF. In (a) & (b), modelled D and Q are shown for 45 m, 24 m, 8m and 1 m above ground level. In (c), leaf-level stomatal conductance, g_s, is calculated at each height; and in (d), canopy conductance is shown for the eddy covariance observations (daytime g_{sc}), the big-leaf model (g_{scb}), and the multilayer model (g_{scm}). The data are for 16th - 19th March, 1994.

model was not skewed with respect to most of the driving variables. However, F_c was underestimated above 20 μmol m^{-2} s^{-1}. The fitted values of J_{max} and V_{max} respectively were 187 and 91 μmol m^{-2} s^{-1}. Leaf respiration in the dark was estimated at 1.7 μmol m^{-2} s^{-1} at 25 °C, whilst the convexity of the photosynthetic response to light, θ, was 0.08. The combined big leaf model was run from the weather station data to yield net canopy assimilation, F_{ecob} (Figure 8.12c).

Multilayer model:

The daily rhythms in photosynthesis differed with height above the ground in a similar way to the measurements shown in Figure 7.1. Data are plotted for four of the six modelled levels in the canopy (Figure 8.12b). At the top, maximum leaf-level rates of 5 - 7 μmol m^{-2} s^{-1} occurred at 1000 or 1100 hrs, and then declined. In contrast, at the bottom of the canopy, maximal irradiance levels were experienced around midday, and since g_s was still not limiting at this hour near ground level, maximal rates of 2 - 3 μmol m^{-2} s^{-1} obtained. Photosynthesis values were scaled to the whole canopy to give estimates of F_{cm}, which were combined with R_t to give F_{ecom}.

Figure 8.12c compares values for measured and modelled F_{eco} for March 16th - 19th. As with stomatal conductance, although the measured F_{eco} trace was less smooth than F_{ecom} and F_{ecob}, there was overall agreement between the three graphs: net assimilation reached a maximum of 12 - 20 μmol m^{-2} s^{-1} around 1100 hrs, and then fell to 0 - 2 μmol m^{-2} s^{-1} near sunset. Respiration rates fell with temperature during the night, averaging 6 - 7 μmol m^{-2} s^{-1}. Overall agreement was closer during the day-time on the 17th and 19th, whilst on the 16th and 18th, the modelled values slightly underestimated F_{eco} during the hours of maximum photosynthesis. Day-time estimates of F_{ecom} and F_{ecob} were similar, though net assimilation in F_{ecob} was less than in F_{ecom} for the peak [morning] values. This difference was accentuated on the 16th and 18th, and almost completely removed on the 17th and 19th. Though variable at night, the *mean* F_{eco} value was similar to that estimated by F_{ecom} and F_{ecob}. These modelled values were identical during complete darkness since R_t was used for both, but at dawn and dusk some differences could be discerned reflecting variation in the modelled balance between leaf photosynthesis and respiration.

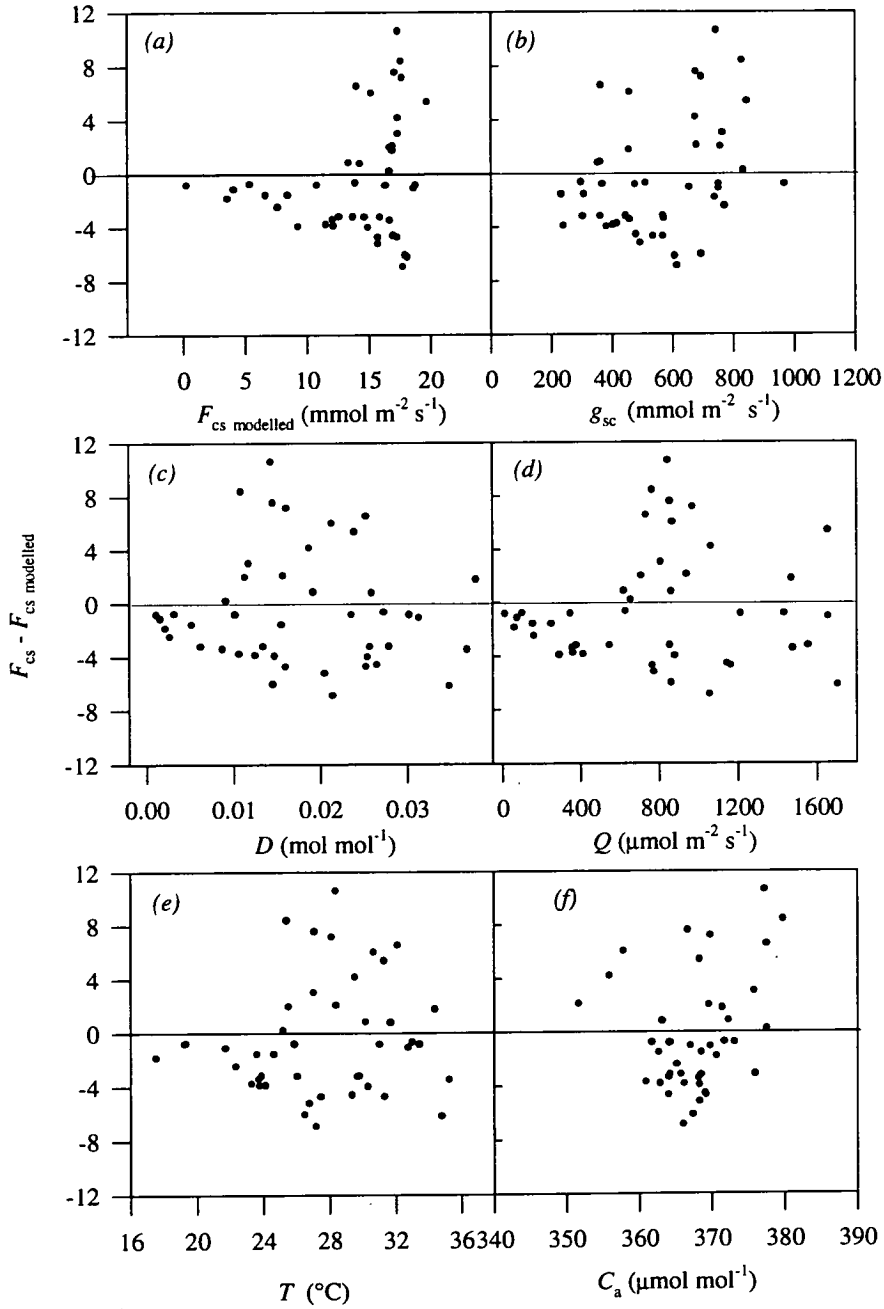

Figures 8.11a-f. Canopy photosynthesis (big-leaf) model results. All graphs plot the residuals as F_{cs} - $F_{cs\ modelled}$ *vs* each of F_{cs}, g_{sc}, D, Q, T, and C_a, respectively. F_{cs} data are F_{eco} values corrected for R_t, total respiration.

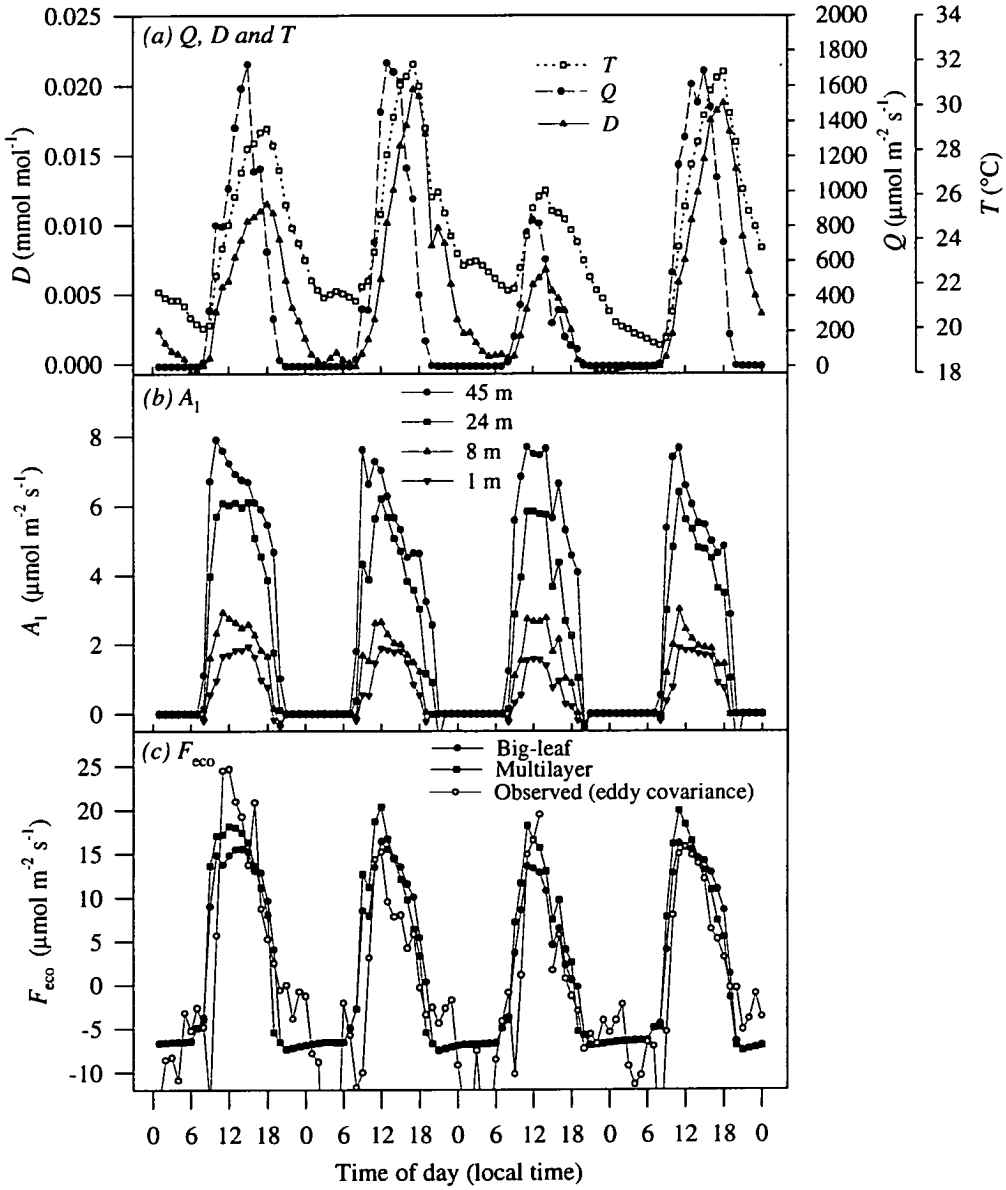

Figures 8.12a-c. Photosynthesis and net assimilation by SRF. In (a) are climate variables for the period 16th March to 19th March: Q, D, and T. In (b), leaf level photosynthesis (A_l) is plotted for leaves at four heights: 45 m, 24 m, 8 m, and 1 m. In (c), net assimilation rates for SRF are shown for the eddy covariance observations (F_{eco}), the big-leaf model (F_{ecob}) and the multilayer model (F_{ecom}). The modelled F_{eco} data (F_{ecob} and F_{ecom}) were obtained by combining gross assimilation (F_{cb} and F_{cm}) with R_t.

SCALING UP FLUX ESTIMATES IN TIME (PRF AND SRF)

Secondary rain forest, Cameroon

The multilayer and big-leaf models for SRF were 'assumed' to give spatially averaged estimates of the hourly changes in net canopy assimilation for the forest as a whole. For each, 46 days of modelled fluxes between forest and atmosphere were compared with the eddy covariance. The observed fluxes indicated the forest to be a source for CO_2 of 1.6 μmol m^{-2} s^{-1}, whilst the simulations predicted a net sink. Of the two models, the multilayer formulation estimated more assimilation (net sink = 0.9 μmol m^{-2} s^{-1}) than did the big-leaf (net sink = 0.7 μmol m^{-2} s^{-1}).

The strong apparent source capacity of the forest as measured by eddy covariance suggested the need for a more detailed appraisal of night-time turbulence that is not presented here. However, a preliminary analysis of the distribution of observed fluxes with wind direction indicated that a large source for CO_2 could be detected over one sector, between 70° and 130° from north (Figure 8.13). These bearings coincided with part of the village of Eboufek (Map 2.2). Consequently, the measurements were thought to be affected by airflows enriched by fuel burning and non-forest land use. After removal of these data, mean night-time efflux values (for the period 2000 - 0400 hrs) were reduced by 50%, whilst mean assimilation rates during daylight hours (1000 - 1600 hrs) were changed by only 7%. The diurnal pattern of wind flow was not fully random (data not shown), and consequently affected overall flux measurements because of a night-time bias towards the 70° - 130° sector (the big-leaf model was fitted to a selected dataset that also had this sector removed).

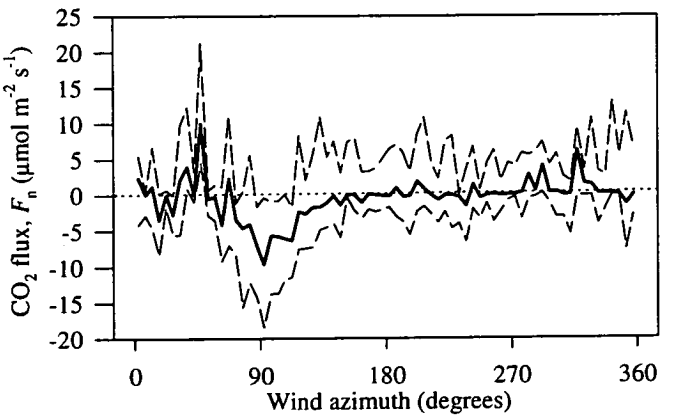

Figure 8.13. The variation in CO_2 flux with respect to wind direction above SRF. The graph shows the median and interquartile range for 2.5 ° bins. The data are net fluxes, F_n, without storage corrections, and are for 9th March to 4th May, 1994.

Climate change scenarios could not be investigated in terms of the annual forest carbon budget for SRF. However, it was possible to re-run the two models for hypothetical conditions during the field campaign. Figures 8.14a-c show the effects of single variable changes in carbon dioxide concentration, radiation and temperature on F_{ecob} and F_{ecom}. The graphs are normalised by the estimates obtained using the true climatological data from February - May 1994. Increased radiation and CO_2 concentration resulted in both models predicting a stronger sink capacity for the forest, whilst for temperature the opposite obtained. The sink strength was most strongly determined by temperature and CO_2 concentration: a warming of 2 °C reduced the sink capacity of the forest by 16%, whilst increasing the CO_2 concentration by 300 μmol mol^{-1} strengthened it by 125%. The multilayer model was less sensitive to changes in C_a and Q, but more sensitive to T than the big-leaf model.

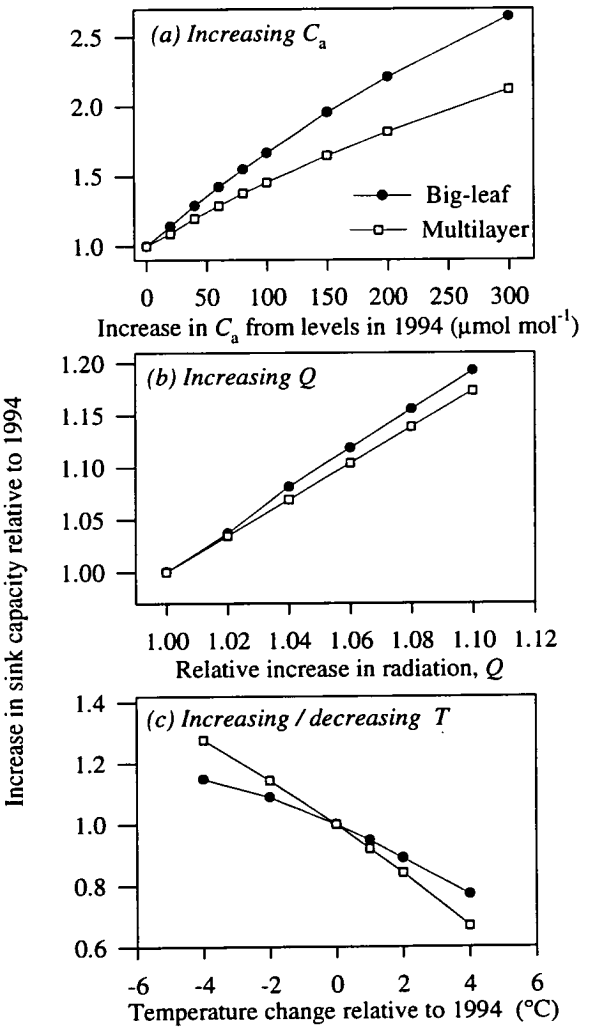

Figures 8.14a-c. The sensitivity in the models for SRF to changes in C_a, Q and T respectively. Each graph shows the relative effect of change in the driving variable on the original estimates from the big-leaf and multilayer models.

Primary rain forest, Brazil

For PRF, a big leaf model was run for one year using the 1992 - 93 weather station data; the detailed results are presented in Grace *et al.* (1995b) and Lloyd *et al.* (1995b). Here, the net assimilation output from that model has been incorporated into the carbon flow diagram shown in Figure 8.15a together with the modelled total respiration, R_t. The forest was found to be a net sink for carbon of 0.9 (±0.2) ton C ha^{-1} yr^{-1} a net difference between gross primary production of 24.1 ton C ha^{-1} yr^{-1} and total respiration, R_t of 23.2 ton C ha^{-1} yr^{-1} (Grace *et al.*, 1995b).

The most significant feature of these results was the higher sensitivity to temperature of respiration over photosynthesis (Grace *et al.*, 1996; Meir *et al.*, 1996). A small change in above-canopy temperature of 1 - 2 °C was found to have a large effect on respiration, but a smaller effect on photosynthesis (Grace *et al.*, 1995b; Grace *et al.*, 1996). The role played by respiration in determining the carbon balance of the forest is considered in Table 8.2 where the largest component contributing to CO_2 efflux, emission from the soil, was estimated for hypothetical temperature records for 1992 - 93. The warming increments used (0.5 - 2.0 °C) were in line with climate change scenarios reported by Houghton *et al.* (1994), and the results show the forest to flip from a net sink to a weak net source of less than 0.3 ton ha^{-1} yr^{-1} under a 2 °C warming. Even a small increase in temperature of 0.5 °C yielded a 28% reduction in the sink strength (from 0.9 - 0.64 ton ha^{-1} yr^{-1}). Clearly inclusion of the above-ground respiratory term would have increased the size of the modelled source. It is emphasised that only the soil component was changed in this simulation, but the results underline those from analogous scenarios described for net assimilation in Grace *et al.* (1995b).

Table 8.2 The effect of temperature on respiration in soil and the net carbon balance of PRF, using annual estimates from Grace *et al.* (1995b). Only estimates for the soil are changed to generate these data. Temperature in (°C); carbon fluxes in ton C ha^{-1} yr^{-1} and negative fluxes indicate a carbon source (physiologist conventions).

Temperature change	Soil CO_2 efflux	New net carbon balance
0	19.5	+0.9
+ 0.5	19.8	+0.64
+ 1.0	20.0	+0.38
+ 2.0	20.7	-0.25

Since an annual estimate for CO_2 fluxes in SRF was not possible, a comparison was made between the two sites by calculating the total amount of carbon metabolised in each component of the forest - leaves, woody tissue and soil. Figures 15b&c show the proportion of the *total* respired and photosynthesised CO_2 that pertains to each. The similarity was striking: none of the components

differed by more than 5% between PRF and SRF, with leaves representing the largest component (60 - 65%), then soil (32 - 37%) and wood (4 - 5%) respectively.

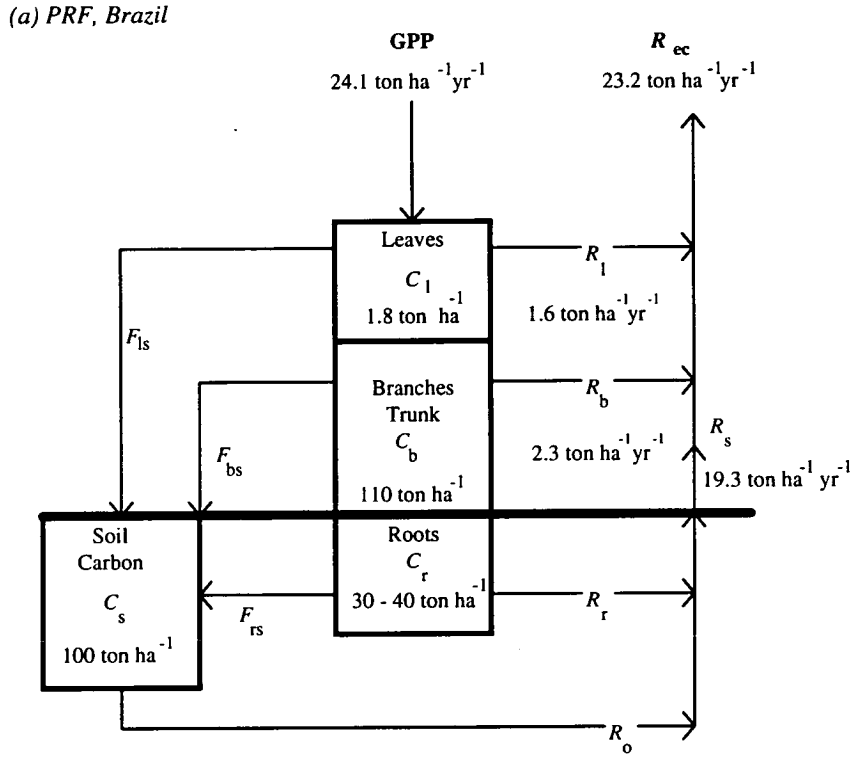

Figure 8.15a. The carbon balance in PRF 1992-3. Estimates are given for the annual fluxes of carbon dioxide within the PRF canopy, and the net exchange between the PRF canopy and the atmosphere (data obtained from this thesis, Grace *et al.*, 1995b & Meir *et al.*, 1996; carbon content of wood, following Matthews (1993) assumed to be 50%). Storage values are in ton C ha^{-1}; fluxes in ton C ha^{-1} yr^{-1}; the soil carbon storage is from Post et al. (1982).

Figure 8.15b&c. The proportion of the *total* metabolic flux of carbon dioxide through different forest components. The data represent the sum of gross respiration and photosynthesis for each component.

8.4 DISCUSSION

DRIVING ENVIRONMENTAL VARIABLES

A late afternoon peak in soil temperature occurred in both forests, and although apparent differences were visible they were not significant (Figure 8.1). The daytime microclimate profiles for the SRF canopy showed the development of vertical gradients in Q, D and T, but the destruction [by turbulence; *c.f.* Figure 4.16b] of nocturnal gradients in C_a, except near ground level (Figures 8.2 - 8.4). The midday vertical gradients visible in T and D resulted from variation in incident radiation, probably because of near-field heating effects. And the efficient mixing seen in C_a also acted on water vapour: the changes in D with height were in response to T rather than water vapour concentration (data not shown). Consequently, the SRF canopy appeared fairly well coupled to the atmosphere during the day. Inspection of Figures 8.6a&c confirms this, and suggests that the decoupling coefficient (Ω; Jarvis & McNaughton, 1986) was low near midday when turbulence was highest, and high (= decoupled) in the morning, when the opposite occurred. Strong coupling was probably responsible for the good estimates obtained for D and T from the above-canopy values.

With all simulated in-canopy microclimate data for SRF, the relationship between measured and predicted values near the ground was significantly noisier than for those near the canopy top (*e.g.*, Figures 8.3b-d and 8.4b-d). For scalars such as temperature and gases, a turbulent mixing model (*e.g.*, Raupach 1988) might improve these estimates, but representation of the radiation field by point sampling is prone to bias from canopy heterogeneity. Consequently, it was difficult to be certain how well the data from one measured profile mimicked the average Q at each height in the forest. For example, the maxima in Figure 8.3a at 1 m are close to 100 μmol m^{-2} s^{-1}; other areas of the forest exhibited peaks of less than this (*personal observation*), and it is possible that the mean Q at 1 m was also less than 100 μmol m^{-2} s^{-1}.

Overall, the SRF in-canopy climate showed some characteristics also found in PRF (McWilliam *et al.*, 1996): vertical daytime gradients in T and D were generated, and light was attenuated with height in an exponential manner. However it was distinguished from PRF by its stronger coupling low in the canopy, lower overall C_a (mean C_a was ~380 - 390 μmol mol^{-1} in SRF *vs* ~ 400 - 410 μmol mol^{-1} in PRF), and by the highly heterogeneous radiation field, especially near ground level.

EDDY COVARIANCE AND CANOPY PHYSIOLOGY (SRF)

Aerodynamic properties

The gradient of the linear relationship between friction velocity and wind speed (Figure 8.5a) was close to that reported in the literature (1.9 in SRF *vs* 1.7: Shuttleworth *et al.*, 1984; Grace *et al.*, 1995a, both working in undisturbed rain forests in Amazonia). The increase in aerodynamic conductance of the forest canopy to heat, water vapour and CO_2 was also a positive function of wind speed (Figure 8.5b) and the gradient of this relationship was marginally greater than that found for the PRF site (Grace *et al.*, 1995a).

The calculation of r_a was subject to some dependency on $\ln(z_{oM} / z_{oH})$ in Equation 8.4. There exists variation in the published value for this term (Verma, 1989), and its effect has been examined elsewhere (Shuttleworth *et al.*, 1988; Monteith & Unsworth, 1990; Grace *et al.*, 1995b). This uncertainty is acknowledged here as r_a and r_s were occasionally of the same order of magnitude, though the good agreement among big-leaf, up-scaled leaf-level measurements and eddy covariance-derived values of canopy conductance suggests that the calculations were reasonable (Figure 8.10d; *c.f.*, Figures 7.2 and 3.5).

Canopy physiology

The 'natural history' of canopy gas exchange appeared like that of a simple leaf (Figure 8.6), though clearly major differences exist. Two of the most important are the inclusion of an 'extra' respiratory component (soil and wood) in the data, and the variability of the sampling 'footprint' inherent to eddy covariance measurements. The heterogeneity in landscape around the SRF site acted as an additional source of variation in the data. The reserve at Mbalmayo was in an area near a small settlement and was composed of a variety of forest types itself, including some areas of swampy forest, as well as the locally dominant moist deciduous forest (Lawson, 1995; Grace *et al.*, unpublished data). Figure 8.13 suggests contamination of the CO_2 signal from one direction and these data were excluded from the subsequent analysis.

Notwithstanding these difficulties, the physiological characteristics of the canopy are consistent with leaf-level measurements made both for this forest, and other tropical moist forests. In particular, the

maximum canopy conductances of 400 - 1000 mmol m^{-2} s^{-1} were congruent with up-scaled leaf data for SRF and PRF, and the diurnal pattern of high morning conductances followed by declining fluxes in the afternoon has previously been found in two tropical rain forests (Shuttleworth, 1989; Roberts *et al.*, 1990; McWilliam *et al.*, 1996).

The responses in net assimilation and conductance to light and water vapour pressure deficit

Net assimilation:

The light response characteristics for SRF (Figure 8.7a) are similar to those found for two Amazonian forests reported by Fan *et al.* (1990; Reserva Ducke, Brazil) and Grace *et al.* (1995a; the PRF site). The estimated dark respiration rate at SRF was 5.8 μmol m^{-2} s^{-1} (at Reserva Ducke it was 6 - 7; at PRF it was 6.5); the quantum requirement at SRF was 40 (at Reserva Ducke it was 60; at PRF it was 40); and the light compensation point at SRF was 230 μmol m^{-2} s^{-1} (at Reserva Ducke it was 260; at PRF it was 280).

A larger discrepancy was found for the maximum assimilation rate where SRF showed greater capacity (25 - 30 μmol m^{-2} s^{-1}) than either the forest at Reserva Ducke or PRF (19 and 15 μmol m^{-2} s^{-1} respectively). Furthermore, whilst the light response curve for SRF was linear up to 800 μmol quanta m^{-2} s^{-1}, it appeared to saturate above 1200 μmol quanta m^{-2} s^{-1}. The Reserva Ducke and PRF canopies did not fully saturate at high Q, but the overall light responses were also curvilinear. Studies in a temperate forest in north eastern USA have also indicated a non-linear light response (Wofsy *et al.*, 1993), though it is possible that such data would show a linear relationship if presented on a daily basis. The asymptotic nature of the F_c - Q response is also suggestive of photosynthetc acclimation within a closed canopy, and the data in Chapter 7 tentatively support this notion. These kinds of analyses may be important for large scale modelling of forest gas exchange (Ruimy *et al.*, 1995; *c.f.*, Sellers *et al.*, 1992; Kruijt *et al.*, 1995) The differences among the tropical sites reflect structural and florisitic variation contingent upon their [bio]geography. But the SRF canopy was also a secondary forest (both Reserva Ducke and PRF were 'primary' sites), and may have contained a greater area of leaves with high nitrogen content and high A_{max} capacity (*c.f.*, Chapters 2 and 7).

Canopy conductance:

Variation in canopy conductance was related to differences in incident radiation and vapour pressure deficit (Figures 8.7b and 8.9). The r^2 value for the stomatal conductance model was 0.61 despite the uncertainties inherent to the eddy covariance technique. Inspection of the response surface in Figure

8.7b revealed some unexpectedly high g_{sc} values at high D (see the triangle in Figure 8.7b). It is possible that these data represented flux measurements contaminated by evaporation from wet or swampy patches in the surrounding forest mosaic. Contamination of the evaporation signal because of poor coupling between the atmosphere and the canopy was less likely, though this may have occurred at low wind speeds. Further anaylsis by wind direction of measurements during the night and late afternoon would permit a more detailed interpretation of the stomatal conductance model.

Possible bias in the selected eddy covariance dataset:

It is reasonable to question how well the selected data in Figure 8.7a adequately represent the general behaviour of the forest. The filters used to select canopy scale data for modelling purposes were chosen to identify physiologically stable conditions and remove transitional states during changing weather conditions. In this sense, the purpose was to locate periods when the canopy could be regarded as equivalent to a leaf placed in a leaf chamber (Chapter 7). Such measurements have previously been used as source data for scaling to the whole canopy (*e.g.*, Caldwell *et al.*, 1986; Roberts *et al.*, 1993; Amthor, 1994). A minimum possible number of points were filtered out, and the consequent photosynthetic light response curve is shown in Figure 8.7a. A detailed analysis (forthcoming) of the F_{eco} data would require the inclusion of verified night-time measurements. As a first step, the inset graph on Figure 8.7a shows the light response of the selected data to be close to that of the parent dataset. Using the same regression method used for the selected data, the light response characteristics in each graph were found to be almost identical: for the inset graph the implied dark respiration rate is 5.9 μmol quanta m^{-2} s^{-1}, the light compensation point is 260 μmol quanta m^{-2} s^{-1}, the quantum efficiency is 43, and the maximum assimilation rate is ~ 25 - 30 μmol quanta m^{-2} s^{-1}. In addition, it is emphasised that the selected data represented a sizeable proportion of the main body of measurements (21%), and were also distributed widely across the normal range of driving environmental variables (Figure 8.9). Together, these observations suggest that the selected data were not significantly biased.

MODELLING RESPIRATION AND PHOTOSYNTHESIS

Respiration (SRF and PRF)

For both forests, soil CO_2 efflux was the largest respiratory component, followed by leaf respiration, and then woody tissue respiration (Figure 8.8). The differences between SRF and PRF reflected their structural and successional states. In this context, the slightly higher mean LAI and greater presence of pioneer species (*e.g.*, *Musanga cecropioides*, *Haumania danckelmaniana*) in SRF (Chapter 3) could explain the higher leaf respiration rates. By the same token, the higher above- and below-ground biomass in PRF resulted in higher estimates for CO_2 efflux from woody tissue and soil. Given the importance of root respiration to total efflux rates from soil (Singh & Gupta, 1977; Raich & Schlesinger, 1992), it is perhaps surprising that the efflux from SRF soil was as high as 5.8 μmol CO_2 m^{-2} s^{-1}. One explanation for this may lie in the recent (1988-9) logging of the Mbalmayo forest: it is possible that a large amount of non-living below-ground litter remains and is continuing to decompose. Over several years this phenomenon would be seen in the overall fluxes as an initial minimum net rate of assimilation (peak in soil respiration relative to gross assimilation) followed by a rise. Indeed, a disturbed secondary forest may have the capacity to act as a temporary source for CO_2 (Uhl, 1987).

The determination of R_t values by component summation is important for the independent verification of eddy covariance measurements over forest (Wofsy *et al.*, 1993; Grace *et al.*, 1996). This is particularly true for 30 or 60 minute night data, as calm and less buoyant nocturnal conditions can reduce aerodynamic conductance to levels not detectable by the eddy covariance technique (Kaimal & Finnigan, 1994). The agreement among measurements in Table 8.2 was encouraging in this respect. But there remains the problem for summation techniques of representing spatial heterogeneity. In this context, above-ground biomass estimates are limited to indirect approaches such as the use of empirical relationships or remote sensing. Some processes are particularly understudied: woody tissue respiration in branches is one example (Sprugel *et al.*, 1996). However, this problem may prove less important in view of the small contribution to total efflux from stems and branches (Figures 8.15b&c). Uncertainty in efflux from the soil is more serious as its contribution to R_t is larger. In this study, the precision of the temperature response in soil CO_2 efflux relied on relatively small sample sizes in a limited range of conditions; a fractional difference in the efflux estimate for soil could result in major changes in the overall forest carbon balance (Meir *et al.*, 1996).

Stomatal conductance and photosynthesis (SRF)

Big-leaf model:

In each case the leaf scale models for stomatal conductance and photosynthesis explained over 60% of the variation in the observed data. The fitted values for the g_{scb} model were similar to those found for individual leaves, though g_{smax} was larger, and α_g was lower than for leaves. The spread of residuals in both fits (Figures 8.9 & 8.11) indicated that the models were fairly robust across a wide range of conditions. But there was a weakness in Figure 8.11a where predicted photosynthesis tended to underestimate F_c at values above 20 μmol m^{-2} s^{-1}. This feature was probably a result of contamination in the g_{sc} signal.

The best fitting value for Rubisco activity, V_{max}, was 187 μmol m^{-2} s^{-1}, for light-saturated electron transport, J_{max}, it was 91 μmol m^{-2} s^{-1} , and for leaf respiration it was 1.7 μmol m^{-2} s^{-1}, whilst the respective parameters for PRF were 130, 68 and 0.7 μmol m^{-2} s^{-1} (Lloyd *et al.*, 1995b). The difference in these fitted values reflects chiefly the higher maximum assimilation rate in SRF, though the abundance of gap-dwelling herbs in this forest may also have had a species specific influence on the fits. Temperature optima for g_{sc} and F_c were not fitted, but estimates from the modelled data indicated lower values for SRF than PRF (respectively: 27.5 °C and 29 °C *vs* 32 °C and 36.5°C for PRF), a probable effect of the lower peak temperatures experienced in SRF.

Multilayer model:

The leaf scale processes underlying the multilayer model have already been discussed in Chapter 7, so only their in-canopy predictions are discussed here (Figures 8.9c and 8.11c).

The response in stomata to D and Q can be observed alternately in the upper-canopy and lower-canopy leaves: the former experienced more radiation but higher vapour pressure deficits than the latter, and the extremes of these combinations provided for the high g_s values in the leaves at these two opposite points in the canopy (Figure 8.10c; *c.f.* Figure 7.2); similar results were found for PRF (McWilliam *et al.*, 1996). The greatest amount of transpiration was undertaken by the sub-canopy layer where the highest leaf area density was found (Figure 3.5). The conductance in some layers also tended to rise in the late afternoon. Both of these features were observed in simulations by Roberts *et al.* (1993) for the forest at Reserva Ducke, Brazil. The radiation environment in SRF may not have been sufficiently well modelled to always generate late afternoon stomatal closure, but the apparent error could also reflect a fault in the fitted g_s model (Equation 7.15). This Jarvis-type formulation drives g_s from Q and

D only. Consequently, if other factors determined afternoon closure, they were not accounted for and an afternoon reduction in D could have resulted in overpredictions of g_{scm}.

The assimilation estimates in Figure 8.12c were determined to some extent by g_{scm}, but the importance of the light environment to photosystem II was made clear by leaves at the top of the canopy showing higher photosynthetic rates than those lower down (5 - 8 μmol m^{-2} s^{-1} at 36 m *vs* 1 - 3 μmol m^{-2} s^{-1} at 1 m). A feature in the measured data (Figure 7.1) retained by this simulation was the tendency for leaves at 1 m to peak later than those at 36 m. This suggests that the model worked well, though the flat (rather than pointed) peak at 1 m indicated that predicted Q and/or g_s may have generated slight overestimates in photosynthesis.

Comparing measured and modelled canopy gas exchange

The comparisons in Figures 8.10d and 8.12c indicate that both multilayer and big-leaf model formulations were reasonably successful. The big-leaf estimates were the most conservative for g_s and F_{eco}. For the F_{eco} simulations (Figure 8.12d), the departure from observed values on duller days with lower D was greater for the big-leaf data, which also tended to underestimate the morning peak in g_s. These obervations suggest that D was limiting for the canopy above 0.015 - 0.025 mol mol^{-1} (all data show agreement at high D), but that insufficient sensitivity to low D in F_{ecob} reduced its accuracy on certain days, in comparison to F_{ecom}. One improvement for both simulations would have been to calculate leaf [canopy] D rather than to use the air values. This could have improved the morning g_{scb} predictions, but would have probably increased further the late afternoon values which already tended to be overestimated, an effect sometimes also visible in the assimilation traces. The phenomenon of an afternoon increase in g_{sc} has been observed elsewhere (*e.g.*, Amthor *et al.*, 1994) and points to a potential gap in our mechanistic understanding of leaf gas exchange. Future improved models may incorporate inhibition feedbacks in photosynthesis or respiration to accommodate this (Herold, 1980; Azcón-Bieto, 1983; Amthor & Cumming, 1988).

Of the two modelling approaches used, the big-leaf is more attractive on several grounds: it provides a large spatial average, the continuously recorded data encompass a wider range of conditions than point measurements, and the relatively simple computations make for suitable application at larger scales (*e.g.*, Sellers *et al.*, 1992; Amthor, 1994). The advantages of a multilayer approach can be seen in this study where the short-comings of the big-leaf formulation could be dissected in the context of detailed physiological information that would not normally be available. For the SRF site, the heterogeneity of

the vegetation resulted in non-uniform whole-canopy gas exchange observations. The multilayer model was therefore particularly useful for this site, and its [generic] use in scaling up and verification purposes has been recognised elsewhere (Caldwell *et al.*, 1986; Reynolds *et al.*, 1992; Roberts *et al.*, 1993; Wofsy *et al.*, 1993).

SCALING UP FLUX ESTIMATES IN TIME (PRF AND SRF)

The focus for up-scaling canopy models to estimate performance over a year is the relative sensitivities to climate of different physiologically active components in the canopy, and their interaction. Currently, such procedures refer exclusively to the effects of 'instantaneous' changes in the environment, not to the longer term effects of climate change on forest structure or growth dynamics, and the feedbacks implied therein. Climatic anomalies in 1992 have recently been attributed to the volcanic aerosols ejected by the eruption of Mount Pinatubo suggesting that models can be tested in this context (Blumthaler & Ambach, 1994). Indeed, year-to-year fluctuations in climate have been found to contribute significantly to variation in the annual rate of CO_2 increase (Sarmiento, 1993).

Before comparing PRF and SRF, the descrepancy between measured and modelled carbon exchange in SRF required consideration. It is rare that a measurement tower is situated with perfect fetch from all directions, and an analysis by wind direction is usually appropriate (*e.g.*, Kruijt, 1993; Wofsy *et al.*, 1993). The effect of a settlement on the measured fluxes was large at SRF, and the tendency for night-time airflows to come from this direction compounded the overestimation of ecosystem respiration. Removal of data from this sector pointed to the forest acting as a carbon sink rather than a source, and this was confirmed by both models. The multilayer formulation predicted a stronger sink than the big-leaf one (0.9 *vs* 0.7 μmol m^{-2} s^{-1}). These numbers were large in comparison to the net assimilation of PRF (0.3 μmol m^{-2} s^{-1}), but similar to recent values obtained for a denser forest in Central Amazonia (Malhi, *personal communication*). They were also obtained from a 46 day period and so may not accurately represent the annual carbon budget in SRF. Whilst F_{ecom} tended to overestimate F_{eco} on some days, F_{ecob} underestimated it on others (Figure 8.12c). The actual behaviour of SRF as a whole probably fell between the two, whilst different sectors of the forest mosaic may have resembled more one model than the other.

A primary role of a model in this case is to estimate behaviour at times other than those where measurement is possible. But the precision in such estimates requires that the model remains accurate across the full annual climatic cycle. This problem is reduced in the tropics, though some seasonality

remains (Culf *et al.*, 1996). For PRF, measurements were made in both the dry and wet seasons before calibrating the model (Grace *et al.*, 1995b). The data included *friagem* periods, though fewer measurements of respiration in soil derived from these dates. Although the predictions for soil behaved well during these intermittent cool spells, further verification of the efflux model in exceptional weather conditions would raise confidence in the annual estimates.

The carbon budget for PRF in Figure 8.15a is a fine balance between respiration and assimilation. The differential sensitivities of photosynthesis and respiration to physical parameters make this balance labile to climatic vicissitudes (Table 8.2; Grace *et al.*, 1996). Figures 8.15b&c indicate a close similarity between PRF and SRF in the proportionation of *total* (24 hour) carbon fluxes to different tissues. The implication is that SRF should behave in a similar way to PRF. Figures 8.14a-c show that net forest assimilation is most strongly sensitive to ambient CO_2 concentrations. But in the context of inter-annual climatic variation, it is likely that radiation and temperature will fluctuate more. Further inspection of Figure 8.14 reveals that the SRF models are especially sensitive to temperature. This is because respiration rises rapidly with temperature, whilst photosynthesis is near its temperature optimum in these conditions. A sensitivity analysis for the PRF model yielded patterns consistent with this result (Grace *et al.*, 1996).

The differences between the two SRF models chiefly reflect differences in the respective fitted photosynthesis parameters, as R_t was used in both. It seems reasonable to assume that photosynthetic physiology was represented better by the multilayer model, as this was parameterised from measurements of leaf tissue only. However, the greater spatial averaging of the big-leaf model calibration may have lead to a more representative estimate of gross productivity.

This work supports a notion that the gas exchange behaviour of well developed tropical moist forest can be generalised despite large differences in geography, structure and floristics. This suggestion has recently been extended to include biomes from different latitudes, such as boreal forest (Jarvis *et al.*, 1995). But there remain important quantitative and qualitative differences. The nature of the canopy photosynthetic response to radiation is one area of contention and may vary importantly with canopy density. Even more clear is the role played at different sites by the temperature response of respiration in soil. This component may determine future changes in the carbon balance and should remain a focus in further studies. However, it is emphasised here that gas exchange models do not exist in isolation; they need to be combined with models of tree growth and below-ground processes before a complete picture of the forest carbon cycle can be drawn.

For use at larger scales, it is stressed that the present results are derived from site-calibrated models. This approach lends itself well to good local estimates of carbon dioxide exchange. But until whole-canopy measured data become available in larger amounts it will not be as widely applicable as more theoretically based models. Fortunately the eddy covariance technique is rapidly gaining currency: this is reflected not only in recent publications (*e.g.*, Wofsy *et al.*, 1993; Hollinger *et al.*, 1994; Grace *et al.*, 1995b; Valentini *et al.*, 1991; Miranda *et al.*, 1996), but also in current and planned international research programmes (ABRACOS, BOREAS, EUROFLUX, LBA). Many more long-term measurements are likely to emerge in the next few years.

8.5 CONCLUSIONS

Whole-canopy gas exchange measurements in SRF were compared with estimates from models derived by two different means. In one, measured leaf-scale photosynthetic parameters were applied to six layers of foliage and the processes scaled to the whole canopy. In-canopy environmental variables were empirically simulated and used to drive assimilation at each level. The second model was parameterised independently using eddy covariance measurements to calibrate a big-leaf type formulation. Both assimilation models were linked to an empirical respiration model so that net forest assimilation rates could be recovered.

Simulation of the in-canopy environment was satisfactory, though spatial representation in the radiation field was limited. Modelled canopy stomatal conductance and photosynthesis were close to the measured values and followed the diurnal pattern correctly. Despite this, each model suffered shortcomings. The multilayer approach was limited by its across-species representation of leaf photosynthetic parameters, and a requirement for detailed environmental data. But its better physiological definition resulted in improved morning conductance estimates, and a greater sensitivity to changes in the environment. The detail in the multilayer model provided analytical insight into the behaviour of the canopy that was not available from the simpler simulation. The big-leaf model gave a good spatial estimate, but the calibrating signal showed a degree of variance because of the forest mosaic surrounding the micrometeorological tower. Slight overestimates of afternoon conductance and assimilation pointed to possible missing elements in the conductance models, but otherwise the results suggested that the representation of leaf-level gas exchange characteristics in the canopy models was satisfactory. The non-linearity of the F_c - Q response for the big-leaf model was

suggestive of photosynthetic acclimation in the canopy, and the leaf-level data used to parameterise the multilayer model indicate that this is at least partly the case.

Results from a similar big-leaf model calibrated for PRF were compared with those from SRF. The broad features of forest gas exchange were shared by both sites. Extension of the PRF model to an annual estimate (Grace *et al.*, 1995b) indicated the forest to be a sink of 0.9 (± 0.2) ton C ha^{-1} yr^{-1} (0.3 (±0.1) μmol C m^{-2} s^{-1}); the SRF site was a stronger sink of 0.7 - 0.9 μmol C m^{-2} s^{-1}, calculated over a 46 day period. Both models were highly sensitive to CO_2 concentration and temperature, but less sensitive to radiation. A small increase in temperature (2 °C) converted the PRF site from a sink for CO_2 to a source. A similar sensitivity in respiration was observed in SRF, though a reduced sink capacity was predicted, rather than a net source. The relatively high fluxes from SRF soil suggested that disturbance can create secondary forests that are temporary sources for carbon dioxide.

Concluding remarks

The goal of estimating larger scale phenomena by measurement of their component parts underpins this thesis. At the level of ecophysiology of the individual, the organ level gas exchange data suggested a way to quantify for whole trees the balance between respiration and photosynthesis (page 96), or explain the fast growth rate of pioneer trees such as *Musanga cecropioides* (page 97). However, the recent development of the eddy covariance technique provided a unique opportunity to test notions of scaling, and hence the primary focus was to understand the major features of the carbon cycle in forests.

Figures 8.15a-c summarise gross features of the forest carbon cycle that have been quantified. Good agreement was found among biomass estimates using different empirical equations based on measurements of basal trunk diameter (Brown *et al.*, 1989; Deans *et al.*, 1996; Chapter 3). The above ground store of carbon is important in the terrestrial carbon cycle, and until recently there has been little certainty in this value for tropical forests. However, respiration in wood represents ~5% of gross ecosystem carbon flows, so uncertainty in this flux is less important than errors in, and changes to, the state variable from which they come. This contrast is not apparent in leaf or soil gas exchange. Foliar biomass is low, but needs to be estimated accurately because 60 - 65% of gross ecosystem carbon fluxes pass through this tissue, most of which is physiologically active. And in soil both the size of the state variable and the flux of carbon to the atmosphere (30 - 40% of gross ecosystem carbon fluxes) are large and require accurate quantification.

The largest single flux in the terrestrial carbon cycle is photosynthesis (Farquhar *et al.*, 1993). Photosynthesis in leaves is relatively well understood (Farquhar & von Caemmerer, 1982) and was modelled in Chapter 7. However, the exact nature of its expression for a forest canopy is unresolved (Ruimy *et al.*, 1995). The overall agreement between measurements and models in Chapter 8 showed the simplified big-leaf approach to work reasonably well, a result consistent with optimisation theories of canopy physiology (Sellers *et al.*, 1992; Kruijt *et al.*, 1995). However, sensitivity to the driving environmental variables was lower for the big-leaf than the multilayer model and represents an area where more detailed research may be needed. Similarly, the interactions between photosynthetic physiology and mesoscale climate variables, such as water vapour and CO_2 concentration, also

determined canopy assimilation rates and require further elucidation before above-canopy eddy covariance data are to be fully appraised (*e.g.*, Grace *et al.*, 1996; Chapter 8).

To retrieve net CO_2 exchange rates, it was also necessary to estimate whole-forest respiration, of which 75% - 85% is derived from the soil. To measure the process of CO_2 production in soil a chamber method was used, but this posed sampling problems because of the spatial heterogeneity characteristic to soil. The agreement between eddy covariance and chamber-derived estimates suggested that spatial variation in gross efflux rates was accounted for adequately. However, given the high sensitivity of the forest carbon balance to the temperature response in soil CO_2 efflux (k in Equation 4.3), there exists a priority to estimate this parameter more precisely (Townsend *et al.*, 1992; Grace *et al.*, 1995b; Chapter 8). One modelling approach may be to use soil nutrient content (especially organic carbon) to predict efflux rates (Chapter 4). But, if longer-term estimates are required, proper feedback mechanisms need to be incorporated: decomposition process models of this type currently exist for non rain forest sites (Parton *et al.*, 1988; Jenkinson, 1990), though they do not explicitly include root respiration (*cf.*, Nadelhoffer & Raich, 1989).

Figures 8.15b&c suggest a close similarity between the cycling of carbon in SRF and PRF; their main distinguishing features in this analysis were structural. However, the comparison ignored the successional processes in each forest, and the different growth patterns and feedbacks implied therein. Feedbacks to changes in climate were also not considered in this thesis, but are needed for longer-term predictions of the terrestrial carbon cycle. The effects in different species of increasing CO_2 concentration on the efficiency of Rubisco, and the consequent effects on the C:N ratio in plant tissue may change the flux of carbon to vegetation, and the relative sizes of the storage components. These effects may be particularly strong at higher temperatures in the tropics (Drake & Dahlman, 1994). Similarly, below-ground production and decomposition in the soil may vary in response to changes in input rates and quality of the fixed organic matter (Zak *et al.*, 1993; Ineson *et al.*, 1995). We have begun to account for the present-day carbon cycle on land; understanding ecosystem feedbacks to climate change is the next major challenge.

Bibliography

Aber JD, Nadelhoffer KJ, Steudler P, Melillo JM (1989). Nitrogen saturation in forest ecosystems. *Biosci* **39**:378-86.

ADC (1990). Instruction manual for LCA3: leaf chamber analysis system. ADC Ltd, Hoddesdon, UK.

Allen SE (1974). *Chemical analysis of ecological materials.* Blackwell Scientific, Oxford, UK.

Amaral Filho ZPd, Neves Filho JP, Viana CDB (1978). Pedologia. *RADAMBRASIL: Levantamento de recursos naturais.* da Luz A.Rio de Janeiro, Brazil: Ministerio das Minas e Energia, Dep. Nacional da Producao Mineral, p. 254-412.

Amthor JS. (1984). The role of maintenance respiration in plant growth. *Plant, Cell & Env* **7**:561-569.

Amthor JS (1989). *Respiration and crop productivity.* Berlin: Springer-Verlag;

Amthor JS (1994). Scaling CO_2-photosynthesis relationships from the leaf to the canopy. *Photosyn Res* **39**:321-50.

Amthor JS (1995). Terrestrial higher-plant response to increasing atmospheric [CO_2] in relation to the global carbon cycle. *Glob Ch Biol* **1**:243-74.

Amthor JS, Cumming JR (1988). Low levels of ozone increase bean leaf maintenance respiration. *Can J Bot* **66**:724-6.

Amthor JS, Goulden ML, Munger JW, Wofsy SC (1994). Testing a mechanistic model of forest-canopy mass and energy exchange using eddy correlation: carbon dioxide and ozone uptake by a mixed oak-maple stand. *Aust J Plant Physiol* **21**:623-51.

Anderson JM, Proctor J, Vallack HW (1983). Ecological studies in four contrasting lowland rain forests in Gunung Mulu National Park, Sarawak, III., Decomposition processes and nutrient losses from leaf litter. *J Ecology* **71**:503-27.

Anonymous (1987). *Manual of dendrology.* Yaounde, Cameroon: ONADEF, Cameroon.

Anten NPR, Hernandez R, Medina E (1996). The photosynthetic capacity and leaf nitrogen content as related to light regime in shade leaves of a montane tropical forest tree *Tetrochidium rubrivenium. Func Ecol [Accepted].*

ap Rees T (1988). Hexose phosphate metabolism by non-photosynthetic tissues of higher plants. *The biochemistry of plants, Vol 14: Carbohydrates.* Preiss J. Academic Press, San Diego, USA, p. 1-33.

ap Rees T (1994). The respiration of plants. 1994; Public lecture abstract. Cambridge University.

Arrhenius S. (1896). On the influence of carbonic acid in the air upon the temperature of the ground. *London, Edinburgh, and Dublin Philosophical Magazine and Journal of Science, Series 5* **41**:237-76.

Azcon-Bieto J. (1983). Inhibition of photosynthesis by carbohydrates in wheat leaves. *Plant Physiol* **73**:681-6.

Azcon-Bieto J, Osmond CB (1983). Relationship between photosynthesis and respiration. *Plant Phys* **71**:574-81.

Baldocchi DD, Hicks BB, Meyers PP (1988). Measuring biosphere-atmosphere exchanges of biologically related gases with micrometeorological methods. *Ecology* **69**:1331-40.

Baldocchi DD Meyers TP.(1991). Trace gas exchange above the floor of a deciduous forest. I. Evaporation and CO_2 efflux. *J Geophys Res* **96**:7271-85.

Baldocchi DD, Verma SB, Matt DR, Anderson DE (1986). Eddy-correlation measurements of carbon dioxide efflux from the floor of a deciduous forest. *J Appl Ecol* 23:967-75.

Ball JT, Woodrow IE, Berry JA (1987). A model predicting stomatal conductance and its contribution to the control of photosythesis under different environmental conditions. *Volume IV.* Dordrecht: Marinus Nijhoff, p. 221-4.

Baysdorfer C, Sicher RC, Kremer DF (1987). Relationship between fructose 2,6-bisphosphate and carbohydrate metabolism in darkened barley primary leaves. *Plant Physiol* **84**:766-9.

Benecke U, Nordmeyer AH (1982). Carbon uptake and allocation by *Nothofagus solandri* var. *ciffortioides* (Hook.f.) Poole and *Pinus contorta* Douglas ex Loudon ssp. *contorta* at montane and subalpine altitudes.*Carbon uptake and allocation in subalpine ecosystems as a key to management: Proceedings of an IUFRO workshop.* Waring RH.Corvallis: For. Res. Lab., Oregon State University, p. 9-21.

Berquist NO (1964). Absorption of carbon dioxide by plant roots. *Bot Not* **117**:249-61.

Blumthaler M, Ambach W (1994). Changes in solar radiation fluxes after the Pinatubo eruption. *Tellus* **46B**:76-91.

Bolin B (1983). *Changing global biogeochemistry: the present and the future.* Brewer P.New York: Springer-Verlag, p. 305-26.

Bolin B, Fung I (1992). Report: the carbon cycle revisited. *Modeling the Earth system.* Ojima D.Boulder, USA: UCAR/Office for Interdiscplinary Earth Studies, p. 151-64.

Bosatta E (1980). Modelling of soil processes - an introduction. *Ecol Bull* **32**:553-64.

Boyle S, Institute of Hydrology (1995). Changes in soil moisture content at Mbalmayo Reserve, Cameroon, 1994 *[Unpublished].*

Bridgham SD, Richardson CJ (1992). Mechanisms controlling soil respiration (CO_2 and NH_4) in southern peatlands. *Soil Biol Biochem* **24**:1089-99.

Brooks A (1986). Effects of phosphorus nutrition on ribulose 1,5 carboxylase activation, photosynthetic quantum yield and amounts of some Calvin cycle metabolites in spinach leaves. *Aust J Plant Physiol* **13**:221-37.

Brooks A, Farquhar GD (1985). Effect of temperature on the CO_2/O_2 specificity of ribulose-1,5-bisphosphate carboxylase/oxygenase and the rate of respiration in the light. *Planta* **13**:221-37.

Brooks JR, Hinckley TM, Ford ED, Sprugel DG (1991). Foliage dark respiration in *Abies amabilis* (Dougl.) Forbes: variation within the canopy. *Tree Physiol* **9**:325-38.

Brown S, Gillespie AJR, Lugo AE (1989). Biomass estimation methods for tropical forests with applications to forest inventory data. *Forest Sci* **35**:881-902.

Brown S, Iverson LR (1992). Biomass estimates for tropical forests. *World Resource Rev* **4**:366-84.

Brown S, Lugo AE (1984). Biomass of tropical forests: a new estimate based on forest volumes. *Science* **223**:1290-3.

Brown S, Lugo AE (1992). Aboveground biomass estimates for tropical moist forests of the Brazilian Amazon. *Interciencia* **17**:8-17.

Brunig EF (1983). Vegetation structure and growth.*Tropical rain forest ecosystems.* Golley FB.Oxford: Elsevier, p. 49-75.

Butler DR, Landsberg JJ (1981). Respiration rates of apple trees, estimated by CO_2 efflux measurements. *Plant, Cell and Env* **4**:153-9.

Byrd GT, Sage RF, Brown RH (1992). A comparison of dark respiration between C_4 and C_3 plants. *Plant Physiol* **100**:191-8.

Caldwell MM, Meister H-P, Tenhunen JD, Lange OL (1986). Canopy structure, light microclimate and leaf gas exchange of *Quercus coccifera* L. in a Portuguese macchia: measurements in different canopy layers and simulations with a canopy model. *Trees* **1**:25-41.

Campbell GS, Norman JM (1989). The description and measurement of plant canopy structure.*Plant Canopies: their growth, form and function.* Russell G, Marshall B, and Jarvis PG.Cambridge, UK: Cambridge Univ. Press,

Cannell MGR, Dewar RC (1994). Carbon allocation in trees: a review of concepts for modelling. *Adv Ecol Res* **25**:59-104.

Carlyle JC (1986). Nitrogen cycling in forested ecosystems. Forestry Abstracts **47**:(5)307-26.

Cavelier J (1992). Fine-root biomass and soil properties in a semi-deciduous and lower montane rain forest in Panama. *Plant & Soil* **142**(2):187-201.

Chapman SB (1979). Some interrelationships between soil and root respiration in lowland *Calluna* heathland in southern England. *J Ecol* **67**:1-20.

Chase WW (1934). The composition, quantity and physiological significance of gases in tree stems. *Minnesota Agr Expt Sta Tech Bull* **99**

Chung H, Barnes RL (1977). Photosynthate allocation in *Pinus taeda*, I. Substrate requirements for synthesis of shoot biomass. *Can J For Res* **7**:106-11.

Ciais P, Tans PP, White JWC (1995). Partitioning of ocean and land uptake of CO_2 as inferred by $\delta^{13}C$ measurements from the NOAA Climate Monitoring and Diagnostics Laboratory Global Air Sampling Network. *J Geophys Res* **100**:5051-70.

Coleman DC (1973a). Compartmental analysis of "total soil respiration" : an exploratory study. *Oikos* **24**:361-6.

Coleman DC (1973b). Soil carbon balance in a successional grassland. *Oikos* **24**:195-9.

Collier DE, Cummins WR, Villar R (1992). Diurnal patterns of respiration in the leaves of four forest tree species. *Physiol Plant* **84**:361-6.

Cowling JE and MacLean SF (1982). Forest floor respiration in a black spruce taiga forest ecosystem in Alaska. *Holarctic Ecol* 4229-37.

Cropper WPJ, Ewel KC, and Raich JW (1985). The measurement of soil CO_2 evolution *in situ*. *Pedobiologia* **28**:35-40.

Culf AD, Esteves JL, Marques Filho A de O, da Rocha HR (1996). Radiation, temperature and humidity over forest and pasture in Amazonia.*Amazonian Deforestation and Climate.* Gash JHC, Nobre CA, Roberts JM, and Victoria RL.Chichester, UK: John Wiley and Sons,

De Jong and Schappert HJV(1972). The calculation of soil respiration and activity from CO_2 profiles in the soil. *Soil Science* **113**:328-33.

Dean TJ, Bell JP, and Baty AJB (1987). Soil moisture measurement by an improved capacitance technique, Part I: Sensor design and performance. *J Hydrol* **93**:67-78.

Deans TD, Moran J, Grace, J (1996). Biomass relationships for tree species in regenerating semi-deciduous tropical rain forest in Cameroon. *For Ecol & Manag [In press]*

Denmead, Bradley (1985). Flux-gradient relationships in a forest canopy. The forest-atmosphere interaction. Hutchinson BA, BB Hicks, D Reidel, Dordrecht, Netherlands, p. 407-420.

Drake BG, Dahlman RC (1994). The potential effect of rising atmospheric CO_2 concentration on carbon accumulation in terrestrial ecosystems. Proceedings of 4th International CO_2 conference, Carqueiranne, France, September.

Edwards NT (1974) A moving chamber design for accurate measurements of soil respiration rates. *Oikos* **25**:97-101.

Edwards NT (1975). Effects of temperature and moisture on carbon dioxide evolution in a mixed deciduous forest floor. *Soil Sci Soc Am Proc* **39**:361-5.

Edwards NT (1982). The use of soda-lime for measuring respiration rates in terrestrial ecosystems. *Pedobiologia* **23**:321-30.

Edwards NT, Shugart HHJ, McLaughlin SB, et al. (1980). Carbon metabolism in terrestrial ecosystems. *Dynamic properties of forest ecosystems.* Reichle DE. Cambridge, UK: Cambridge University Press,

Ehleringer JR, Field CB (1993). *Scaling physiological process: Leaf to Globe.* San Diego, USA: Academic Press.

Enting IG, Trudinger CM, Francey RJ (1995). A synthesis inversion of the concentration and $\delta^{13}C$ of atmospheric CO_2. *Tellus* **47B**:35-52.

Evans JR (1987). The dependence of quantum yield on wavelength and growth irradiance. *Aust J Plant Physiol* **14**:69-79.

Evans JR (1989). Photosynthesis and nitrogen relationships in leaves of C_3 plants. *Oecologia* **78**:9-19.

Evans JR (1993a). Photosynthetic acclimation and nitrogen partitioning within a lucerne canopy, I. Canopy characterisitcs. *Aust J Plant Physiol* **20**:55-67.

Evans JR (1993b). Photosynthetic acclimation and nitrogen partitioning within a lucerne canopy, II. Stability through time and comparison with a theoretical maximum. *Aust J Plant Physiol* **20**:69-82.

Ewel KC, Cropper WP, Gholz HL (1987). Soil CO_2 evolution in Florida slash pine plantation, II. Importance of root respiration. Can J For Res **17**:330-3.

Fan S, Wofsy SC, Bakwin PS, and Jacob DJ.(1990) Atmosphere-biosphere exchange of carbon dioxide and ozone in a Central Amazon forest. *J Geophys Res* **9**516851-64.

Fang C, Moncrieff JB (1995). An improved dynamic chamber technique for measuring CO_2 evolution from the soil. *Func Ecol* **9**: 743-754.

Fang C, Moncrieff JB (1996). Measuring and modelling the flux of CO_2 from soil (in preparation).*[Unpublished]*

Farquhar GD (1989). Models of integrated photosynthesis in cells and leaves. *Phil Trans Roy Soc, London, B* **323**:357-68.

Farquhar GD, Lloyd J, Taylor JA, Flanagan LB, Syvertsen JP, Hubick KT, Wong SC, Ehleringer JR (1993). Vegetation effects on the isotope composition of oxygen in atmospheric CO_2. *Nature* **363**:439-43.

Farquhar GD, von Caemmerer S (1982). Modelling of photosynthetic response to environmental conditions.*Water Relations and Carbon Assimilation. Encyclopaedia of Plant Physiology 12(B).* Lange OL, Nobel PS, Osmond CB, and Ziegler H.New York, USA: Springer-Verlag, p. 550-87.

Farquhar GD, von Caemmerer S, Berry JA (1980). A biochemical model of photosynthetic CO_2 assimmilation in leaves of C_3 species. *Planta* **149**:78-90.

Farquhar GD, Wong SC (1984). An empirical model of stomatal conductance. *Aust J Plant Physiol* **11**:191-210.

Fearnside PM, Newton LJ, Fernandes FM (1993). Rain forest burning and the global carbon budget: biomass, combustion efficiency, and charcoal formation in the Brazilian Amazon. *J Geophys Res , D* **98**:16733-43.

Field CB (1983). Allocating leaf nitrogen for the maximisation of carbon gain: leaf age as a control on the allocation program. *Oecologia* **56**:341-7.

Field CB (1988) On the role of photosynthetic responses in constraining the habitat distribution of rain forest plants. *Aust J Plant Physiol* **15**:343-58.

Field CB, Ball JT, Berry JA (1989). Photosynthesis: principles and field techniques. *Plant physiological ecology: field methods and intrumentation.* Pearcy RW, Ehleringer J, Mooney HA, Rundle PW. Chapman & Hall, London, UK, p209-253.

Field CB, Mooney HA (1986). The photosynthesis-nitrogen relationship in wild plants.*The economy of plant form and function.* Givnish TJ.Cambridge, UK: Cambridge University Press, p. 25-55.

Foaham, A. (1982). Etude du comportement general du Framire a Bilik: contribution a l'etude de la sylviculture artificiele du Framire. Yaounde, Cameroon. Centre de Rech. For. de Nkolbisson.

Folster H, de las Salas G, Khanna P (1976). A tropical evergreen forest site with perched water table, Magdalena valley, Colombia. Biomass and bioelement inventory of primary and secondary vegetation. *Oecologia Plant* **11**:297-320.

Foote KC, Schaedle M (1976). Diurnal and seasonal patterns of photosynthesis and respiration in stems of *Populus tremuloides* Michx. *Plant Physiol* **58**:651-2.

Foster Brown I, Martinelli LA, Wayt Thomas W, Moreira MZ, Cid Ferreira CA, Victoria RA (1995). Uncertainty in the biomass of Amazonian forests: an example from Rondonia, Brazil. *For Ecol & Manag* **75**: 175-189.

Francey RJ, Tans PP, Allison CE, Enting IG, White JWC, Trolier M (1995). Changes in oceanic and terrestrial carbon uptake since 1982. *Nature* **373**:326-30.

Friedli H, Loetscher H, Oeschger H, Siegenthaler U, and Stauffer B (1986). Ice core record of the $^{13}C/^{12}C$ record of atmospheric CO_2 in the past two centuries. *Nature* **324**:237-8.

Fung IY, Tucker CJ, Prentice KC (1987). Application of advanced very-high resolution radiometer vegetation index to study atmosphere-biosphere exchange of CO_2. *J Geophy Res* **92**:2999-3015.

Garratt JR (1992). *The Atmospheric Boundary Layer.* Cambridge, UK: Cambridge University Press;

Gifford RM (1994). The global carbon cycle: a viewpoint on the missing sink. *Aust J Plant Physiol* **21**:1-15.

Gillespie AJR, Brown S, Lugo AE (1992). Tropical forest biomass estimation from truncated stand tables. *For Ecol and Man* **48**:69-87.

Goodwin RH, Goddard DR (1940). The oxygen consumption of isolated trees. *Amer J Bot* **27**:234-7.

Grace J (1983). *Plant-atmosphere relationships.* London, UK: Chapman and Hall.

Grace J (1991). Physical and ecological evaluation of heterogeneity. *Functional Ecology* **5**:192-201.

Grace J, Lloyd J, McIntyre J, Miranda A, Meir P, Miranda H, Moncrieff J, Massheder J, Wright I, and Gash J (1995a). Fluxes of carbon dioxide and water vapour over an undisturbed tropical forest in south-west Amazonia. *Glob Ch Biol* **1**(1):1-12.

Grace J, Lloyd J, McIntyre J, Miranda AC, Meir P, Miranda H, Nobre C, Moncrieff J, Massheder J, Malhi Y, et al. (1995b). Carbon dioxide uptake by an undisturbed tropical rain forest in SW Amazonia, 1992 to 1993. *Science* **270**:778-80.

Grace J, Malhi Y, Lloyd J, McIntyre J, Miranda AC, Meir P, and Miranda H (1996). The use of eddy covariance to infer the net carbon dioxide uptake of Brazilian rain forest.*Glob Ch Biol* **2**

Grace J, Okali DUU, Fasehun FE (1982). Stomatal conductances of two tropical trees during the wet season in Nigeria. *J App Ecol* **19**:659-70.

Grahammer K, Jawson MD, and Skopp J (1991). Day and night soil respiration from a grassland. *Soil Biol Biochem* **23**:77-81.

Griffiths, G (1993). The carbon content of trees. ITE, Edinburgh, UK. ITE.

Hagihara A, Hozumi K (1981). Respiration consumption by woody organs in a *Chamaecyparis obtusa* plantation. *J Jpn For Soc* **63**

Hagihara A, Hozumi K (1991). Respiration. *Physiology of trees.* Raghavendra AS. New York, USA: John Wiley and Sons, p. 87-110.

Hanson PJ, Wullschleger SD, Bohlman SA, and Todd DE (1993) Seasonal and topographic patterns of forest floor CO_2 efflux from an upland oak forest. *Tree Phys* **13**:1-15.

Hari P, Nilson T, Salminen R, Kaipiainen L, Ross J (1984). Nonlinear dependence of photosynthetic rate on irradiance and its consequences for estimates of the amount of saccharides formed. *Photosynthetica* **18**:28-33.

Hari P, Nygren P, and Korpilahti E (1991). Internal circulation of carbon within a tree. *Can J For Res* **21**:514-5.

Harley PC, Tenhunen JD, Lange OL (1986). Use of an analytical model to study limitations on net photosynthesis in *Arbutus unedo* under field conditions. *Oecologia* **70**:393-401.

Harley PC, Thomas RB, Reynolds JF, Strain BR (1992). Modelling photosynthesis of cotton grown in elevated CO_2. *Plant, Cell and Env* **15**:217-82.

Henderson-Sellers A (1991). A commentary on: Tropical deforestation, albedo and the surface energy balance. *Climate Change* **19**:135-7.

Herold A (1980). Regulation of photosynthesis by sink activity - the missing link. *New Phytol* **86**:131-44.

Hodnett MG, Oyama MD, Tomasella J (1996). Comparisons of long-term soil water storage behaviour under pasture and forest in three areas of Amazonia. *Amazonian deforestation and climate.* Gash JHC, Nobre CA, Roberts JM, and Victoria RL.Chichester, UK: John Wiley.

Holdridge L (1967) *Life zone ecology.* San Jose, Costa Rica: Tropical Science Center.

Hollinger, DY, Kelliher, FM, Byers, JN, Hunt, JE, McSeveny, TM, Weir, PL (1994). Carbon dioxide exchange between an undisturbed old-growth temperate forest and the atmosphere. *Ecology* **75**: 134-150.

Honzak M (1996). The estimation of wood and leaf biomass in secondary tropical forest.*Amazonian deforestation and climate.* Gash JHC, Nobre CA, Roberts J, and Victoria RL.Chichester, UK: John Wiley and Sons,

Houghton JT et al. (1994). *Climate Change: The IPCC Scientific Assessment.* Cambridge University Press, Cambridge, UK.

Houghton RA (1995). Land-use change and the carbon cycle. *Glob Ch Biol* **1**:275-88.

Houghton RA and Woodwell GM (1979) Global climatic change. *Sci Am* **260**:36-44.

Howard PJA and Howard DM.(1979) Respiration of decomposing litter in relation to temperature and moisture. *Oikos* **33**457-65.

Hubbard RM, Ryan MG, Lukens DL. (1995)A simple, battery-operated, temperature controlled cuvette for respiration measurements. *Tree Phys* **15**:175-9.

Hulett JR (1956). Deviations from the Arrhenius equation. *Quarterly Rev* **18**:227-42.

Hutchinson GL, Livingston GP (1993). Use of chamber systems to measure trace gas fluxes. *Agricultural Ecosystem Effects on Trace Gases and Global Climate Change.* Anonymous Madison, WI, USA: *Soil Sci. Soc. Am.***13** p. 63-78.

IBAMA (1992). *Alternativas de desenvolvimento dos cerrados: manejo e conservacao dos recrusos naturais renovaveis.* IBAMA, Governo do Brasil.

IBGE (1993). Censores do Brasil: Uma visaopanoramica da nossa Natureza. Sao Paulo. Governo do Brasil; Sao Paulo.

Ineson P, Cotrufo MF, Howson G (1995). CO_2 fertilisation effects on decomposition processes. *Annual report to TIGER committee.* Grange-over-Sands, Cumbria, January 1995.

Irving DE, Silsbury JH (1987). A comparison of the rate of maintenance respiration in some crop legumes and tobacco determined by three methods. *Ann Bot* **59**:257-64.

James WO (1953). *Plant respiration.* Oxford, UK: Clarendon Press;

Jansson SL, Persson J (1982). Mineralisation and immobilisation of soil nitrogen.Stevenson FJ p. 292-52.

Jarvis PG (1976). The interpretation of the variations in in leaf water potential and stomatal conductance found in canopies in the field. *Phil Trans Roy Soc London (B)* **273**:593-610.

Jarvis PG (1995). Scaling processes and problems. *Plant, Cell and Env* **18**:1079-89.

Jarvis PG, Dewar RC (1993). Forests in the global carbon balance: from stand to region.*Scaling physiological process: Leaf to Globe.* Ehleringer JR and Field CB.San Diego: Academic Press, p. 191-221.

Jarvis PG, Grace J, Moncrieff JB, et al. (1995). Looking for the missing carbon sink in tropical and boreal forests.*Photosynthesis: from light to biosphere.* Mathis P.London, UK: Kluwer Academic, p. 773-8.

Jarvis PG, McNaughton KG (1986). Stomatal control of transpiration: scaling up from leaf to region. *Adv Ecol Res* **15**:1-49.

Jarvis PG, Miranda HS, Muetzelfeldt RM (1985). Modelling canopy exchanges of water vapour and carbon dioxide in coniferous forest plantations.*The Forest-Atmosphere Interaction.* Hutchison BA and Hicks BB.Dordrecht, The Netherlands: Reidel, p. 521-42.

Jenkinson DS (1990) The turnover of organic carbon and nitrogen in soil.. *Phil Trans R Soc Lond B* **329**:361-8.

Jenkinson DS, Adams DE, Wild A (1991). Model estimates of CO_2 emissions from soil in response to global warming. *Nature* **351**:304-6.

Johansson N (1933). The relation between the tree stem's respiration and growth. *Svenska Skogvaords Tidskr* **31**:53-134.

Johnson IR, Thornley JHM (1985). Temperature dependence of plant and crop processes. *Ann Bot* **55**:1-24.

Jones HG (1992) *Plants and Microclimate.* 2nd ed. Cambridge, USA: Cambridge University Press;

Jones MB, Leafe EL, Stiles W, Collett B (1978). Pattern of respiration of a perennial ryegrass crop in the field. *Ann Bot* **42**:693-703.

Jordan C (1985). Soils of the Amazon rain forest.*Amazonia.* Prance GT and Lovejoy TE.Oxford: Pergamon Press, p. 83-94.

Jordan CF, Uhl C (1978). Biomass of a terra firme forest of the Amazon Basin. *Oecologia Plant* **13**:387-400.

Junk WJ, Furch K (1985). The physical and chemical properties of Amazonian waters and relationships with the biota.*Amazonia.* Prance GT and Lovejoy TE.Oxford, UK: Pergamon Press, p. 3-17.

Kaimal JC, Finnigan JJ (1994). *Atmospheric boundary layer flows.* Oxford, UK: Oxford University Press.

Kaimal JC, Wyngaard JC, Izumi Y, Cote OR (1972). Spectral characteristics of surface-layer turbulence. *Q J Royal Met Soc* **98**:563-89.

Kato R, Tadaki Y, Ogawa H (1978). Plant biomass and growth increment studies in Pasah Forest. *Malay Nat J* **30**:211-24.

Kawahara T, Hatiya K, Takeuti I, Sato A (1976). Relationship between respiration rate and nitrogen concentration of trees. *Jap J Ecol* **26**:165-70.

Keeling CD (1994). *The global carbon cycle.* Heinmann M.Berlin, Germany: Springer-Verlag,

Keeling CD, Whorf TP, Whalen M, van der Plicht J (1995). Interannual extremes in the rate of rise of atmospheric carbon dioxide since 1980. *Nature* **375**:666-70.

Keller M, Kaplan WA, Wofsy SC (1986). Emission of N_2O, NH_4, and CO_2 from tropical forest soils. *J Geophys Res* **91**:11791-802.

Kira T, Shidei T (1967). Primary production and turnover of organic matter in different forest ecosystems of the western Pacific. *Jap J Ecol* **17**:70-87.

Kirschbaum MUF, Farquhar GD (1984). Temperature dependence of whole leaf photosynthesis in *Eucalyptus pauciflora* Sieb. ex Spreng. *Aust J Plant Physiol* **11**:519-38.

Klinge H, Rodrigues WA, Brunig E, et al. (1975). Biomass and structure in a central Amazonian rain forest.*Tropical ecological systems.* Golley FB and Medina E.New York: Springer-Verlag, p. 115-22.

Koch GW, Amthor JS, Goulden ML (1994). Diurnal patterns of leaf photosynthesis, conductance and water potential at the top of a lowland rain forest canopy in Cameroon: measurements fromthe *Radeau de Cimes. Tree Physiol* **14**:347-60.

Koike F, Syahbuddin Y (1993). Canopy structure of a tropical rain forest and the nature of an unstratified layer. *Func Ecol* 7(2):230-235.

Korner C (1995). Biodiversity and CO_2: global change is under way. *Gaia* **4**:234-43.

Koyama H (1981). Photosynthetic rates in lowland rain forest trees of Peninsular Malaysia. *Jap J Ecol* **31**:361-9.

Kramer PJ, Kozlowski TT (1960). *Physiology of Trees.* New York, USA: McGraw-Hill;

Kruijt, B (1994). Turbulence over a forest downwind of an edge. PhD thesis, *University of Groningen.*

Kruijt B, Ongeri S, Jarvis PG (1995). Scaling up from leaf to canopy.*Scaling Up.* Van Gardingen P, Foody G, and Curran P.Cambridge, UK: Cambridge University Press,

Kull O, Jarvis PG (1995). The role of nitrogen in a simple scheme to scale up photosynthesis from leaf to canopy. *Plant, Cell and Env* **18**:1174-83.

Ladd JN, Amato M, and Oades JM (1985). Decomposition of plant material in Australian soils 3:Residual organic and microbial biomass-C and biomass-N from isotope labelled legume material and soil organic matter decomposing under field conditions. *Aus J Soil Res* **23**:603-11.

Lambers H, Szaniawski RK, de Visser R (1983). Respiration for growth, maintenance and ion uptake. An evaluation of concepts, methods, values and their significance. *Physiol Plant* **58**:556-63.

Landsberg JJ (1986). *Physiological Ecology of Forest Production.* London, UK: Academic Press;

Lang ARG (1987). Simplified estimates of leaf area index from transmittance of the sun's beam. *Agric For Meteorol* **41**:179-86.

Lang ARG, Yuequin X (1986). Estimation of leaf area index from transmission of direct sunlight in discontinuous canopies. *Ag For Met* **37**:229-43.

Lang ARG, Yuequin X, and Norman JM (1985). Crop structure and the penetration of direct sunlight. *Ag For Met* **35**:83-101.

Lanthony, P (1958). Travaux d'amelioration de la regeneration naturelle en foret classee de Mbalmayo (Cameroun). CCTA Pub. 43 of Inter-African Forestry Conference. p.123

Laties GG (1982). The cyanide-resistant, alternative path in higher plant respiration. *Ann Rev Plant Physiol* **33**:519-55.

Lawson, G.J. (1995). Growth of indigenous tree plantations in the Mbalmayo Forest Reserve, Cameroon. ITE, Edinburgh, UK. ITE.

Leal JWL, Silva GH, dos Santos DB, et al. (1978). Geologia. *RADAMBRASIL: Levantamento de recursos naturais.* Luz AA.Rio de Janeiro, Brazil: Ministerio das Minas e Energia Dep. Nac. da Producao Mineral, p. 28-184.

Ledig FT, Drew AP, Clark JG. (1976) Maintenance and constructive respiration, photosynthesis, and net assiimilation rate in seedlings of pitch pine. *Ann Bot* **40**:289

Lehto T, Grace J (1994). Carbon balance of tropical tree seedlings - a comparison of two species. *New Phyt* **127**:455-63.

Lemon E, Allen LH, Muller L (1970). Carbon dioxide exchange of a tropical rain forest. *Bioscience* **20**:1054-69.

Lemur J (1973). A method for simulating the direct solar radiation regime in sunflower, Jerusalem artichoke, corn and soybean canopes using actual stand structure data. *Agric Meteorol* **12**:229-47.

Letouzey, R. (1985). Notice sur la carte phytogeographique du Cameroun au 1: 500 000; domaine de la foret dense humide semi-decidue caducifoliee; domaine de la foret dense humide toujours verde. Toulouse, France. IRA Cameroun - ICIV, Toulouse.

Leuning R (1995). A critical appraisal of a combined stomatal-photosynthesis model for C_3 plants. *Plant, Cell and Env* **18**:339-55.

Leuning R, Moncrieff JB (1990) Eddy covariance CO_2 flux measuurements using open and closed path analysers: corrections for analyser water vapour sensitivity and damping of fluctuations in air sampling tubes. *Bound Layer Met* **53**:63-7.

Leverenz JW (1981). Photosynthesis and transpiration in large forest-grown Douglas fir: diurnal variation. *Can J Bot* **59**:349-56.

Levy EB, Madden EA (1932). The point method of pasture analysis. *N Z J Agric* **46**:267-79.

Levy, P.(1995). Carbon dioxide exchange of Sahelian vegeatation. PhD thesis, *University of Edinburgh.*

Linder S. (1985). Potential and actual production in Australian forests.*Research for forest management.* Landsberg JJ and Parsons W.Melbourne, Australia: CSIRO, p. 11-35.

Linder S, Troeng E (1980). Photosynthesis and transpiration of 20-year-old Scots pine. *Structure and function of northern coniferous forests - an ecosystem study.* T. Persson. *Ecol Bull* **32**: 165-181.

Linder S, Axelsson B (1982). Changes in carbon uptake and allocation patterns as a result of irrigaiton and fertilization in a young *Pinus sylvestris* stand.*Carbon uptake and alocation in subalpine ecosystems as akey to management: Proceedings of an IUFRO workshop.* Waring RH.Corvallis, USA: Forest Res. Lab., Oregon State Univ. p. 38-44.

Lisboa PLB (1990). *Rondonia: colonizacao e floresta.* Rel. de Pesq. 9 ed. Sao Paulo, Brazil: SCT/PR CNPq;-220.

Lloyd J, Grace J, Miranda AC, Meir P, Wong SC, Miranda HS, Wright I, Gash JHC, McIntyre J (1995b). A simple calibrated model of Amazon rain forest productivity based on leaf biochemical properties. *Plant, Cell and Env* **18**:1129-45.

Lloyd J, Taylor JA (1994). On the temperature dependence of soil respiration. *Functional Ecology* **8**:315-23.

Lloyd J, Wong SC, Styles JM, Batten D, Priddle R, Turnbull C, McConchie CA (1995a). Measuring and modelling whole-tree gas exchange. *Aust J Plant Physiol* **22**:987-1000.

Lohammar T, Larsson S, Linder S, Falk SO (1980). FAST - Simulation models of gaseous exchange in Scots Pine. *Ecol Bull* **32**:505-23.

Luizao FJ, Schubart HOR (1987). Litter production and decomposition in a terra-firme forest of Central Amazonia. *Experientia* **43**:259-65.

Lundegardh H (1927). Carbon dioxide evolution of soil and crop growth. *Soil Science* **23**:417-53.

MacArthur RH, MacArthur JW (1961). On bird species diversity. *Ecology* **42**:594-8.

Marland G, Andres RJ, Boden TA (1994). Global, regional and national CO_2 emissions.*Trends '93: A compendium of data on global change.* Anonymous, Tenessee, USA: Oak Ridge, National Lab. p. 508-84.

Marshall JD, Ehleringer JR (1990). Are xylem-tapping mistletoes partially heterotrophic? *Oecologia* **84**:244-8.

Marshall JD, Ehleringer JR, Schulze E-D, Farquhar GD (1994). Carbon isotope composition, gas exchange and heterotrophy in Australian mistletoes. *Functional Ecology* **8**:237-41.

Massheder JM, Moncrieff JB (1996). EdiSol [computer program]. Univerisity of Edinburgh.

McCracken, PJ (1993). Turbulent exchange of momentum and carbon dioxide of a sitka spruce plantation. PhD thesis, *University of Edinburgh.*

McCree KJ (1970). An equation for the rate of dark respiration of white clover plants grown under controlled conditions. *Prediction and measurement of photosynthetic productivity.* Setlik I.Wageningen, Netherlands: Center for Agric. Publishing.

McCree KJ (1983). Carbon balance as a function of plant size in sorghum plants. *Crop Sci* **23**:1173-7.

McCune B, Menges ES (1986). Quality of historical data on midwestern old-growth forests. *Amer Mid Naturalist* **116**:163-72.

McDermitt DK, Loomis RS (1981). Elemental composition of biomas and its relation to energy content, growth efficiency,and growth yield. *Ann Bot* **48**:275-90.

McWilliam AL, Cabral OMR, Gomes BM, et al. (1996). Forest and pasture leaf gas exchange in SW Amazonia. *Amazonian deforestation and climate.* Gash JHC, Nobre CA, Roberts J, and Victoria RL.Chichester, UK: John Wiley and Sons,

McWilliam ALC, Roberts JM, Cabral OMR, Leitao MVBR, de Costa ACL, Maitelli GT, Zamparoni CAGP (1993). Leaf area index and above-ground biomass of terra firme rain forest and adjacent clearings in Amazonia. *Func Ecol* **7**:310-7.

Medina E, Klinge H (1983). Productuvity of tropical forests and tropical woodlands.*Ecosystem processes: Mineral cycling, productivity and Man's influence.* Lange OL, Nobel PS, Osmond CB, and Ziegler H.Berlin, Germany: Springer-Verlag, p. 281-303.

Medina E, Klinge H, Jordan C, Herrera R (1980). Soil respiration in Amazonian rain forests in the Rio Negro basin. *Flora* **170**:240-50.

Meir P, Grace J, Miranda AC, et al. (1996). Soil respiration in a rain forest in Amazonia, and in cerrado in Central Brazil.*Amazonian Deforestation and Climate.* Gash JHC, Nobre CA, Roberts JM, and Victoria RL.London, UK: John Wiley and Sons,

Melillo JM, Aber JD, Muratore JF (1982). Nitrogen and lignin control of hardwood leaf litter docomposition dynamics. *Ecology* **63**:621-6.

Miranda AC, Miranda HS, Lloyd J, Grace J, Francey RJ, McIntyre J, Meir P, Riggan P, Lockwood R, Brass J (1996). Fluxes of carbon, water vapour and energy over Brazillian cerrado: an analysis using eddy covariance and stable isotopes. *Plant, Cell and Env submitted*

Moncrieff JB, Malhi Y, Leuning R (1996). The propagation of errors in long-term measurements of land-atmosphere fluxes. *Glob Ch Biol* **2**

Moncrieff JB, Massheder JM, de Bruin H, et al. (1996). A system to measure surface fluxes of energy, momentum and carbon dioxide.. *J Hydrology [In Press]*

Moncrieff JB, Verma SB, Cook DR (1992). Intercomparison of eddy correlation carbon dioxide sensors during FIFE 1989. *J Geophys Res* **97**:18725-30.

Monsi M, Saeki T (1996). Uben den Lichtfaktor in den Pflanzengesellschaften und seine Bedeutung fur die Stoff produktion. *Jap J Bot* **14**:22-52.

Monteith JL (1995). A reinterpretation of stomatal responses to humidity. *Plant, Cell and Env* **18**:357-64.

Monteith JL, Unsworth MH (1990). *Principles of Environmental Physics.* London, UK: Edward Arnold.

Moore CJ (1986). Frequency response corrections for eddy correlation systems. *Bound Layer Met* **38**:147-69.

Mosier AR (1989). Chamber and isotope techniques.*Exchange of Trace Gases between Terrestrial Ecosystems and the Atmosphere.* M.O.Andreae and D.S.Schimel.New York: John Wiley, p. 263-80.

Nadelhoffer KJ, Raich JW (1992). Fine root estimates and below-ground carbon allocation in forest ecosystems. *Ecology* **73**(4):1139-47.

Nadkarni NM (1981). Canopy roots - convergent evolution in rain forest nutrient cycles. *Science* **214**:1023-4.

Nadkarni NM, Parker GG (1994). A profile of forest canopy science and scientists. *Selbyana* **15**:38-50.

Nakayama FS (1990). Soil respiration. *Remote Sens Reviews* **53**:11-21.

Negisi K (1979). Bark respiration rate in stem segments detached from young Pinus densiflora trees in relation to velocity of artificial sap flow. *J Jpn For Soc* **61**:88-93.

Neller JR (1918). Studies on the correlation between the production of carbon dioxide and the accumulation of ammonia by soil organisms. *Soil Sci* **5**:225-41.

Nepstad DC, de Carvalho CR, Davidson EA, Jipp PH, Levebre PA, Negreiros GH, da Silva ED, Stone TA, Trumbore SE, Vieira S (1994). The role of deep roots in the hydrological and carbon cycles of Amazonian forests and pastures. *Nature* **372**:666-9.

NERC (1993). TIGER: Programme report and science highlights, 1990-1992. London, UK: NERC.

Newton JD (1923). Measurement of the carbon dioxide evolved from the roots of various crop plants. *Sci Agric* **4**:268-74.

Ngeh, CP (1989). Effects of land clearing methods on a tropical forest ecosystem and the growth of *Terminalia ivorensis* (A. Chev.) *University of Edinburgh.*

Ninomiya I, Hozumi K (1981). Night-time respiration in standing forest trees, *Pinus densi-thunbergii* Uyeki and *Chamaecyparis obtusa* Endl. measured by the enclosed standing tree method.*Proceedings of the XVII IURFO World Congress, Div. 2.* Anonymous, IUFRO, p.113

Njib, G (1987). Catenary relationship in tropical forest soils: Mbalmayo area *Enschede, Netherlands;*

Norman JM, Campbell GS (1991). Canopy structure.*Plant Physiological Ecology: field methods and instrumentation.* 2nd ed. Pearcy RW, Ehleringer J, Mooney HA, and Rundel PW.London. Chapman and Hall, p. 301-26.

Norman JM, Garcia R, Verma SB (1992). Soil surface CO_2 fluxes and the carbon budget of a grassland. *J Geophys Res* **97**:18845-53.

Odum HT (1970). Summary: an emerging view of the ecological system at El Verde.*A tropical rain forest.* Odum HT and Pigeon RF.Washington, USA: Div. Tech. Info. AEC,

Odum HT, Lugo A, Cintron G, et al. (1970). Metabolism and evapotranspiration of some rain forest plants and soil. *A Tropical Rain Forest.* Anonymous, Springfield, Va: US: US AEC, p. 103-64.

Orchard VA, Cook FJ (1983). Relationship between soil respiration and soil moisture. *Soil Biol Biochem* **15**:447-53.

Paembonan SA, Hagihara A, Hozumi K (1992). Long-term respiration in relation to growth and maintenance processes of the above-ground parts of a hinoki forest tree. *Tree Physiol* **10**:101-10.

Parker LW, Miller J, Steinberger Y, Whitford WG (1983). Soil respiration in a Chihuahuan desert rangeland. *Soil Biol Biochem* **15**:303-9.

Parkinson KJ (1981). An improved method for measuring soil respiration in the field. *J Appl Ecol* **18**:221-8.

Parkinson KJ (1983). Porometry.*Instrumentation for environmental physiology.* Woodward FI.Cambridge, UK: Cambridge University Press,

Parton WJ, Stewart JWB, Cole CV (1988). Dynamics of C, N, P, and S in grassland soils. *Biogeochem* **5**:109-31.

Paulson CA (1970). The mathematical representation of wind speed and temperature profiles in the unstable suface layer. *J App Met* **9**:857-61.

Pearcy RW (1987). Photosynthetic gas exchange responses of Australian tropical forest trees in canopy, gap and understorey micro-environments. *Func Ecol* **1**:169-78.

Pelkonen P, Vapaavuori EM, Vuorinen H (1985). HCO_3^- uptake through the roots in willow and sunflower and effect of HCO_3^- uptake on the productivity of willow cuttings.*Energy from biomass.* Palz W, Coombs J, and Hall DO.London, UK: Elsevier, p. 417-21.

Penning de Vries FWT (1975). The cost of maintenance processes in plant cells. *Annals of Botany* **39**:77-92.

Penning de Vries FWT, Brunsting AHM, van Laar HH (1974). Products, requirements and efficiency of biosynthesis: a quantitative approach. *J Theor Biol* **45**:339-77.

Pennington, D (1994) The taxonomy and molecular systematics of *Andira.* DPhil thesis *University of Oxford* p196.

Pires JM, Prance GT (1985). The vegetation types of the Brazilian Amazon.*Amazonia.* Prance GT and Lovejoy TE.Oxford, UK: Pergamon Press, p. 109-45.

Plass, GN (1956). The carbon dioxide theory of climatic change. *Tellus* **8**:140-154.

Quarrie J (1992). *Earth Summit 1992.* London, UK: Regency Press Corps p140.

Raich J, Schlesinger WH (1992). The global carbon dioxide flux in soil respiration and its relationship to climate. *Tellus* **44B**:81-99.

Raich JW (1983). Effects of forest conversion on the carbon budget of a tropical soil. *Biotropica* **15**:177-84.

Raupach MR (1988). Canopy transport processes.*Flow and transport in the natural environment: advances and applications.* Steffen WL and Denmead OT.Berlin, Germany: Springer-Verlag, p. 95-127.

Raven JA, Farquhar GD (1989). Leaf apoplast pH estimation in *Phaseolus vulgaris .Plant Membrane Transport: The Current Position.* Dainty J, de Michels MI, Marre E, and Rasi-Caldogno F.Amsterdam, Netherlands: Elsevier, p. 607-10.

Rayment MB, Jarvis PG (1996). Another improved method for measuring soil CO_2 effluxes in the field. *Submitted*

Reed KL, Hamerly ER, Dinger BE, Jarvis PG (1976). An analytical model for field measurements of photosynthesis. *J App Ecol* **13**:925-32.

Reich PB, Walters MB (1994). Photosynthesis-nitrogen relations in Amazonian tree species, II. Variations in nitrogen vis-a-vis specific leaf area influences mass- and area-based expressions. *Oecologia* **97**:73-81.

Reich PB, Walters MB, Ellsworth DS, Uhl C (1994). Photosynthesis-nitrogen relations in Amazonian tree species, I. Patterns among species and communities. *Oecologia* **97**:62-72.

Revilla Cardenas, JD (1986). Estudos de ecologia e controle ambiental na regiao do reservatorio da UHE de Samuel: Estimativa da Fitomass. Manaus, Brazil. INPA.

Reyes G, Brown S, Lugo AE (1992). Wood densities of tropical tree species. New Orleans, Louisiana. USDA, Forest Service. SO-88.

Reynolds JF, Chen J, Harley PC, Hilbert DW, Dougherty RL, Tenhunen JD. (1992). Modelling the effects of elevated CO_2 on plants: extrapolating leaf response to a canopy. *Agric For Met* **61**:69-84.

Roberts J, Cabral OMR, Fisch G, Molion LCB, Moore CJ, Shuttleworth WJ. (1993) Transpiration from an Amazonian rain forest calculated from stomatal conductance measurements. *Agric For Meteor* **65**:175-96.

Roberts J, Cabral OMR, de Aguiar LF (1990). Stomatal and boundary layer conductances in an Amazonian terra firme rain forest. *J App Ecol* **27**:336-53.

Rochette P, Desjardins RL, Pattey E (1991). Spatial and temporal variability of soil respiration in agricultural fields. *Can J Soil Science* **71**:189-96.

Ross J. (1981) *The radiation regime and architecture of plant stands.* The Hague, Denmark: Junk;

Ruimy A, Jarvis PG, Baldocchi DD, Saugier B (1995). CO_2 fluxes over plant canopies and solar radiation: a review. *Adv in Ecol Res*

Ryan MG (1989). Sapwood volume for three subalpine conifers: predictive equations and ecological implications. *Can J For Res* **19**:1397-401.

Ryan MG (1990). Growth and maintenance respiration in stems of *Pinus contorta* and *Picea engelmannii*. *Can J For Res* **20**:48-57.

Ryan MG (1991). A simple method for estimating gross carbon budgets for vegetation in forest ecosystems. *Tree Physiol* **9**:255-66.

Ryan MG (1996). Foliar maintenance respiration of subalpine and boreal trees and shrubs. *[In Press]*

Ryan MG, Hubbard RM, Clark DA, Sanford RL (1994). Woody-tissue respiration for *Simarouba amara* and *Minquartia guianensis*, two tropical wet forest species with different growth habits. *Oecologia* **100**:213-20.

Ryan MG, Waring RH (1992). Maintenance respiration and stand development in a subalpine lodgepole pine forest. *Ecology* **73**:2100-8.

Salati E (1985). The climatology and hydrology of Amazonia.*Amazonia.* Prance GT and Lovejoy TE.Oxford, UK: Pergamon Press, p. 18-48.

Sarmiento JL (1993). Atmospheric CO_2 stalled. *Nature* **365**:697-8.

Schaedle M (1975). Tree photosynthesis. *Ann Rev Plant Syst* **26**:101-15.

Schlesinger WH (1977). Carbon balance in terrestrial detritus. *Ann Review Ecol Systematics* **8**:51-81.

Schlesinger WH, Melack, JM (1981). Transport of organic carbon in the world's rivers. *Tellus* **33**: 172-187.

Schulze E (1967). Soil respiration of tropical vegetation types. *Ecology* **48**:652-3.

Schulze E-D, Kelliher FM, Korner C, Lloyd J, Leuning R (1994). Relationships among maximum stomatal conductance, ecosystem surface conductance, carbon assimilation rate and plant nitrogen nutrition: A global ecology scaling exercise. *Annu Rev Ecol Syst* **25**:629-60.

Sellers PJ, Berry JA, Collatz GJ, Field CB, Hall FG (1992). Canopy reflectance, photosynthesis and transpiration, III. A reanalysis using improved leaf models and a new canopy integration scheme. *Remote Sens Environ* **42**:187-216.

Sharpe PJ, de Michelle DW (1977). Reaction kinetics of poikilotherm development. *J Theor Biology* **64**:649-70.

Shinozaki K, Yoda K, Hozumi K, Kira T (1964). A quantitative analysis of plant form - the pipe model theory. *Jap J Ecol* **14**:97-132.

Shuttleworth WJ (1989). Micrometerology of temperate and tropical forest. *Phil Trans Roy Soc, London B* **324**:299-334..

Shuttleworth WJ, Gash JHC, Lloyd CR, McNeil DD, Moore CJ, Wallace JS (1988). An integrated micrometeorological system for evaporation measurement. *Agric For Met* **43**:295-317.

Shuttleworth WJ, Gash JHC, Lloyd CR, Moore CJ, Roberts J, Marques Ad, Fisch G, Silva Filho VdS, Ribiero MdG, Molion LCB, et al. (1984). Eddy correlation measurements of energy partition for Amazonian forest. *Quart J Roy Met Soc* **110**:1163-9.

Siegenthaler U, Sarmiento JL (1993). Atmospheric carbon dioxide and the ocean. *Nature* **365** :119-25.

Singh JS, Gupta SR (1977). Plant decomposition and soil respiration in terrestrial ecosystems. *Botanical Review* **43**:449-58.

Sokal RR, Rohlf FJ (1981). *Biometry.* New York, USA: W.H. Freeman.

Sorensen LH (1981). Carbon-nitrogen relationships during the humification of cellulose in soils containing different amounts of clay. *Soil Biol Biochem* **13**:313-21.

Sprugel DG (1990). Components of woody-tissue respiration in young *Abies amabilis* trees. *Trees* **4**:88-98.

Sprugel DG, Benecke U (1991). Measuring woody-tissue respiration and photosynthesis.*Techniques and Approaches in Forest Tree Ecophysiology.* Lassoie JP and Hinckley TM.Berlin. CRC Press, p. 329-55.

Sprugel DG, Ryan MG, Brooks JR, et al. (1996). Respiration from organ level to the stand.*Physiological ecology of coniferous forests.* Smith WK and Hinckley TM.

Stark N, Jordan CF (1978). Nutrient retention by the root mat of an Amazonian rain forest. *Ecology* **59**:434-7.

Stumm W, Morgan JJ (1981). *Aquatic Chemistry.* New York, USA: John Wiley and Sons

Svensson BH (1980). Carbon dioxide and methane fluxes from the ombotrophic parts of a subarctic mire. *Ecol Bulletin* **30**:235-50.

Swaine MD, Whitmore TC (1988). On the definition of ecological species groups in tropical rain forests. *Vegetatio* **75**:81-6.

Szaniawski RK, Kilkiewicz M (1982). Maintenance and growth respiration in shoots and roots of sunflower plants grown at differnt root temperatures. *Physiol Plant* **54**:500-4.

Tans PP, Fung IY, Takahashi T (1990). Observational constraints on the global atmospheric CO_2 budget. *Science* **247**:1431-8.

Tchoundjeu Z, Roby AJ (1995). Projet d'Amenagement et de regeneration forestiere de Mbalmayo. Regenerating and protecting the forests of Cameroon. Proceedings of the 2nd Assembly of the Professional Foresters Association of Cameroon, Yaounde, Cameroon, 1993.

Tesarova M, Gloser J (1976). Total CO_2 output from alluvial soils with two types of grassland communities. *Pedobiologia* **16**(364):372

Thornley JHM (1970). Respiration, growth, and maintenance in plants. *Nature* **227**:304-5.

Thornley JHM (1977). Growth, maintenance and respiration: a re-interpretation. *Ann Bot* **41**:1191-203.

Tickell C (1977). *Climatic change and world affairs.* London, UK: Pergamon Press;

Townsend AR, Vitousek PM, Holland EA (1992). Tropical soils dominate the short-term carbon cycle feedbacks to atmospheric carbon dioxide. *Climatic Change* **22**:293-303.

Trewartha GT (1954). *An introduction to climate.* New York:

Uhl C (1987). Factors controlling succession following slash-and-burn agriculture in Amazonia. *J Ecol* **75**:377-407.

Valentini R, Scarascia Mugnozza GE, de Angelis P, Bimbi R (1991). An experimental test of the eddy correlation technique over a Mediterranean machia canopy. *Plant, Cell and Env* **14**:987-94.

Vapaavuori EM, Pelkonen P (1985). HCO_3^- uptake through the roots and its effect on the productivity of willow cuttings. *Plant, Cell and Env* **8**:531-4.

Verma SB (1989). Aerodynamic resistances to transfers of heat, mass and momentum. *Estimation of areal evapotranspiration.* Proceedings of a workshop held at Vancouver, BC. IAHS Publ. no 177.

Verma SB (1990). Micrometeorological methods for measuring surface fluxes of mass and energy. *Remote Sens Review* **5**:99-115.

Vertregt N, Penning de Vries FWT (1987). A rapid method for determining the efficiency of biosynthesis of plant biomass. *J Theor Biol* **128**:109-19.

von Caemmerer S, Evans JR (1991). Determination of the average partial pressure of CO_2 in chloroplasts from leaves of several C_3 plants. *Aust J Plant Physiol* **18**:287-305.

von Caemmerer S, Evans JR, Hudson GS, Andrews TJ (1994). The kinetics of Rubisco inferred from measurements of photosynthesis in leaves of transgenic tobacco. *Planta* **195**:88-97.

Vuorinen AH, Vapaavuori EM, Lapinjoki S (1989). Time course of uptake of dissolved inorganic carbon through willow roots in light and in darkness. *Phys Plant* **77**:33-8.

Wang YP, Jarvis PG (1990). Description and validation of an array model - MAESTRO. *Agric Forest Met* **51**:251-80.

Waring RH, McDonald AJS, Larsson S, Ericsson T, Wiren A, Arwidsson E, Ericsson A, Lohammar T (1985). Differences in chemical composition of plants grown at constant relative growth rates with stable minertal nutrition. *Oecologia* **66**:157-60.

Warren Wilson J, Reeve JE (1960). Inclined point quadrats. *New Phytol* **59**:1-8.

Warren-Wilson J (1965). Stand structure and light penetration I. Analysis by point quadrats. *New Phytol* **58**:92-101.

Webb EK, Pearman GI, Leuning R (1980). Correction of flux measurements for density effects due to heat and water vapour transfer. *Quart J Roy Meteorol Soc* **106**:85-100.

White RE (1987). *Introduction to the practice and principles of soil science.* Oxford, UK: Blackwell Scientific.

Whitehead D, Okali DUU, Fasehun FE (1981). Stomatal response to environmental variables in two tropical forest species during the dry season in Nigeria. *J App Ecol* **18**:571-87.

Whitmore TC (1984). *Tropical rain forests of the Far East.* 2nd ed. Oxford, UK: Clarendon Press.

Whittaker RH, Woodwell GM (1967). Surface area relations of woody plants and forest communities. *Am J Bot* **54**:931

Williams KF, Percival F, Merino J, Mooney HA (1987). Estimation of tissue consturction cost from heat of combustion and organic nitrogen content. *Plant, Cell and Env* **10**:725-34.

Wofsy SC, Goulden ML, Munger JW, Fan SM, Bakwin PS, Daube BC, Bassow SL, Bazzaz FA (1993). Net exchange of CO_2 in a mid-latitude forest. *Science* **260**:1314-7.

Wofsy SC, Harriss RC, Kaplan WA (1988). Carbon dioxide in the atmosphere over the Amazon Basin. *J Geophys Res* **93**:1377-87.

Yoda K (1967). Comparative ecological studies on three main types of forest vegetation in Thailand, III. Community respiration. *Nature and Life in SE Asia* **5**:83-148.

Yoda K (1974). Three-dimensional distribution of light intensity in a tropical rain forest of West Malaysia. *Jap J Ecol* **24**:247-54.

Yoda K (1983). Community respiration in a lowland rain forest in Pasoh, Peninsular Malaysia. *Jap J Ecol* **33**:183-97.

Zak DR, Pregitzer KS, Curtis PS, Teeri JA, Fogel R, Randlett DL (1993). Elevated atmospheric CO_2 and feedback between carbon and nitrogen cycles. *Plant & Soil* **151**:105-117.

Appendices

APPENDIX A

A1. DESIGN OF SOIL TEMPERATURE PROBE

Copper-constantan junctions were positioned at different levels down a 50 cm plastic rod, and referenced against a known temperature measured using a a temperature-calibrated '107' thermistor (Figure A1). All wires were sealed into the plastic rod using epoxy resin. In order to minimise the response time to temperature changes the thermocouple junctions were electrically insulated from the soil by a thin layer of varnish.

Wiring Diagram for Soil Temperature Probes

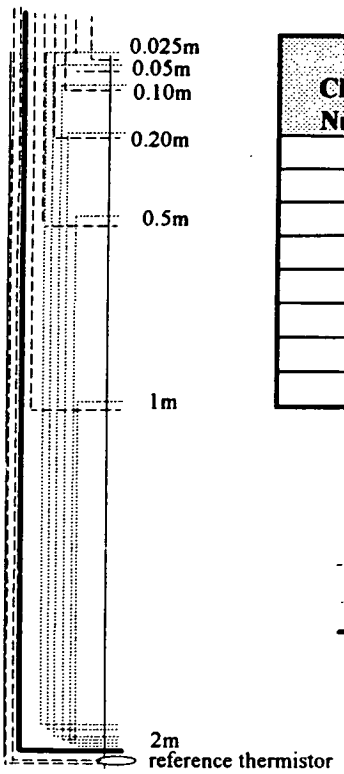

21X Channel Number	Descriptor
1	Ref - 1m differential Thermocouple
2	Ref - 0.5m differential Thermocouple
3	Ref - 0.20m differential Thermocouple
4	Ref - 0.10m differential Thermocouple
5	Ref - 0.05m differential Thermocouple
6	Ref - 0.025m differential Thermocouple
7	Temperature @ 2m (Thermistor)
8	Soil heat flux plates

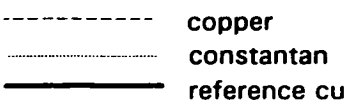

APPENDIX B

B1. WOODY TISSUE RESPIRATION IN LIGHT AND DARK

The effect on respiration rates of placing a shroud over stem tissue was investigated in Chapter 5 (Table A1). The radiation flux incident to the stem was also measured by placing a PPFD sensor normal to the plane of the stem. An illness prevented the collection of more data.

Table B1. Comparison of CO_2 efflux rates normalised to 24 °C with the chamber shrouded or unshrouded; Q is incident photon flux density. All units: $\mu mol\ m^{-2}\ s^{-1}$.

Species	*Without shroud (in light)*	*With shroud (in dark)*	*Maximum Q*
Musanga cecropioides	0.94	1.2	500
Trema orientalis	0.84	0.82	300

APPENDIX C

C1. THE MEASUREMENT OF PHOTOSYNTHESIS USING THE LCA3

The foliar exchange of CO_2 and water vapour was measured in SRF using a portable infra-red gas analyser, in conjunction with a Parkinson leaf chamber (LCA3 and PLC(N), ADC, Hoddesdon, UK). Air drawn from a 2 m sample line is pumped into the leaf chamber via a 1 dm^3 buffer tank and through chemicals that may remove CO_2 (soda lime) or humidify the air (ferrous sulphate). A sample of this 'reference' line is also delivered to the optical bench for the measurement of CO_2 concentration and subsequently followed by 'analysis' air that has passed through the chamber with the leaf in it. The IRGA works as an open system drawing air continuously through the sample cell. A solenoid switching system delivers air in a four stroke, 10 second sequence: reference air - CO_2 free air - analysis air - CO_2 free air.

The infra-red source emits in the 4.26 μm band; the absorption of this signal varies according to the CO_2 concentration, and is detected by a pyroelectric detector. The absolute sensitivity to water vapour in the 4.26 μm band is very small. Corrections are made for the broadening of the CO_2 absorption band by water vapour, and the dilution of CO_2 by evaporation into the analysis stream. Humidity is measured by two Coreci sensors positioned in the PLC inlet and outlet. They operate as a hygroscopic

polymer film separating two metal electrodes. The capacitance of the polymer changes with humidity,and one of the metal plates is very thinly plated (~0.02 μm) to ensure response times of less than a second. Response times are a little slower at very high humidity (> 85%), and some hyteresis may be experienced. Air and leaf temperature are measured using 'Betatherm' precision thermistors, respectively mounted in the chamber head and placed inside the chamber, against a leaf. The software can also be used to calculate leaf temperature from the energy balance (Parkinson, 1983). Radiation is sensed in the 0.4 - 0.7 μm band as photosynthetic photon flux density (Q) using a filtered selenium photocell mounted on top of the chamber.

Calibration:

Calibration for CO_2 was carried out in the field using the LCA3 software and gas of a known CO_2 concentration (400 μmol mol^{-1}) that had been pre-prepared using precision mixing pumps (Wösthoff, Germany) in the laboratory in Edinburgh, and then shipped to the field site. Calibration for the humidity sensors was done using a portable precision water vapour generator (Licor 610, Licor, Nebraska, USA). The response of each sensor can be fine-tuned with a small potentiometer located inside the handle of the PLC. The CO_2 calibration tends to be robust over 1 - 3 days, but was checked every morning; the humidity sensors have a tendency to drift and recalibrated up to 4 times a day, before each measurement session.

The leaf temperature sensors were calibrated using standard resistors of 2 kΩ (equivalent to 25 °C), and 1.15 kΩ (equivalent to 40 °C) connected to plugs that were then inserted into the thermistor socket. The air temperature thermistor could not be calibrated. Independent checks were made of the temperature measurements by placing the PLC in a cool box in the shade together with a Cu-Cn thermocouple, and the data logged for 60 minutes.

Boundary layer resistance and system response time:

The boundary layer resistance, r_b, of a leaf placed in the chamber needs to be measured so that the stomatal resistance (or conductance) can be derived from changes in the water vapour pressure of reference and analysis air. To do this a piece of wet filter paper (i.e., simulating a leaf with no stomatal resistance) was sandwiched between two layers of plastic with a 2 cm^2 circular hole cut to expose the filter paper, and this was then placed in the chamber as a leaf would be. The mean value obtained for r_b in this chamber was 0.21 m^2 s mol^{-1}. The response time of the PLC depends on the chamber volume and flow rate used. It is important to know this value as some idea is required of the

time for equilibration after placing a leaf in the chamber. The PLC(N) has a volume of 12 cm^3, which at a flow rate of 250 - 300 cm^3 min^{-1} reaches equilibrium after around 30 seconds.

C2. ANALYTICAL SOLUTION FOR A_j

Following Farquhar and von Caemmerer (1982), the rate of CO2 assimilation is found as the minimum of either the Rubisco-limited (A_v) or electron transport-limited (A_j) rate. The following gives the derivation for an analytical solution to A_v and A_j using V, J, g_i, g_c, Q, T, and R_d (Lloyd *et al.*, 1995a).

Addressing A_v first, from Equation 7.1, $A_v = \dfrac{V_{max}\left(C_c - \Gamma^*\right)}{\left(K_c\left[1 + pO / K_o\right] + C_c\right)} - R_d$

where pO is the ambient concentration of oxygen; K_c and K_o are the Michaelis-Menten constants for carboxylation and oxygenation by Rubisco, C_c is the concentration of CO_2 in the chloroplast, Γ^* is the CO_2 compensation concentration in the absence of dark respiration, and R_d is the rate of respiration at $Q = 0$. A_v can also be expressed as a function of the internal conductance to CO_2 diffusion (g_i), as:

$$A = g_i (C_{st} - C_c) \qquad \text{Equation B1}$$

where C_{st} is the concentration of CO_2 at the site of evaporation within the sub-stomatal cavity. If Equation B1 is combined with 7.1,

$$A_v + R_d = V_{max}\left(\frac{C_{st} - A_v / g_i - \Gamma^*}{K_c\left(1 + pO / K_o\right) + C_{st} - A_v / g_i}\right) \qquad \text{Equation B2}$$

which can be re-arranged to form Equation B3:

$$A_v^2 - \left[g_i\left(K_c\left(1 + \frac{pO}{K_o}\right) + C_{st}\right) + V_{max} - R_d\right]A_v - R_d g_i\left(K_c\left(1 + \frac{pO}{K_o}\right) + C_{st}\right) + V_{max} g_i\left(C_{st} - \Gamma^*\right) = 0$$

This quadratic could now be solved using a standard route, but it is desirable to express A_v as a function of CO_2 and C_a, rather than C_{st}, and hence an equivalent form of Equation B1 can be written:

$$A = g_c (C_a - C_{st}) \qquad \text{Equation B4}$$

where g_c is the stomatal conductance to CO_2 (g_s / 1.6; Jarvis, 1976). This can now be combined with Equation B3 to give:

$$A_v^2 - \left[g_i \left(K_c \left(1 + \frac{pO}{K_o} \right) + C_a - \frac{A_v}{g_c} \right) + V_{max} - R_d \right] A_v$$

$$- R_d g_i \left(K_c \left(1 + \frac{pO}{K_o} \right) + C_a - \frac{A_v}{g_c} \right) \qquad \text{Equation B5}$$

$$+ V_{max} g_i \left(C_a + \frac{A_v}{g_c} - \Gamma^* \right) = 0$$

After further rearrangement a, b, and c can be defined for the standard quadratic, $aA_v^2 + bA_v + c = 0$:

$a = -g_i - g_c$ Equation B6a

$b = g_i g_c(K_c(1 + pO/K_o) + C_a) + (g_i + g_c)(V_{max} - R_d)$ Equation B6b

$c = g_i g_c(R_d(K_c(1 + pO/K_o) + C_a) - V_{max}(C_a - \Gamma^*))$ Equation B6c

Addressing A_j, from Equation 7.3, $A_J = \frac{J}{4}\left(\frac{C_c - \Gamma^*}{C_c + 2\Gamma^*}\right) - R_d$

Equations 7.3 and B1 can be combined to give:

$A_j^2 - (g_i(C_{st} + 2\Gamma^*) + J/4 - R_d)A_j - R_d g_i(C_{st} + 2\Gamma^*) + g_i(C_{st} - \Gamma^*)J/4 = 0$ Equation B7

And, as before, by substituting Equation B4 into B7, an expression for A_j can be obtained in terms of conductances to CO_2 diffusion, and the underlying metabolism, where $aA_j^2 + bA_j + c = 0$, where:

$a = -g_i - g_c$ Equation B8a

$b = g_i g_c(C_a + 2\Gamma^*) + (g_i + g_c)(J/4 - R_d)$ Equation B8b

$c = g_i g_c(R_d(C_a + 2\Gamma^*) - J/4(C_a - \Gamma^*))$ Equation B8c

The photosynthetic rate of the leaf is taken as the minimum of the two quadratics given above for A_v and A_j.

APPENDIX D

D1: FORMULAE USED TO CALCULATE λ, e_s, s, ρ_a, γ, Ψ_M AND Ψ_H:

i) Latent heat of vaporisation of water vapour,

λ (J g^{-1}) = -2.496 T + 2501, Equation D1a

where T = temperature in °C

ii) Saturated water vapour pressure (Tetens formula),

$$e_s \text{ (kPa)} = 0.611 \exp\left[\frac{17.27T}{T+(273.15-36)}\right] \quad \text{Equation D1b}$$

where T = temperature in °C.

iii) Slope of saturation vapour pressure *vs* temperature (by differentiation of Tetens formula),

$$s \text{ (Pa K}^{-1}) = \frac{5004799371}{5000}\exp\left[\frac{1727}{5}\frac{T}{(20T+4743)}\right]\frac{P}{(20T+4743)^2} \quad \text{Equation D1c}$$

where T = temperature in °C and P is pressure.

iv) The density of dry air,

ρ_a (kg m^{-3}) = 1.292 - 0.00428T where T = temperature in °C Equation D1d

v) The psychrometer constant at a given temperature, T,

$$\gamma \text{ (Pa K}^{-1}) = \frac{P c_p}{\left(\frac{M_{H_20}}{M_{air}}\right)\lambda} \quad \text{Equation D1e}$$

where c_p is the specific heat of dry air (1012 J kg^{-1} K^{-1}), λ is the latent heat of vaporisation of water vapour, and M_{H20} and M_{air} are the molecular weights of water vapour and air respectively.

vi) As described in section 8.2, the aerodynamic resistance of the canopy, r_a, is partly determined by the term [ln(z_{oM} / z_{oH}) + ψ_M - ψ_H] in Equation 8.4. The estimated value for ln(z_{oM} / z_{oH}) was 1.5 (Garratt, 1992; Grace *et al.*, 1995a), while ψ_M and ψ_H are defined in unstable conditions as (Paulson, 1970; Lloyd *et al.*, 1995b):

$$\psi_M = 2\ln[(1 + x)/2] + \ln[(1 + x^2)/2] - 2\tan^{-1} x + \pi/2 \qquad \text{Equation D1f}$$

$$\psi_H = 2\ln[(1 + y)/2] \qquad \text{Equation D1g}$$

where $x = (1 - 16\zeta)^{1/4}$, $y = (1 - 16\zeta)^{1/2}$ and $\zeta = (z - d)/L$, where z is the reference height above the ground, d is the zero place displacement, and L is the Monin-Obukhov length,

$$L = -(u*^3\, T\, c_p\, \rho_a) / (kgH) \qquad \text{Equation D1h}$$

where $u*$ is the friction velocity, T is air temperature, c_p is the heat capacity dry air, ρ_a is the density of dry air, k is von Karmen's constant (~0.41), g is acceleration due to gravity, and H is the sensible heat flux. In stable conditions it is assumed that $\psi_M = \psi_H = -5\zeta$ (Garratt, 1992; Lloyd *et al.*, 1995b).

D2. EMPIRICAL RELATIONSHIPS USED TO OBTAIN IN-CANOPY METEOROLOGICAL VARIABLES

All in-canopy variables were derived from above-canopy measurements using empirical relationships based on short-term in-canopy measurements in SRF.

1) In-canopy air temperature, T, and woody tissue temperature, T_w, was related to above canopy temperature, T_c, using a series of regressions (Tables D2.i.a & D2.i.b); no in-canopy measurements of T were made at 7 m or 22 m, so values for those heights were estimated as the mean of the two neighbouring measurements.

Table D2.i.a. Regressions relating T at height, h (m), with T_c. Data are given for measured heights at 1 m, 15 m, 33 m and 46 m; temperature units are in °C. The form of the equation is $T_{ah} = aT_c + b$.

h	a	b	r^2	n
1	0.6586	6.452	0.87	288
15	0.9552	-0.026	0.96	288
33	0.9941	-0.856	0.98	288
46	0.9632	0	0.98	288

Table D2.i.b. Regressions relating T_w at height, h (m) with T_c. Data are given for five measured heights, at 8 m, 12 m, 20 m, 30 m and 40 m; temperature units are in °C. The form of the equation incorporates a lag to account for the heat capacity of woody tissue: $T_w = (\cos(t + a))\ b + cT_c + dT_c^2 + e$, where t is time in radians (π rads = midday).

h	*a*	*b*	*c*	*d*	*e*	r^2	*n*
8	2.45	2.97	-0.81	0.02	30.04	0.84	288
12	-0.73	-3.32	-1.10	0.03	33.16	0.83	288
20	5.46	-3.86	-1.63	0.04	40.26	0.86	288
30	5.36	-4.57	-3.21	0.07	61.69	0.84	288
40	5.88	-3.75	2.31	-0.03	-9.26	0.83	288

2) In-canopy air vapour pressure deficit, D, was related to above-canopy vapour pressure deficit, D_c, using a similar procedure to that for temperature (Table D2.ii).

Table D2.iii. Regressions relating D at height, h (m), with D_c. Data are given for measured heights at 1 m, 15 m, 33 m and 46 m; D units are in mol mol^{-1}. The form of the equation is D at $h = aD_c + b$, except for D at $h = 1$ m, where a quadratic fitted the data better: D (at h=1 m) = $aD_c^2 + b$.

h	*a*	*b*	r^2	*n*
1	57.64	0.0018	0.91	140
15	0.9854	2.05×10^{-4}	0.92	140
33	1.0318	1.36×10^{-4}	0.96	140
46	0.9687	0	0.94	140

3) In-canopy daytime CO_2 concentration, C_a, was driven from above canopy CO_2 concentration, C_{ac}. C_a from 7 m to C_{ac} was assumed to be identical between 0900 hrs and 1600 hrs (*i.e.*, the mean profile was vertical; see Figure 8.4); for the times between 0600 hrs - 0800 hrs and 1700 hrs - 1900 hrs regressions by height were used to predict mean C_a (C_a*) between 7 m and the canopy-top (Table D2iii.a). C_a at 1m was defined for each hour as a mean constant fraction of C_a at 7 m (Table D2iii.b).

Table D2.iii.a. Regressions fitted to estimate C_a* at height h (m) between 7 m and the canopy-top (C_{ac}) for hours when the C_a profile was not vertical. The form of the regression is $C_a^* = ah + b$; C_a units are µmol mol^{-1}, where n represents average concentrations (mean of 24 measurements) for each of 5 heights (Figure 8.4). Estimates of C_a for a specific hour were then calculated according to: $C_a = (C_{ac} / C_{ac}^*)C_a^*$

Hour	*a*	*b*	r^2	*n*
0600	-0.95	452.3	0.99	5
0700	-0.56	436.8	0.99	5
0800	-0.10	405.9	0.94	5
1700	-0.16	376.3	0.69	5
1800	-0.24	385.1	0.79	5
1900	-0.45	398.1	0.89	5

Table D2.iii.b. The mean proportional increase, x, in C_a* from 7 m to 1m for individual hours between 0600 hrs - 1900 hrs; $C_{a(1\ m)} = xC_{a(7\ m)}$, units for C_a = μmol mol^{-1}.

Hour	0600	0700	0800	0900	1000	1100	1200
x	1.022	1.049	1.057	1.091	1.051	1.047	1.045
Hour	1300	1400	1500	1600	1700	1800	1900
x	1.056	1.060	1.073	1.078	1.084	1.054	1.040

4) In-canopy Q was driven from above-canopy measurements, Q_c. The extinction in mean Q, (Q*),with height, h, was linearised using a ln$Q$ transformation. Data from three different groups of hours were found to show similar extinction patterns with height (section 8.3). Regressions were fitted to these data to permit the estimation of Q* at height h, Q_h*; Q_h for specific hours was calculated by scaling Q_h* according to the difference between measured Q_c and Q_h* at h = the canopy-top (Table D2.iv).

Table D2.iv. Regressions between ln$Q$* and height, h (m), for three groupings of hours. The form of the regression is lnQ_h* = $bh + c$. Q_h can now be estimated according to Equation 8.2, where Q_h = exp[$a_t(bh + c)$], or Q_h = exp[a_t lnQ_h*]. Units for Q are in μmol quanta m^{-2} s^{-1}.

Hour groupings	*b*	*c*	r^2	*n*
0600, 0700, 1800	0.85	0.075	0.65	12
0800, 0900, 1600, 1700	2.82	0.066	0.88	20
1000 - 1500 inclusive	3.98	0.064	0.89	30

APPENDIX E

Table E1. List of all species in SRF and PRF upon which gas exchange measurements were made.

(1) PRF, BRAZIL

Family	*Species*
Anacardiaceae	*Astronium lecointei* Ducke
Annonaceae	*Xylopia* sp
Arecaceae	*Orbigynia speciosa*
Burseraceae	*Protium polybotrium* (Turcz) Engl.
Chrysobalanaceae	*Licania* sp
Euphorbiaceae	*Hironima* sp
Erythroxylaceae	*Erythroxylum* c.f. *microcarpum* Mart.
Lauraceae	*Ocotea* cf *caudata* (Nees.) Mez
Lecythidaceae	*Bertolettia* sp
Leguminoseae; Caes.	*Sclerolobium* sp

Leguminoseae; Mim.	*Inga sp*
Leguminoseae; Pap.	*Derris pterocarpa* (DC)
Loganaceae	*Strychnos amazonicus* Krukoff
Meliaceae	*Cedrela odorata* L.
Meliaceae	*Guarea kunthii* A. juss.
Meliaceae	*Trichilia quadrijuga* H.B.K.
Moraceae	*Cecropia ficilifolia* Snethl.
Moraceae	*Cecropia sciadophylla* Mart.
Moraceae	*Naucleopsis glabra* Spr. ex Baill
Moraceae	*Naucleopsis krunnii* (Standl) C.C. Berg.
Moraceae	*Pseudomeldia* sp.
Moraceae	*Sorocea guilleminiana* Grand.
Moraceae	*Trymatococcus amazonicus* Poepp et Endl.
Myristicaceae	*Virola calophylla* Warb.
Myristicaceae	*Virola michelii* Hackel
Palmae	*Maximilliana maripa* (Corre Serra) Drude
Sterculiaceae	*Sterculia pruriens* (Aubl.) Schum
Sterculiaceae	*Theobroma microcarpum* Mart.
Sterculiaceae	Unknown
Violaceae	*Leonia glycicarpa* Ruiz
Violaceae	*Rinorea pubiflora* (Benth.) Spreng.

(2) SRF, CAMEROON

Family	*Species*
Annonaceae	*Xylopia etiopica*
Asteraceae	*Vernonia conferta*
Burseraceae	*Santira trimera* (Oliv.) Aubr.
Combretaceae	*Terminalia superba* Engl. & Diels
Dichapetalaceae	*Dichapetalum sp*
Leguminoseae; Caes	*Amphimas pterocarpoides* Harms.
Leguminoseae; Caes	*Distemonanthus benthamianus* Baill.
Leguminoseae; Pap.	*Ptercarpus soyauxii* Taub.
Icacinaceae	*Desmostachys tenuifolius*
Irvingaceae	*Desbordesia glaucescens* (Engl.) Van Tiegh.
Irvingaceae	*Kainedoxa gabonensis* Pierre ex Engl. var oblongifolia
Meliaceae	*Trichilia sp*
Marantaceae	*Haumaniana dankelmaniana* M-Redh
Marantaceae	*Megaphrynium macrostachyum*
Marantaceae	*Hypsodelphis violacea* (Ridl.) M-Redh.
Moraceae	*Musanga cecropoides* R.Br.
Myristicaceae	*Coelocaryon preussi* Warburg
Myristicaceae	*Staudtia stipitata* Warburg
Ochnaceae	*Lophira alata* Banks ex Gaertn.f.
Olacaceae	*Panda oleosa* Pierre
Sterculieaceae	*Triplochiton scleroxylon* K. Schum.
Ulmaceae	*Celtis adolfi-friderici* Engl.
Ulmaceae	*Celtis mildbraedi* Engl.
Ulmaceae	*Trema orientalis* (Linn.) Bl.
Verbenaceae	*Vitex grandifolia*